IMPACT OF THE CLOSING PANAMANIAN SEAWAY IN THE LATE MIOCENE TO PLIOCENE ON COCCOLITHOPHORE EVOLUTION, BIOGEOGRAPHY AND PALAEOPRODUCTIVITY

Monographische Dissertation

zur Erlangung des Doktorgrades
der Mathematisch-Naturwissenschaftlichen Fakultät
der Christian-Albrechts-Universität zu Kiel

vorgelegt von

Jeannette Lezius

Kiel, 2008

Referent	Prof. Dr. Priska Schäfer
Koreferent	PD Dr. Mara Weinelt
Tag der Disputation	30.01.2009
Zum Druck genehmigt	15.04.2009
Der Dekan	Prof. Dr. Lutz Kipp

EIDESSTATTLICHE ERKLÄRUNG

Hiermit erkläre ich an Eides statt, dass die vorliegende Dissertation mit dem Titel 'Impact of the closing Panamanian Seaway in the late Miocene to Pliocene on coccolithophore evolution, biogeography and palaeoproductivity', abgesehen von der Beratung durch meine akademischen Lehrer, in Inhalt und Form meine eigene Arbeit darstellt. Ferner habe ich weder diese noch eine ähnliche Arbeit an einer anderen Hochschule im Rahmen eines Prüfungsverfahrens vorgelegt.

Kiel, den 16.12.2008

_____

J. Lezius

ABSTRACT

The closure of the Panamanian Seaway acted as a critical threshold in the late Neogene ocean circulation patterns with strong impact on climate and plankton evolution. Evaluation of feedback mechanisms between palaeoceanography and marine biota related to the uplift of the Isthmus of Panama emphasises the fundamentally changed palaeoceanographic conditions. A high-resolution multi-proxy approach on sediments of two ODP Sites from the eastern equatorial Pacific (Site 1241) and the central Caribbean Sea (Site 1000) highlights the prominent role of calcareous nannoplankton to provide insights into this turning point in Earth's history. Whithin this thesis the following points regarding the biostratigraphy, evolution and ecology, accumulation rates and stable carbon and oxygen isotope composition of coccolithophores are addressed:

(1) The detection of local and global nannofossil bioevents suggests a set of mechanisms that is controlled by intrinsic and extrinsic factors triggering coccolithophorid evolution independently of the Panamanian Seaway Closure. Synchrony is observed in the Top of the paracme interval of *R. pseudoumbilicus* (7.135-7.058 Ma), the first occurrence (FO) of *R. rotaria* (7.2-7.18 Ma) and the last occurrence (LO) of *S. abies* (3.624-3.618 Ma). Diachrony exists for the LO of *R. rotaria* (6.9 Ma; 6.34 Ma). (2) Distinct morphological patterns provide evident influence of the gateway closure. Gradual and punctual changes in intrageneric and intraspecific coccolith size occur, which distinguish the eutrophic eastern equatorial Pacific as preferred ecological niche for the assemblage-dominating r-selective *Reticulofenestra* spp. They show the largest coccolith sizes, strongest size increases and longest durations of dominance of large species as well as the highest abundances in the more eutrophic, open-seaway conditions of the late Miocene eastern equatorial Pacific. Large reticulofenestrids could have passed through the seaway to the central Caribbean, but due to the lack of ecologically preferred conditions, they do not reach significant numbers in the fossil record. Small cell sizes dominate the consistingly more oligotrophic conditions of the Caribbean, and also gain higher abundances in the Pliocene eastern equatorial Pacific. (3) With closed-seaway conditions, palaeoproductivity decreases (*F. profunda*, MARs, nannoARs) in the eastern equatorial Pacific due to the changed palaeo-location off the equatorial divergence and preceding the high-producitivity event of the 'Biogenic Bloom'. This may superimpose the general trend of post-closure palaeoproductivity increase in the tropical eastern Pacific (e.g. Schneider and Schmittner, 2006). The observed increase in palaeoproductivity (*F. profunda*) in the central Caribbean after the Panamanian Seaway Closure, however, is not concordant with the decreased coccolith accumulation rates, which might be a result of short-lived seasonal productivity events in an overall oligotrophic regime. (4) Stable isotopic composition proved changes in the central Caribbean due to isthmus closure, with changes in ecology, productivity and salinity. Strong influence of bank-derived aragonite in the Pliocene, however, indicates the necessity of a multi-proxy approach to detect possible

influences of the isotopic signal of the bulk fine-fraction, i.e. the coccolith isotope signature. (5) Improvement of its understanding confirmed the reliability of the isotopic signal of the bulk fine-fraction due to a constant offset to the isotopic signal of quasi-monospecific subgroups. Isotopically heavy and light groups exist within species-specific isotopic signatures depending on coccolith size. The signal of larger species is generally depleted by 1 ‰ in both, stable carbon and oxygen isotopes compared to the smaller fractions and the bulk fine-fraction signal. (6) The 'Late Miocene Carbon Shift' is apparent in the bulk fine-fraction of both, the eastern equatorial Pacific and the central Caribbean. The amplitude of the depletion in carbon isotopic composition is similar in coccoliths and foraminifers, with a decrease of about 1 ‰. The decrease of planktonic and benthic isotope signals, as well as the decrease in accumulation rates and changes in assemblage composition suggest the necessity of other mechanisms to explain the 'Late Miocene Carbon Shift' than solely productivity changes. (7) This interval, however, is marked by a two-fold prominent increase in carbonate accumulation. It is accounted for by (a) an increase in coccolith sizes before, and (b) an increase in coccolith productivity after 6.7 Ma. These patterns clearly indicate the so-called 'Biogenic Bloom' to be a coccolithophorid bloom.

KURZFASSUNG

Der Seeweg von Panama spielte eine entscheidende Rolle für die Ozeanzirkulation im späten Neogen. Seine Schließung hatte starke Auswirkungen auf das globale Klima und die Evolution von Plankton-Organismen. Die Auswertung von Rückkopplungsmechanismen zwischen der Paläozeanographie und marinen Biota bestätigt die grundlegend veränderten paläozeanographischen Bedingungen durch die Hebung des Isthmus von Panama. Ein hochauflösender Multi-Proxy Ansatz an Sedimenten von zwei ODP Kernen aus dem östlichen äquatorialen Pazifik (Site 1241) und der zentralen Karibik (Site 1000) betont die außergewöhnliche Rolle von kalkigem Nannoplankton (i.w.S Coccolithophoriden) bei der Untersuchung dieses Wendepunkts in der Erdgeschichte. Diese Arbeit befasst sich mit dem Einfluss der Schließung des Seeweges von Panama auf die Biostratigraphie, Evolution und Ökologie, Paläoproduktivität sowie Zusammensetzung von stabilen Kohlenstoff- und Sauerstoffisotopen von Coccolithophoriden.

(1) Die Bestimmung von lokalen und globalen biostratigraphischen Ereignissen unter Nannofossilien weist auf eine Reihe von Mechanismen, die von intrinsischen und extrinsischen Faktoren kontrolliert werden. Diese beeinflussen die Evolution von Coccolithophoriden unabhängig von der Schließung des Panama-Seeweges. Synchronität wurde im Top des Paracme-Intervals von R. *pseudoumbilicus* (7.135-7.058 Ma), dem ersten Auftreten (FO) von *R. rotaria* (7.2-7.18 Ma) und dem letzten Auftreten (LO) von *S. abies* (3.624-3.618 Ma) beobachtet. Diachronität erscheint beim letzten Auftreten von *R. rotaria* (6.9 Ma; 6.34 Ma). (2) Bestimmte morphologische Muster weisen deutlich auf den Einfluss der Schließung des Seeweges hin. Graduelle und punktuelle Größenänderungen innerhalb von Gattungen und Arten treten auf, was den östlichen äquatorialen Pazifik als bevorzugte ökologische Nische für die dominierenden r-Strategen *Reticulofenestra* spp. erkennen lässt. Diese weisen größte Coccolithengrößen, stärkste Größenzunahmen, längste Dauer an Dominanz großer Formen und höchste Häufigkeiten unter den leicht eutrophen Bedingungen des äquatorialen Pazifiks zu Zeiten mit offenem Seeweg auf. Große Reticulofenestren treiben durch den Seeweg in die zentrale Karibik, wo sie allerdings aufgrund ungünstiger ökologischer Bedingungen nur in geringem Masse in fossilen Sedimenten zu finden sind. Kleine Coccolithengrößen überwiegen in den oligotrophen Bedingungen der Karibik, und gewinnen auch im Pliozänen äquatorialen Pazifik an Bedeutung. (3) Unter den Bedingungen des geschlossenen Seeweges nimmt die Paläoproduktivität (*F. profunda*, MARs, nannoARs) aufgrund der veränderten Paläo-Lokation mit Entfernung zur äquatorialen Divergenz und der vorangegangenen stark erhöhten Produktivität des „Biogenic Bloom“ Intervals im östlichen equatorialen Pazifik ab. Dies mag die generell beobachtete Zunahme der Paläoproduktivität im tropischen Ostpazifik (Schneider and Schmittner, 2006) überlagern. Der Anstieg der Paläoproduktivität (*F. profunda*) in der zentralen Karibik nach der Schließung des Seeweges ist wiederum nicht vereinbar mit den stark verringerten

Akkumulationsraten von Coccolithen, was ein Ergebnis von kurzlebigen, saisonal geprägten Produktivitäts-Ereignissen in einem sonst durchgehend oligotrophen Regime zu sein scheint. (4) Die Zusammensetzung stabiler Isotope belegt schließungsbedingte Änderungen von Ökologie, Produktivität und Salinität in der Karibik. Hier tritt im Pliozän starker Eintrag von Aragonit von den umliegenden Karbonatbänken auf. Mögliche Einflüsse auf das Isotopensignal der Gesamtfeinfraktion müssen geklärt werden. (5) Generell wird die Gesamtfeinfraktion von Coccolithen präsentiert. Die detaillierte Untersuchung verschiedener Größenfraktionen (quasi-monospezifische Unterfraktionen) bezüglich ihrer Isotopensignale bekräftigte die Verlässlichkeit der Gesamtfeinfraktion als geochemischen Proxy anhand eines konstanten Versatzes untereinander. Hierbei wurden, in Abhängigkeit von ihrer Coccolithengröße, isotopisch leichte und schwere Gruppen ausgemacht. Das Signal der großen Arten ist hierbei in den Kohlenstoff- und Sauerstoffisotopen generell um 1 ‰ leichter als das der kleineren Fraktionen und der Gesamtfeinfraktion. (6) Der sogenannte „Late Miocene Carbon Shift“ tritt in der Gesamtfeinfraktion von Pazifik und Karibik auf. Die Amplitude des Coccolithen- und Foraminiferenisotopensignals ist mit einer Abnahme von 1 ‰ sehr ähnlich. Die niedrigsten Kohlenstoffisotopenwerte treten um 6.7 und 5.9 Ma auf. Die Abnahme von bentischen und planktonischen Isotopensignalen, gekoppelt mit der Abnahme der Akkumulationsraten, sowie Vergesellschaftunsänderungen zeigen, dass der „Late Miocene Carbon Shift“ nicht alleine mit Änderungen in der Produktivität erklärt werden kann. (7) Dennoch ist dieser Intervall ist von einem zweifachen, starken Anstieg der Karbonatakkumulationsraten gekennzeichnet. Diese werden hervorgerufen durch (a) eine Zunahme der Coccolithengröße (Intervall älter als 6.7 Ma) und (b) eine Zunahme der Coccolithenproduktivität (Intervall jünger als 6.7 Ma). Dieses Modell identifizierte den „Biogenic Bloom“ Intervall eindeutig als Produktions-Ereignis von Coccolithophoriden.

CONTENTS

CHAPTER 1 INTRODUCTION

1.1 Aim of the study, strategy, and structure of thesis

This thesis aims to evaluate the influence of the closure of the Panamanian Seaway on the evolution, biogeography and palaeoproductivity of coccolithophores. Main object of this study is to investigate causes and consequences of plankton evolution in relation to the gateway closure to understand feedback mechanisms between biota and the global carbon cycle. Focus was placed on a remarkable event of enhanced biogenic accumulation during the late Miocene, the so-called 'Biogenic Bloom' interval, to evaluate the coccolithophorid response to fundamentally changing palaeoceanographic patterns on both sides of the emerging Panamanian Isthmus.

1.1.1 Objectives

The opening and closure of oceanic gateways are considered as important mechanisms that changed ocean circulation and affected global climate and biota. The DFG Research Unit 'Impact of Gateways on Ocean Circulation, Climate and Evolution' was established at University of Kiel in 2001 to provide palaeoceanographic evidence of these mechanisms. Major questions addressed the role of oceanic gateways on global thermohaline circulation, climate, and the evolution of marine organisms.

This study was part of the sub-project 'Influence of ocean gateways on evolution of marine plankton: A biometric approach'. It documents the role of calcareous nannoplankton as a main carbonate producer in the ocean in relation to changes in ocean circulation and global climate in the late Miocene to Pliocene. Target is to assess the influence of the closure of a low latitude gateway, the Panamanian Seaway, on the evolution and biogeography of planktonic nanno-organisms and on their influence on the carbon cycle. Main focus of this study is the prominent change of carbonate accumulation rates in all ocean basins during the so-called 'Biogenic Bloom' interval, for which quantitative biostratigraphic as well as morphometrical, ecological, and geochemical investigations on coccolithophores were carried out.

More specifically, major objectives of this thesis are:

- **Biostratigraphy**
  - → Synchrony/diachrony of nannofossil bioevents based on orbitally tuned high-resolution records
  - → Differences between first and last occurrences among K-selective (oligotrophic specialists) and r-selective (eutrophic opportunists) taxa
  - → Temporal and spatial biostratigraphic schemes

- **Biometry**
  - → Intrageneric and intraspecific species variations
  - → Patterns of evolution (gradualistic and/or punktualistic)
  - → Differences between K-selective (oligotrophic specialists) and r-selective (eutrophic opportunists) taxa
  - → Correlation between evolution- induced change of coccolith size and the closing history of the Panamanian Seaway

- **Absolute and relative abundances**
  - → Biodiversity of the coccolithophorid assemblages
  - → Differences in biogeography related to the isthmus closure
  - → Ecology
  - → Calculation of accumulation rates
  - → Species-specific carbonate fluxes
  - → Linkage between carbonate accumulation rates and evolution- induced changes in coccolithophores (increase in productivity or in size)

- **Particle size distribution of the fine-fraction**
  - → Influence of ecological and evolutionary patterns in coccolithophores on grain size distribution

- **Stable carbon and oxygen isotope values**
  - → Species-dependent isotope fractionation
  - → Influence of evolution- and/or ecology- induced changes in coccolithophorid assemblages on the stable isotope signal of fine-fraction
  - → Correlation of foraminifer and bulk fine-fraction isotope records with emphasis on the Biogenic Bloom interval / Late Miocene Carbon Shift and Panamanian Seaway Closure

1.1.2 Outline

This thesis has been divided into three main parts:

The first part (chapters 1 and 2) contains an **introduction** to the dissertation. Chapter 1 provides main objectives, strategies with a short overview on site locations and the quality of the sample material, and background information. This serves a general introduction into the hydrography of the late Miocene to Pliocene tropical East Pacific and Caribbean Sea, as well as a compendium of the closing history of the Panamanian Seaway. Finally an overview on coccolithophores is presented. Chapter 2 includes a detailed description into sample treatment and analytical methods.

The second part (chapters 3 to 8) presents and discusses the **results** of this dissertation.

Topics of that second part cover the objectives listed before in chapter 1.1.1, including biostratigraphy, morphometry, accumulation patterns, grain size variations, and stable carbon and oxygen isotopes of the bulk fine-fraction. Integrated and slightly modified manuscripts are presented in:

· Chapter 6:

Lezius, J. and Kinkel, H., The uplift of Panama and the carbonate budget: the coccolith side of the story. Manuscript in preparation for Palaeogeography, Palaeoclimatology, Palaeoecology.

· Chapter 7:

Lezius, J. and Kinkel, H., Sedimentological grain size analysis as a proxy in micropalaeontology – the coccolithophorid assemblage during the late Miocene to Pliocene Biogenic Bloom interval in the eastern equatorial Pacific. Manuscript in preparation for Marine Geology.

The last part (chapters 9 and 10) gives a **synthesis** of all discussed results (chapter 9) and summarizes the main conclusions (chapter 10) by considering questions and objectives previously raised in chapter 1.

References cited in chapters 1-10 are listed in a combined reference register at the end of the thesis. All data that were generated by the author within the framework of this thesis and are provided in the **appendices** (A1-A3).

1.1.3 Strategy

1.1.3.1 Site selection, observed time intervals, sampling interval

In order to obtain insights into the influence of changes in circulation patterns and hydrography related to the closure of the Panamanian Seaway, two ODP sites (Fig. 1.1.3.1-1) were chosen for this study, one in the **eastern equatorial Pacific** (**Site 1241**), the other in the **central Caribbean Sea** (**Site 1000**). These sites have been extensively studied by the DFG Research Unit 'Impact of Gateways on Ocean Circulation, Climate and Evolution'. Main focus for this thesis was placed on an interval with open-gateway-conditions around 7.7 to 5.5 Ma, the so-called '**Biogenic Bloom**' interval. A second time interval covers the final phase of the closure of the Panamanian Seaway in the mid-Pliocene between 3.7 and 3.3 Ma.

From the Pacific Site 1241, samples were taken every 50 cm in the older, and every 100 cm in the younger part of the late Miocene section due to a supposed change in sedimentation rate (Mix, Tiedemann, Blum et al., 2003a; Mix et al., 2003b). The time resolution is around 13.5 kyr. Caribbean Site 1000 has a sampling interval of consistently 50 cm for the late Miocene, reflecting a temporal resolution of around 11.5 kyr.

For the younger '**Final Closure**' interval, samples were taken every 10 cm, resulting in a time resolution of less than 3 kyr at both the Pacific and the Caribbean site.

A sampling gap exists at Site 1241 between Hole A Core 9 Transect H Section 7 and Hole A Core 10 Transect H Section 2 causing a gap in the Pacific record from 3.5475 to 3.4576 Ma.

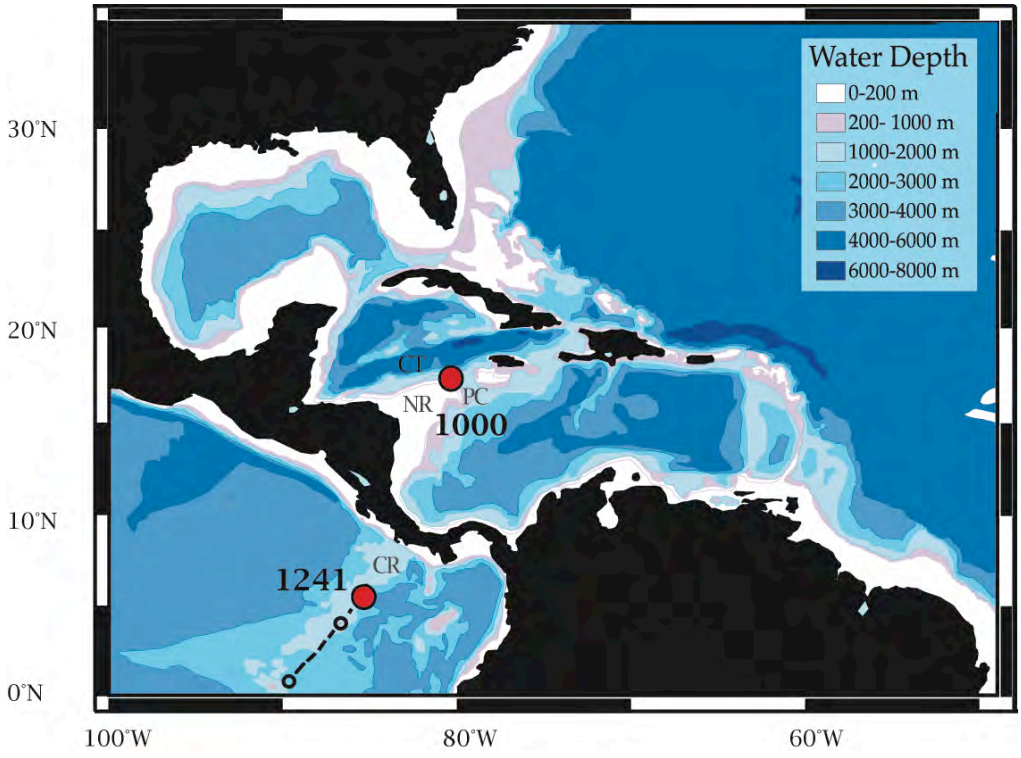

Fig. 1.1.3.1-1 Geography and bathymetry of the central Caribbean and eastern equatorial Pacific with locations of studied ODP Sites 1241 and 1000 (red circles). Tectonic backtracking of Site 1241 is marked with dashed line, small circles indicate positions at 7.5 and 3 Ma (after Pisias et al., 1995). CR = Cocos Ridge, NR = Nicaragua Rise, CT = Cayman Trough, PC = Pedro Channel.

1.1.3.2 Site locations, sample material

ODP Site 1241

Sediment records obtained during ODP Leg 202 provide a palaeoceanographic transect to assess climate and oceanographic changes in the southeast Pacific over Neogene time. The eastern equatorial Pacific ODP Site 1241 (Fig. 1.1.3.1-1) was drilled during that Leg at 5°50N, 86°26´W in the Guatemala Basin on the northern flank of Cocos Ridge at 2027 m water depth (Mix et al., 2003a). Tectonic backtracking of today's position on the Cocos Ridge moves Site 1241 southwestward (around 4°N, 87°10´W at 3 Ma; 1,5°N, 89°30´W at 7.5 Ma, Fig. 1.1.3.1-1) (after Pisias et al., 1995). Thus, during the investigated time intervals, Site 1241 was probably located close to the equator and probably at shallower depth (Mix et al., 2003a). As Site 1241 was located fairly close to the final gateway region throughout the late Miocene to Pliocene, it was considered as an ideal position to examine closure-related changes in the tropical east Pacific surface hydrography on marine biota.

The observed sediments are composed of foraminifera-bearing nannofossil oozes. All samples from both investigated time intervals from the late Miocene and the Pliocene contain very abundant and diverse nannofossil assemblages. Due to its relatively shallow depth, preservation of the calcareous micro- and nannoplankton at Site 1241 is excellent. This is supported by Lyle et al. (1995) who proposed that the carbonate compensation depth was established at a depth of about 3400 m from 10 Ma onward, with maximum deepening toward modern values of 3600 m in the Plio-Pleistocene.

ODP Site 1000

The Central Caribbean ODP Site 1000 (Fig. 1.1.3.1-1) was obtained during Leg 165. It is situated at 16°33´N, 79°52´W within the Pedro Channel on the Northern Nicaraguan Rise at 916 m water depth (Sigurdsson et al., 1997). Sediments deposited during the investigated time intervals are a mixture of pelagic and bank-derived neritic carbonates. All samples from both investigated time intervals from the late Miocene and the Pliocene contain very abundant and diverse nannofossil assemblages. The shallow-water depth of the site in comparison with the depth of the modern lysocline at 4000 m (Archer, 1996) implies that carbonate dissolution is negligible. Samples show an excellent preservation of calcareous micro- and nannofossils. Fragile structures of coccoliths and even delicate holococcoliths are well preserved in all samples.

1.1.3.3 Oceanographic settings

ODP Site 1241 - eastern equatorial Pacific

Site 1241 on the Cocos plate is separated from the west coast of Central America by the Middle American Trench (Fig. 1.1.3.3-1), which traps most terrestrial sediments shed from the Central American Volcanic Arc. Terrestrial influence has remained a minor factor at this site. As Jiang and Wise (2007) proposed that no intra-plate variation in geological and tectonic settings on Cocos plate occurred during the Miocene to Pliocene, the nature of

deposition in the eastern equatorial Pacific has been influenced mainly by surface water productivity. The sedimentary sources are mainly biogenic calcite and to a minor extent biogenic silica, which determine sedimentation rates confirmed by the relationship of mass accumulation rates (MARs) between bulk sediments and the main sedimentary components (Jiang et al., 2007). Today´s distribution pattern of surface-water productivity helps to explain the spatial and temporal variations of palaeoproductivity in the eastern equatorial Pacific. Jiang and Wise (2007) found diminishing productivity away from the equator in the sedimentary records of the eastern equatorial Pacific, compared with today´s situation (Paytan et al., 1996). They observed substantially higher sedimentation rates under highly productive waters, affected by equatorial divergence or strong influence of the Peru upwelling system. Assuming that regional hydrography remains constant and the only change in the system is the tectonically induced drift of the site location relative to this fixed oceanographic background, tectonic backtracking indicates higher productivity during the late Miocene and Pliocene at Site 1241 than today, due to proximity to equatorial divergence and South Equatorial Current (Figs. 1.1.3.1-1; 1.1.3.3-1), suggesting colder and less saline conditions with a much shallower pycnocline than today (Mix et al., 2003a).

Today´s surface hydrography (Fig. 1.1.3.3-1) in the tropical Pacific is strongly controlled by seasonal variations in wind strength, causing seasonal changes in thermocline depth. The ocean current and wind system in the eastern equatorial Pacific is closely linked to the Intertropical Convergence Zone (ITCZ). This is the zone of convergence of the northeast and southeast trade winds. Trade winds drive the North Equatorial Current (NEC) and South Equatorial Current (SEC) towards the west. The SEC is fed by the Peru Current, which advects cool, nutrient-rich waters from the southeast Pacific into the Galápagos region, and by the North Equatorial Counter Current (NECC), which carries eastward the nutrient-depleted return-flow surface waters from the Western Pacific Warm Pool (WPWP). The Equatorial Under Current (EUC) below the SEC flows towards the East in a depth from around 300 m in the WPWP to a depth of around 30 m in the east Pacific, parallel to the shoaling thermocline. During El Niño-like conditions, the warm waters of the WPWP move to the East due to weak easterly winds over the tropical Pacific. This causes the cessation of upwelling, a decreasing temperature gradient between the WPWP and the east Pacific, and a deepening of the thermocline in the east Pacific (Wallace et al., 1998). Generally, the present day eastern Pacific is characterized by relatively low temperatures. Southeast trade winds cause strong upwelling along the Peruvian coast and along the equator, thus forming the Pacific Cold Tongue, which extends towards the equatorial divergence (Mitchell and Wallace, 1992). Accordingly, the thermocline in these areas is very shallow (< 50 m).

ODP Site 1000 - central Caribbean Sea

Prior to the middle Miocene, the Nicaragua Rise (NR) was a large carbonate platform that separated the Cayman Trough (CT) and the Yucatan Basin from the Caribbean Sea (Droxler et al., 1991; Droxler et al., 1992). This megabank became segmented due to teconical activity

along the northern Caribbean plate boundary. The Pedro Channel (PC), where Site 1000 is located, represents one of the largest segments of this once continuous platform (Fig. 1.1.3.1-1). The collapse of the periplatform followed the movement of the strike-slip fault along the Cayman Trough around 10.71 to 9.36 Ma, initiating the northward Caribbean Current (Kameo and Sato, 2000). The opening of that new gateway for the North Atlantic Western Boundary Current, caused an intensification of the Loop Current - Gulf Stream - system thus strengthening the thermohaline overturn.

This high tectonic activity strongly influenced sedimentation patterns in the Caribbean Sea. Mainly pelagic carbonates were deposited at Site 1000 mixed with fine-grained biogenic neritic carbonates delivered from adjacent carbonate banks, together with a minor component of terrigenous sediments (Sigurdsson et al., 1997). Prior to shoaling of the Panamanian Seaway, the Caribbean Sea was under mesotrophic conditions. The ongoing constriction of the Panamanian Seaway caused a gradual decrease in palaeoproductivity (Jain and Collins, 2007). Today (Fig. 1.1.3.3-1), the uppermost water column in the southern part of the Carribean Sea is composed of relatively fresh Caribbean Water (CW, 0-80 m) and highly saline Subtropical Under Water (SUW, 80-180 m) that forms the permanent Caribbean thermocline (100-150 m) (Wüst, 1964). The CW presents a mixture of Amazonas and Orinoco River outflow and equatorial surface water. The salinity-enriched SUW originates from the subtropical gyre. The Caribbean Current passes the Yucatan Channel and the Florida Straits where it merges with the Antilles Current to form the Gulf Stream. A strong salinity gradient of 1.0 to 1.5 determines the differences between the Caribbean Sea / Western Atlantic Warm Pool (WAWP) and the eastern equatorial Pacific today. It is mainly determined by the net transport of water vapour from the Caribbean Sea over central America into the Pacific by means of the trade winds (Broecker and Denton, 1989).

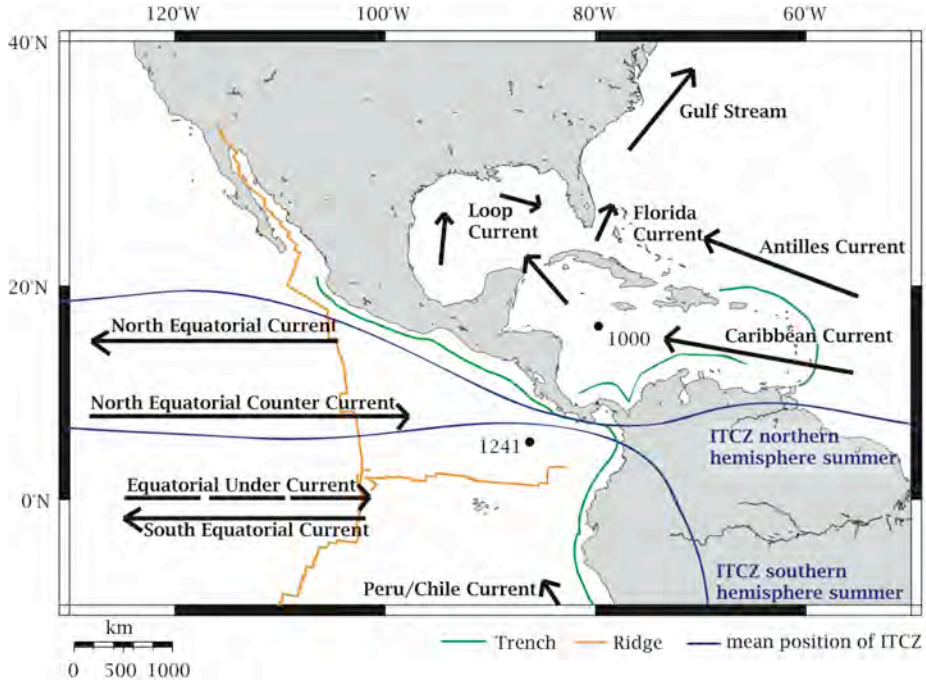

Fig. 1.1.3.3-1 General circulation in the Caribbean Sea and tropical eastern Pacific. Showing site locations, major surface and subsurface currents, and changes in the position of the ITCZ.

1.1.3.4 Age models

An accurate time calibration of sediment sequences is of crucial importance to precisely date geological events and determine rates of change. It provides the basis for all interpretations concerning the history of ocean circulation, climate and the evolution of biota. The astronomical tuning method is based on the fact that cyclic changes in climate proxy records respond statistically convincing to variations in insolation. Age models were constructed by matching patterns of cyclic variation in climate proxy records with patterns of changes in solar radiation that are controlled by cyclic variations in Earth's orbital parameters (e.g. Hays et al., 1976; Imbrie and Imbrie, 1980). The astronomical tuning technique is at present the most accurate absolute dating method for sediment records spanning the time interval of the last 35 Ma for which astronomers provide a valid and precise orbital solution for variations in Earth´s orbital parameters (eccentricity, obliquity, precession) (Laskar, 1999). Thus, correlation of sedimentary cycles to orbital parameters has resulted in the development of very accurate timescales for the Neogene (e.g. Laskar et al., 1993; Hilgen et al., 1995; Hilgen et al., 1999; Hilgen et al., 2003) and culminated in the 'Astronomically Tuned Neogene Time Scale' (ATNTS2004) (Lourens et al., 2004), recently improved by Lisiecki and Raymo (2005) and Hüsing et al. (2007). An astronomical time scale integrates a framework of magnetostratigraphy, biostratigraphy, tephrachronology and oxygen isotope stratigraphy.

Generally, preliminary on-bord age models use biostratigraphic, palaeomagnetic, and other data like e.g. physical properties, to construct an age-depth model. For Sites 1241 (Mix, Tiedemann, Blum et al., 2003) and 1000 (Sigurdsson, Leckie, Acton et al., 1997), nannofossil biostratigraphic datums were used to construct age-depth models (Flores et al., 2006; Kameo and Sato, 2000). Refinement of these preliminary age-depth models was done within the DFG Research Unit 'Ocean Gateways' (see below).

The Pliocene age model of tropical east Pacific Site 1241 was based on correlation of benthic $\delta^{18}O$ and $\delta^{13}C$ stratigraphies with Atlantic Site 925/926 and on tuning high frequency variations in GRA density (gamma-ray attenuation; e.g. Blum, 1997), percent sand of carbonate fraction, and benthic carbon and oxygen isotopes to the orbital solution of Laskar et al. (1993). This astronomically derived age model is in agreement with the most recent astronomical tuned oxygen isotope stack (Lisiecki and Raymo, 2005) and with other orbitally tuned age models (e.g. Tiedemann and Franz, 1997) and offers a clear developed 41-kyr-signal, especially in the $\delta^{13}C$ record (Tiedemann et al., 2007). The establishment of the age model is described in detail in Tiedemann et al. (2007) from 6–2.5 Ma. The age model of the Biogenic Bloom interval at Site 1241 was based on visual correlation of benthic $\delta^{13}C$ values with south-eastern Pacific Site 1237, resulting in a continuous Miocene stratigraphic sequence extending from 7.5 to 5.8 Ma (Fig. 1.1.3.4-1(A)).

Steph et al. (2006b) developed an astronomically calibrated age model for the Pliocene section of Site 1000 (5.5-2.5 Ma). The age model was established on the $\delta^{18}O$ record of the

benthic foraminifer *C. wuellerstorfi*. Since no composite depth model exists for Site 1000, a preliminary age model was constructed by identifying major $\delta^{18}O$ isotopic stages according to the nomenclature of Shackleton et al. (1995b), but using the age model and the $\delta^{18}O$ - reference record from ODP Site 925/926 from Ceara Rise (Bickert et al., 1997; Shackleton and Hall, 1997; Tiedemann and Franz, 1997). The final age model revealed the presence of dominant precession cycles in the planktonic $\delta^{18}O$ record, which were then used to fine-tune the age model from Site 1000 (Steph et al., 2006b). Lack of foraminiferal isotopic values, the age model for the Biogenic Bloom interval at Site 1000 is based on tuning high frequency variations in GRA density (gamma-ray attenuation; e.g. Blum, 1997) filter output with 409- and 100 kyr-insolation and fine fraction carbon and oxygen isotopes to the orbital solution of Laskar et al. (1993). It was developed by T. Bickert, University of Bremen (unpubl. data), resulting in a continuous and astronomically tuned Miocene stratigraphic sequence extending from 8 to 5.5 Ma (Fig. 1.1.3.4-1(B)).

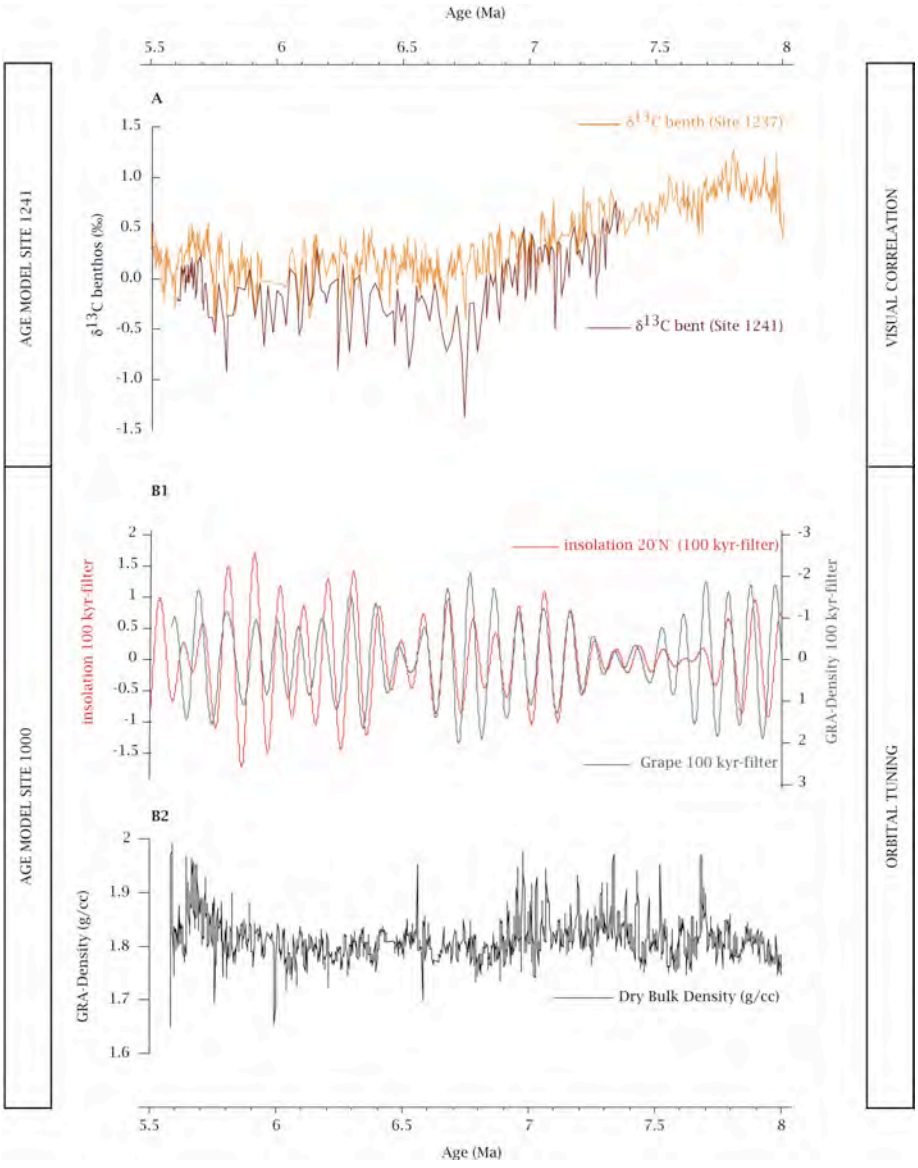

Fig. 1.1.3.4-1 Establishment of age models of late Miocene Sites 1241 (A) and 1000 (B). A: Visual correlation of benthic $\delta^{13}C$ values between Sites 1241 and 1237 was done by A. Sturm. B: orbital tuning of Site 1000 by courtesy of T. Bickert, GRA-density filtered with 100 kyr insolation (B1), raw GRA-density (B2).

1.2 Background Information

1.2.1 Palaeoceanography and climate of the late Miocene to Pliocene and their impact on biota

The Cenozoic era is characterized by a long-term global cooling trend from early Paleogene ice-free 'greenhouse' conditions towards the Neogene 'icehouse' regime (for an overview see Zachos et al., 2001a). The Mid-Miocene climate transition is a major cooling step in the Cenozoic climate evolution (Zachos et al., 2001a). The warm phase of the early Miocene, peaked in the Middle Miocene Climatic Optimum (MMCO; 17-14.5 Ma), was followed by the generally long-term cooling trend of the middle to late Miocene. The pronounced global cooling of the late Miocene marks a turning point in climate history (e.g. Shackleton and Kennett, 1975b). The subsequent early to mid-Pliocene represents the most recent period in Earth´s history of sustained global warmth (e.g. Dowsett et al., 1992; Ravelo and Andreasen, 2000; Billups, 2002) preceding the dramatic cooling associated with the onset of Northern Hemisphere Glaciation (NHG) at 2.74 Ma (e.g. Raymo et al., 1996; Dowsett et al., 1999; Bartoli et al., 2005) as final step towards our recent climatic conditions.

Earth´s orbital geometry is a primary force that drives climate. Rhythms related to Earth´s orbital parameters of eccentricity, obliquity, and precession oscillate around a climatic means that is constantly drifting in response to gradual changes in Earth´s major boundary conditions, largely controlled by plate tectonics. Continental geography and topography, as well as oceanic gateway location and bathymetry, and concentrations of greenhouse gases constitute major boundary conditions. Major events occurred during the late Neogene as trigger of the climate: (1) **tectonically driven events** as the uplift of the Tibetan Plateau (e.g. Raymo et al., 1988; Ruddiman and Raymo, 1988; Raymo and Ruddiman, 1992; Raymo, 1994; Ruddiman, 1998; Zisheng et al., 2001), constriction of the Indonesian Seaway (e.g. Li et al., 2004; Ravelo et al., 2004) and the uplift of the Isthmus of Panama (e.g. Duque-Caro, 1990; Coates et al., 1992; Haug et al., 2001b); (2) **changes in the ocean-continent climate system** including ice-sheet expansion, sea-level fluctuations, cooling of surface and deep water masses, onset of thermohaline overturn (Savin et al., 1975; Shackleton and Kennett, 1975a; Woodruff, 1989; Miller et al., 1991; Wright and Miller, 1996; Billups, 2002); (3) **changes in biota**, with basin-to-basin asymmetry in silica accumulation between North Atlantic and North Pacific (Keller et al., 1989; Farrell et al., 1995b; Cortese et al., 2004), as well as prominent shifts in carbonate accumulation rates in all ocean basins (e.g. Farrell et al., 1995b; Lyle et al., 1995), and expansion of C4 plants (e.g. Cerling et al., 1997; Pagani et al., 1999; Hoorn et al., 2000; Retallack et al., 2002).

1.2.1.1 Uplift history of the Isthmus of Panama and possible impacts

The Panamanian Seaway acted as a critical threshold in late Neogene ocean circulation patterns with its strong impact on ocean circulation forcing climate change and feedbacks in

biota. This major tectonic event of shoaling of the seaway is responsible for changes in the Atlantic and Pacific deep and surface water circulation regime and the intensification of the thermohaline circulation in the North Atlantic due to increasing salt and heat transport to high northern latitudes (Maier-Reimer et al., 1990; Haug and Tiedemann, 1998; Billups et al., 1999; Haug et al., 2001a; Nisancioglu et al., 2003). Thus it may play an important role in the initiation of the northern hemisphere glaciation, which started during the mid-Pliocene (Driscoll and Haug, 1998; Haug and Tiedemann, 1998; Bartoli et al., 2005) and is therefore considered to trigger the last cooling step in the Cenozoic climate change.

The geological history of the Panamanian Seaway, by means of step-like uplift and final emergence of the Isthmus of Panama, has been reconstructed from pelagic sediment records (e.g. Keigwin, 1978; Keigwin, 1982a; Keigwin, 1982b; Keller et al., 1989; Haug and Tiedemann, 1998; Kameo and Sato, 2000; Haug et al., 2001b; Lear et al., 2003; Steph, 2005; Steph et al., 2006a; Steph et al., 2006b), marine sediment records exposed on land (Duque-Caro, 1990; Collins et al., 1996; e.g. Coates et al., 2003), and from terrestrial environments (e.g. Marshall et al., 1982; Lundelius et al., 1987).

The tectonic closure of the Panamanian Seaway from 13 to 1.8 Ma resulted from the subduction of the Pacific Cocos- and Nazca plates beneath the North and South American plates and later the Caribbean plate (Coates and Obando, 1996; Meschede and Frisch, 1998; Hoernle et al., 2002). Complementary data come from reconstruction of palaeoceanographic events by comparing microfossil assemblages and their isotope signals between Caribbean Sea and Pacific (e.g Haug et al., 2001). Thus, several studies used benthic and planktonic foraminifers as well as calcareous nannoplankton to monitor the Neogene oceanographic changes related to the closing history of the Isthmus (e.g. Duque-Caro, 1990; Collins et al., 1996; Kameo and Sato, 2002). During the early middle Miocene (15.1 Ma) tectonic disturbances triggered the uplift of the Panama sill, and the deep-water connection between east Pacific and Caribbean Sea was cut off (Duque-Caro, 1990), but a free exchange of water masses down to intermediate depth still existed (sill depth about 2000 m) (Keller and Barron John, 1993). Proceeded shoaling of the Panama sill from the middle to late Miocene (13-12 Ma) to a depth of around 1000 m interrupted the intermediate water connection between Pacific and Caribbean Sea (Duque-Caro, 1990; Coates et al., 1992). In the late Miocene, from about 12 to 6 Ma, the Panamanian sill rose further and a significant interoceanic, biogeographic barrier had formed at around 8 Ma (Collins et al., 1996) with sill depths between 200 and 500 m (Keller et al., 1989; Duque-Caro, 1990; Chaisson and Ravelo, 2000; Jain et al., 2007). First terrestrial faunal exchange between North and South America (raccoons and sloths) is recorded at 9.3 to 8 Ma (Marshall et al., 1982; Webb, 1985; Webb, 1991; Webb et al., 1995; Webb and Rancy, 1996), indicating the existence of an extended archipelago with relatively close spacing of islands in Central America since the late Miocene (Fig 1.2.1.1-1). At about 5 Ma, the subduction of the Cocos Ridge, which formed during the

passage of the Cocos Plate over the Galápagos hotspot, dramatically elevated the Central American volcanic arc and led to the final phase of the closure (Hoernle et al., 2002).

Most modelling studies indicate that the main transport of water masses was directed from the Pacific into the Atlantic (Maier-Reimer et al., 1990; Mikolajewicz et al., 1993; Nisancioglu et al., 2003; Prange and Schulz, 2004). The inflow of lower salinity waters from the Pacific into the Atlantic prevented a significant salinity increase in the Caribbean Sea prior to the closure. Additionally, a certain amount of North Atlantic Deep Water, or all of it, may have escaped from the Atlantic into the Pacific with a sill depth below 1000 m (Nisanciolgu et al., 2003), which would greatly reduce the salinity difference with respect to modern times in case of an open isthmus. From 4.6 to 4.2 Ma, the restriction of the Panamanian sill reached a critical threshold for upper water mass exchange (Haug and Tiedemann, 1998). This was inferred from the divergence between Pacific-Caribbean planktonic oxygen isotope records (Keigwin, 1982; Haug et al., 2001), indicating the development of the modern Pacific-Atlantic contrast in sea surface salinities, with higher surface water salinity in the Caribbean Sea. The evolutionary divergence of near-shore faunas on both sides of the Isthmus around 3.5 Ma suggests the gateway to be effectively closed by this time (Coates et al., 1992). Crudeli (2005) described changes in evolutionary radiation of Caribbean coccolithophores during that early Pliocene interval of gradual shoaling. Divergence of nannoplankton assemblages between the eastern equatorial Pacific and the Caribbean Sea indicate the final closure of the Panamanian Seaway at 2.76 Ma (Kameo and Sato, 2000). Although a few mammals from South America crossed into North America and vice versa before around 3 Ma, the major Great American Biotic Interchange of vertebrates appeared between 2.7 and 2.6 Ma (Marshall et al., 1982; Webb, 1985; Lundelius et al., 1987; Webb et al., 1995; Webb and Rancy, 1996). These dates are coincident with the glacial- induced sea-level drop during the main intensification of the northern hemisphere ice-sheet growth as start of the Northern Hemisphere Glaciation (NHG) at around 3.0 to 2.5 Ma.

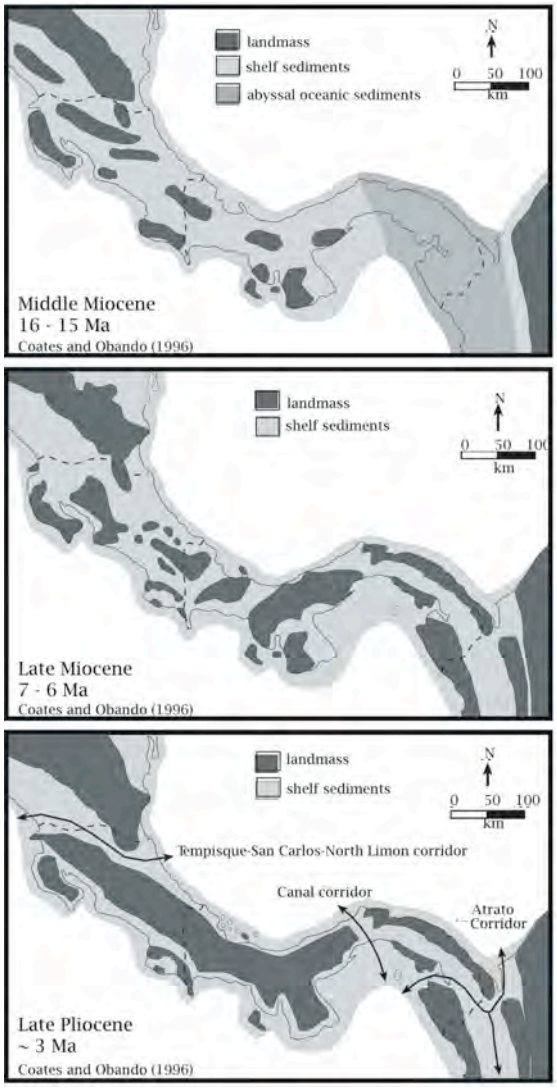

Fig. 1.2.1.1-1 The progressive closure of the Panamanian Seaway. A schematic palaeo-geographic interpretation of the Panamanian Isthmus between 16 to 3 Ma. Modified from Coates and Obando (1996).

Molnar (2008) scrutinised the role of the emerging Isthmus of Panama and its inference to cause, trigger or facilitate the climate change leading to the waxing and waning of ice sheets on the Northern Hemisphere. Other authors also questioned the role of the seaway closure (Dowsett et al., 1992; Mudelsee and Raymo, 2005; Lunt et al., 2008), or even hypothesised that the closure delayed the Ice Age (Berger and Wefer, 1996; Klocker et al., 2005). Contrary, increased central Caribbean surface temperatures and salinities (Groeneveld, 2005) are thought to be a possible trigger or necessary pre-condition for the onset of the NHG (Driscoll and Haug, 1998; Haug and Tiedemann, 1998). The final closure of the Panamanian Seaway is expected to have significantly strengthened the Western Boundary Current, diverted large volumes of warm and salty water northward, and increased the production of North Atlantic Deep Water (NADW) (e.g. Raymo et al., 1989; Maier-Reimer et al., 1990; Bartoli et al., 2005). Enhanced evaporation in the North Atlantic would provide the necessary water vapour to build ice sheets, while increased density of the remaining water would further intensify thermohaline circulation (Tiedemann and Franz, 1997; Haug and Tiedemann, 1998; Meier-Reimer et al., 1990; Nisanciouglu et al., 2003; Prange and Schulze, 2004).

1.2.1.2 Climate and biota

The Neogene cooling trend was superimposed by several punctuated periods of intensive glaciations (Mi-Events) (Miller et al., 1991; Westerhold et al., 2005). The latest Miocene glacial period lasted from 6.26-5.5 Ma (Hodell et al., 2001). Intensifications within this **late Miocene glacial period** (6.26-5.5 Ma) observed by Hodell et al. (2001), consisted of 18 glacial-to-interglacial oscillations that were controlled by the 41-kyr-cycle of obliquity (Hodell et al., 2001). The most prominent glacial stages during that interval were marine isotope stages TG20 at 5.75 Ma and TG12 at 5.51 Ma (Shackleton et al., 1995a; Shackleton and Crowhurst, 1997). This intensification of glaciation is supported by comparison of benthic oxygen isotope records with records of ice-rafted debris (Jansen and Sjoholm, 1991), but concrete estimations of sea-level lowering during that interval are vague and arguable (Aharon et al., 1993; Braga and Martin, 1996).

A negative carbon isotope shift (0.5-1.5 ‰) in marine sediments occurs during the late Miocene chron C3AR termed **Late Miocene Carbon Shift** (Loutit and Kennett, 1979; Keigwin and Shackleton, 1980; Vincent et al., 1980; Keigwin, 1982b; Hodell et al., 2001; Grant and Dickens, 2002) and is dated between 7.6 and 5.0 Ma. The isotope excursion has been observed in benthic and planktonic foraminifers as well as in bulk sediments (e.g. Keigwin, 1979; Vincent et al., 1980; Hodell et al., 1991c; Shackleton and Hall, 1997; Hodell et al., 2001) and has been considered as a globally synchronous chemostratigraphic datum (Loutit and Kennett, 1979; Keigwin and Shackleton, 1980; Loutit and Keigwin, 1982; Loutit et al., 1983). This rapid global change in the $\delta^{13}C$ values marks a major perturbation in the global carbonate budget and has been placed in context with factors like the change in the vegetation type (Cerling et al., 1997) related to increasing seasonality and aridity (Molnar,

2005) and reintroduction of organic carbon from erosion of shelf reservoirs to the oceans driven by regression (Vincent et al., 1980). Increased flux of marine and terrigenous organic matter (Loutit and Keigwin, 1982; Delaney and Boyle, 1987) correlates well with dissolution spikes and enhanced remineralisation of organic matter, what has been observed by several authors (e.g. Müller et al., 1991; Bickert et al., 2004; Diester-Haass et al., 2005). The late Miocene $\delta^{13}C$ shift has also been associated with elevated primary productivity (Bender and Keigwin, 1979; Vincent et al., 1980; Loutit and Keigwin, 1982; Vincent and Berger, 1985; Grant and Dickens, 2002), which provides a mechanism for decreasing benthic foraminiferal $\delta^{13}C$ values, but would not explain the shift in planktonic foraminifers. However, Diester-Haass et al. (2006) found good agreement in the timing of the foraminiferal $\delta^{13}C$ decrease and an increase in marine productivity at several sites from the Indian and Pacific Oceans.

There are two remarkable palaeoceanographic events of drastic variations in the pelagic carbonate deposition known within this time interval of the late Miocene, which are characterized by prominent changes in carbonate accumulation rates between 12 and 5 Ma in all ocean basins (Peterson et al., 1992; e.g. Berger et al., 1993; Mix et al., 2003b). These variations in carbonate accumulation rate are associated with the so called **'Carbonate Crash'** and '**Biogenic Bloom**' intervals (Farrell et al., 1995b; Lyle et al., 1995), which are thought to have been influenced by changes in deep-water circulation and shoaling of the CCD in case of the Carbonate Crash interval (Peterson et al., 1992; Farrell et al., 1995b; Lyle et al., 1995; Roth et al., 2000; Lyle, 2003), or, respectively, by an increase in palaeoproductivity for the Biogenic Bloom period (Dickens and Owen, 1999; Hermoyian and Owen, 2001; Diester-Haass et al., 2004). About 12 to 9 Ma ago, several sharp drops in $CaCO_3$ concentration occurred in equatorial latitudes of the Pacific and Indian Oceans (e.g. Peterson et al., 1992; Berger et al., 1993; Farrell et al., 1995b; Jiang et al., 2007), in the equatorial and south-east Atlantic (King et al., 1997; Krammer et al., 2006), and the Caribbean Sea (Roth et al., 2000). Several hypotheses have been put foreward to explain this crash in carbonate sedimentation. Dilution by non-carbonate sediments (Diester-Haass et al., 2004) or enhanced dissolution associated due to changes in deep-water circulation and shoaling of the CCD and/or lysocline (e.g. Lyle et al., 1995, Farrell et al., 1995; Roth et al., 2000) as well as enhanced dissolution due to increased productivity and decomposition of organic matter (Archer, 1991) have been attributed to this dramatic reduction of $CaCO_3$ in sediments. Jiang et al. (2007), however, pointed to a causative mechanism related to surface-circulation-induced low productivity, thus explaining the carbonate crash not as a dissolution event, but as a consequence of lowered productivity (Jiang et al., 2007). Opposite, the Biogenic Bloom interval between around 8 to 4 Ma, with extraordinary high biogenic accumulation rates, has been described from the Atlantic (Hermoyian and Owen, 2001; Diester-Haass et al., 2004; Diester Haass et al., 2005), Pacific (Farrell et al., 1995b; Lyle et al., 1995; Grant and Dickens, 2002; Lyle, 2003) and Indian Ocean (Peterson et al., 1992; Berger et al., 1993; Dickens and Owen, 1999; Hermoyian and Owen, 2001). Surface water productivity increased significantly

(Peterson et al., 1992; Berger et al., 1993; Delaney and Filippelli, 1994; Dickens and Owen, 1994), implying a fundamental change in global nutrient cycling. This has been supported by several independent proxy-records of enhanced palaeoproductivity (carbonate and biogenic silica MARs, phosphorus, faunal assemblages) and proxies for lower dissolved oxygen at intermediate depth (benthic faunal assemblages, benthic carbon isotopes, manganese fluxes and Mn/Sc ratios). Two possible scenarios could be responsible for the increase in productivity: a global increase in nutrient supply to the oceans related to enhanced continental weathering due to tectonic uplift processes of the Tibetan Plateau (e.g. Filippelli and Delaney, 1994; Farrell et al., 1995a; Hermoyian and Owen, 2001; Gupta et al., 2004), Raymo and Ruddiman, 1992) or Papua New Guinea (Wells et al., 1999), and/or a redistribution of nutrients within the ocean due to circulation changes (basin-basin-fractionation) (Berger et al., 1993; Dickens and Owen, 1994; Dickens and Owen, 1999; Schneider and Schmittner, 2006). Ziegler et al., (2008) revised the relationship between Papua New Guinea tectonism and central equatorial Pacific biogenic sedimentation patterns and postulate large scale interoceanic reorganisations of nutrient inventories related to variability in upstream nutrient utilization as potential causes for the changes in export production. Hermoyian and Owen (2001) however, clearly demonstrated that this event is of global nature and may not be the result of nutrient redistribution between different ocean areas or enhanced upwelling, by detecting the Biogenic Bloom signal in several low-productivity areas. Grant and Dickens (2002), however, pointed out the complexity of the Biogenic Bloom for regional water mass changes and vertical mass structure, an idea also supported by Diester-Haass et al. (2005) who found timing discrepancy of the global extent of the Biogenic Bloom.

The late Miocene is also a time of major vegetation changes. The dramatic **expansion of C4-plants** occurred between 8 to 6 Ma (Hoorn et al., 2000; 1995; Retallack et al., 2002; Cerling et al., 1997, Hodell et al., 1994; Pagani et al., 1999). C4-photosynthezising plants can internally concentrate CO_2 (Hatch-Slack-Cycle) before carbon is fixed by the Calvin Cycle and subsequently avoid energetic costs of photorespiration. Additionally, the ability to increase internal leaf CO_2, decreases the stomatal conductance, what increases water-use efficiency. Thus, C4 plants can survive hot climatic conditions with high irradiance and water stress as well as high minimum temperatures with low pCO_2 levels (Cerling et al., 1997; Fig. 1.2.1.2-1). Thus, C4 grasslands flourished under global cooling, drying and declining atmospheric levels of CO_2 in the late Miocene (Cerling et al., 1997). Since that vegetation change had significant impact on mammal diet, a worldwide faunal change was observed (Cerling et al., 1997) and thus represents a turning point in plant-animal co-evolution (Retallack et al., 2002; Retallack, 2004). C4 plants, which thrive in seasonally dry climates typical of savannas, prevails in cold periods, but C3 plants, which dominate vegetation in humid environments, characterize the warmer periods (Molnar, 2008). Thus, benefiting from conditions where ratios of atmospheric CO_2 to O_2 are low, C4 floras would have been favoured by the early

Miocene. Pagani et al. (1999) concluded that the pCO_2 level was not sufficient to trigger the late Miocene shift in vegetation. Indeed, during late Carboniferous to Permian glaciation, pCO_2 levels were low enough and some plants independently evolved the C4 pathway, which was subsequently lost in Mesozoic when CO_2 levels rose again (Cerling et al., 1997). Pagani et al. (1999) suggest that the development of low-latitude seasonal aridity and changes in growing conditions on a global scale, rather than a decrease in pCO_2 led to the sudden expansion of C4-dominated ecosystems in the late Miocene (Pagani et al., 1999).

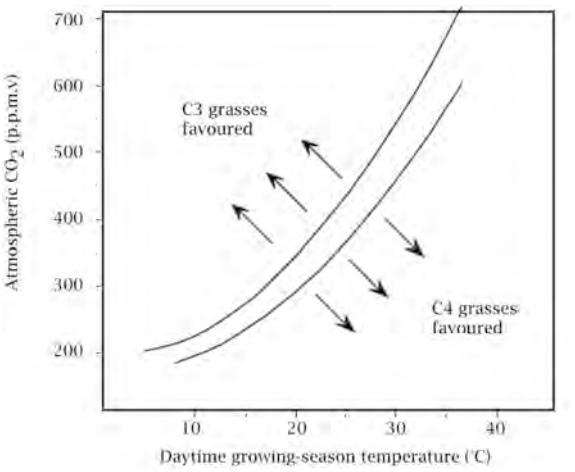

Fig. 1.2.1.2-1 Modelling results for predicting C3/C4 dominance of grasses related to temperature and partial pressure of CO_2. Modified from Cerling et al. (1997).

The ecological response on the decrease in atmospheric CO_2 below the threshold that favoured C3-photosynthesizing plants triggered a change in terrestrial carbon isotopic composition (Cerling et al., 1993). The shift from C3-dominated to C4-dominated ecosystems resulted in a terrestrial $\delta^{13}C$ increase (C3 plants: -22 ‰ (water-stressed/high light conditions) to -35 ‰, C4 plants: -11.4 ‰ to -12.7 ‰ (Cerling et al., 1997)), which is opposite to the observed marine carbon isotope shift (Hodell et al., 1994; see above). Additionally, the floral shift from C3 to C4 pathway was also accompanied by an overall decrease in global biomass (Schlesinger, 1991), which may have caused the marine decrease in $\delta^{13}C$ values during late Miocene (Cerling et al., 1997).

The complexity of forces driving climate change with their control on Earth´s major boundary conditions clearly reveals implications for palaeoceanography and biota. The fundamental role of the oceans indicates the importance of marine biota and their influence on climatic changes. The role of marine biota may thus provide insights into the understanding of climate.

1.2.2 Marine biota and the global biogeochemical cylces

The Earth´s climate has been exposed to major changes over geologic timescales, driven by the complex interaction of several processes like orbital parameters, solar output, tectonic processes, as well as their internal responses and feedback mechanisms. Since a possible greenhouse warming due to increased release of carbon dioxide by combustion of fossil fuels was proposed (‘Keeling-curve’, Keeling et al., 1995; Keeling et al., 1996), the global carbon cycle is one of the most important topics in environmental sciences. Here, the oceans play an important role in atmospheric changes due to their capability to store large amounts of heat and CO_2. The drawdown of atmospheric CO_2 by photosynthesis of marine organisms

and its conversion into organic matter ('biological pump', Berger et al., 1987) counteracts the calcification in the upper layers of the ocean, and its sink and partly storage in the geological archive ('carbonate pump') (Fig. 1.2.2-1).

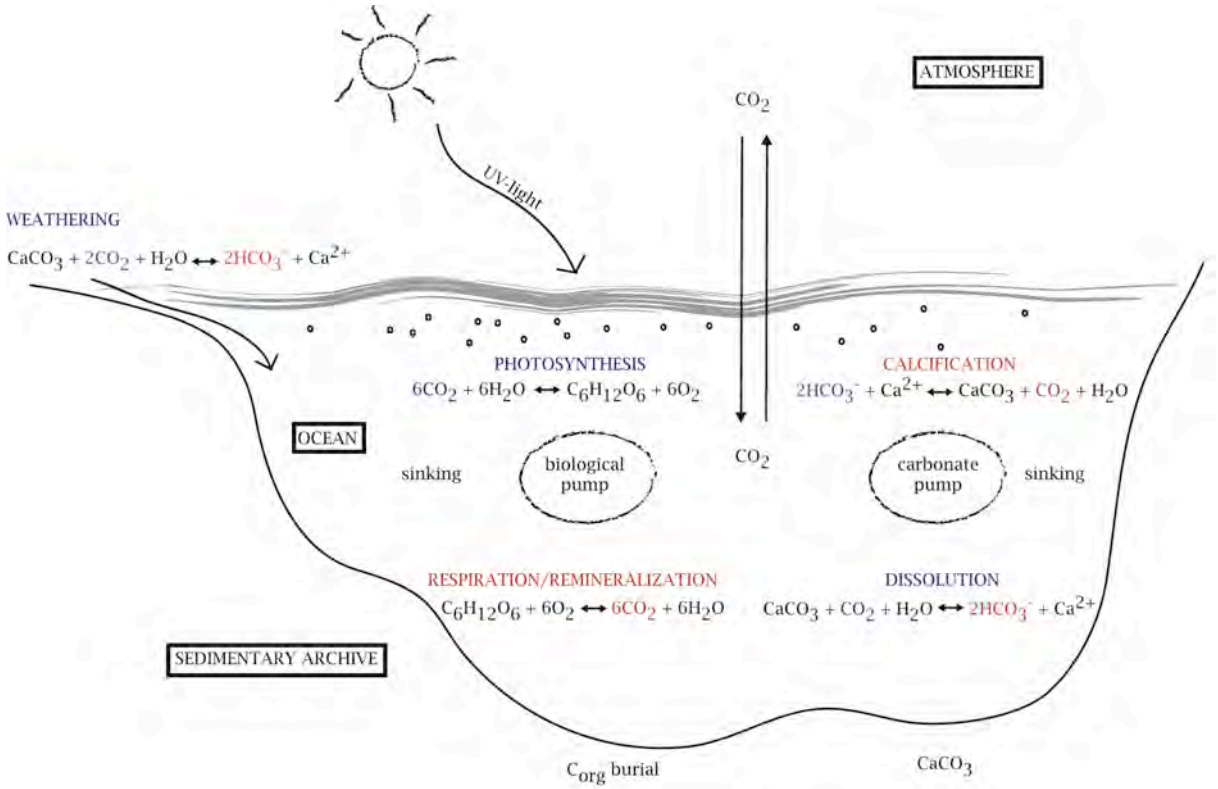

Fig. 1.2.2-1 Schematic representation of the complex role of the oceans and the marine organisms, principally coccolithophores, within the carbon cyle. Modified from Baumann et al. (2004).

Carbonate biomineralisation first occurred around the Precambrian – Cambrian boundary (Wood et al., 2002; Porter, 2007). Next major development took place several hundred million years later, with the Mesozoic proliferation of planktic calcifiers (Roth, 1987; Martin, 1995) and the establishment of the modern mode of carbonate cycling. Although benthic foraminifers and other bottom-dwelling calcifiers evolved early in the Phanerozoic, it was not until the Mesozoic that a marked proliferation in coccolithophorid and planktic foraminiferal diversity and abundance is observed (Martin, 1995; Hart, 2003). The first occurrence of nannofossil-generated pelagic carbonates is recorded at the Jurassic/Cretaceous boundary, based on a switch from radiolaria-dominated siliceous sediments to nannofossil-dominated carbonates in the western Tethys (Baumgartner, 1987). Several major evolutionary steps in the development of calcareous plankton have led to further changes in the carbon cycle, favouring the deep sea as a site of carbonate deposition (Roth, 1987; Hay, 2004). The shift of carbonate sedimentation from shallow shelves to the deep sea, with its creation of a responsive deep-sea sedimentary sink of $CaCO_3$, had major impact on the global carbon cycle and stability of Earth´s climate (Ridgwell and Zeebe,

2005). This Mesozoic shift affected deep-ocean carbonate budgets, calcite compensation depths, and geological carbonate turnover rates (Kennett, 1982; Bown et al., 1998).

Following these evolutionary modes of the marine carbonate cycle, Zeebe and Westbroek (2003) conceptualised three distinct models of carbonate saturation states of the ocean: (A) The geochemical-ruled Precambrian $CaCO_3$ cycle resembles a carbonate ocean, in which biogenic precipitation of $CaCO_3$ is essentially absent ('Strangelove'-ocean). It is characterized by high-supersaturation and generally inorganic formation of carbonates. (B) Following the appearance of biomineralisation in the Cambrian, biologically controlled carbonate precipitation in shallow-water environments became significant ('Neritan' ocean). (C) The Mesozoic shift towards widespread pelagic biomineralisation finally led to a significant stabilization of the marine $CaCO_3$ saturation state ('Cretan' ocean). In this 'Cretan' ocean, the $CaCO_3$ production is entirely biologically controlled and to a large degree independent of the external supersaturation. In this model $CaCO_3$ production occurs in the open ocean.

Although $CaCO_3$ precipitation may also occur as cements and coatings in the marine environment, it is primarily associated with the biomineralisation of living organisms, such as corals, benthic algae and shelly animals, and plankton species. Here, coccolithophores and planktonic foraminifers form the largest part of the pelagic carbonate production, with lesser contributions by pteropods and calcareous dinoflagellates (Milliman, 1993).

Coccolithophores play an exceptional role in the global climate system, since they significantly influence biogeochemical cycles in several ways. The following chapter addresses these remarkable marine organisms.

1.2.3 Coccolithophores

Coccolithophores are a major group of marine, unicellular phytoplankton. They have great potential as palaeoceanographic tool since they hold a unique role in the global carbon cycle because of their combined effect on both the organic carbon and the carbonate pump (Bown and Young, 1998; Baumann et al., 2004; Baumann et al., 2005; Fig. 1.2.2-1). Due to their great abundances, fast turnover rates, and their capability to carry out photosynthesis and calcification, these haptophyte algae are significant components of the Earth's biogeochemical cycles (Bown and Young, 1998). As main open-ocean primary producers, coccolithophores strongly influence marine pelagic biogeochemistry and the marine ecosystem (Winter and Siesser, 1994; Bown et al., 1998). Their minute external calcite scales, the coccoliths, consitute the single most important component of deep-sea sediments. From a quantitative point of view, coccolithophores are the most important pelagic calcifying organisms in the modern ocean (Baumann et al., 2004; Bown et al., 2004; Hay, 2004; Rost and Riebesell, 2004). Together with planktonic foraminifers, they produce the largest reservoir of carbonate rocks. Estimations on the relative contribution of different calcifying organisms to the global pelagic marine carbonate production suggest, that about 20-60 % is provided by coccoliths (Milliman, 1993; Steinmetz, 1994; Baumann et al., 2004; Schiebel et

al., 2004). Sediment-trap studies proved the relation between primary production and particle flux out of the eutrophic zone (e.g. Steinmetz 1994 and references therein). Hence estimates of the volume of extant coccoliths (Honjo, 1976; Samtleben and Bickert, 1990; Steinmetz, 1991; Beaufort and Heussner, 1999; Young and Ziveri, 2000) allow the conversion of coccolith fluxes into carbonate fluxes. These estimates are mostly used in sediment-trap studies (e.g. Knappertsbusch and Brummer, 1995; Ziveri et al., 1995; Broerse et al., 2000; Sprengel et al., 2002) but are also reliable for sediment records (e.g. Tremolada and Young, 2002; Boeckel and Baumann, 2004). As for most primary producers, coccolithophorid distribution is controlled by several parameters (Winter et al., 1994), like nutrient availability and temperature, which themselves are linked to the large-scale feature of oceanic circulation (Bown and Young, 1998). Thus, biogeographic distribution patterns of calcareous nannoplankton assemblages are commonly used to infer surface water patterns as temperature conditions and circulation patterns as well as productivity gradients (Brummer and van Eijden, 1992; Kinkel et al., 2000), since their remains in sediments reflect the physical and chemical characteristic of overlying surface water masses (Roth, 1994). The effort to understand the behaviour of taxa related to limiting factors as sea-surface temperature or nutrient distribution was improved by several workers (e.g. McIntyre and Bé, 1967; Okada and McIntyre, 1977; Lohmann and Carlson, 1981; Chepstow-Lusty et al., 1989; Molfino and McIntyre, 1990; Young, 1994; Beaufort et al., 2001; Flores et al., 2005). Calcareous nannoplankton arguably provides the most complete record of biodiversity of any group of organisms (Bown et al., 2004). Detailed morphometric studies of coccoliths in fossil records have improved biostratigraphic resolution (Backman and Hermelin, 1986; Colmenero-Hidalgo et al., 2002; Hagino and Okada, 2006), exposed evolutionary trends (Young, 1990; Bollmann, 1997; Raffi et al., 1998; Knappertsbusch, 2000) and have shown its good potential use in palaeoceanographic proxy studies (Henderiks and Renaud, 2004; Mattioli et al., 2004). Because of additional optical (albedo), biochemical (DMS) and ballasting effects (see chapter 1.2.3.4), they are likely to produce extra feedbacks to climate change (Charlson et al., 1987; Westbroek et al., 1993). Thus, besides their biostratigraphic importance, the exceptional fossil record of coccolithophores preserves remarkable signals for interpreting global change in the geological record.

1.2.3.1 Fossil record

Calcareous nannofossils first occur in the fossil record in Late Triassic sediments. First nannoliths and calcareous dinoflagellates were documented from the Carnian (225 Ma; Bown et al., 2004), coccoliths are present from the Norian (220 Ma; Di Nocera and Scandone, 1977; Jafar, 1983; Bralower et al., 1991; Bown et al. 1998) as abundant but low-diversity assemblages (maximum 5 species). These first taxa were very small (2 to 3 µm) and apparently restricted to low latitudes (Bown 1998, Bown et al., 2004). There is evidence, that 80 % of Late Triassic calcareous nannofossil species did not survived the mass extinction

event at the Triassic/Jurassic boundary, but coccolithophores re-established again and became dominant forms in Jurassic to Cretaceous marine realms (Bown, 1998). Most major coccolithophorid families were established during the Early Jurassic radiation (Fig. 1.2.3.1-2). Their diversity (Fig. 1.2.3.1-1) increased throughout the Mesozoic and reached a diversity peak in the Late Cretaceous. Calcareous nannoplankton underwent fatal diversity loss at the Cretaceous/Paleogene boundary, but recovered rapidly in the early Palaeocene from a small number of survivor species (Bown, 2005), reaching a second diversity peak in the Mid-Eocene. The Paleocene radiation was more rapid and more diverse than the Mesozoic one (Fig. 1.2.3.1-2), resulting in the establishment of significantly different coccolithophorid families. After a decline in the Oligocene, coccolithophores diversity increased in the Miocene, but suffered a diversity loss during the past 5 Ma (Fig. 1.2.3.1-1). This Pliocene diversity decline is distinguished by extinction of species that dominated primary productivity throughout the entire Neogene, reticulofenestrids, *Sphenolithus* and *Discoaster*, but also a radiation of few eutrophic forms, *Pseudoemiliania* and *Gephyrocapsa*.

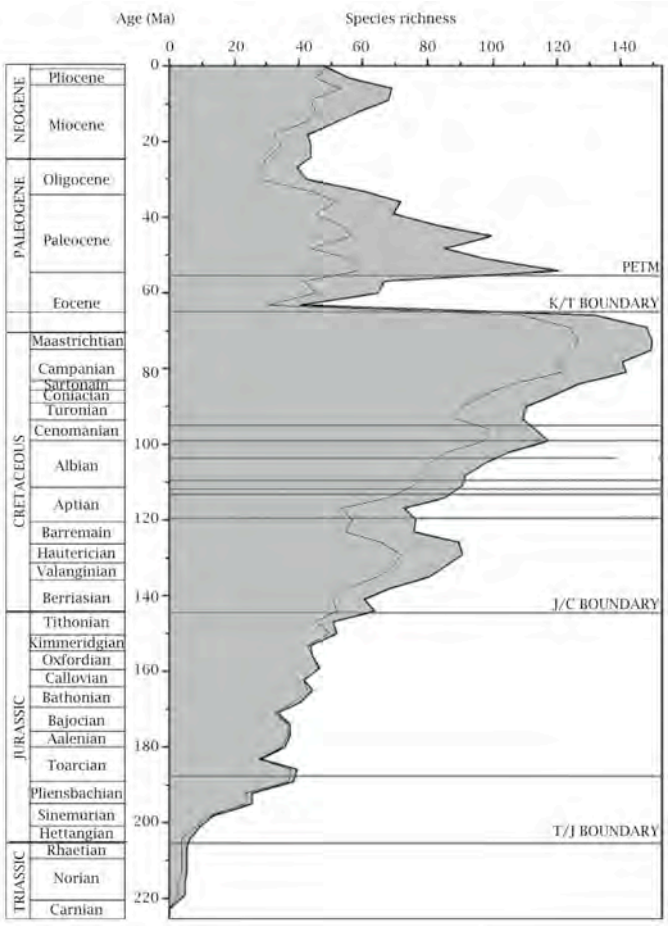

Fig. 1.2.3.1-1 Species richness of coccolithophores (light line) and total nannofossil diversity (dark line), from Bown et al. (2004).

1.2.3.2 Biology, biogeography, ecology and evolution

Coccolithophores are minute (< 20 µm) marine unicellular flagellate algae belonging to the class Prymnesiophyceae (Hibberd, 1976) of the division Haptophyta (Edvardsen et al., 2000) (Taxonomic notes given in Appendix A2). They are characterized by possessing two smooth flagella and a third flagellum-like organelle, the haptonema, as well as golden-brown chloroplasts.

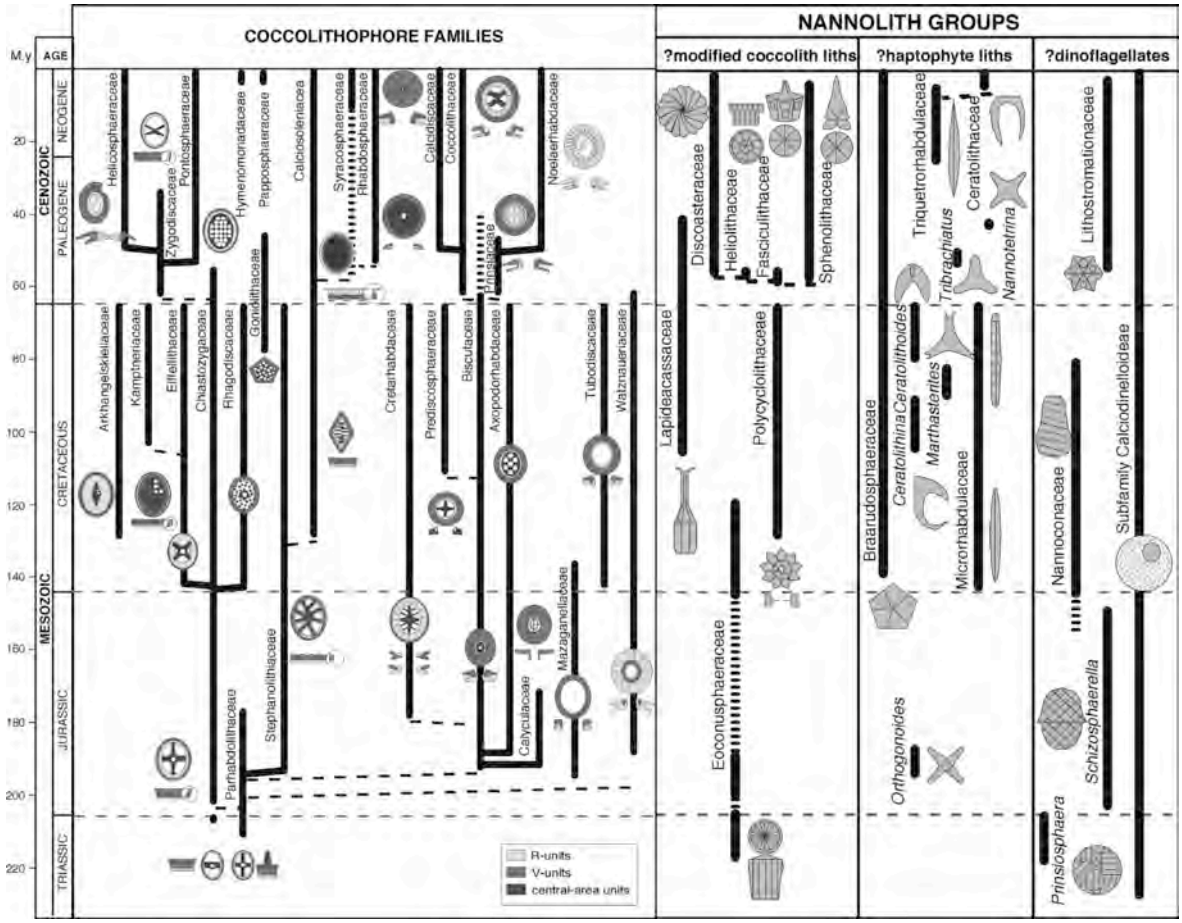

Fig. 1.2.3.1-2 Phylogenetic model for calcareous nannofossils, from Bown et al. (2004).

Coccolithophores have a diplo-haplontic life-cycle (Fig. 1.2.3.2-1), with the haploid and diploid phase being independently capable of photosynthesis and asexual binary reproduction (Pienaar, 1994). The life cycle phases are characterised by distinct biomineralisation modes. They produce different types of highly characteristic calcified scales, heterococcoliths (diploid stage) and holococcoliths (haploid stage), or occasionally nannoliths (Geisen et al., 2002). Coccoliths can be monomorphic (e.g. *Coccolithus*), dimorphic (e.g. *Scyphosphaera*) or polymorphic (e.g. *Syracosphaera pulchra*) as well as variomorphic (e.g. *Helicosphaera*) with one (e.g. *Scyphosphaera*) or more (e.g. *Emiliania*, *Florisphaera*) discrete layers of liths. Some species are known to calcify only in the diploid phase (*Emiliania*, *Pleurochrysis*), in some others (Family Noelaerhabdaceae), diploid, non-motile heterococcolith-bearing cells (C-cells) alternate with haploid, motile organic-scale bearing cells (S-cells) during life-cycle, where also non-motile naked cells (N-cells) appear as mutant diploid stage (Billard and Inouye, 2004). There are also life cycles described involving heterococcolithophores and stages with aragonitic coccoliths (*Alisphaera*, Manton and Oates, 1980), as well as combination of nannoliths/holococcoliths with heterococcoliths linked to complex life cycles (Cros et al., 2000).

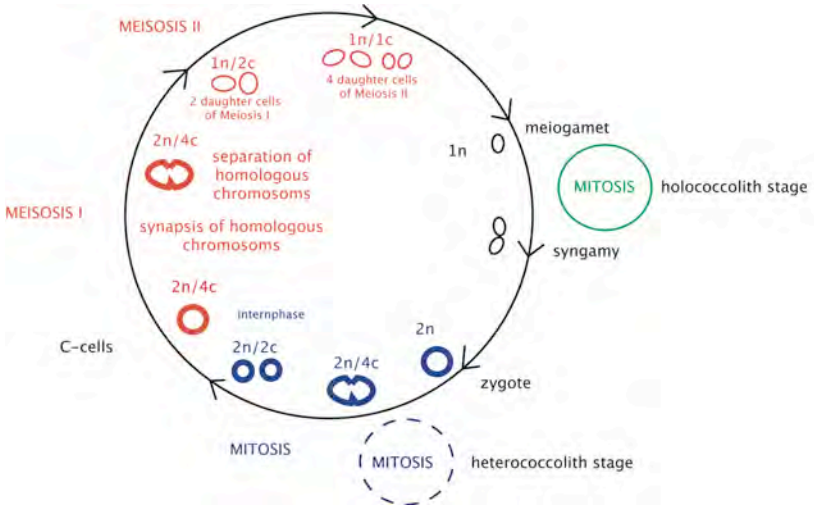

Fig. 1.2.3.2-1 Schematic representation of coccolithophorid basic life cycle. Both, haploid and diploid phases are chloroplast-bearing and can reproduce indefinitely by asexual binary fission (small mitosis circles). Both phases can calcify producing hetero- (diploid, thick lines) and holo- (haploid, thin lines) coccoliths respectively.

Coccolithophores live in the photic zone where light levels are sufficient to carry out photosynthesis. Additionally, their horizontal and vertical distribution is controlled by latitude, ocean currents, water masses and their nutrient requirements, salinity and temperature profiles, light energy regimes, trace elements and vitamins (Brand, 1994; Winter et al., 1994; Bown and Young, 1998).

Modern coccolithophores generally show a widespread oceanic distribution within the photic zone, with highest diversities at low latitudes. They constitute the most significant phytoplankton group in warm, stable and relatively low nutrient domains where they often display high biodiversity (Jordan and Winter, 2000; Winter et al., 2002; Young, 2003), but numbers of species have very broad ecological tolerances. So, *E. huxleyi* offers a wide temperature and salinity range between 1 to 31˚C (McIntyre et al., 1970; Brand, 1994) and 11 to 41 psu (Hay and Honjo 1989; Winter et al., 1994). Also, one freshwater form has been documented (see Bown, 1998). Modern biogeographic distribution resulted in a first biogeographic zonation scheme by McIntyre and Bé (1967) due to certain temperature dependences of coccolithophores. The distribution of coccolithophores follows broad latitudinal belts or zones basically separated by frontal systems (see Winter et al., 1994, Table 1 and Fig. 3). These zonal boundaries are highly dynamic, seasonally variable and characterized by a specific assemblage. Additionally, coccolithophore communities show limited vertical stratification, presented by a distinctive lower photic zone assemblage (*Florisphaera profunda*, *Gladiolithus flabellatus*) occurring in or below the thermo-nutricline, and utilizing the less competitive low-light - low-temperature - high-nutrient niche (see Winter et al., 1994, Table 2 and Fig. 4). Typically, phytoplankton communities are dominated by small cells under oligotrophic conditions (e.g. oceanic gyres), whereas larger phytoplankton cells are more abundant at continental margins and in upwelling zones, where nutrient concentrations tend to be higher and more variable (Chisholm, 1991). The

particular environments are dominated by characteristic assemblages, which can be distinguished by their coccolith types and coccosphere morphology (Young, 1994). Young (1994) divided the coccolithophores into different groups according to ecological and morphological criteria (Fig. 1.2.3.2-2):

A) Placolith bearing r-selective opportunistic species adapted to exploit variable eutrophic conditions. These are highly productive species found in upwelling areas (equatorial divergence and coastal upwelling) and in the temperate regions. They include *Emiliania huxlei*, *Gephyrocapsa* spp., *Reticulofenestra* spp., and *Umbilicosphaera* spp., with coccoliths composed of a proximal and a distal shield joined by a central area.

B) Umbelliform K-selective specialised species adapted to stable oligotrophic conditions. These are low-productive species found in the upper 100 m of the subtropical ocean gyres (10-30° latitude), composed of *Umbellosphaera* spp. and *Discosphaera tubifera*, with distally flaring coccoliths.

C) Floriform deep dwelling species, low-light adapted, and highly productive; possibly r-selective. They mainly characterize the lower photic zone assemblage with *Florisphaera profunda* or *Gladiolithus flabellatus* in a stable water column of low- to mid latitudes. Their dense asymmetrical mass of liths surrounds the much smaller cell.

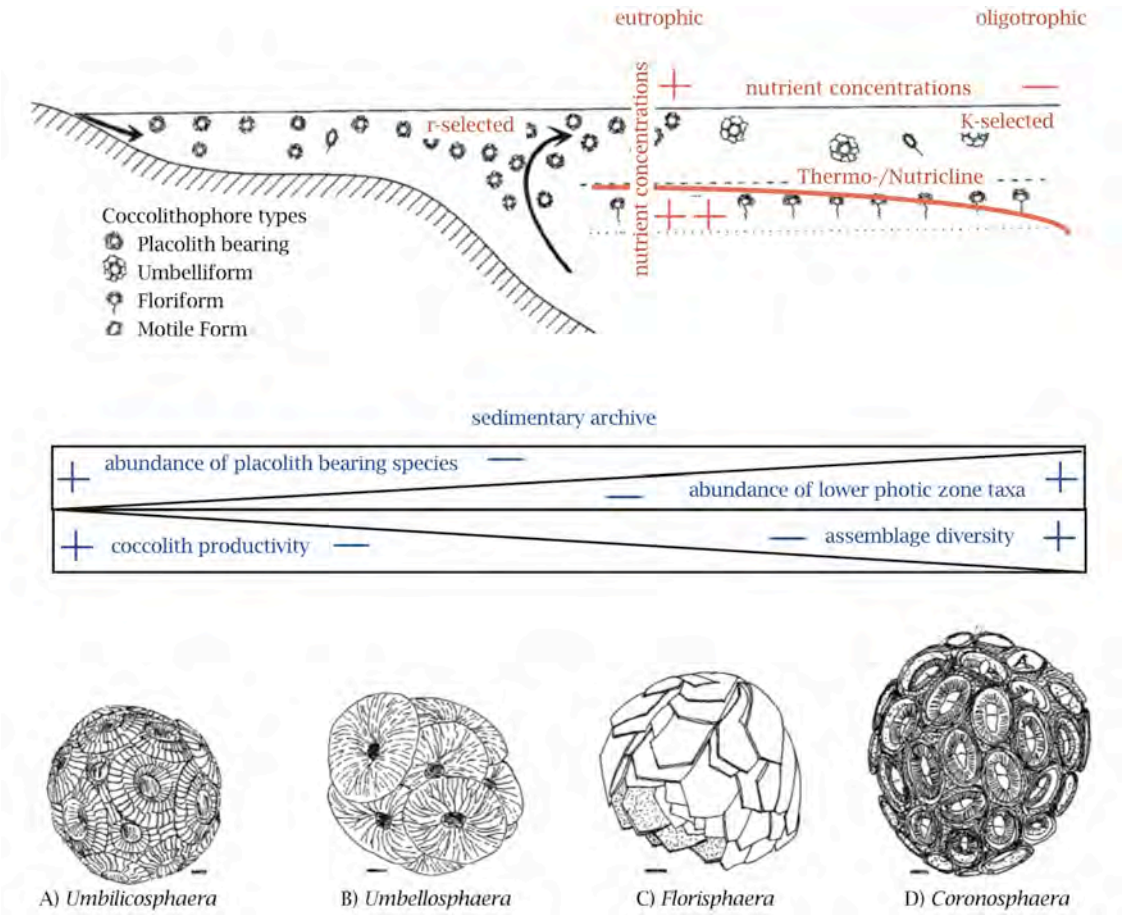

Fig. 1.2.3.2-2 Model of ecological distribution of coccolithophore types and their response to changing surface water nutrient concentrations and its sedimentary outcome. Cartoon to illustrate different communities discussed in the text: A) Placolith dominated, B) Umbelliform dominated, C) Floriform dominated, D) Motile species. Modified from Young (1994) and Kinkel et al. (2000).

The modern diversity of coccolithophores distinguishes into 180 species (Jordan and Kleijne, 1994; Billard and Inouye, 2004) based on morphological criteria. This number of morpho-species is certainly overestimated, because most, if not all, coccolithophores display complex haploid life cycles (see above) with the expression of 2 or even 3 radically different coccoliths during the different stages (Geisen et al., 2002). Numbers of classically determined 'morpho-species' are in fact monophyletic clusters of a sibling, biological species, separated by subtle morphological characters (De Vargas et al., 2004). Based on presence of these (pseudo-) cryptic sibling species, De Vargas et al. (2004) introduced the concept of super-species. These are assemblages of allopatric (geographical or temporal) species of monophyletic origin, which often show distinct morphological differences (de Vargas et al., 2004). Thus, the habitat segregation of these morphotypes indicates that the global distributions observed for these major taxa are mixtures of several discrete subspecies (Ziveri et al., 2004; Hagino and Okada, 2006), which may be composed of two or more genotypically discrete species (or sub-species) with often subtle morphological differences but rather strong ecological differences. Thus, body size is a central feature, as it reflects the evolutionary history, physiology and ecology of marine micro-organisms (e.g. Schmidt et al., 2006). Hence, size changes can influence global biogeochemical cycles and have implications for efficiency contributed to deposition of deep-sea carbonates. Also, cell geometry has substantial influence on fractionation of stable isotopes in both coccolith carbonate (biocalcification) (Ziveri et al., 2003) and haptophyte organic compounds (photosynthesis) (Popp et al., 1998) that are used in palaeoceanographic reconstructions (e.g. Pagani et al., 2005).

1.2.3.3 Biomineralisation and function of coccoliths

Besides purely organic scales, distinct features of coccolithophores are their coccoliths, built of calcium carbonate in association with an organic matrix. In general, two major, morphologically distinct types of coccoliths can be distinguished, heterococcoliths and holococcoliths. They are characterized by their mode of formation and the stage within the life cycle during which they are produced (Bown, 1998). Heterococcoliths are formed of a radial array of interlocked, complex crystal units of variable shape whereas holococcoliths are formed of numerous minute (< 0.1 µm) identical, non-interlocked, euhedral crystallites (Young et al., 1992). Calcification of heterococcoliths takes place intracellularly and is consequently under strong cellular control (Westbroek et al., 1989; Young et al., 1992; Pienaar, 1994). In contrast, biomineralisation of holococcoliths apparently occurs outside the cell membrane (Rawson et al., 1986). Information on holococcoliths biomineralisation is scarce because forms are extremely small in size and culture observations are limited. Heterococcolith formation on the other hand has been extensively studied, especially in *Emiliania huxleyi* and *Pleurochrysis* (Westbroeck et al., 1993; Pienaar, 1994). Calcite precipitation of heterococcoliths takes place inside a special vascular system derived from

the Golgi body (details given in Fig. 1.2.3.3-1)(Westbroek et al., 1984; Young et al., 1999) and is thus isolated from the surrounding water as well as from other cellular processes. Initiation is the buildup of an organic scale, called base-plate. Nucleation of calcite crystallites is located on the rim and gives rise to a ring of simple rhomb-shaped crystals, the proto-coccolith ring (Fig. 1.2.3.3-2). A distinct feature of heterococcolith formation is the V/R model of nucleation, where crystals have approximately radial (R-units) and vertical (V-units) c-axis orientations. The coccolith is transported to cell surface and extruded via exocytosis to finally become part of the coccosphere. Regulation of crystal growth is a result of interaction between inorganic and organic systems. Simple calcite crystals are heavily modified as compared to the regular inorganic form. The final shape of the coccoliths is thus the result of biologically controlled biomineralisation processes within the vesicle (Young and Henriksen, 2003). Still, the functions of calcification in relation to photosynthesis and nutrient acquisition are still debated (Brownlee and Taylor, 2004). Calcification may enhance the biogeochemical efficiency of the cell, since a possible coupling between production of carbon dioxide from the calcification process and utilization during photosynthesis may be of energetic advantage (Nimer et al., 1992; Sikes and Fabry, 1994; Nimer and Merrett, 1995). For the functional use of coccoliths for

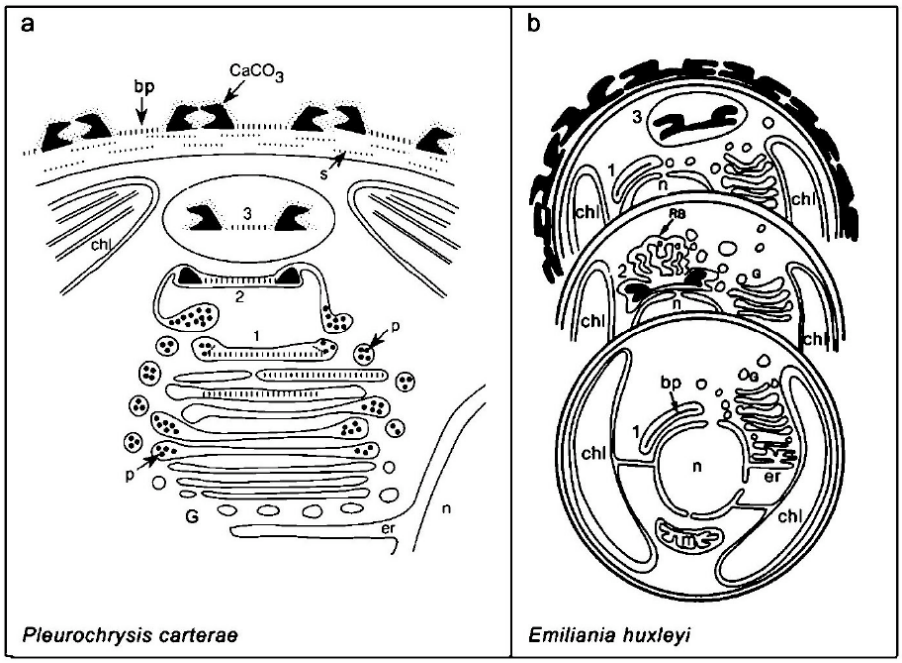

Fig. 1.2.3.3-1 Intracellular pathway of coccolith formation in (a) *P. carterae* and (b) *E. huxleyi*. Coccolith vesicle is shown (1) before, (2) during and (3) after mineral deposition. Polysaccharide and calcium containing particles (p), reticular body (RB), base plate (bp), chloroplast (chl), Golgi stacks (G), endoplasmatic reticulum (er), nuclei (n), mitochondrion (m), unmineralized scales (s). From Langer (2005), reproduced from Marsh (2003).

Fig. 1.2.3.3-2 Potential proto-coccolith rim on reticulofenestrid coccosphere of late Miocene Site 1241.

coccolithophores no definite explanation has been found so far (Young, 1994). Although coccolithophores are grazed and ingested by copepods and other zooplankton with no distinction between a coccolith-bearing and a naked cell, size and calcification may still be adaptive for lowering ingestion by other organisms (Njestgaard et al., 1996), or as protection of the delicate wall from mechanical damage, microbial or chemical attack (Young, 1994). Coccoliths may also be able to regulate reflection of light into the cell allowing life in the lower photic zone, or, reversed, allowing life in the photic zone. This additionally alters the albedo of the surface ocean, increases the temperatures in surface waters (Holligan, 1991) and makes coccolithophorid blooms visible to satellite sensors.

The understanding of biomineralisation patterns and processes improves the ability to interpret the geochemical signal preserved within coccoliths.

1.2.3.4 Biogeochemical impact of coccolithophores

Coccolithophores may be small in size, but they occur in huge numbers in the surface layers of the oceans, sometimes forming blooms with cell densities larger than a million cells per liter. The high reflectance of large blooms (traceable even from satellites) significantly alters the ocean´s albedo. The balance, that distinguishes if coccolithophores, and especially the large blooms they form, act as a source or sink for atmospheric CO_2 is the ratio between calcification and photosynthesis (Van der Wal et al., 1995; Buitenhuis et al., 1999). The assumption, that calcification is a source for CO_2 is based on equations for inorganic carbonate precipitation (see Fig. 1.2.2-1), but this might not be the case for coccolithophores. Since calcification and photosynthesis occur intracellularly in coccolithophores, a possible coupling between production of carbon dioxide from the calcification process and utilization during photosynthesis may be of energetic advantage (Nimer et al., 1992; Sikes and Fabry, 1994; Nimer and Merrett, 1995). It seems possible, that coccolithophores possess the ability to supply their own CO_2 for photosynthesis via calcification. However, studies have shown that general phytoplankton growth can be limited by the availability of dissolved CO_2 in seawater (Raven, 1993; Riebesell et al., 1993). This effect especially controls organic and siliceous phytoplankton but coccolithophores may counteract this limitation by producing their own CO_2 via bicarbonate consumption during calcification (Buitenhuis et al., 1999). Nimer et al. (1997) have shown in culture studies, that coccolithophores only use their intracellular CO_2 source under very limiting CO_2 conditions. In contrast, Rost and Riebesell (2004) have revealed that calcification in coccolithophores is not a prerequisite for efficient photosynthesis. Non-calcifying cells can photosynthesise as efficiently as, or even more efficiently than calcifying ones (Rost and Riebesell, 2004). Measurements of stable carbon isotope discrimination also indicate that *Emiliania huxleyi* can accumulate inorganic carbon, but that calcification is not used directly to supply photosynthesis with carbon (Rost et al., 2002).

Marine biota act as a carbon pump by producing particulate and dissolved organic matter, which is then exported to deeper layers in the ocean where it is respired to inorganic nutrients (Siegenthaler and Sarmiento, 1993) and redistributed in the water column. The remaining fraction reaches the sediment. Here, sinking particles are the major pathway for transport of particulate organic carbon (POC) from the surface to the ocean interior and sediments (McCave, 1975; Honjo, 1996). Besides marine snow or fecal pellets (e.g. Suess, 1980), mineral ballast (silicate and carbonate minerals and lithogenic material) is the major constituent of sinking particles (Klaas and Archer, 2002), often comprising more than half the mass of particles leaving the surface (Honjo, 1996). Being denser than either seawater or typical organic matter, these minerals normally provide a large part of the density differential needed to allow these particles to sink (McCave, 1975, Honjo, 1996). Armstrong et al. (2002) implicated from the 'ballast' model, that organic carbon sinking fluxes correlate tightly with material fluxes. The ballast thus either increases the sinking speed of the adherent POC (Honjo, 1996), or it could provide some physical protection from degradation (Klaas and Archer, 2002). Geographical differences in POC-fraction (Armstrong et al., 2002) led Klaas and Archer (2002) to synthesise data of a global long-term sediment trap study to document the relationship between different forms of mineral ballast. They proposed that most of the organic carbon rain in the deep sea (up to 83 %) is carried by calcium carbonate. It is more abundant than terrigenous material, and, since calcium carbonate is the densest of marine components (Honjo, 1996), the carrying coefficient (i.e. the mineral-associated organic carbon fraction (Klaas and Archer, 2002)) of calcium carbonate is three times higher than that for opal (Klaas and Archer, 2002). This theory of major 'ballasting' of organic carbon carried by calcium carbonate highlights the role of coccolithophores as trigger of POC-sink and -storage in sediment, due to their exceptional position within the carbon cycle. Their combined effect on the oceanic pumps of organic carbon and carbonate (Fig. 1.2.2-1) together with the 'ballast' model (Fig. 1.2.3.4-1) strengthens the position of coccolithophores as major impact on the surface ocean CO_2 balance. Besides the biological and the carbon pump, a third major process has been proposed by which coccolithophores may influence the global climate system over time: A large-scale albedo effect may be linked to the release of dimethylsulfoniopropionate (DMSP) produced by coccolithophores. This is a metabolite, which is extracellularly reduced and converted by enzymatic activity to dimethylsulfide (DMS). DMS is a crucial component in global climate regulation, and the most abundant biological sulfur compound emitted to the atmosphere (Simpson et al., 1999). Its oxidation product, sulphuric acid, has potential to create aerosols, which act as cloud condensation nuclei. Through this interaction with cloud formation and linkage to acid rain (Fig. 1.2.3.4-1), the massive production of atmospheric DMS over the oceans may have a significant impact on the Earth's climate (Malin et al., 1992). Therefore, coccolithophores and cloud formation seem to be linked, in particular when a lot of DMS is released over a coccolithophorid bloom area (Westbroek et al., 1993).

Dimethylsulfoniopropionate is additionally thought to have a toxic effect on zooplankton (Wolfe et al., 1997) which might turn predatory grazers to convert to another food source, e.g. diatoms, instead of DMSP producing coccolithophores (Njestgaard et al., 1996).

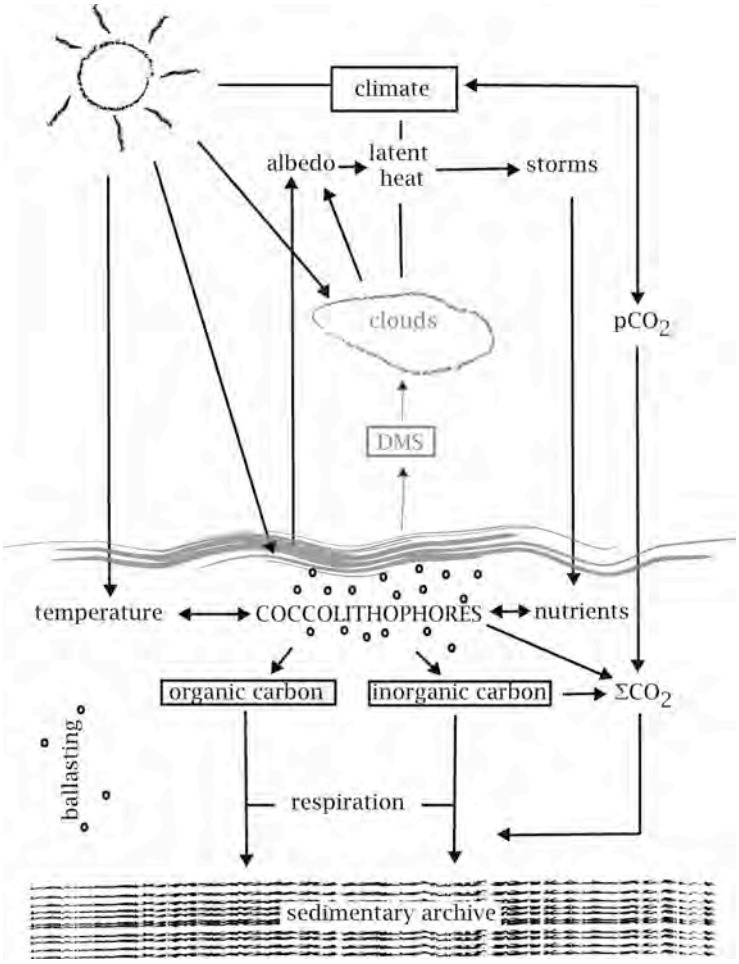

Fig. 1.2.3.4-1 Model of the biogeochemical impact of a coccolithophorid bloom on the carbon and carbonate cycle and its possible feedback on the climate system. Modified from Westbroeck (1995).

1.2.3.5 Coccolith-based geochemical proxies

Calcareous nannoplankton has been used as a tool in studies of global climate change, though advantages in its application have been slow, with most palaeoceanographic investigations concentrating on data from foraminifers. Use of coccoliths was initially confined to biostratigraphy and ecological studies, even they provide an exceptional tool for reconstruction of past oceanographic, environmental, and biological conditions and possess certain unique advantages over foraminifers. Both, the organic and inorganic remains of coccolithophores in sediments provide proxies for palaeoceanographic and thus palaeoclimatic patterns. Dependence of incorporation of trace elements and stable isotopes into biogenic calcium carbonate has been recognized for decades. The isotopic compostition and the trace metal to calcium ratio of biogenic calcium carbonate were therefore used to reconstruct environmental parameters. Coccolith carbonate is used to receive indicators from the elemental chemistry (Sr/Ca, Mg/Ca). It has been shown, that elemental chemistry of **Sr/Ca** of coccolith calcite can provide a useful proxy for coccolithophorid productivity as well as growth rates (Stoll and Schrag, 2000; Stoll and Ziveri, 2004). The strong temperature dependence of Mg incorporation in calcite is increasingly used for palaeothermometry on foraminifers following initial work of Nürnberg et al. (1996). But due to methodological problems in measuring **Mg/Ca**-ratios and their much lower Mg content (compared to foraminifers), the alkenone undersaturation ratio of **alkenone biomarkers** (U_{37}^{K}) of coccolithophores is the more common, reliable index for temperature reconstructions (e.g. Brassell et al., 1986; Prahl et al., 2000). These haptophyte

molecular organic markers in form of long-chain alkenons and their molecular distribution and carbon isotopic composition are widely used as a tool in palaeoceanography and palaeoclimatology (e.g. Laws et al., 2001; Schneider, 2001). Besides the application of the alkenone $U_{37}^{K'}$ index for estimation of palaeotemperatures, their carbon isotopic fractionation ($\varepsilon_{alkenone}$) is utilised to reconstruct past atmospheric CO_2 concentrations (e.g. Jasper and Hayes, 1990; Pagani et al., 1999). Stable isotopic measurements in biogenic calcite are a key tool for palaeoceanographic studies. For all marine carbonates, the **stable oxygen isotope** ratio depends on temperature and salinity conditions at which the carbonate precipitates as well as the isotopic composition of the seawater from which it forms. Primary ice-volume control on benthic oxygen isotope records has led to their use in the approximation of past sea-level variations (Cooke and Rohling, 2001). The **stable carbon isotope** ratio largely reflects the carbon isotopic composition of dissolved inorganic carbon (DIC) in the ocean, and is used in studying water mass movements and palaeoproductivity (Cooke and Rohling, 2001).

Oxygen isotopic variations of polyspecific coccolith-dominated sediment fine-fractions was found to co-vary with those measured in planktonic foraminifers (Margolis et al., 1975; Anderson and Steinmetz, 1981; Dudley and Nelson, 1989; Paull and Thierstein, 1990; Dudley and Nelson, 1994), but shows significant offsets from equilibrium (Anderson and Cole, 1975; Dudley and Goodney, 1979; Dudley et al., 1980). Culture experiments show that oxygen isotope fractionation of coccolithophores correlates with temperature (Dudley et al., 1986) and that this apparent temperature effect is not caused by underlying growth rate changes (Ziveri et al., 2003). The especially wide range of so called 'vital effects' in oxygen isotopic composition (Dudley et al., 1986; Ziveri et al., 2003) may hamper the application of bulk fine-fraction $\delta^{18}O$ over major paleoceanographic events where there is significant change in the nannofossil assemblage (Bralower, 2002). However, Ziveri et al. (2003) provided species-specific correction factors for oxygen and carbon vital effects in coccoliths. Techniques were developed to separate quasi-monospecific coccolith fractions from bulk sediment (Minoletti et al., 2001; Stoll and Ziveri, 2002). These methods might be the best approach to use the unique advantage of coccoliths for standard applications in palaeoceanography. Improvements of this are presented in chapter 8.2.2.

CHAPTER 2 METHODS

2.1 Sample processing

The original samples were splitted into a main sample and an archive sample. An additional series of samples was used for stable isotope analyses of foraminifers. Individual steps of sample processing are summarized in Fig. 2.1-1.

A list of all samples is given in Appendix A3-1. Samples are labelled with 'BB' for the Biogenic Bloom Interval and 'FC' for the Final Closure Interval. 'P' indicates samples from Pacific Site 1241 and 'C' specifies samples from Caribbean Site 1000. This results in sample codes 'BBP' and 'BBC', or 'FCP' and 'FCC', respectively.

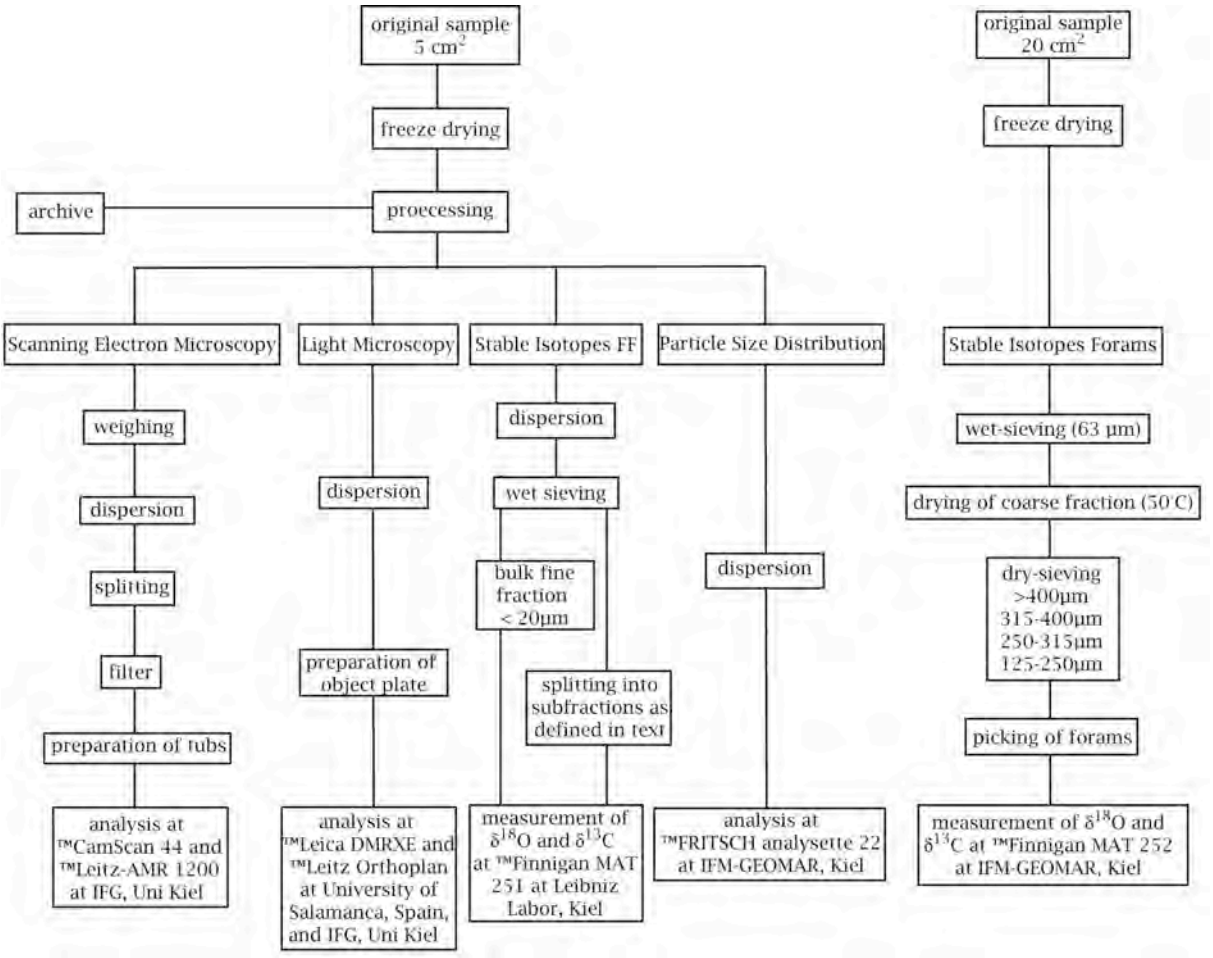

Fig. 2.1-1 Summary of individual steps of the sample preparation of this study.

2.2 Scanning Electron Microscopy (SEM)

Samples were prepared with the combined dilution/filtration technique of Backman and Shackleton (1983) and the improved method of Andruleit (1996) as standard preparation for SEM samples. For our coccolithophorid analyses 60 mg of dry bulk sediment were used for the Miocene samples, 80 mg for the Pliocene samples. Carbonate saturated tap water was

used to dilute the sediment. Sonification is the most effective tool for disaggregation of carbonate-rich sediments, but has to be applied carefully, since fragmentation of whole fragile microfossil tests may create new, smaller particles (Aiello and Kellet, 2006). However, tests of non-destructive disaggregation support the work of Bairbakhish et al. (1999), that coccolith breakage in ultrasonic bath (in our test up to 60 min) is negligible. To disintegrate aggregates, the suspension was sonified in 1-3 cycles for a total of 15-120 seconds. The samples were wet-splitted to $^{1}/_{100}$ with an electronic rotary sample divider (™FRITSCH laborette 27). The splitted aliquot with 0.6 mg, respectively 0.8 mg was filtered with a low-pressure vacuum pump onto a polycarbonate membrane filter (™Schleicher & Schuell, Satorius, 50 mm diameter, 0.4 µm pore size). After drying in the oven with 40-50°C for 24 hours, small pieces were cut out of each filter and fixed onto carbon sticky tabs on SEM-aluminium-stubs and coated with gold/palladium. SEM investigation was done with a ™CamScan 44 (used for determination of assemblage composition) and a ™Leitz AMR-1200 (used for biometric analyses) at IFG, University of Kiel, at a magnification of 5000 ×.

2.2.1 Biometry

Digital photographs made with an ™Leitz-AMR 1200 SEM with Spektrum mono 2,00 at IFG, University of Kiel, were used for morphometric analysis. The analysis was done using image analysis software ImageJ 1.36 (available free on web: http:// rsb.info.nih.gov/ij/). The individual lengths of maximal 400 individual specimens per species were measured per sample.

2.2.2 Data processing for abundance and flux calculations

For abundance calculations about 300-600 individual liths per sample were counted at the SEM. According to Dennison and Hay (1967), the probability of failure is 5-0.5 % in detecting all species with proportions over 1 %. Since the number of specimens counted per unit area is approximately proportional to the selected species per gram sediment (Backman and Shackleton, 1983), the analysis of species composition and abundances on a measured transect leads to the calculation of coccolith absolute abundances (see Andruleit, 1996; Boeckel and Baumann, 2004):

$$N = (F \times C \times S)/(A \times W)$$

with N = coccolith density (no. of individual coccoliths × g^{-1}), F = filter area (mm^2), C = number of counted coccoliths, A = investigated filter area (mm^2), W = weight of sample (g) and S = split factor.

Quantification of the contribution of single taxa to coccolith carbonate was calculated by using the mass equation of Young and Ziveri (2000). For that, the parameters shape (k_s), mean length (l), and calcite density (2.7 g/cm^3) were considered:

$$\text{Coccolith mass } m = 2.7 \times k_s \times l^3$$

From this the weight-balanced nannoplankton carbonate concentration follows as:

$$\text{Nannoplankton carbonate (wt \%)} =$$

$$\Sigma\,[N_{\text{individual species}}\ (\text{no.} \times g^{-1}) \times m_{\text{individual species}} \times 0.001] \times 10000 \,/\, CaCO_3(\text{wt\%})$$

This equation gives weight-percentages of coccolith carbonate built up from species with available shape factors. Extrapolation permits a 'calculated' indication of total weight percent of coccolith carbonate, which is used as 'Coccolith carbonate (wt %)' in this study. We used the calculated shape factors for single species (k_s) given in Young and Ziveri (2000) and Beaufort and Heussner (1999).

Relative abundances of the dominant species include an indeterminable group (indet.) that allows numbers to add up to 100 %. In contrast to this, the relative contribution to coccolith carbonate cannot attain 100 % for lack of the indispensable shape factor for some species. All species included in the mass calculations are mentioned in the respective section (chapter 6). Values of coccolith mass can vary especially due to size, so the presented data in this thesis are averaged values. For the calculation of coccolith carbonate, the species-specific carbonate contribution is necessary as well as the carbonate content per sample.

Mass fluxes were calculated using the formulas (given by Lototskaya et al., 1998):

$$\text{bulkMAR} = SR \times DBD$$

$$\text{cMAR} = SR \times DBD \times CaCO_3\,\% \times 0.01$$

$$\text{nMAR} = \text{bulkMAR} - \text{cMAR}$$

where MAR = mass accumulation rate ($g \times cm^{-2} \times ka^{-1}$), SR = sedimentation rate ($cm \times ka^{-1}$), DBD = dry bulk density ($g \times cm^{-3}$), c = carbonate, $CaCO_3$ % = weight percent carbonate of bulk sediment, and n = non-carbonate. Coccolith accumulation rates were calculated using the following formulas (Lototskaya et al., 1998; Ziveri et al., 2000; Ziveri and Thunell, 2000):

$$\text{cocAR} = SR \times DBD \times N$$

$$\text{xAR} = SR \times DBD \times X$$

where cocAR = total coccolith accumulation rate ($\text{no.} \times cm^{-2} \times ka^{-1}$) and xAR = accumulation rate of species x ($\text{no.} \times cm^{-2} \times ka^{-1}$) with X = absolute abundance of species x ($\text{no.} \times g^{-1}$ sediment).

2.3 Light Microscopy (LM)

Preparation of smear slides for light-microscope examination followed standard procedures, using a toothpick and a drop of water to distribute a thin layer of sediment on a glass microscope slide (e.g. Backman and Shackleton, 1983; Bown and Young, 1998). Analysis was carried out with a ™Leica DMRXE combined with the ™Leica QWin-Photo-Programm at the University of Salamanca, and a ™Leitz Orthoplan at the University of Kiel.

2.4 Stable isotopes of the bulk fine-fraction and quasi-monospecific subfractions

Stable isotope analysis of the fine-fraction was done on the fraction < 20 µm. For this, dispersed sediment was wet-sieved with ethanol absolute. Supernatant was removed by

centrifugation with a ™Eppendorf MiniSpin plus. Residual sediment was dried in a heating oven and stored in analyser-containers. To create a complete stable isotopic record of the late Miocene to Pliocene, supplementary samples were analysed to close the gap between the two observed intervals of the late Miocene (BB) and the Pliocene (FC).

As shown in Fig. 2.4-1, isotopic composition does not vary fundamentally (max 0.5 ‰) between samples treated with tap water and alcohol. $\delta^{18}O$ values do not differ categorically, but $\delta^{13}C$ values show consistently lower values in samples washed with tap water. As will be shown in chapter 8.2.3, this could be due to dissolution of the small-sized clay fraction. To avoid any effect on the isotope signal by tap water, processing of samples was solely done with ethanol absolute.

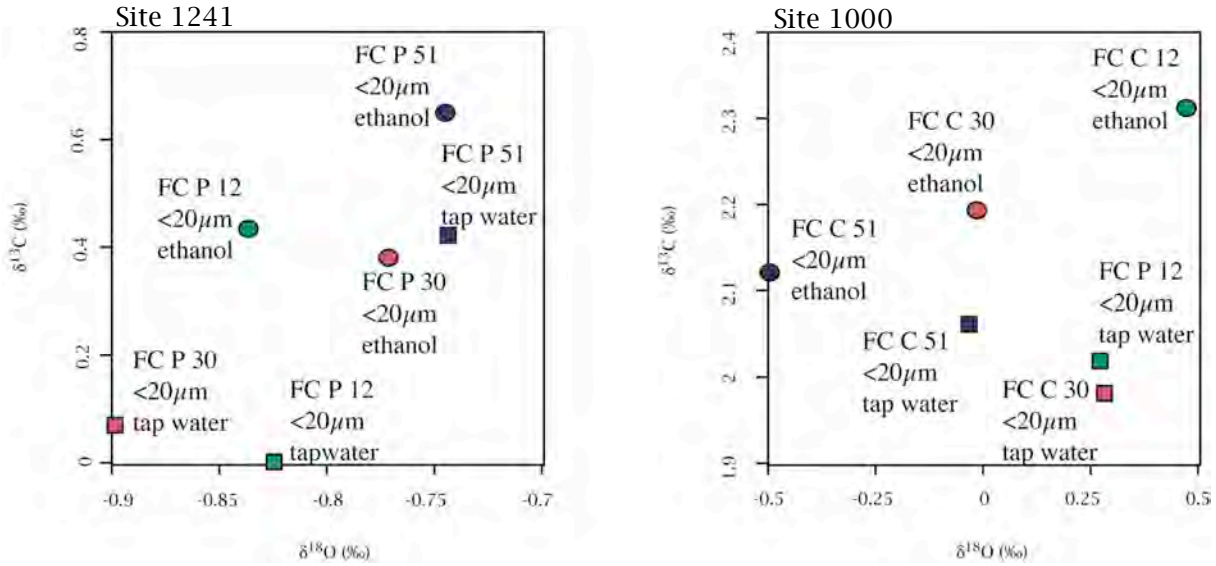

Fig. 2.4-1 Isotopic composition of samples treated with tap water and ethanol absolute. Squares represent samples treated with tap water, circles represent samples treated with ethanol. Left graph show results of Pliocene Site 1241 (FCP - labels), right graph shows results of Pliocene Site 1000 (FCC-labels).

Subfractions were determined depending on specific assemblage composition of each sample. Thus, certain species represent a certain grain size class. Stokes´ law is applied to estimate the size of a particle due to the different settling velocities in a fluid medium. Basic principle is the dependence of size on density of a particle and the parameters of the carrier liquid. That gravitational fractionation combined with wet sieving was used to separate different subfractions. After improvement of that methodology of grain size separation at the ™Sigma 310K centrifuge, the following grain size classes were determined for chosen samples: < 1 µm, 1-3 µm, 3-5 µm, 5-8 µm, 8-11 µm, and 11-20 µm. A more detailed description of the methodology of grain size separation is given in chapter 8.2.2.

Measurements of stable oxygen and carbon isotopes were carried out with a ™Finnigan MAT 251-mass spectrometer with automated Kiel carbonate preparation device (with analytical precision better than ± 0.07 ‰ for $\delta^{18}O$ and ± 0.04 ‰ for $\delta^{13}C$; $\pm 1\sigma$) at Leibniz-Laboratory for Radiometric Dating and Stable Isotope Research, Kiel.

2.5 Foraminiferal stable isotopes

Determination of oxygen and carbon isotopes on planktonic and benthic foraminifers was done by S. Steph, IFM-GEOMAR, Kiel on samples from the Pliocene for both, Site 1241 and Site 1000 (Steph, 2005).

For the late Miocene Site 1241, 10 to 20 specimens of the planktonic foraminifer *G. sacculifer* were selected from the size fraction 315-400 µm for each stable isotope measurement ($\delta^{18}O$ and $\delta^{13}C$). For the benthic isotope records, 1-5 tests of the epibenthic species *C. wuellerstorfi* or *C. mundulus* (> 250 µm) were analysed. Measurements of stable oxygen and carbon isotopes were carried out at IFM-GEOMAR, Kiel with a ™Finnigan MAT 252-mass spectrometer with automated Kiel carbonate preparation device (with analytical precision better than ± 0.07 ‰ for $\delta^{18}O$ and ± 0.04 ‰ for $\delta^{13}C$; $\pm 1\sigma$).

No measurements were done on late Miocene samples of Site 1000 due to insufficient preservation of foraminifers.

2.6 Grain size analysis

Particle size analysis by laser diffraction was carried out at the IFM-GEOMAR, Kiel using the ™FRITSCH analysette 22 NanoTec Laser Particle Sizer (Fritsch GmbH, Idar Oberstein, Germany). The Laser Particle Sizer is based on the system of low-angle laser light scattering (LALLS), i.e., the diffraction of scattered light caused by particles passing through a laser beam. No separate sample preparation was necessary prior to measurement, since complete dispersion can be achieved by applying a built-in ultrasonification unit. The NanoTec Laser Particle Sizer works with a HeNe-Laser (wavelength λ = 655 nm) and measures particles with a convergent laser beam (reversed Fourier-Optic) and the model-independent evaluation by Fraunhofer theory (Fritsch – Instruction manual analysette 22; Pabst et al., 2000; Gregorová et al., 2006), which was used as standard report of the scattered light information due to its advantages for homogeneity of samples. Thus, analyses used foreward scattered light falling on the photosensitive sensor rings, enabling a particle size range from 0.1-2000 µm to be analysed. Multiple measurements with a measuring range of 204 channels with 200 scans each was selected to increase resolution. In order to exclude measuring artefacts, after initial tests, all adjustable parameters concerning sample treatment during measurement (volumetric flow rate, stirrer speed and ultrasonics) were kept constant for all measurements. The entire system of the ™FRITSCH analysette 22 NanoTec works with distilled water. The turbulent flow through the measuring cell guarantees a statistical distribution of particles; reproducibility of the Laser Particle Sizer measurements is high.

CHAPTER 3 ECOLOGY

The overall geographic distribution and ecologic requirements of coccolithophores have changed substantially over geological time. Whereas calcareous nannoplankton was cosmopolitan and diverse in the Mesozoic with high abundances in coastal and oceanic as well as polar and equatorial waters, today´s coccolithophores are less diverse, and dominate temperate and tropical, nutrient-poor offshore waters (Brand, 1994). In modern nannoplankton assemblages, diversity is strongly correlated with environmental stability. Salinity and nutrient levels are thought to be the primary factors controlling the composition of nannoplankton assemblages (e.g. Wade and Bown, 2006, see chapter 1.2.3.2). They are typically differentiated in upper photic and deeper photic zone communities separated by the thermocline (Winter et al., 1994). High-diversity assemblages characterize stable, oligotrophic, mid ocean gyre habitats, whereas a decreased diversity is typical for highly fluctuating, eutrophic, unstable environments with extreme ecological conditions (e.g. Brand, 1994; Roth, 1994; Tab. 3-1). The latter life strategy is characterized by early maturity, rapid growth, small body sizes and short life span. This r-selective opportunistic strategy is an adaption to an ecologically unpredictable, mostly eutrophic environment, known from noelaerhabdacean coccolithophore genera, such as *Reticulofenestra*, *Gephyrocapsa*, and *Emiliania.* Contrary, the life strategy of K-selective specialists in oligotrophic environment, like *Sphenolithus* and *Discoaster*, is characterised by slow development, low mortality, late maturity and reproduction, large body size and long life span as an adaption to relatively constant environments. The fact that calcareous nannoplankton is predominantly K-selective complicates nutrient supply as an important control mechanism on their distribution. Under eutrophic conditions, coccolithophores are outcompeted by diatoms (e.g. Negri and Villa, 2000).

Tab. 3-1 Coccolithophore ecology and distribution.

high diversity but low standig stocks	**high standing stocks but low diversity**
seasonally stable, deep thermocline	instable, deep seasonal mixing, shallow thermocline
oligotrophic	eutrophic
e.g. tropical / subtropical mid-ocean gyres	e.g. continental shelves, upwelling areas, polar divergence, river mouths
	→ outcompeted by diatoms → coccolithophorid blooms following depletion of silica

The late Miocene to Pliocene calcareous nannofossil assemblages at Sites 1241 and 1000 show typical open-marine species compositions, with high diversities and dominance of seven taxa/species, *Florisphaera profunda*, *Sphenolithus abies,* *Reticulofenestra* spp., *Umbilicosphaera* spp., *Coccolithus pelagicus*, *Calcidiscus leptoporus* and *Helicosphaera* spp. (Appendix A1).

The major ecological characteristics of these taxa are as follows:

(1) ***Florisphaera profunda*** is a unique deep-dwelling species, whose affiliation to coccolithophores is still not clear, and thus classified as *incertae sedis* (Young et al., 2003). *F. profunda* inhabits the lower photic zone below 100m, centered at 150m with water temperatures > 10°C (Okada and Honjo, 1973; Okada and McIntyre, 1977; Reid, 1980; Molfino and McIntyre, 1990) and is thus adapted to low light and high nutrient conditions of that layer (Brand, 1994; Quinn et al., et al., 2005). Molfino and McIntyre (1990a; b) assigned variations in the abundance of *F. profunda* to monitor climate control of nutricline depth. Thus, changes in the abundance of *F. profunda* through the geological record are used as a proxy to model palaeonutricline dynamics (Molfino and McIntyre, 1990). A decrease in *F. profunda* has also been inferred from an increase in turbidity (Ahagon et al., 1993). An inverse relationship between Florisphaera fluxes and the diatom export production shows that *F. profunda* is inversely related to the intensity of upwelling (Jordan and Kleijne, 1994; Jordan et al., 1996; Ziveri and Thunell, 2000). Beaufort et al. (1997; 2001) indicated that the abundance of this taxa is a function of the primary productivity and, thus, providing a robust transfer function for palaeoproductivity estimates. *F. profunda* holds therefore great potential as a tool for the reconstruction of past oceanographic conditions.

Together with rarely abundant ***Gladiolithus flabellatus***, which inhabits the same ecological niche, they build the so-called **Lower Photic Zone Taxa (LPZ)** grouped in this study.

Sphenolithus abies is interpreted as a dominant species in warm waters, with oligotrophic and stable environments (e.g. Haq and Lohmann, 1976; Lohmann and Carlson, 1981; Perch-Nielsen, 1985a). In contrast, Wade and Bown (2006) discussed sphenoliths to be an opportunistic taxon with a wide range of occupied environments. *S. abies* is generally grouped with ***Discoaster*** **spp**., which are known to be lower photic zone inhabitants, with similar ecological tolerance as *F. profunda* (Flores et al., 2005). Sure is, that these taxa signalise a low productivity environment, thus *F. profunda* and *S. abies* were grouped, together with *Discoaster* spp., ***Rhabdosphaera clavigera*** and ***Discosphaera tubifera***, as **Low Productivity Indicator Taxa (LPI)**.

(2) ***Reticulofenestra*** **spp.** provide evidence that these forms are important palaeoecological and palaeoceanographic indicators (Negri and Villa, 2000). Small reticulofenestrids thrive in tropical upwelling settings (Okada and Honjo, 1973) and periods of high fertility (Biekart, 1989; Wade and Bown, 2006). Okada (2000) indicated a generally reversed stratigraphic trend of 'small placoliths' opposite to *F. profunda*, indicating changes in palaeoproductivity. At Sites 1241 and 1000 *Reticulofenestra* spp. are represented by *R. minuta*, *D. productus*, *R. minutula*, and *R. haquii*, which are related to a shallow, instable thermocline (Flores et al., 2005). These species may have tolerated eutrophic environments with a broad range in salinity (Wade and Bown, 2006). Rare abundances of *R. rotaria* and *R. pseudoumbilicus* have been observed. Flores et al., 2005 recognized abundances of *R. rotaria* to peak due to an increase of surface water temperature, but also due to decreasing salinity, however, ecology of that taxa is not well known, despite it´s good applicability as a biostratigraphic marker

(as shown in chapter 4) (Negri et al., 1999; Negri and Villa, 2000). All observed reticulofenestrids are part of the typical late Miocene temperate nannoflora (Lohmann and Carlson, 1981). Only few small *Gephyrocapsa* were present in the Pliocene sediments of Site 1000, these species are recorded as indicative of higher temperature in surface waters and higher productivity (Colmenero-Hidalgo et al., 2004). Moreover, the abundance changes in small reticulofenestrids and small *Gephyrocapsa* have been related to stability fluctuations in the environment, and their increase indicates poorer stratification of surface waters (Gartner et al., 1987).

(3) *Umbilicosphaera* spp. have a widespread distribution in the fossil record (Flores et al., 2003). Umbilicospheres are used as a reliable marker of oligotrophic conditions (e.g. Okada and McIntyre, 1979; Roth, 1987; Griaudeau, 1992). Flores et al. (2005) proposed the behaviour of *U. jafari* to be not related to temperature, silica minimum or salinity increase, whereas Wade and Bown (2006) hypothesised *U. jafari* to reflect an ability to flourish in shallow waters and hypersaline conditions with no response to changed nutrient levels.

(4) *C. pelagicus* is a cold eutrophic species (McIntyre et al., 1970; Roth and Berger, 1975; Okada and McIntyre, 1979; Lohmann and Carlson, 1981; Brand, 1994; Winter et al., 1994; Samtleben et al., 1995; Vazquez et al., 2000; Flores et al., 2003; Flores et al., 2005; Hagino and Okada, 2006) sometimes associated with an increase in productivity (Roth and Berger, 1975; Roth, 1994; Cachao and Moita, 1995; Andruleit et al., 2000; Boeckel and Baumann, 2004), sometimes without any relation to productivity characteristics (Filippelli et al., 2003; Flores et al., 2005).

(5) *C. leptoporus* is a cosmopolitan species (McIntyre and Bé, 1967; Geitzenauer et al., 1976). Warm and oligotrophic environmental patterns control the distribution of that taxon (Geitzenauer et al., 1977; Okada and McIntyre, 1977; Lohmann and Carlson, 1981; Giraudeau, 1992; Brand, 1994; Ziveri et al., 2000; Flores et al., 2003; Hagino and Okada, 2004; Hagino and Okada, 2006). Some ecological preferences for eutrophic environments have also been inferred (Giraudeau, 1992; Young, 1994; Flores et al., 2003). *C. leptoporus* is considered to be one of the most dissolution-resistant species (Schneidermann, 1977), thus its relative increase in abundances in more fertile areas has been supposed to be related to selective dissolution in organic rich sediments rather than to a true increase in abundance (Baumann et al., 2004). A similarity between fluxes and abundances of *C. leptoporus* and *Helicosphaera* has been observed (Ziveri et al., 1995; Ziveri et al., 2000; Ziveri and Thunell, 2000), whereby highest fluxes have been associated with low to intermediate nutrient concentrations and high coccolithophorid productivity (Flores et al., 2003).

(6) *Helicosphaera* spp. is known to have affinities to warm waters and moderately elevated nutrient conditions (McIntyre and Bé, 1967; Giraudeau, 1992; Flores et al., 2003; Baumann et al., 2005; Flores et al., 2005; Wade and Bown, 2006). *Helicosphaera* species appear to be able to thrive in shallow, eutrophic environments, with enhanced abundances in hemipelagic, near-continental environments (Perch-Nielsen, 1985a), upwelling regions, and gyre margin

waters with a higher fertility (Giraudeau, 1992). *H. carteri* has also been documented in eutrophic, hyposaline waters (Giraudeau, 1992, Flores et al., 2005) and estuarine environments (Cachao and Moita, 2000). Flores et al., 2003 described similar patterns of *Helicosphaera carteri* to that observed for *C. leptoporus*, but opposite patterns to that of *C. pelagicus*.

CHAPTER 4 BIOSTRATIGRAPHY

4.1 Neogene nannofossil biozonation

Calcareous nannofossils are exceptionally useful for biostratigraphy in pelagic settings since they are abundant, planktonic, rapidly evolving and largely cosmopolitan. The huge amount of data on the stratigraphic distribution of single species since their first appearance in the early Carnian is synthesized in a number of relatively stable biostratigraphic zonation schemes (notably Martini and Worsley, 1970; Okada and Bukry, 1980; Bown et al., 1998). These nannofossil biozonations are based on changes in the abundance patterns of taxa. Such changes may represent the first occurrence (FO) or last occurrence (LO) of taxa, a distinct rise or decline in abundance, an interval of peak abundance (Acme) or conversely, an interval of absence bracketed by presence (Paracme), or a prominent change in dominance between different taxa (Raffi et al., 2006). Biostratigraphic schemes are continuously refined (e.g. Raffi, 1999 and references therein) as well as tested on their reliability (e.g. Raffi et al., 1993; Wei, 1993; Raffi et al., 1995; Backman and Raffi, 1997). Nannofossil biozonation of the late Neogene time intervals investigated in this study are given in Fig. 4.1-1, a detailed list of all expected bioevents that have been described by other authors is given in Tab. 4.1-1.

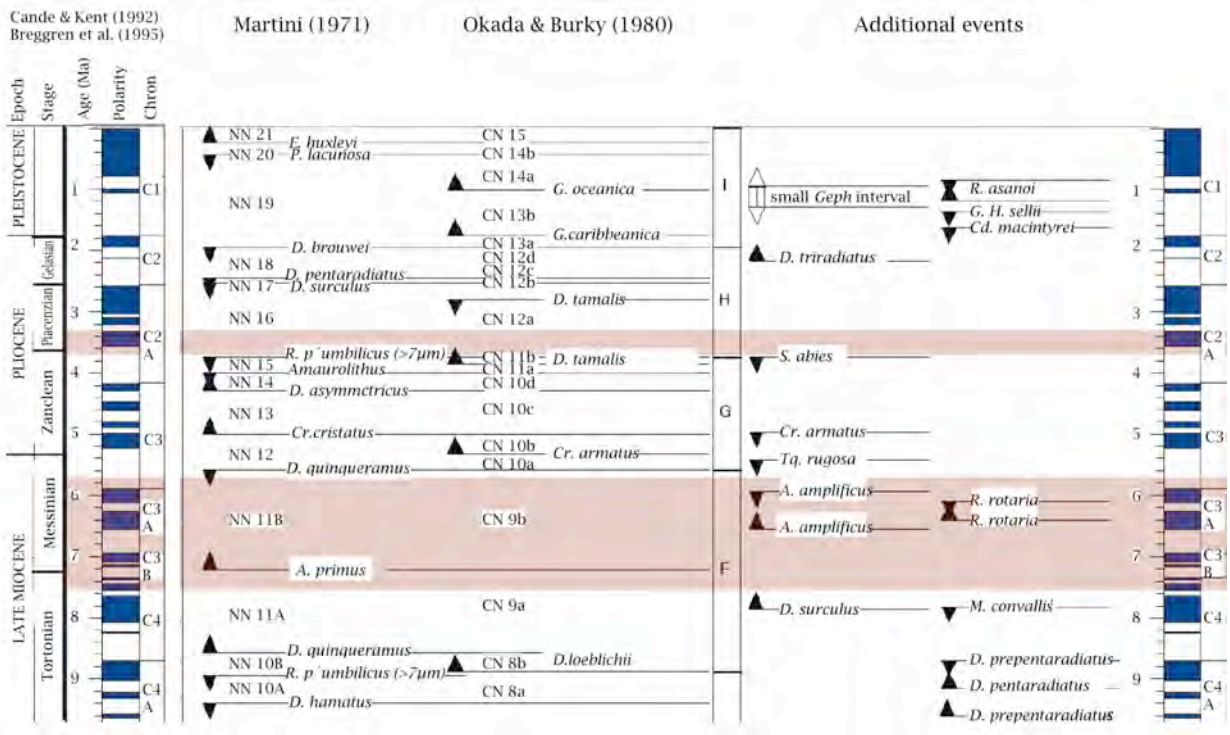

Fig. 4.1-1 Summary of late Neogene nannofossil biostratigraphic zonation schemes and bioevents (after Young, 1998), red bars indicate investigated time intervals worked on in this study.

Tab. 4.1-1 Expected bioevents in time intervals of this study. FO = first occurrence; LO = last occurrence; T = Top.

Nannofossil Biovent	References	Age (Ma)	Location	Age model
LO *S. abies*	Gibbs et al. 2005	3.56-3.52	ODP Sites 926, 662, 659	orbitally tuned
	Shackleton 95 (c)	3.66	ODP Leg 138	Biostratigraphy (Raffi and Flores (1995), plaeomagnetic time scales (Breggen et al. 1985, Cande and Kent (1992)
	Kameo and Bralower, 2000	3.65-3.524	ODP Site 1000	calcareous nannofossil schemes of Burky (1973, 1975) and Okada and Burky (1980)
	Flores (unpublished)	3.614-3.569	ODP Site 1241	Correlated with orbitally tuned age model of Tiedemann et al. (2007)
LO *R. pseudoumbilicus*	Gibbs et al., 2005	3.82-3.81	ODP Sites 926, 662, 659	orbitally tuned
	Kameo and Bralower, 2000	3.852-3.8	ODP Site 1000	calcareous nannofossil schemes of Burky (1973, 1975) and Okada and Burky (1980) correlated with orbitally tuned age model of Steph et al. (2006)
	Flores (unpublished)	3.8-3.742	ODP Site 1241	Correlated with orbitally tuned age model of Tiedemann et al. (2007)
LO *A. primus*	Kameo and Bralower, 2000	4.8-4.37	ODP Site 1000	calcareous nannofossil schemes of Burky (1973, 1975) and Okada and Burky (1980) correlated with orbitally tuned age model of Steph et al. (2006)
FO *C. rugosus*	Kameo and Bralower, 2000	5.04-4.93	ODP Site 1000	calcareous nannofossil schemes of Burky (1973, 1975) and Okada and Burky (1980) orbitally tuned age model of Steph et al. (2006)
	Backman and Raffi, 1997	5.046	ODP site 926	orbitally tuned
LO *C. actus*	Kameo and Bralower, 2000	5.04-4.978	ODP Site 1000	calcareous nannofossil schemes of Burky (1973, 1975) and Okada and Burky (1980) orbitally tuned age model of Steph et al. (2006)
	Backman and Raffi, 1997	5.046	ODP site 926	orbitally tuned
FO *C. actus*	Kameo and Bralower, 2000	5.367-5.34	ODP Site 1000	calcareous nannofossil schemes of Burky (1973, 1975) and Okada and Burky (1980) orbitally tuned age model of Steph et al. (2006)
	Backman and Raffi, 1997	5.372	ODP site 926	orbitally tuned
LO *A. amplificus*	Kameo and Bralower, 2000	5.88	ODP Site 1000	calcareous nannofossil schemes of Burky (1973, 1975) and Okada and Burky (1980)
	Backman and Raffi, 1997	5.993	ODP site 926	orbitally tuned
FO *A. amplificus*	Kameo and Bralower, 2000	6.5	ODP Site 1000	calcareous nannofossil schemes of Burky (1973, 1975) and Okada and Burky (1980)
	Backman and Raffi, 1997	6.84	ODP site 926	orbitally tuned
T paracme *R. pseudoumbilicus*	Kameo and Bralower, 2000	6.8	ODP Site 1000	calcareous nannofossil schemes of Burky (1973, 1975) and Okada and Burky (1980)
	Backman and Raffi, 1997	7.1	ODP site 926	orbitally tuned
	Flores (unpublished)	6.939-6.862	ODP Site 1241	Correlated with our orbitally tuned age model
LO *R. rotaria*	Negri et al., 1999	6.771-6.760	N-Apennines	orbitally tuned
FO *R. rotaria*	Negri et al., 1999	FO: 7.405-7.398	N-Apennines MCS	orbitally tuned
		FCO: 7.226-7.218	N-Apennines MCS	orbitally tuned
	Jiang and Wise, 2007	6.32	ODP Site 1256	calcareous nannofossil schemes of Martini and Müller (1986) and Okada and Burky (1980); magnetostratigraphy (Breggren et al., 1995)
	Negri and Villa, 2000	FO: 7.423-7.419	Crete Faneromeni	orbitally tuned
		FCO: 7.267-7.262	Crete Faneromeni	orbitally tuned
	Jiang and Wise, 2007	7.18	ODP Site 1256	calcareous nannofossil schemes of Martini and Müller (1986) and Okada and Burky (1980), magnetostratigraphy (Breggren et al., 1995)

4.2 Methodology

The standard methodology for biostratigraphy is based on Light Microscopy (LM) observations, because of its undeniable advantage of easy and fast processing. Additionally, certain species are easy to determine in LM due to high birefringence (*Discoaster* spp., *Amaurolithus* spp.). I decided to focus on the examination of coccoliths with Scanning Electron Microscopy (SEM) since Bollmann et al. (2002) demonstrated the number of species obtained in high diversity samples to be much higher with SEM than with LM. For that, samples were prepared with the combined dilution/filtration technique of Andruleit (1996) (see chapter 2), examination was carried out with a ™CamScan 44 at the University of Kiel.

Even though higher diversity and greater confidence of identification (especially of small liths, e.g. *R. calicis* bioevent, see below) is obtainable with SEM compared to LM (Baumann et al., 2002), for refining (low) SEM resolution for detailed biostratigraphic questions at significant points, additional samples for Light Microscope observations were prepared as smear slides using standard techniques. Analysis was done with a ™Leica DMRXE at the University of Salamanca, and a ™Leitz Orthoplan at the University of Kiel.

In retrospect, there also emerged an important species only to be detected in LM not in SEM, *Reticulofenestra rotaria*.

4.3 Late Miocene to Pliocene bioevents at Sites 1241 and 1000

4.3.1 Reliability

Precision and accuracy of nannofossil biostratigraphic correlations have been discussed extensively (e.g. Hills and Thierstein, 1989; Wei and Wise, 1989; Spencer-Cervato et al., 1994; Raffi, 1999) since biostratigraphy should be treated carefully. Besides factors such as preservation state and productivity rate, re-working, downhole contamination and the presence of rare and discontinuous species blur the sharpness of the biohorizons. Since a geological sample represents a time-averaged assemblage, it is difficult to define diachrony in nannofossil communities. Yet in biostratigraphic work, it is generally assumed that species first and last occurrences appear more or less simultaneously throughout a broad geographic range (Bolli et al., 1985). Relatively few cases of diachronous extinctions in nannofossil events are calibrated by orbital stratigraphy (Raffi et al., 1993; Chapman and Chepstow, 1997). Even though it is often assumed that bioevents are synchronous at the level of typical biostratigraphic resolution (> 100 ka), a number of studies demonstrated remarkable synchrony on orbital timescales (< 100 ka) (Backman and Shackleton, 1983; Raffi et al., 1993).

All examined samples of Sites 1241 and 1000 contain very abundant and diversified nannofossil assemblages with exceptional good preservation (chapter 1.1.3.2). The biostratigraphic analyses of this study partly encountered above-named problems, especially since some nannofossil events are based on species with extremely rare occurrences.

ODP biostratigraphy of Site 1241 (Flores et al., 2006) documented less bioevents than the high-resolution record of this study. In contrast, ODP Site 1000 biostratigraphy (Kameo and Bralower, 2000) shows several occurrence data *(e.g. Amaurolithus amplificus, Ceratolithus actus* and *Ceratolithus rugosus* and *Amaurolithus primus* (Tab. 4.1)) that were not identified within this study, neither in SEM nor LM.

4.3.2 Results

The observed Biogenic Bloom interval is generally characterized by small coccoliths, mainly reticulofenestrids (Young, 1998). Following a 'small *Reticulofenestra* Interval' at about 8.6 Ma (Young, 1990), reticulofenestrids show a wide range of size variations. A dramatic event that is not included in the standard zonation is placed within this interval, the paracme of *R. pseudoumbilicus*. This paracme interval has also been observed in the equatorial Indian Ocean (Rio et al., 1990; Young, 1990), in the western equatorial Pacific Ocean (Takayama, 1993), the eastern equatorial Pacific (Raffi and Flores, 1995), and the western equatorial Atlantic (Backman and Raffi, 1997) and Caribbean Sea (Kameo and Bralower, 2000). The reappearance of *R. pseudoumbilicus* is used by Raffi and Flores (1995) to define the top of the paracme interval of *R. pseudoumbilicus*. This abrupt recurrence of large *R. pseudoumbilicus* has been dated by Backman and Raffi (1997) at 7.1 Ma. In samples of Site 1241, large *Reticulofenestra* specimens appear at 7.058 Ma (Fig. 4.3.2-1), but since the abundance of that species is negligible, the exact determination of that bioevent is difficult. This problem is even more pronounced in the Caribbean samples, where *R. pseudoumbilicus* abundances are even lower (FO 7.135 Ma; Fig. 4.3.2-2), in practice visible in only few (less than 5) individual coccoliths.

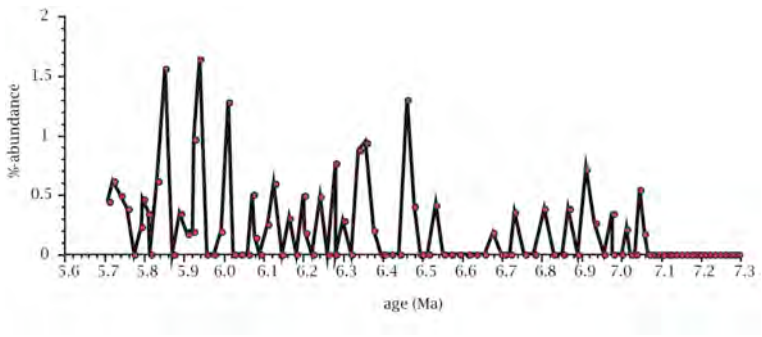

Fig. 4.3.2-1 Top of paracme of *R. pseudoumbilicus* at Site 1241.

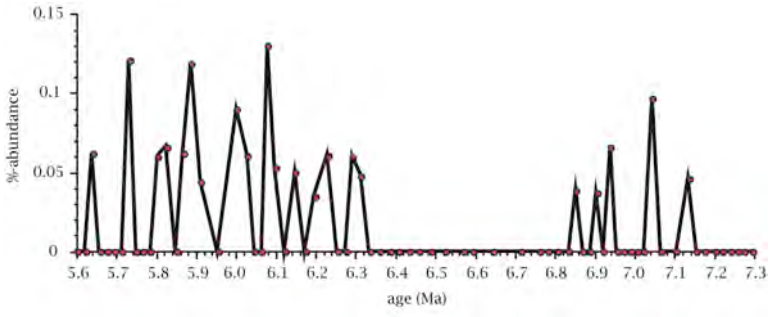

Fig. 4.3.2-2 Top of paracme of *R. pseudoumbilicus* at Site 1000.

Between 7.5 and 6.3 Ma there is a short interval in which nearly circular *Reticulofenestra* specimens are present. This *R. rotaria* (Theodoridis, 1984) has a short stratigraphic range restricted to nannofossil Subzone NN11b in the Mediterranean area (Theodoridis, 1984) and in the eastern equatorial Pacific Ocean (Raffi and Flores, 1995). Negri et al. (1999) and Negri and Villa (2000) dated the FCO (first common occurrence) between 7.22 and 7.26 Ma and the LCO (last common occurrence) from 6.76 to 6.77 Ma in astronomically dated sediments from the North Apennine and Crete. Based on biostratigraphy and magnetostratigraphy, Jiang and Wise (2007) assigned ages for the FO and LO of *R. rotaria* to 7.18 and 6.32 Ma, respectively, at eastern equatorial Site 1256. At Site 1241 a first occurrence of *R. rotaria* at 7.33 Ma is followed by common occurrence starting at 7.2 Ma (Fig. 4.3.2-3), whereas in sediments of Site 1000 the first occurrence is detected at 7.18 Ma (Fig. 4.3.2-4). *R. rotaria* LO is 6.36 Ma in the equatorial east Pacific and 6.89 Ma in the central Caribbean Sea.

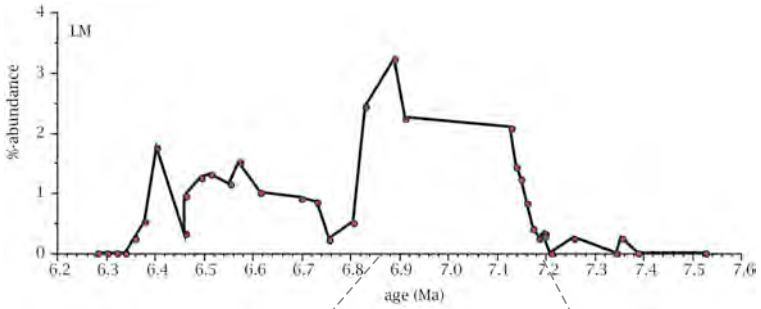

Fig. 4.3.2-3 occurrence of *R. rotaria* at Site 1241.

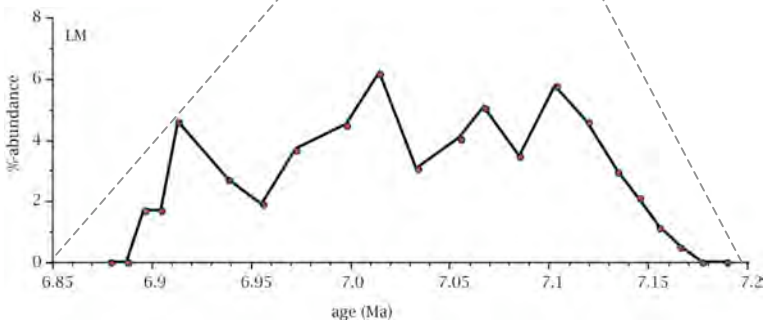

Fig. 4.3.2-4 occurrence of *R. rotaria* at Site 1000.

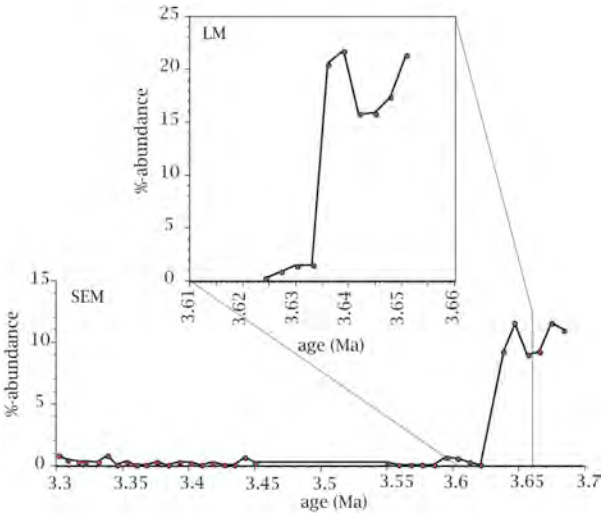

Fig. 4.3.2-5 Top *Sphenolithus abies* at Site 1241. SEM and refined LM data.

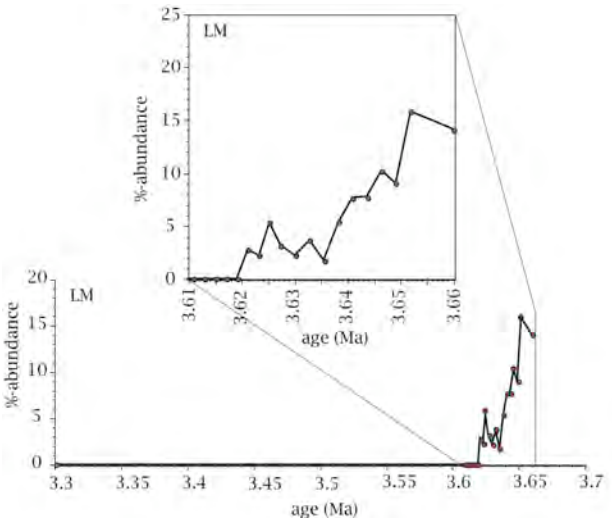

Fig. 4.3.2-6 Top *Sphenolithus abies* at Site 1000. LM data.

The second observed interval of the 'Final Closure' is marked by the prominent and biostratigraphically important last occurrence datums of *R. pseudoumbilicus* and *S. abies*. The latter has been detected in the samples of Site 1241 and Site 1000, but the LO of *R. pseudoumbilicus* is subjected to the difficulty of rare and discontinuous abundances. Last specimens of *R. pseudoumbilicus* were identified at 3.621 Ma in the Pacific samples, but in the Caribbean samples no single specimen has been identified. Gibbs et al. (2005) dated the last occurrences of *R. pseudoumbilicus* in the equatorial and subequatorial Atlantic to be synchronous between 3.81 and 3.82 Ma. They identified a decline in *S. abies* between 3.71 and 3.67 and its extinction between 3.56 and 3.52 Ma. At Site 1241, *S. abies* rapidly decreases between 3.64 and 3.635 Ma with a LO at 3.624 Ma observed in both, SEM and, with refined resolution, with LM (Fig. 4.3.2-5). At Site 1000 the decrease of *S. abies* started at 3.655 Ma with a LO at 3.619 (Fig. 4.3.2-6, only LM observations).

4.3.3 Synchrony / Diachrony

The large number of nannofossil biostratigraphic datums that appear to be synchronous in the geological record makes coccoliths an ideal biostratigraphic tool. However, this observed pattern is in conflict with general evolutionary theories, which predict a geographic and ecological control on dispersal of marine plankton. This consequently should lead to diachronous first and last appearance datums among planktonic organisms (Norris, 2000).

Precession and accuracy of nannofossil biostratigraphic events need to be defined cautiously. Within orbitally tuned high-resolution time series like those of late Miocene to Pliocene Sites 1241 and 1000, dating of bioevents is more reliable than supposed events in the low-resolution ODP shipboard data. But still, determination of synchrony or diachrony is highly dependent on the applied age model. As described in chapter 1.1.2, the age models of tropical east Pacific Site 1241 and central Caribbean Site 1000 are based on tuning high frequency variations in GRA density, percent sand of carbonate fraction and benthic $\delta^{13}C$ to the orbital solution of Laskar et al. (1993) and correlation with reference benthic and planktonic $\delta^{18}O$ and $\delta^{13}C$ records (Sites 925 and 926) (Steph et al., 2006). The latter parameters are in constant phase relation with the obliquity cycle. This, in turn, guarantees a maximum error of 41 kyr due to fixed tie points of the age model. Compared to ODP shipboard biostratigraphic resolution (Kameo and Bralower, 2000), this allows very precise work on biostratigraphic datums within the given error. And, even the above-criticised end of paracme of *R. pseudoumbilicus* offers persuasive synchronity at both Sites (Fig. 4.3.3-1).

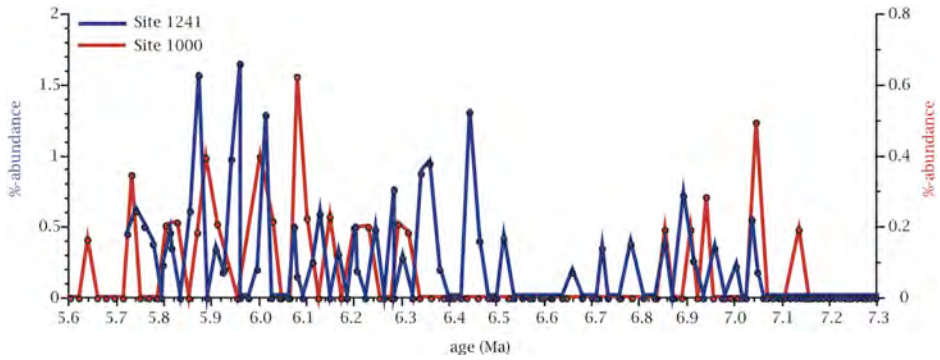

Fig. 4.3.3-1 Top paracme *R. pseudoumbilicus*, synchrony, Site 1241 (blue) and Site 1000 (red).

Appearance datums of *R. rotaria* in the Caribbean Sea are restricted to a short occurrence interval from 7.18 until 6.89 Ma. In the Pacific they show a wider range between 7.33, and common abundances around 7.2 Ma, and 6.36 Ma. Synchronous common appearance of that species occurs at around 7.19 Ma, but diachrony exists in its last occurrence (Fig. 4.3.3-2). The first occurrence datums of *R. rotaria* are perfectly synchronous with reference data of Negri et al. (1999), Negri and Villa (2000) and Jiang and Wise (2007) around 7.2 Ma. Last occurrence of *R. rotaria* is observed around 6.9 Ma at Site 1000 as well as dated by Negri et al. (1999) and Negri and Villa (2000) in sediments from North Apennine and Crete. Last occurrence of *R. rotaria* at Site 1241 is found around 6.34 Ma, synchronous to data of Jing and Wise (2007) (eastern equatorial ODP Site 1256). Thus, the stratigraphic occurrence of *R. rotaria* in the Caribbean Sea is similar to that of the Mediterranean, with an early last occurrence, wheras the stratigraphic range in Site 1241 is similar to the equatorial Pacific (Site 1256). It is noteworthy, that the diachronous last occurrence between the Pacific and the Caribbean Sea takes place prior to a significant separation of the two oceans, due to the closure of the Panamanian Seaway.

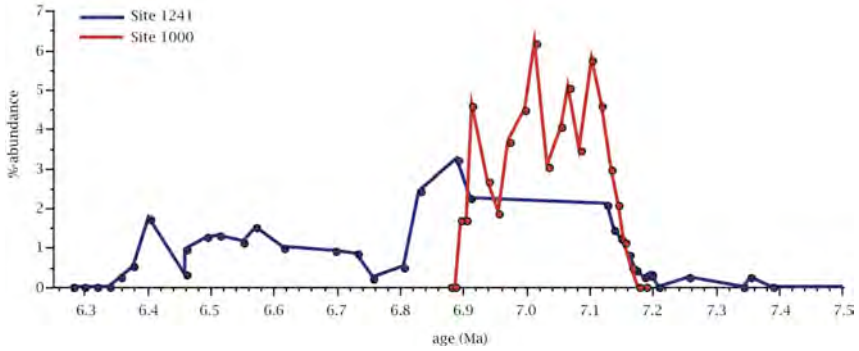

Fig. 4.3.3-2 Top *R. rotaria*, synchrony/diachrony, Site 1241 (blue), Site 1000 (red).

Another nannofossil bioevent around the closure of the Panamanian Seaway, the occurrence of *Reticulofenestra calicis*, was detected by Crudeli (2005). This hitherto undescribed species has a very short stratigraphic range, but shows synchronous first and last occurrences in both sites (Fig. 4.3.3-3). To what extend this event is synchronous on a

more global scale could not be answered, since this species has not yet been observed in sediments from other regions, due to lack of SEM observations.

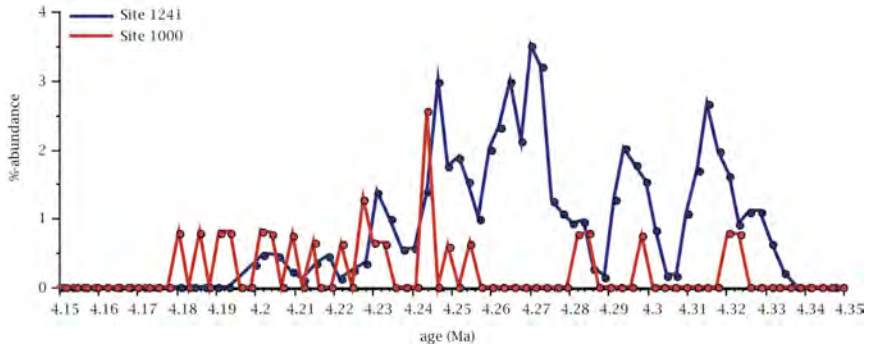

Fig. 4.3.3-3 *R. calicis*, synchrony, Site 1241 (blue), Site 1000 (red). Data of Crudeli (2005), kindly provided by H. Kinkel.

Synchronous last occurrence datums of *Sphenolithus abies* (Fig. 4.3.3-4) between 3.624 and 3.619 Ma at both sides of the Panamanian Isthmus correlate well with data from the equatorial and subequatorial Atlantic of Gibbs et al. (2005). Since that time the closure of the Panamanian Seaway is already completed (references see chapter 1.2.1.2), synchrony requires additional mechanisms for the decline of *Sphenolithus abies*, such as its response to the intensification of glacial conditions as suggested by Gibbs et al. (2005).

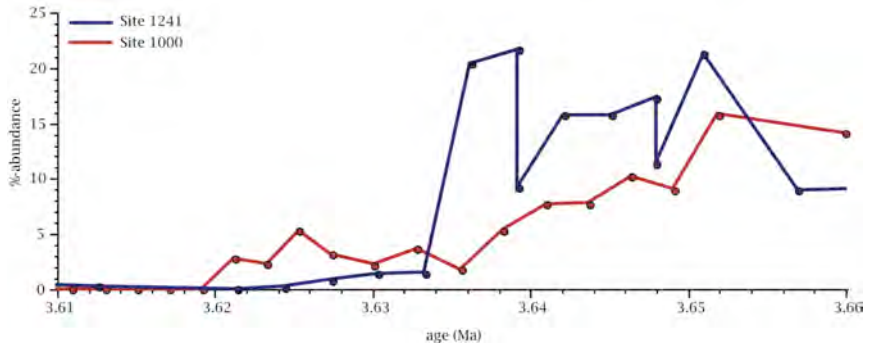

Fig. 4.3.3-4 Top *Sphenolithus abies*, synchrony, Site 1241 (blue), Site 1000 (red).

4.3.4 Conclusions and perspectives

Along with the sampling interval, the biostratigraphic results of the late Miocene to Pliocene eastern equatorial Pacific Site 1241 and Central Caribbean Site 1000 guarantee several nannofossil bioevents. Datums of *R. pseudoumbilicus* (T paracme), *R. rotaria* (FO and LO), *R. calicis* (FO and LO) and *S. abies* (LO) have been identified and correlated to detect temporal and spatial biostratigraphic schemes related to the Panamanian Seaway Closure (summarized in Tab. 4.3-1):

(1) T paracme *R. pseudoumbilicus* synchron at around 7.1 Ma
correlation with Raffi et al. (2006, and references therein)

(2) FO *R. rotaria* synchron at around 7.19 Ma
correlation with Negri et al. (1999), Negri and Villa (2000) and Jiang and Wise (2007)

(3) LO *R. rotaria* diachron
- Site 1000 at around 6.9 Ma correlates with Negri et al. (1999), Negri and Villa (2000)
- Site 1241 at around 6.34 Ma correlates with Jiang and Wise (2007)

(4) FO *R. calicis* synchron at around 4.33 Ma

(5) LO *R. calicis* synchron at around 4.19 Ma

(6) LO *S. abies* synchron at around 3.621 Ma
correlation with Shackleton (1995c) and Gibbs et al. (2005)

The closure of a gateway causes dramatical changes in all palaeoceanographic conditions. Synchronity in detected bioevents, with open- and closed-gateway conditions, clearly point on a set of mechanisms that forced nannoplankton evolution independently of the Panamanian Seaway Closure. Especially, synchrony of nannofossil bioevents related to a closed Panamanian Seaway raises questions on nannoplankton evolution since geographic and ecologic control on dispersal of planktonic organisms changed fundamentally. One would expect lack of migration of a new species if oceanographic changes due to the gateway are relevant, and thus a diachrony in FO-datums, but synchrony, as observed in *S. abies* and *R. calicis*, is remarkable and requires additional factors beyond. Consideration of a variety of factors and mechanisms need to be discussed for interpretation of possible causes for bioevents. Due to the difference in oceanographic settings in both observed sites, ongoing chapters of this study discuss ecology (chapter 3) and evolution (chapter 5), assemblage composition (chapter 6), as well as palaeoceanographic conditions (chapter 8) and will be synthesised in chapter 9.

Species-level taxonomy is based primarily on coccolith morphology, applied to studies of their ecology, biogeography, sediment flux and evolution (Perch-Nielsen, 1985; Jordan and Kleijne, 1994; Bown, 1998; Young et al., 2003). Morphometric studies are of basic importance for understanding the comprehensive role of coccolithophores in the geological record. This has been done in this study, with focus on size variations of *Reticulofenestra* and *Calcidiscus* specimens and will be presented in chapter 5.

Tab. 4.3-1 Summary of calcareous nannofossil horizons of this study with astronomical age estimates and correlation with published references: 1: Gibbs et al. 2005; 2: Shackleton 95 (c); 3: Kameo and Bralower, 2000; 4: Flores (unpublished data); 5: Jiang and Wise, 2007; 6: Negri et al., 1999; 7: Negri and Villa, 2000, 8: Raffi et al., 2006.

Nannofossil Biovent	Age (Ma)	Location	Synchrony / diachrony Panama	Synchrony with reference	Location references
LO *S. abies*	3.624	eastern equatorial Pacific	Synchrony	1, 2, 3, 4	eastern equatorial Pacific, Central Atlantic
	3.618	Caribbean		1, 2, 3, 4	eastern equatorial Pacific, Central Atlantic
LO *R. calicis*	4.2	eastern equatorial Pacific	Synchrony		
	4.18	Caribbean			
FO *R. calicis*	4.336	eastern equatorial Pacific	Synchrony		
	4.325	Caribbean			

LO *R. rotaria*	6.34	eastern equatorial Pacific	Diachrony	5	eastern equatorial Pacific
	6.9	Caribbean		6, 7	Mediterranean
FO *R. rotaria*	7.2 (7.36)	eastern equatorial Pacific	Synchrony	5, 6, 7	eastern equatorial Pacific, Mediterranean
	7.18	Caribbean		5, 6, 7	
T paracme *R. pseudoumbilicus*	7.058	eastern equatorial Pacific	Synchrony	8 and references therein	worldwide
	7.135	Caribbean		8 and references therein	

CHAPTER 5 MORPHOMETRY

5.1 Coccolith intra-specific size variability

The use of calcareous nannofossils for biostratigraphical purpose or analysis of palaeoenvironmental conditions requires the adoption of consistent taxonomic concepts. Due to its high consistency, this can be achieved by the identification of morphological endmembers within a genus. Thus, detailed morphometric studies of coccoliths in fossil records have improved biostratigraphic resolution (Backman and Hermelin, 1986; Colmenero-Hidalgo et al., 2002; Hagino and Okada, 2006), have exposed evolutionary trends (Young, 1990; Bollmann, 1997; Knappertsbusch, 2000; Raffi et al., 2006) and have shown its good potential use in palaeoceanographic proxy studies (Henderiks and Renaud, 2004; Mattioli et al., 2004). Moreover, coccolith size is a useful proxy to estimate calcite production and carbonate burial by coccolithophores (Broerse et al., 2000; Young and Ziveri, 2000; Sprengel et al., 2002; Henderiks, 2008b). It exerts a substantial influence on fractionation of stable isotopes in both, coccolith carbonate (Ziveri et al., 2003) and haptophyte organic compounds (Popp et al., 1998) as well as on the incorporation of trace elements (Henderiks, 2008b).

The presence of intermediate morphotypes between endmembers representing distinct species sheds light on phylogenetic relationships (Raffi et al., 1998). Despite the absence of fossil documentation for ancestor-descendant relationships and the insufficiency of information about the ultrastructure of most known nannofossils, several studies have investigated the evolutionary relationships between and within different genera and species (Gartner, 1969; Burky, 1971; Haq and Lohmann, 1976; Samtleben, 1980; Raffi et al., 1998). These studies base mainly on qualitative observations of affinities in simple morphological features. To unravel the assumption of phenotypic vs. genotypic variations in calcareous nannoplankton (Renaud et al., 2002; Quinn et al., 2003), recent studies on living coccolithophores were done. They revealed that morphological variations in many apparently globally distributed coccolithophorid species often reflect genetic differences (Cachao and Moita, 2000; Geisen et al., 2002; Sáez et al., 2003; Schroeder et al., 2005). Several of the ‘morpho-species’ are in fact monophyletic clusters of a sibling, biological species, separated by subtle morphological characters (de Vargas et al., 2004). De Vargas et al. (2004) introduced the concept of ‘super-species’, which is based on the presence of (pseudo-) cryptic sibling species. These species are morphologically identical (or have minor but recognizable morphological characteristics), but discernible by correlating their genetical, physiological or behavioural characters (Sáez et al., 2003). Such ‘super-species’ are assemblages of allopatric (geographical or temporal) species of monophyletic origin, which often show distinct morphological differences (de Vargas et al., 2004). Thus, the habitat segregation of these morphotypes indicates that the global distributions observed for these major taxa are mixtures of several discrete subspecies (Ziveri et al., 2004; Hagino and Okada,

2006) which may be composed of two or more genotypically discrete species (or sub-species) with often subtle morphological differences but rather strong ecological differences.

5.2 Body sizes and evolutionary changes

Size is an obvious morphological characteristic. It is easy to measure, conspicuous, comparable across taxa, extremely variable through time and readily preserved in the fossil record. Besides profound influences on nutrient uptake kinetics, photosynthesis, respiration, growth, and sinking rates, carbon cycling, and isotopic composition, cell geometry and size strongly determine the physiology of unicellular algae, whilst also affecting their ecological and evolutionary patterns. The size of a single specimen is constrained by its genome, ontogeny and environment (Seilacher 1992; Hunt and Roy, 2006). Causal mechanisms for a change can be intrinsic or extrinsic. A variety of passive and active selection pressures likely influence these changes, with specific abiotic and biotic factors determining trends over time.

In general, size changes occur due to simply improved adaptions to the environment or specialisations during major diversification events, with or without major niche transitions (Stanley, 1973; Smith et al., 1995). Here, the tendency for lineages to evolve to larger body size, Cope´s Rule, is widely seen as a pervasive evolutionary pattern in biology (see Jablonski (1997) and references therein). Correlations between body size and temperature have led to the suggestion that Cope´s Rule may simply be an evolutionary manifestation of Bergmann´s Rule. This ecogeographic rule inversely correlates between body size and temperature. Thus, phenotypic evolution in response to climate change can be an important determination of trends in body size (Hunt and Roy, 2006). But still there is contradiction between assets and drawbacks of larger body sizes, and studies across a wide range of taxa have supported (Brown and Maurer, 1986; Alroy, 1998) and rejected (Arnold et al., 1995; Jablonski, 1997) it, but none has yet confirmed suggestions empirically (Hone and Benton, 2005; Hunt and Roy, 2006). However, Jablonski (1997) supposed a directional net increase in body size to be no more frequent than an increase in size range among species or a net evolutionary size decrease. Hypotheses suggest, that large size may be inhibitory to speciation (Arnold et al., 1995), because of the nonlinear changes of metabolic rates and foraging efficiency with increasing size (Peters, 1983). For the same reasons and because large-sized taxa tend to be more specialised, they may be more prone to extinction (Norris, 1991). Anyway, it is arguable whether Cope´s rule is easy to apply on simple single-celled life or not merely represents a statistical artefact.

As a visible proxy for life history events, size can be used to determine evolutionary patterns. Morphological characteristics are often influenced by evolution of a taxon, thus speed of evolutionary and hence morphological change is a fundamental point. Evolutionary changes are gradual or abrupt within lineages. Punctuated equilibrium and phyletic gradualism are theoretical end members of a wide spectrum of possible evolutionary

patterns (Sheldon, 1990). Phyletic gradualism assumes that lineages evolve without a tendency for evolutionary acceleration during speciation events. This contrasts sharply with the rapid evolutionary changes interrupting stasis in fossil lineages (Eldredge and Gould, 1988; Eldredge et al., 2005). Endmembers of the hypothetical models of morpho-genetic evolution represent different degrees of disconnection (simple or complex spatio-temporal) between the morphological, genetic, and ecological differentiations (de Vargas et al., 2004).

Still, it is unclear if biotic or abiotic factors were more important in the initiation of speciation and extinction (Smetacek, 2001; Finkel et al., 2007). In case of plankton evolution, Schmidt et al. (2004a; 2004b) clearly supported the stationary mode of Stenseth and Maynard Smith (1984) as an evolutionary model in planktonic foraminifers (i.e. evolution is largely driven by abiotic changes). Finkel et al. (2005; 2007) supported the strong correlation between evolutionary changes and changes of the physical environment as a reason for size decreases in diatoms and dinoflagellates and suggest that an universal abiotic driver related to climate is responsible for evolutionary changes in size structure. Henderiks and Pagani (2008) demonstrated that potential phenotypic size response within the coccolithophorid *Reticulofenestra* is affected by several biotic and/or abiotic factors, since species composition and regional ecology seem to be the major driving forces of the observed size variability. This is supported by Young (1990), who interpreted the systematic size variation patterns of Neogene reticulofenestrids with two extreme possibilities, namely the effect of change in ecological factors such as climate on a genetically unchanging population, or an evolutionary change without environmental change. He suspected direct control to be evolutionary with likely ecological influence, but size variation patterns being a product of genotypic variation.

5.3 Methodology

Morphological data of late Miocene to Pliocene coccoliths morphometry of ODP Sites 1241 and 1000 was attained with SEM analysis. Samples for SEM observation were prepared as described in chapter 2.2. About 50 to 80 digital photographs per sample were done with a ™Leitz-AMR 1200 SEM at a magnification of 2000 ×. Accurate morphometric measurements were carried out with ImageJ 1.36 (available free on web: http://rsb.info.nih.gov/ij/). Since coccolith cell size is strongly linearly correlated to both, coccospheres and cell diameter (Henderiks, 2008a), the overall coccolith length was measured on the most important taxa. Thus, measurements have been accomplished for individuals of the genera *Reticulofenestra* and *Calcidiscus*. Around 200 to 400 individuals of *Reticulofenestra* were measured per sample. Because auf its lower abundances, all detectable specimens of *Calcidiscus* are captured for size determination (between one to 61 individuals per sample). A total of 22761 measurements were carried out on *Reticulofenestra* and 1809 measurements on *Calcidiscus*.

5.4 Late Miocene to Pliocene coccolith size variabilities at Sites 1241 and 1000

5.4.1 Size variations in *Reticulofenestra* coccoliths

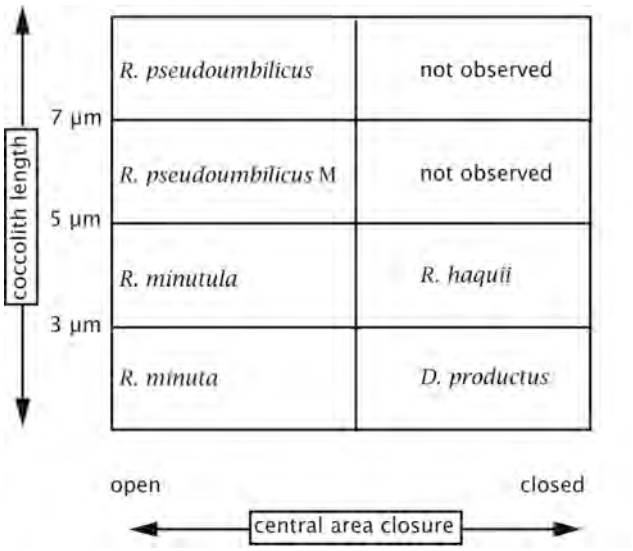

Fig. 5.4.1-1 Applied scheme of conventional taxonomic subdivision of Miocene *Reticulofenestra* coccoliths, modified for his study after Backman (1980), Flores and Sierro (1989) and Young (1990).

Reticulofenestra specimens appear in Eocene until Holocene sediments and dominate coccolith assemblages in the Neogene (Young, 1990). Several species of that genus are used as biostratigraphic index fossils (Martini, 1971; Burky, 1973) or as palaeobiogeographic indicators of palaeoenvironmental change (Haq and Lohmann, 1976; Lohmann and Carlson, 1981; Driever, 1988). Reticulofenestrid coccolith ultrastructure and morphometry are rather simple, thus usually the size of the placolith diameter and the size of the central opening are the most important morphological features used for morphological determination of species (Takayama, 1993). The modified scheme applied for *Reticulofenestra* taxonomy at Sites 1241 and 1000 is given in Fig. 5.4.1-1, specified by length of liths and structure of central area. This resulted in the distinction of *Dictyococcites productus* and *R. minuta* (1-3 µm), *R. haquii* and *R. minutula* (3-5 µm), as well as the medium form of *R. pseudoumbilicus, R. pseudoumbilicus* M (5-7 µm), and *R. pseudoumbilicus* (> 7 µm) (see also Appendix A1). Many authors (see Young, 1990) do not place coccoliths with a closed central area into a separate genus, thus the species concerned were grouped (*D. productus* / *R. minuta* - group and *R. haquii* / *R. minutula* - group respectively). Taxonomy of *R. pseudoumbilicus* is controversy discussed in literature, since for biostratigraphy it became generally accepted to base separation of that species on sizes > 7 µm (e.g. Rio et al., 1990; Raffi et al., 1995). *R. pseudoumbilicus* M is thus defined as morpho-species of *R. pseudoumbilicus* ranging from 5 to 7 µm, wheras *R. pseudoumbilicus* represents species larger than 7 µm. Detailed description of taxonomy and species identification is given in Appendix A1, ecology is discussed in chapter 3, examples of Neogene reticulofenestrids of this study are presented in plate 1 (Appendix A1-1).

Numerous authors have observed systematic patterns of size variation within this Neogene genus. Kameo and Bralower (2000) examined size distribution patterns of reticulofenestrids in order to interpret the biostratigraphic utility of changes in size. Takayama (1993) divided various *Reticulofenestra* species into four groups based on their sizes and showed

characteristic stratigraphic distribution patterns of them throughout the Neogene. Young (1990) studied microevolutionary changes within the Neogene *Reticulofenestra* through biometric analyses and defined size variation patterns of reticulofenestrids from Middle Miocene to Recent. He reported disappearance of large *Reticulofenestra pseudoumbilicus*, resulting in a 'small *Reticulofenestra* event' (SRE), where specimens larger than 5 µm virtually vanish between 8.92 and 7.1 Ma.

Biostratigraphic data of Sites 1241 and 1000 are discussed in chapter 4 of this study. Apparent limitation of biostratigraphical data due to low abundances of certain species was demonstrated for instance with the Top of the Paracme event of *R. pseudoumbilicus* (7.135-7.058 Ma). The latter has been recognized with SEM, but since frequencies of this species are rare, a precise dating of that bioevent is difficult (see chapter 4.3.1 and 4.3.2) and biometric analysis becomes even more important. Thus, due to its definition depending on lith size (*R. pseudoumbilicus* > 7 µm*)*, this bioevent can be determined in samples of the eastern equatorial Pacific Site 1241 and central Caribbean Site 1000 on the basis of morphometric analysis (Figs. 5.4.1-2 and 5.4.1-3).

At Site 1241, size variability within the *Reticulofenestra* genus displays the following pattern (Fig. 5.4.1-2): The intermediate *R. pseudoumbilicus* M is mainly represented between 7.1 and 6.3 Ma. The *R. haquii / R. minutula* - group with sizes ranging from 3 to 5 µm show highest abundances from 7.7 to 7.3 Ma and 6.2 to 5.7 Ma. Inbetween, from 7.3 to 6.7 Ma and 6.5 to 6.2 Ma, the small *D. productus / R. minuta* - group gains dominance. At Site 1000, this small reticulofenestrid group is of persistent predominance with a few subordinate peaks of the 3 to 5 µm group (Fig. 5.4.1-3). Generally, reticulofenestrids are smaller at Site 1000 than at Site 1241. A much wider range of coccolith lengths is represented at Site 1241 with sizes between 2.5 and 5.5 µm. At Site 1000 the majority of reticulofenestrid sizes range between 2.5 and 3.5 µm. Similarly larger specimens (*R. pseudoumbilicus* M) occur only infrequently at that site, whereas their quantities are more numerous at Site 1241.

The found patterns of size variations in reticulofenestrids badge in an obvious tripartition of both records (Figs. 5.4.1-4 and 5.4.1-5). Site 1241 emphasises the dominance of the 3 to 5 µm *R. haquii / R. minutula* - group between 7.7 and 7.3 Ma (interval BBP-A). Within that section an increase within the *R. haquii / R. minutula* - group size range becomes apparent, which proceeds within an interval (interval BBP-B) of generally larger lith sizes from 7.3 until 6.3 Ma. A wide range of lith sizes is present in that interval, with predominance of sizes around 3 µm until 6.7 Ma, where the increase in largest coccolith sizes contemporaneously recedes. An abrupt end of this development towards larger coccolith sizes occurs at 6.3 Ma where large liths disappear and coccoliths around 3 µm gain high abundances with an increasing trend towards slightly larger lith sizes (interval BBP-C). Generally, all three reticulofenestrid sections of Site 1241 show a tendency towards increasing lith sizes.

Measurements of reticulofenestrid coccolith lengths at Site 1000 clearly show a predominance of small *D. productus / R. minuta* - group < 3 µm from 7.3 to 6.4 Ma (interval

BBC-A) and 5.9 until 5.6 Ma (interval BBC-B). The central section (interval BBC-B) offers a wide range of liths sizes with intermediate abundances of all size classes. It is the only interval with larger reticulofenestrid coccoliths at that site.

A few control measurements were done on samples from the Final Closure Interval (Figs. 5.4.1-6 and 5.4.1-7). No dramatical size changes within *Reticulofenestra* occur. A strong dominance of the small *D. productus / R. minuta* - group is conspicuous. Larger individuals appear only sparsely.

What is obvious is the fact that reticulofenestrid coccoliths are generally smaller in the Caribbean Site 1000 compared to the Pacific Site 1241. Due to palaeoceanographic conditions, this pattern clearly supports the straightforward allometric rule, which dictates, that small cells have higher nutrient-uptake and faster growths rates than larger ones (Raven, 1998). This would explain why larger cell sizes are missing at Site 1000. Its oligotrophic conditions favour the smaller cell sizes, contrary to the generally larger sizes that appear at the more eutrophic late Miocene Site 1241 (chapter 1.1.3.3). Generally, smaller individuals during the Final Closure Interval reconfirm the advantage of small cell sizes to cope with low nutrient conditions in the Pliocene hegemonic characteristic on both sides of the isthmus (chapters 1.1.3.3 and 5).

Moreover, the overall trends in lith size variations are similar at both sites in the late Miocene, with an obvious trisection around centred size maxima (intervals B), but with a shift in the timing of these intervals between the two sites. Site 1241 proceeds with the size-steps at 7.3 and 6.4 Ma, whereas at Site 1000 similar shifts occur at 6.7 and 5.9 Ma respectively. Even since large lith sizes are not as pronounced as at Site 1241, the middle (large) Interval B is clearly detectable at Site 1000, but covers a drastically reduced time interval (0.5 Ma compared to 0.9 Ma at Site 1241). Possibly, a delay in the initiation of (the large) interval B at Site 1000 may occur due to an eastward drifting of larger species from the Pacific towards the Caribbean Sea through the Panamanian Seaway. Here, in the more oligotrophic conditions, these larger individuals would suffer from lower nutrient levels and disappear much more rapidly than in the ecological preferred niche of the eastern equatorial Pacific. This ecological preference would also support the tendency of increasing lith sizes within the three reticulofenestrid size- dependent subintervals at Site 1241.

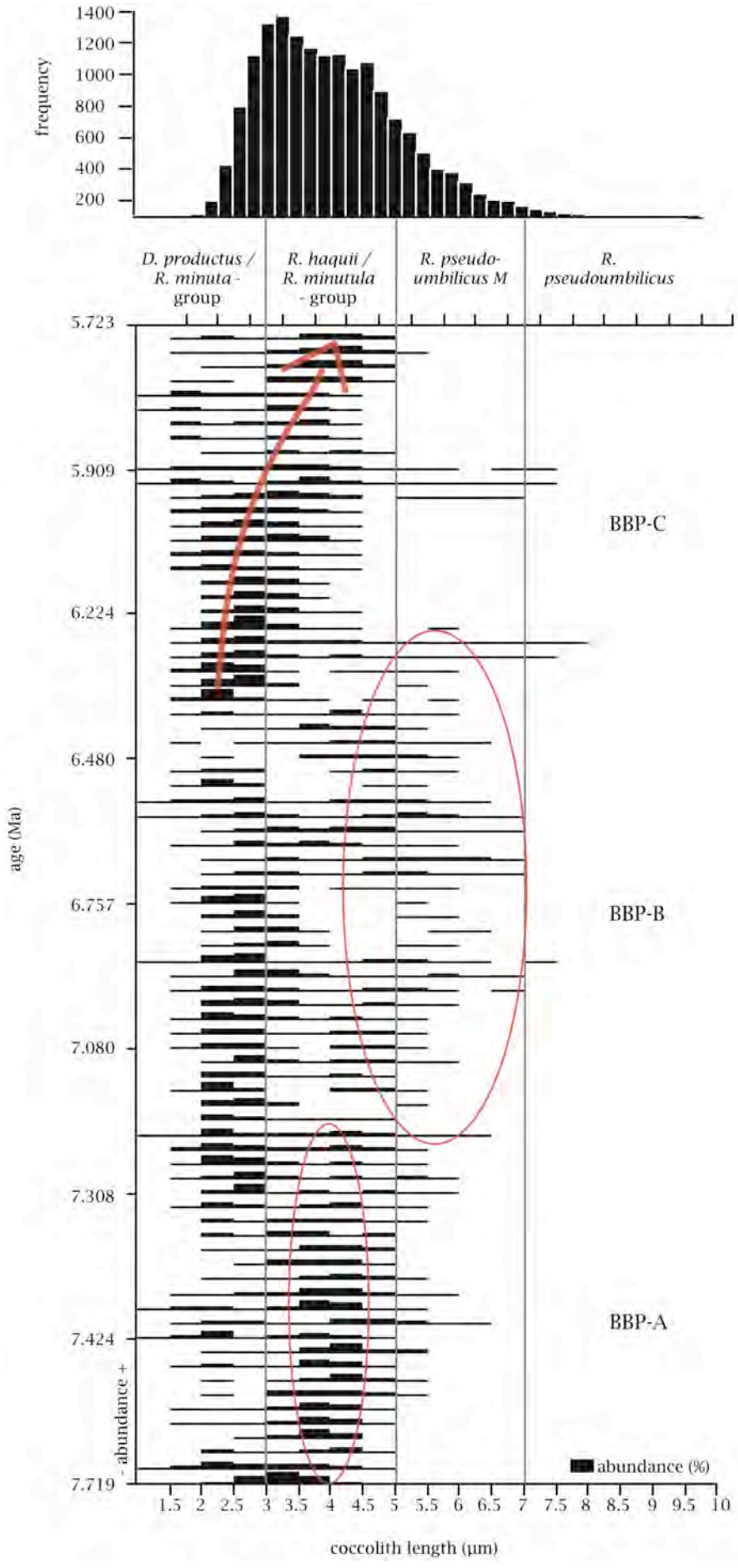

Fig. 5.4.1-2 Size distribution of *Reticulofenestra* specimens at Site 1241 during late Miocene Biogenic Bloom interval (BBP). N = 14617. Abundance of individual coccoliths shown in percentage relative to total measurements of coccoliths. Non-linear age model.

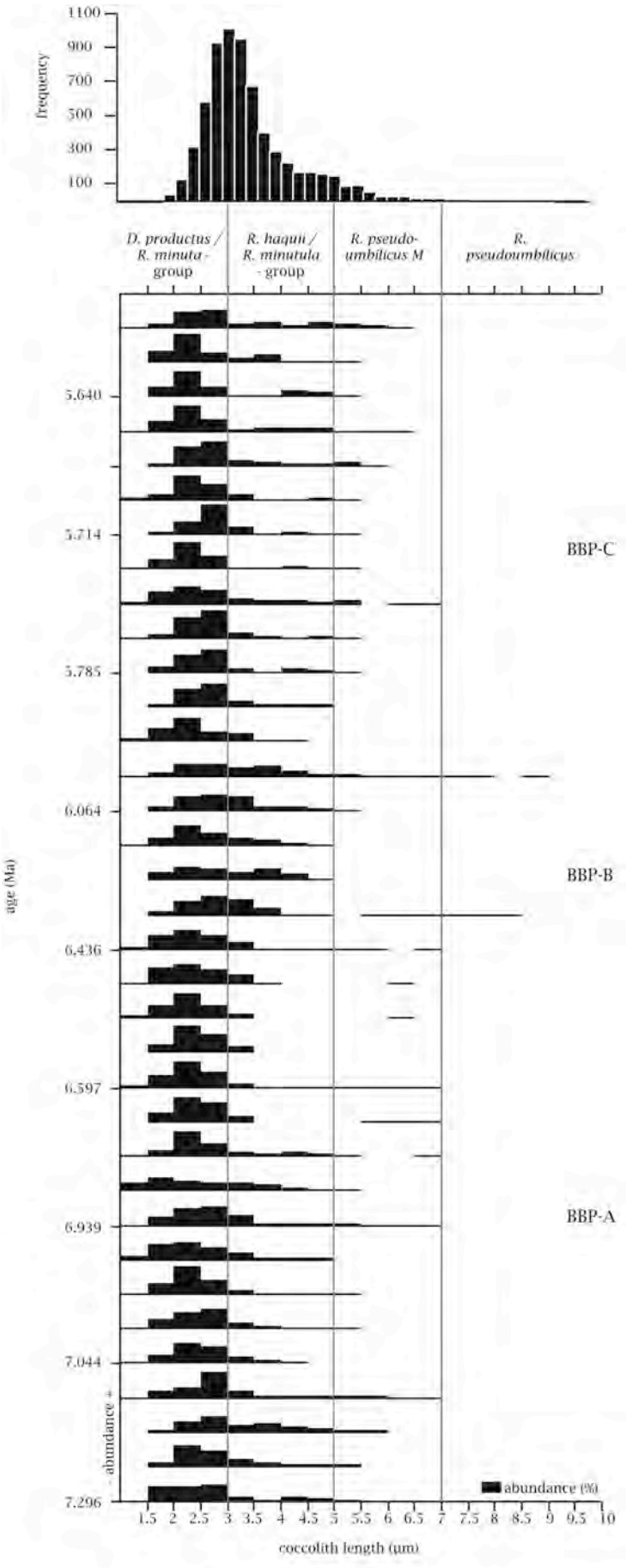

Fig. 5.4.1-3 Size distribution of *Reticulofenestra* specimens at Site 1000 during late Miocene Biogenic Bloom interval (BBC). N = 6553. Abundance of individual coccoliths shown in percentage relative to total measurements of coccoliths. Non-linear age model.

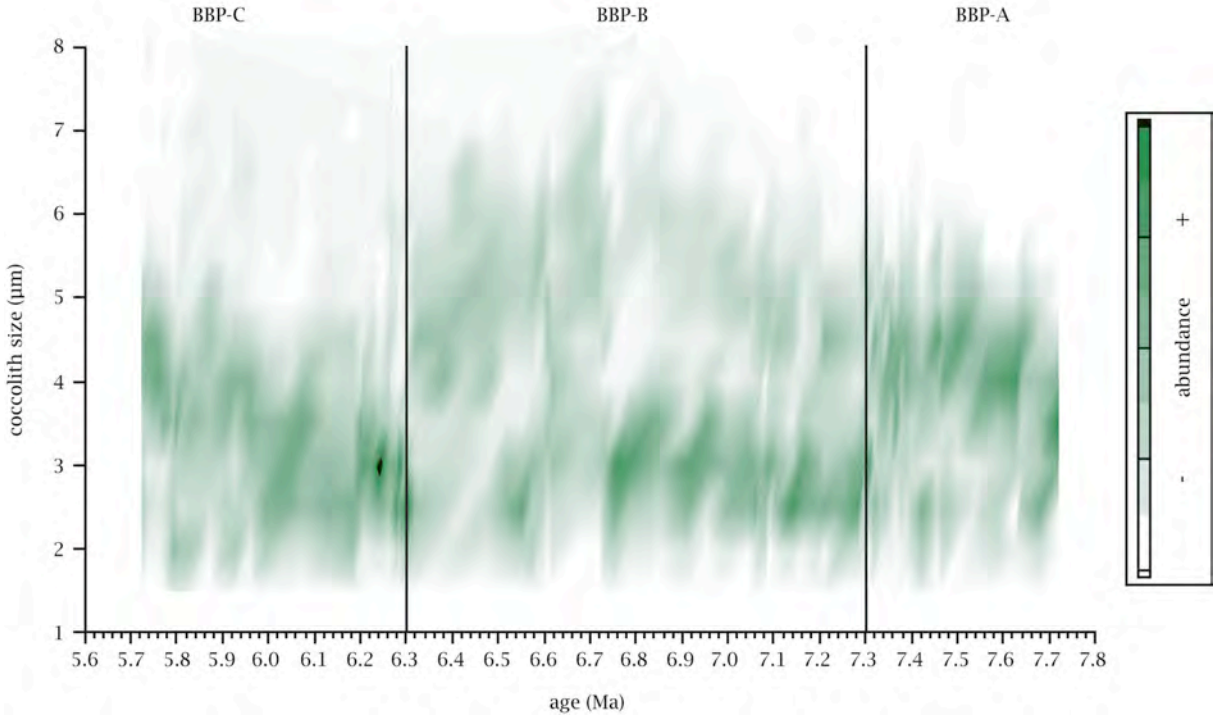

Fig. 5.4.1-4 %-abundances of coccolith size distribution of *Reticulofenestra* specimens at Site 1241 during late Miocene Biogenic Bloom interval. Partitioning into three sub-sections represented as intervals BBP-A, BBP-B and BBP-C.

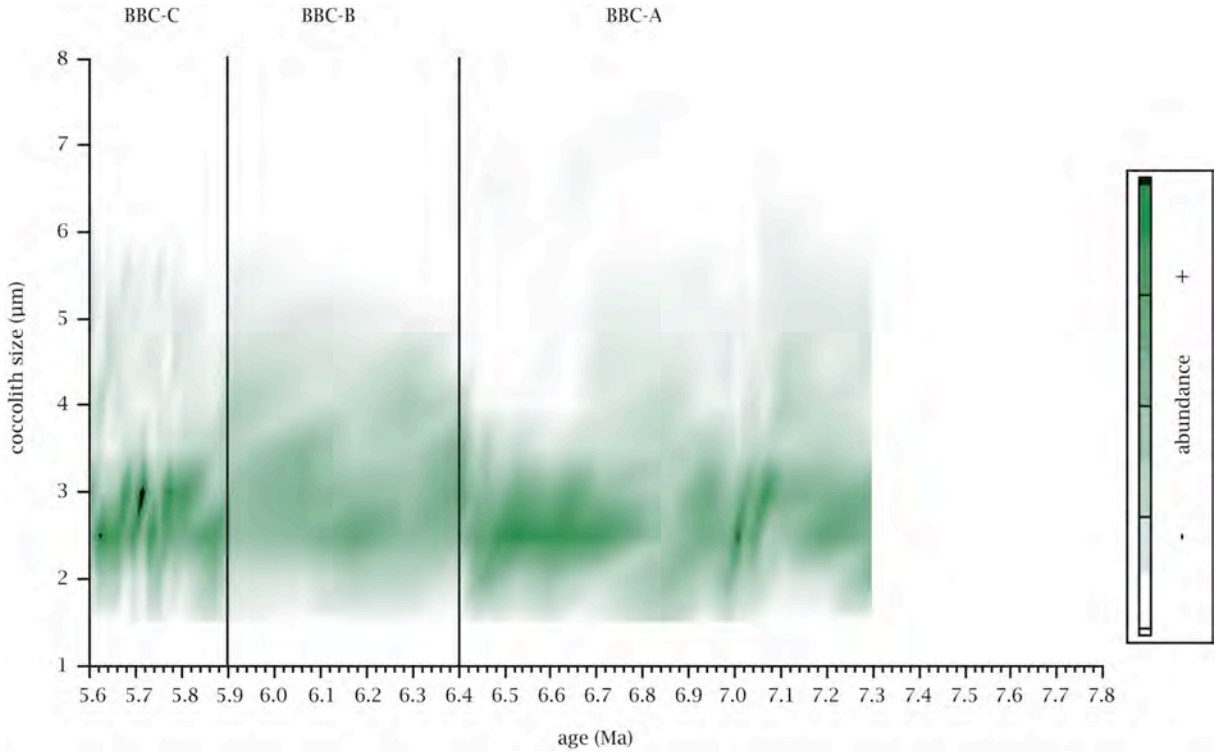

Fig. 5.4.1-5 %-abundances of coccolith size distribution of *Reticulofenestra* specimens at Site 1000 during late Miocene Biogenic Bloom interval. Partitioning into three sub-sections represented as intervals BBC-A, BBC-B and BBC-C.

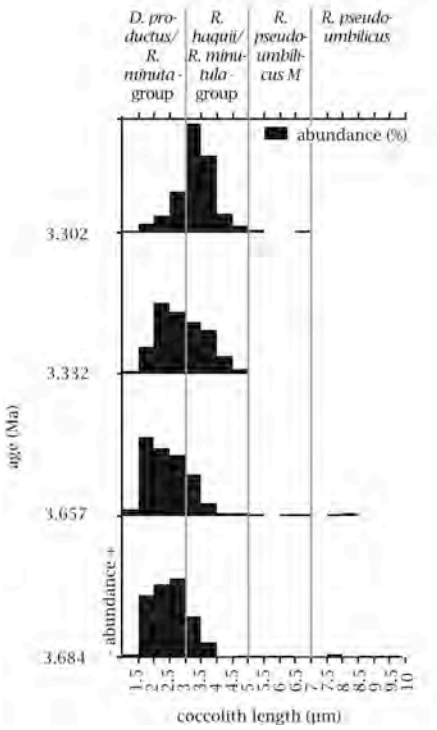

Fig. 5.4.1-6 Size distribution of *Reticulofenestra* specimens at Site 1241 during Pliocene Final Closure Interval. Abundance of individual coccoliths shown in percentage relative to total measurements of coccoliths. Non-linear age model.

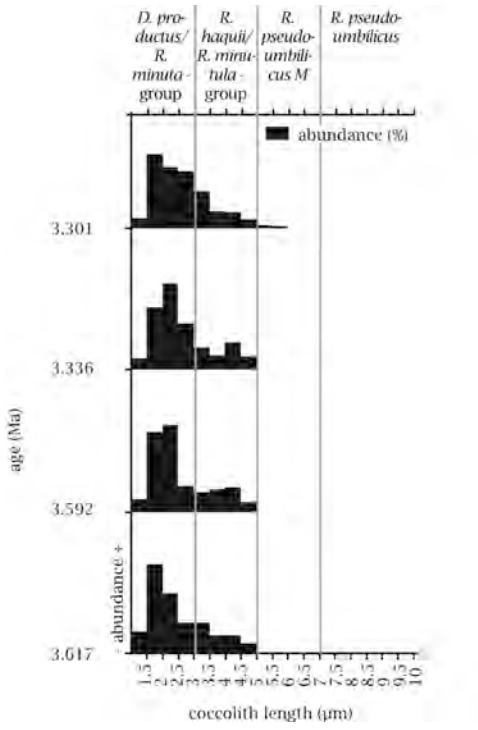

Fig. 5.4.1-7 Size distribution of *Reticulofenestra* specimens at Site 1000 during Pliocene Final Closure Interval. Abundance of individual coccoliths shown in percentage relative to total measurements of coccoliths. Non-linear age model.

5.4.2 Size variations in *Calcidiscus* coccoliths

The coccolithophorid species *Calcidiscus leptoporus* is often chosen for morphometrical studies because it has a long stratigraphic record (lowermost Miocene to Recent), is cosmopolitan today (McIntyre and Bé, 1967), successfully grown in culture (Dudley et al., 1980; Dudley et al., 1986), and shows considerable variability in morphology. Investigations of the morphological evolution of *C. leptoporus* revealed very complex microevolutionary patterns (Knappertsbusch, 2000). Using the diameter of the coccoliths and the number of elements per cycle in shields (Fig. 5.4.2-1), various authors have distinguished several morphological variants of *C. leptoporus* in both living (Knappertsbusch et al., 1997; Renaud and Klaas, 2001; Quinn et al., 2003) and fossil assemblages (McIntyre and Bé, 1967; Knappertsbusch et al., 1997; Knappertsbusch, 2000; Baumann and Sprengel, 2000; Quinn et al., 2004). The determination of these morphotypes based on diameter versus elements is still not yet firmly established because patterns within these morphotypes exhibit substantial overlap. *C. macinteyrei*, for example, a large extinct morphovariant, is considered as a separate species by stratigraphers, whereas other investigators treat it as an informal morphovariant (Knappertsbusch et al., 1997, Knappertsbusch, 2000).

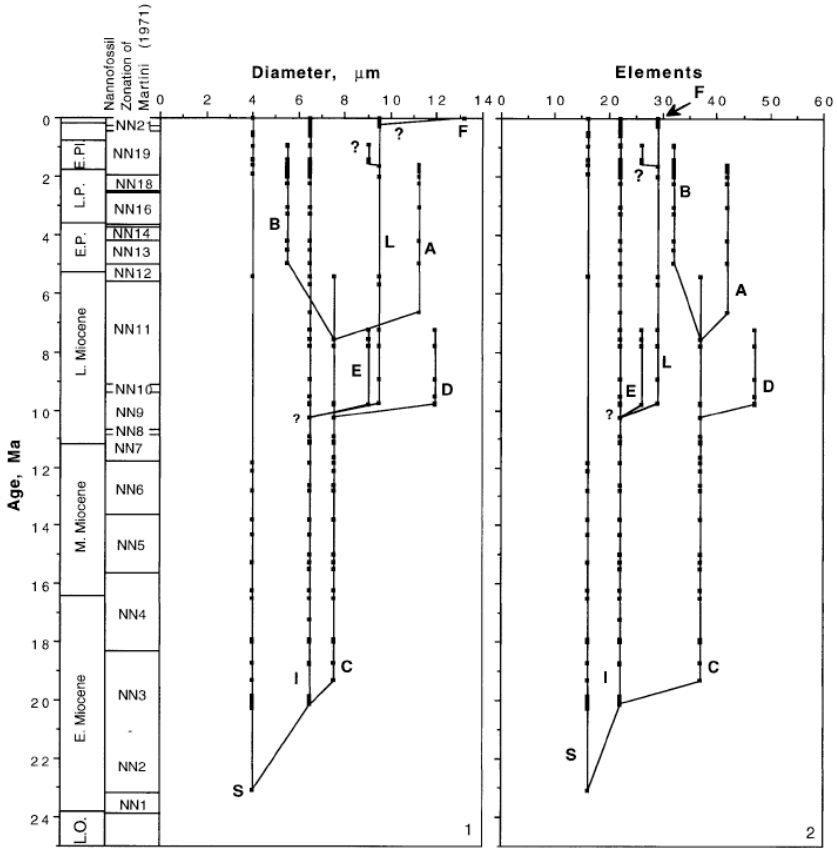

Fig. 5.4.2-1 Reconstruction of the hypothetical bivariate phylogenetic relationships among *C. leptoporus* morphotypes from Miocene to recent after Knappertsbusch (2000).
Left side: Supposed relationship between morphotypes showing evolution of diameters.
Right side: Supposed relationship between morphotypes showing evolution of elements.
From Knappertsbusch (2000).

Grouping of coccolith measurements into different morphotypes resulted in four subdivisions within the late Miocene to Pliocene samples of Site 1241 and Site 1000 identified after Knappertsbusch (2000) and Quinn et al. (2004) into *C. leptoporus* S (< 5 µm = *C. fuscus* (Janin, 1987)), *C. leptoporus* I (5-8 µm), *C. leptoporus* L (8-10 µm), *C. leptoporus* XL (> 10 µm, = *C. macintyrei* (Loeblich and Tappan, 1978)).

Generally, *Calcidiscus* spp. shows highest frequency of the intermediate (I-) type in all samples. Whereas samples of the late Miocene eastern equatorial Pacific show consistent distribution within that (I-) morphotypes (Fig. 5.4.2-2), central Caribbean samples clearly indicate a dominance of the largest coccolith size within that I-morphotype-range (Fig. 5.4.2-3). Also, the smallest *C. leptoporus* S is presented by high numbers, whereas the larger morphotypes *C. leptoporus* L and *C. leptoporus* XL are sparsely spread over samples of the observed interval. Largest individual sizes up to 12.8 µm appear in samples of Site 1241, at Site 1000 individuals reach maxima sizes of 10 µm. Clear distribution patterns or notable general trends in size changes are scarcely observable, especially due to rare measurements of individuals at Site 1000.

As seen in the size variation patterns of reticulofenestrid coccoliths, larger cell sizes occur in higher abundances at less oligotrophic conditions. Same is true with *C. leptoporus*, which shows generally larger sizes at Site 1241. Expectedly, *C. leptoporus* has generally higher abundances at Site 1241 (chapter 6), since its ecologically favoured niche in the tropical eastern Pacific offers slightly colder and less oligotrophic conditions compared to the central Caribbean Sea (chapter 1.1.3.3). Size distribution patterns of the Pliocene *C. leptoporus* morphotypes are not presented here due to rare measurements. Their temporal and spatial abundance patterns are given in chapter 6.

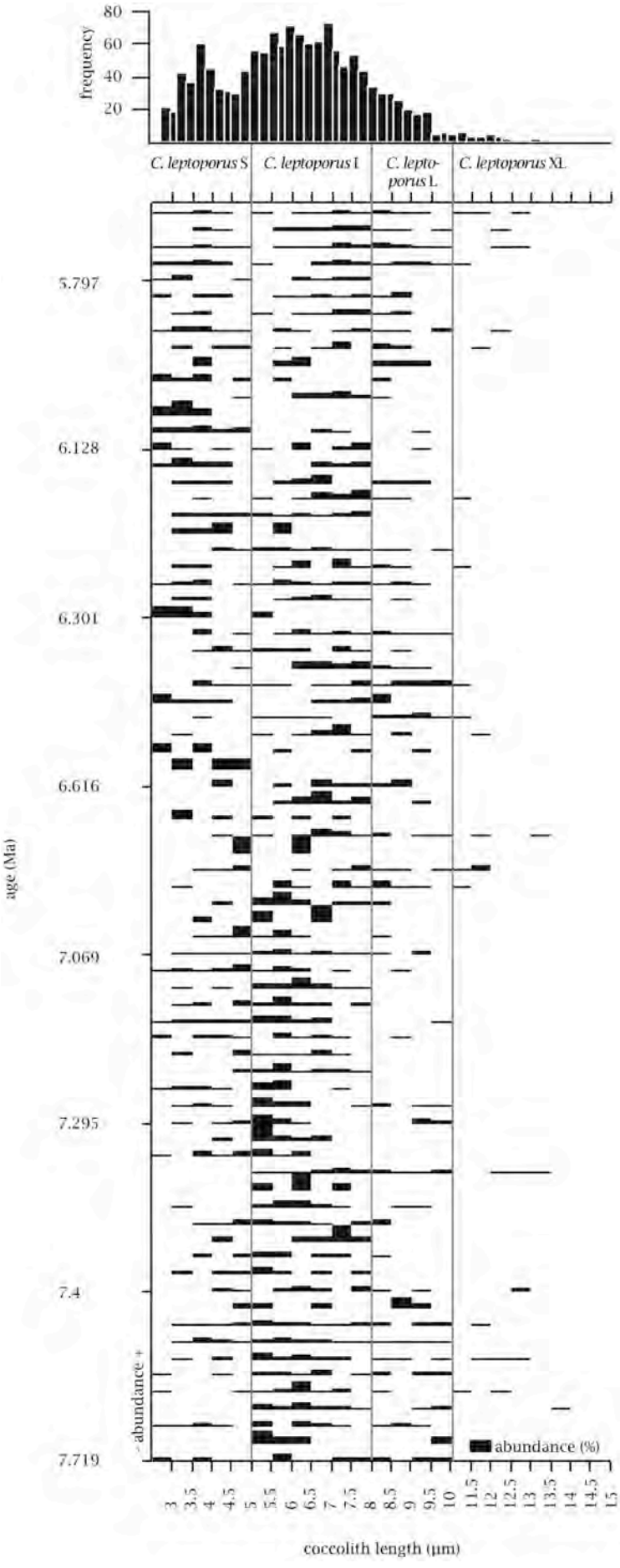

Fig. 5.4.2-2 Size distribution of *Calcidiscus* specimens at Site 1241 during late Miocene Biogenic Bloom interval. N = 1350. Abundance of individual coccoliths shown in percentage relative to total measurements of coccoliths.

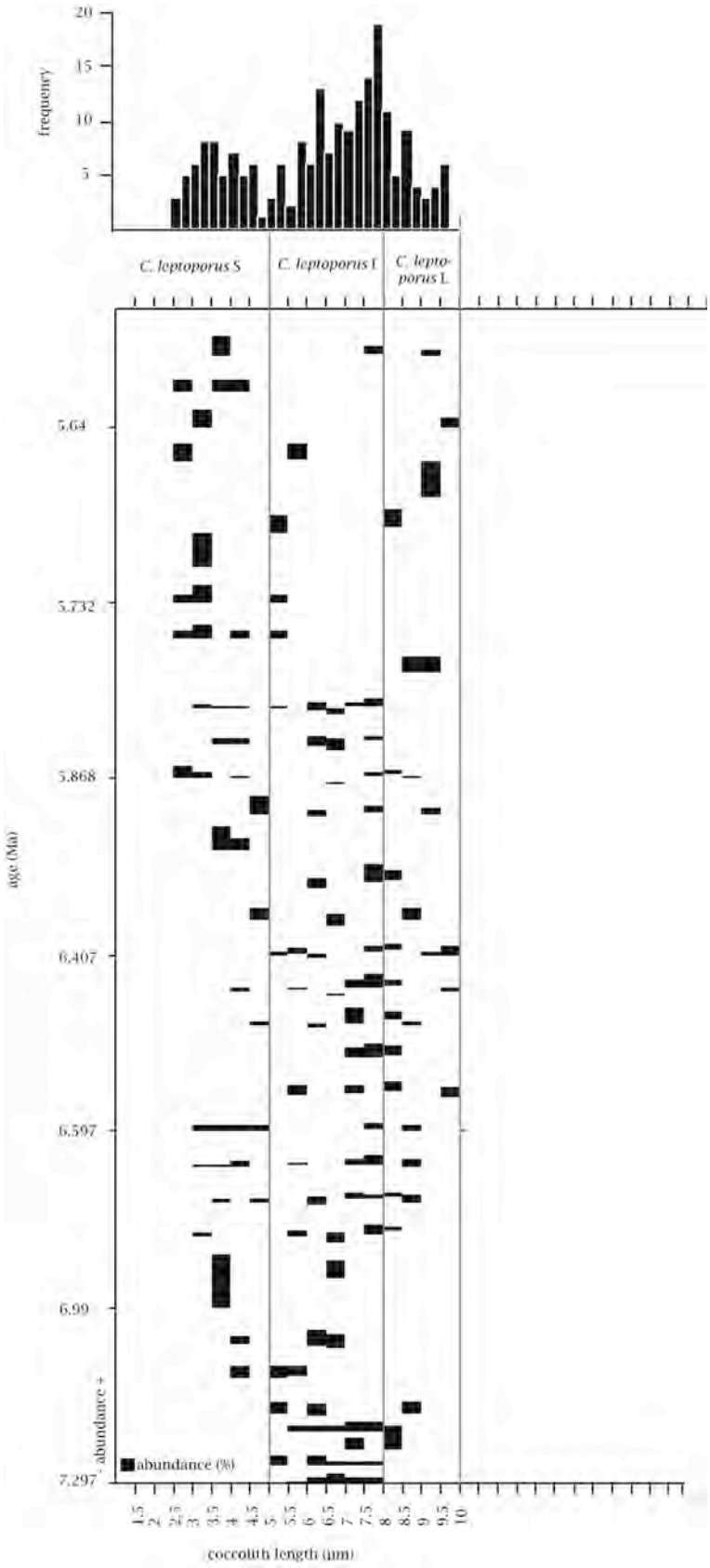

Fig. 5.4.2-3 Size distribution of *Calcidiscus* specimens at Site 1000 during late Miocene Biogenic Bloom interval. N = 212. Abundance of individual coccoliths shown in percentage relative to total measurements of coccoliths.

5.4.3 Size patterns

Schmidt et al. (2006) combined several microfossil groups in order to understand ecosystem-wide interactions of size ranges. They noted a dramatic size increase in Neogene foraminifers, highly variable size patterns in radiolarian and a reduction in size range of coccolithophores. The overall macro-evolutionary (evolutionary change at or above level of species) size decrease in coccolithophores during the Cenozoic (Bown et al., 2007; Henderiks and Pagani, 2008) is punctuated by distinct size decreases and biogeographic marginalization of major taxa in the Miocene (Henderiks, 2008b). Since then, small taxa have become more dominant.

On species level, however, data of the late Miocene to Pliocene ODP Sites 1241 and 1000 do not confirm a size reduction, neither within *Reticulofenestra* nor *Calcidiscus* (Figs. 5.4.3-1,2,3,4). During the entire observed intervals only little variability within the size patterns are noticable.

Mean sizes of coccoliths of *Reticulofenestra* slightly fluctuate around 3.55 µm at Site 1241 (Fig. 5.4.3-1), with strongly elevated values between 6.72 and 6.32 Ma. Here, a 1.65 fold mean lith size increase occurs (interval BBP-B, chapter 5.4.2). A same trend emerges within reticulofenestrid maximum lith sizes (95th percentile) at Site 1241 starting at 7.3 Ma, which points on an increase in size maxima towards younger ages, whereas the size of small coccoliths is constant (5th percentile). A two-step-change in reticulofenestrid lith sizes occurs at Site 1241, a gradual increase in maximum coccolith sizes starting at around 7.3 Ma combined with an increase in mean lith sizes between 6.7 and 6.3 Ma.

At Site 1000, *Reticulofenestra* coccoliths vary around mean sizes of 2.83 µm (Fig. 5.4.3-2). In the central Caribbean Sea, reticulofenestrids thus show distinct smaller lith sizes than in the eastern equatorial Pacific. Additionally, there is no evidence of a general increase in large lith sizes at Site 1000. Just a slight (1.4 fold) increase in mean size is observed (interval BBC-B, chapter 5.4.2) between 6.4 and 5.9 Ma, as well as a possible trend towards smaller maximum lith sizes starting at 5.9 Ma.

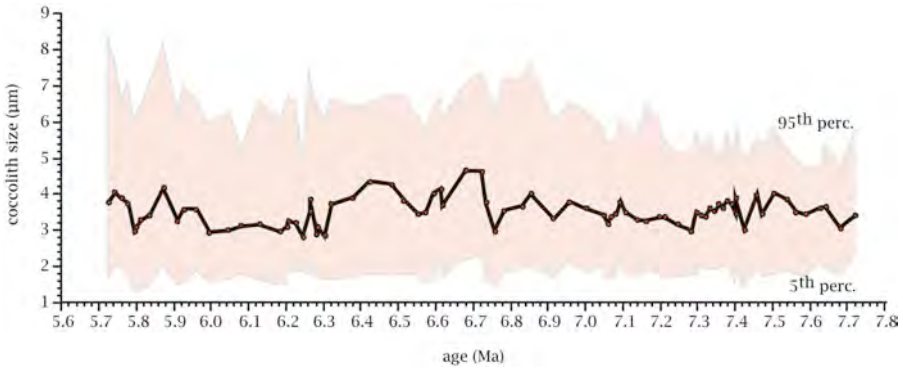

Fig. 5.4.3-1 Mean size (black line), as well as an envelope (coloured band) of 5th and 95th percentile size of reticulofenestrids at Site 1241. Mean sizes vary around 3.55 µm

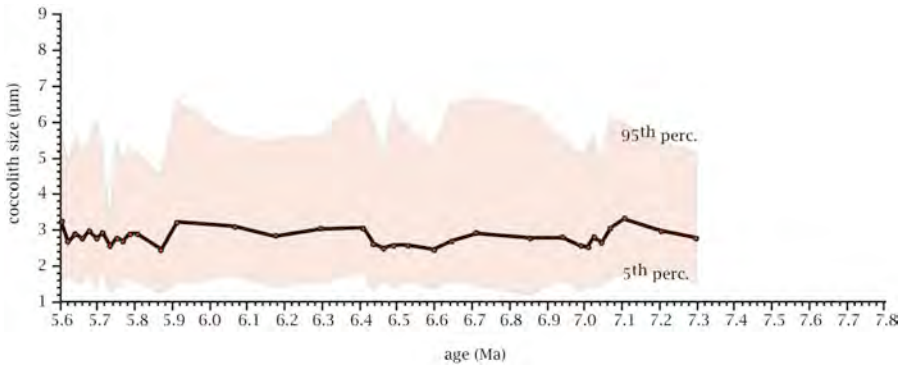

Fig. 5.4.3-2 Mean size (black line), as well as an envelope (coloured band) of 5th and 95th percentile size of reticulofenestrids at Site 1000. Mean sizes vary around 2.83 µm.

Coccoliths of *Calcidiscus* are more scarce in all observed samples, thus a calculation of percentiles is not reliable (Figs 5.4.3-3 and 5.4.3-4). In any case, *Calcidiscus* shows highly fluctuating size variabilities and no significant patterns at both sites.

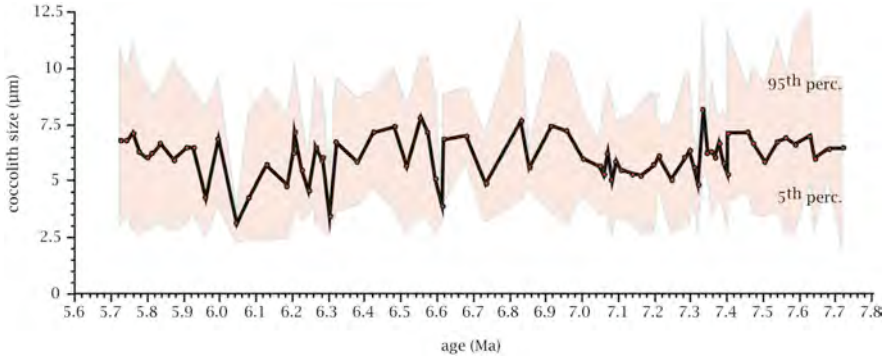

Fig. 5.4.3-3 Mean, as well as an envelope of 5th and 95th percentile size of *Calcidiscus* at Site 1241.

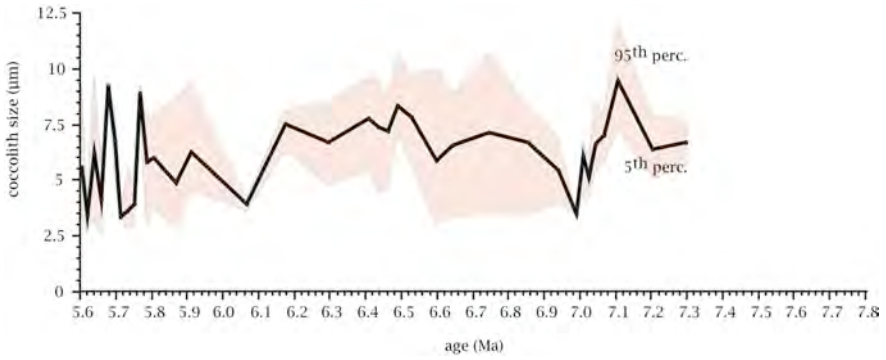

Fig. 5.4.3-4 Mean, as well as an envelope of 5th and 95th percentile size of *Calcidiscus* at Site 1000.

5.4.4 Discussion and conclusions

Morphometric analyses of late Miocene to Pliocene coccoliths of *Reticulofenestra* and *Calcidiscus* at Sites 1241 and 1000 offer distinct patterns in size distributions and variabilities that can be explained with respect to ecology- and evolution- induced changes. (1) Generally, coccoliths are smaller under oligotrophic conditions. (2) Both, *Reticulofenestra* and *Calcidiscus* show largest lith sizes in the late Miocene Pacific, benefiting from the more eutrophic conditions of that site, due to its palaeo-location closer to the equatorial divergence (chapter 1.1.3.3). The northward teconical- induced drift of the site location results in decreased reticulofenestrid lith sizes in Pliocene samples of the eastern equatorial Pacific, similar to Caribbean lith sizes. (3) In the late Miocene, the dominating reticulofenestrids show a distinct tripartition of both records, with a centered interval of larger lith sizes. These three subdivisions (4) proceed in the eastern equatorial Pacific. Additionally, their individual duration is (5) longer at Site 1241 than at Site 1000 and is (6) marked by internal lith-size increases. These patterns possibly point on a scenario related to the prevailing open-isthmus conditions in the late Miocene: Migration of large reticulofenestrids from the more eutrophic Pacific could import these large species towards the oligotrophic Caribbean Sea, but since they prefer a more eutrophic ecological niche, they disappear there within a short time range. On the other side, the more eutrophic conditions in the eastern equatorial Pacific offer the possibility of increases in species lith sizes within the individual subdivisions at Site 1241.

Overall large-scale patterns of evolution- induced changes seem to be triggered by smaller-scaled patterns of ecology- induced changes within the morphometry of late Miocene to Pliocene reticulofenestrids at Sites 1241 and 1000. The partitioning into sub-sections with gradual increases and abrupt decreases in size, combined with the different timing and duration of respective intervals at both sites, is thus initiated by ecological parameters, which affect morphometrical characteristics.

The observed overall size decrease in coccoliths during the Cenozoic (Schmidt et al. 2006; Bown et al., 2007; Henderiks and Pagani, 2008) is not observed in the late Miocene samples of Sites 1241 and 1000. The existing lack of large *Reticulofenestra* species in the Pliocene samples (Figs. 5.4.1-4 and 5.4.1-5) results in a decrease in the 95th percentile, and thus affirms the overall macro-evolutionary coccolithophorid size decrease within that single and dominating genus. But since there is no obvious general size pattern determinable within single coccolithophorid genera in the late Miocene to Pliocene interval at both investigated locations, it seems necessary to determine size variations within the entire fine-fraction. Only then it is possible to state about a general 'coccolithophorid size trend', since other authors (e.g. Schmidt et al., 2006) analysed and grouped the entire spectrum of specimens. Due to the two-step-change (change in mean sizes and change in maximum sizes), especially, its necessary to determine the temporal and spatial variations within the assemblage

compositions (chapter 6) and support this with analysis of the grain size distribution within the fine-fraction (chapter 7).

The influence of abiotic forcing on size-related evolutionary changes in planktic organisms is difficult to judge from the studies so far, since most of them have a rather crude resolution (around 1 Ma) taking into account only long term global patterns in abiotic forcing mechanisms, such as temperature. Due to their rapid turnover rates, coccolithophores should more likely be subjected to rapid (kyr) changes in abiotic forcing mechanisms. A multi-proxy approach seems necessary to evaluate driving forces for evolutionary trends with respect to all in- and external influences. Together with variations in compositions of coccolithophorid assemblages, as well as grain size analyses and stable isotopic compositions of coccoliths and foraminifers, this will be discussed in chapter 9.

CHAPTER 6 PALAEOPRODUCTIVITY

THE UPLIFT OF PANAMA AND THE CARBONATE BUDGET: THE COCCOLITH SIDE OF THE STORY

(This chapter is a manuscript in preparation for Palaeogeography, Palaeoclimatology, Palaeoecology. Minor text modifications have been made.)

6.1 Introduction

The Miocene to Pliocene was a period of transition in global climate and ocean circulation systems associated with major turnovers in marine and terrestrial biota and changes in biological productivity. The climate system was affected by expansion of Antarctic ice sheets, cooling of surface and deep water masses, aridification of continents, as well as tectonic processes leading to the uplift of the Tibetan Plateau and Himalayas and emergence of the Panamanian Isthmus (Shackleton and Kennett, 1975b; Kroon et al., 1991; Prell and Kutzbach, 1992; Raymo and Ruddiman, 1992; Hodell et al., 1994; Cerling, 1997; Haug and Tiedemann, 1998; Pagani et al., 1999; Pagani et al., 2000; Haug et al., 2001b; Qiang et al., 2001; Zachos et al., 2001a; Retallack et al., 2002). In particular, the Panamanian Seaway acted as a critical threshold in late Neogene ocean circulation patterns, with strong impact on climate and plankton evolution. The shoaling of the seaway is responsible for changes in the Atlantic and Pacific deep and surface water circulation regime and the intensification of the thermohaline circulation in the North Atlantic due to increasing salt and heat transport to high northern latitudes (Maier-Reimer et al., 1990; Haug and Tiedemann, 1998; Billups et al., 1999; Haug et al., 2001a; Nisancioglu et al., 2003). Thus, this region may play an important role in the initiation of the northern hemisphere glaciation, which started during the Mid-Pliocene (Driscoll and Haug, 1998; Haug and Tiedemann, 1998).

Geographical and temporal distribution as well as biostratigraphic studies of micro- and nannofossil assemblages provide evidence of profound changes in Neogene circulation patterns associated with the uplift of Panama (Keigwin, 1978; Gartner et al., 1987; Keller et al., 1989; McDougall, 1996; Kameo and Sato, 2000; Kameo, 2002). In order to reconstruct these changes we investigated Neogene coccolithophorid assemblages on both sides of the Isthmus with respect to palaeoproductivity.

Coccolithophores are a major group of marine, unicellular phytoplankton. They have a great potential as a tool for palaeoceanographic reconstructions since they hold a unique role in the global carbon cycle. This is because of their combined effect on both the organic carbon and the carbonate pump (Bown and Young, 1998; Baumann, 2004; Baumann et al., 2004; Baumann et al., 2005). Due to their great abundances, fast turnover rates, and their capability to carry out photosynthesis and calcification these haptophyte algae are significant components of the Earth's biogeochemical cycles (Bown and Young, 1998). As main open-ocean primary producers coccolithophores strongly influence marine pelagic biogeochemistry and the marine ecosystem (Winter and Siesser, 1994; Bown et al., 1998). Their minute external calcite scales, the coccoliths, constitute one of the most important

components of deep-sea sediments. Thus, the exceptional fossil record of coccolithophores preserves remarkable signals for interpreting global change in the geological record. From a quantitative point of view, coccolithophores are the most important pelagic calcifying organisms in the modern ocean (Baumann et al., 2004; Hay, 2004). Estimations on the relative contribution of different calcifying organisms to the global pelagic marine carbonate production suggest, that about 20-60 % is provided by coccoliths (Milliman, 1993; Steinmetz, 1994; Baumann et al., 2004).

We did a multi-proxy approach to quantify the contribution of coccolithophorid carbonate to pelagic sediment. Volume estimations were combined with grain size analyses to respect palaeoecological changes. We aim to interpret the different patterns in relation to gradual changing oceanographic settings. Here we focus on coccolithophorid assemblages on both sides of the Panamanian Seaway before and during the phase of its final closure. We chose two ODP cores, Site 1241 on the Cocos Ridge on the Pacific side off Panama, and Site 1000 in the central Caribbean Sea and analysed samples of the late Miocene (about 7.5–5.5 Ma), when the Isthmus was still open, and of the final closure interval in the late to middle Pliocene (3.3–3.7 Ma). Special focus was placed on the late Miocene, the so called 'Biogenic Bloom' interval (Farrell et al., 1995b), a period where sediments from all ocean basins contain evidence for enhanced accumulation of biogenic components. Extraordinarily high biogenic carbonate accumulation rates in this interval have been described from the Atlantic (Hermoyian and Owen, 2001; Diester-Haass et al., 2004; Diester Haass et al., 2005), the Pacific (Farrell et al., 1995b; Lyle et al., 1995; Grant and Dickens, 2002; Lyle, 2003) and the Indian Ocean (Peterson et al., 1992; Berger et al., 1993; Dickens and Owen, 1999; Hermoyian and Owen, 2001). Surface water productivity increased significantly (Peterson et al., 1992; Berger et al., 1993; Delaney and Filippelli, 1994; Dickens and Owen, 1994), implying a fundamental change in global nutrient cycling. This is supported by proxy-records of enhanced palaeoproductivity (carbonate MARs, biogenic silica, phosphorus, faunal assemblages) and proxies for lower dissolved oxygen at intermediate depth (benthic faunal assemblages, benthic carbon isotopes, manganese fluxes and Mn/Sc ratios). Two possible scenarios are thought to be responsible for that increase in productivity: (1) A global increase in nutrient supply to the oceans possibly related to enhanced continental weathering due to tectonic uplift processes (e.g. Filippelli and Delaney, 1994; Farrell et al., 1995a; Hermoyian and Owen, 2001; Gupta et al., 2004), and/or (2) a redistribution of nutrients within the ocean due to circulation changes (basin-basin-fractionation; Berger et al., 1993; Dickens and Owen, 1994, 1999; Schneider and Schmittner, 2006). Hermoyian and Owen (2001) detected the Biogenic Bloom signal in several low-productivity areas, clearly demonstrating that this event is of global nature and not the result of nutrient redistribution between different ocean areas or enhanced upwelling. Grant and Dickens (2002), however, pointed out the complexity of the Biogenic Bloom for regional water mass changes and

vertical mass structure. This was supported by Diester-Haass et al. (2005) who found timing discrepancy of the global extent of the Biogenic Bloom.

In order to test these hypotheses, we questioned the mechanisms of the Biogenic Bloom event to evaluate patterns within changing oceanographic regimes related to the closure of the Panamanian Isthmus. There is no information available to what extent the change in productivity due to changes in certain calcareous plankton groups had an impact on the observed patterns. Thus we focused on one of the most important producers of calcium carbonate, the coccolithophores to define (1) the contribution of coccoliths to the Biogenic Bloom, (2) the link between the prominent trends in carbonate accumulation rates and evolutionary/ecological changes in calcareous marine nannoplankton, and (3) implications of temporal and spatial changes concerning one of the most prominent events during the late Neogene: the closure of Panamanian Seaway.

6.2 Materials and methods

6.2.1 ODP samples

ODP Site 1241

Sediment records obtained during Leg 202 provide a palaeoceanographic transect to assess climate and oceanographic changes in the southeast Pacific over Neogene time. The tropical east Pacific ODP Site 1241 was drilled during that Leg at 5°50N, 86°26´W in the Guatemala Basin on the north flank of Cocos Ridge at 2027 m water depth (Mix, Tiedemann, Blum et al., 2003a). Tectonic backtracking of today's position on the Cocos Ridge moves Site 1241 southwestward (around 4°N, 87°10´W at 3 Ma; 1,5°N, 89°30´W at 7.5 Ma) (after Pisias et al., 1995). During the investigated time intervals, Site 1241 was probably located close to the equator and probably at shallower depth. The observed sediments are composed of foraminifera-bearing nannofossil oozes. Due to its relatively shallow depth, preservation of the calcareous nannoplankton at Site 1241 is excellent. As proposed by Lyle et al. (1995), the carbonate compensation depth in the Guatemala Basin was established in a depth of about 3400 m from 10 Ma onward, with maximum deepening toward modern values of 3600 m in the Plio-Pleistocene.

ODP Site 1000

The Central Caribbean ODP Site 1000 was obtained during Leg 165. It is situated at 16°33´N, 79°52´W within the Pedro Channel on the Northern Nicaraguan Rise at 916 m water depth (Sigurdsson, Lecki, Acton et al. 1997). Sediments deposited during the investigated time intervals are a mixture of pelagic and bank-derived neritic carbonates. The shallow-water depth of the site in comparison with the depth of the modern lysocline at 4000 m (Archer, 1996) implies that carbonate dissolution is negligible and samples show an excellent preservation of calcareous micro- and nannofossils. Fragile structures of coccoliths and even delicate holococcoliths are well preserved in all samples.

6.2.2 Samples and observed time intervals

For nannofossil distribution, a total of 650 samples were examined to cover two different time intervals at both sites.

The older interval includes the Biogenic Bloom period around 7.7-5.5 Ma, and represents the conditions with an open Panamanian Seaway. From the Pacific Site 1241 (273-176 mcd), samples were taken every 50 cm in the lower, and every 100 cm in the upper part due to a supposed change in sedimentation rate (Mix, Tiedemann, Blum et al., 2003a). The time resolution is around 13.5 kyr. Caribbean Site 1000 has a sampling interval of consistently 50 cm (278-175 mbsf) for the Biogenic Bloom, reflecting a temporal resolution of ~ 11.5 kyr. (future labelled as sample code BBP and BBC respectively)

The younger time interval covers the final phase of the closure of the Panamanian Gateway in the Pliocene. In this interval (about 3.7 to 3.3 Ma) samples were taken every 10 cm, resulting in a time resolution of better than 3 kyr at both, the Pacific and the Caribbean site. (future labelled as sample code FCP and FCC respectively)

A sampling gap exists at Site 1241 between Hole A Core 9 Transect H Section 7 and Hole A Core 10 Transect H Section 2, which causes a gap in the Pacific record from 3.5475 to 3.4576 Ma.

Sand content was determined via sieve analysis, for the younger time interval FCP and FCC by Steph (2005), and by T. Bickert, University of Bremen, for the BBC (pers. com.). Carbonate measurements were carried out with a ™LECO-CS 125-analyser by Steph (2005) for the Pliocene interval. Carbonate contents for the older interval BBP and BBC were provided by ODP (http://iodp.tamu.edu /janusweb/links/ links_all. shtml).

All sediment samples were freeze-dried before qualitative and quantitative examination.

6.2.3 Age models

Astronomically tuned age models were constructed by matching patterns of cyclic variation in climate proxy records with patterns of changes in solar radiation that are controlled by cyclic variations in Earth's orbital parameters (Steph, 2005).

The age models of tropical east Pacific Site 1241 and central Caribbean Site 1000 are based on tuning high frequency variations in GRA density, percent sand of carbonate fraction and benthic $\delta^{13}C$ to the orbital solution of Laskar et al. (1993) and benthic and planktonic $\delta^{18}O$ records. These astronomically derived age models are in agreement with the most recent astronomical polarity time scale (Lisiecki and Raymo, 2005) and with other recent orbitally tuned age models (e.g. Tiedemann and Franz, 1997; Site 1237, R. Tiedemann, unpubl. data). The establishment of the age models are described in detail by Sturm (unpublished data) (and chapter 1.1.2) for Site 1241 from 7.7–5.7 Ma and Tiedemann et al. (2007) from 5.5–2.5 Ma, and for Site 1000 by Bickert (unpublished data) from 8–5.5 Ma, and Steph et al. (2006a) from 5.5–2.5 Ma.

6.2.4 Calcareous nannofossil quantification

The determination of absolute and relative coccolithophore abundances was carried out with Scanning Electron Microscopy (SEM). Samples were prepared with the combined dilution/filtration technique of Backman and Shackleton (1983) and the improved method of Andruleit (1996) as standard preparation for SEM samples (chapter 2.2). SEM investigation was done with a ™CamScan 44 at Institute for Geosciences, University of Kiel at a magnification of 5000 x. Taxonomic identification follows Farinacci (1969), Perch-Nielsen (1985a), Jordan and Kleijne (1994), Young (1998) and Young et al. (2003) as given in Appendix A2. About 300-600 individual liths per sample were counted, according to Dennison and Hay (1967) having a probability of failure of 5-0.5 % in detecting all species with proportions over 1 %. Since the number of specimens counted per unit area is approximately proportional to the selected species per gram sediment (Backman and Shackleton, 1983), the analysis of species composition and abundances on a measured transect leads to the calculation of coccolith absolute abundances (see Andruleit, 1996; Boeckel and Baumann, 2004) (chapter 2.2.2). Quantification of the contribution of single taxa to coccolith carbonate was calculated by using the mass equation of Young and Ziveri (2000). These calculations give weight-percentages of coccolith carbonate build up from species with available shape factors (Young and Ziveri, 2000). Extrapolation permits a 'calculated' indication of total weight percent of coccolith carbonate, which is used as 'coccolith carbonate (wt %)' in this study. We used the calculated shape factors for single species (k_s) given in Young and Ziveri (2000) and Beaufort and Heussner (1999). The measurements of coccolith lengths, needed for coccolith mass calculations, was done using digital photos of a ™Leitz-AMR 1200 SEM working with Spektrum mono 2.00 and analysed with the Program ImageJ 1.36 (available free on web: http://rsb.info.nih.gov/ij/). Hence for each sample a discrete calculation of species-specific volume calculation was carried out. For the calculation of mass fluxes and coccolith accumulation rates, formulas were used represented in detail in Lototskaya et al. (1998), Ziveri et al. (2000) and Ziveri and Thunell (2000) (chapter 2.2.2).

There are significant sources of uncertainty in these calculations: the calculation of shape factors, the application of these shape factors on species which have not explicitly been determined by Young and Ziveri (2000) as well as the indispensable measurement of length (see chapter 6.4.1). Both, absolute and relative abundances are discussed, because absolute abundances may be biased by changes in sedimentation processes in addition to changes in the primary production (Beaufort and Heussner, 1999). However, our data appear to be reasonable in comparison to all relations and therefore are expected to be a good approximation for the real nannofossil carbonate content.

In this paper we examined abundances and mass fluxes of species, which are important for palaeoproductivity. Thus, focus was laid on abundance and accumulation patterns of a high productivity group (*Reticulofenestra* spp., small *Gephyrocapsa* ssp., *Umbilicosphaera* spp.)

and a low productivity group (*F. profunda*, *G. flabellatus*, *S. abies*, *Discoaster* spp., *R. clavigera*, *D. tubifera*) as well as patterns of massive carbonate producers like *C. leptoporus*, *C. pelagicus* and *Helicosphaera*.

6.2.5 Sedimentological grain size analyses

For grain size analyses, measurements were made on a total of 210 samples from both sites on which also assemblage counts at the SEM were conducted. Laser diffraction was carried out with a ™FRITSCH analysette 22 NanoTec Laser Particle Sizer (Fritsch GmbH, Idar Oberstein, Germany) at IFM-GEOMAR Kiel. The Laser Particle Sizer is based on the system of low-angle laser light scattering (LALLS), i.e., the diffraction of scattered light caused by particles passing through a laser beam. The ™FRITSCH analysette 22 uses a HeNe laser (wavelength λ = 632.8 nm) with reversed Fourier-Optic and model-independent evaluation by Fraunhofer theory (Pabst et al., 2000; Gregorova et al., 2006). No separate sample preparation was necessary prior to measurement, since complete dispersion can be achieved by applying the built-in ultrasonification unit. The laser scattering light claims a working range in wet dispersion from 0.01 to 2000 µm. The suspension is pumped through a sample cell placed in the convergent laser beam, the foreward scattered light falls on the photosensitive sensor rings. For considerably high resolution we selected the multiple measurement with a measuring range of 204 channels with 200 scans each. Turbulent flow through the measuring cell guarantees a statistical distribution of particles (pers. com. C. Berthold, University of Tübingen); reproducibility of the Laser Particle Sizer measurements is high. A detailed discussion about laser grain size analysis and its use in micropalaeontology is given in chapter 7.

As introduced by Stuut et al. (2002b), we used a log-ratio of the relative abundances of the two fractions to correlate coccolith dominance with other fragments. We defined this Coccolith Carbonate Index (CCI) as 'CCI-coarse', where faction A was considered as 2-10 µm and fraction B as 10-63 µm (after Robinson and McCave, 1994) to relate between the coccolith-fraction and the foraminiferal plus biosilicious fossil fragments. 'CCI-fine' is defined as log-ratio between 2-10 µm and < 2 µm to express the dominance of coccoliths against the clay fraction.

6.3 Results

6.3.1 Total abundances Fig. 6.3-1A-D(1)

Numbers of total calcareous nannoplankton liths in all samples vary amounting to giga (10^9) individual coccoliths per gram sediment. During the Biogenic Bloom interval (7.7-5.5 Ma) mean value of total liths is about 20 $\times 10^9 \times g_{sediment}^{-1}$ in the Pacific and 24.2 $\times 10^9 \times g_{sediment}^{-1}$ in the Caribbean Sea. Average values shift towards higher data from 6.3 Ma onward with the maximum of > 40 $\times 10^9$ at the Pacific site. At the Caribbean site, highest values of up to 38 $\times 10^9$ occur during the Biogenic Bloom interval after 6.1 Ma.

The absolute number of liths deposited during the Final Closure Interval (3.7-3.3 Ma) is 24.8×10^9 individual coccoliths per gram sediment in the Pacific, and $14.7 \times 10^9 \times g_{sediment}^{-1}$ in the Caribbean Sea.

6.3.2 Coccolith carbonate Fig. 6.3-1A-D(2)

Calculated weight percentages of coccolith carbonate strongly fluctuate over all observed intervals and never exceed 50 %. The proportion of carbonate produced by coccoliths in the late Miocene shows mean values of 25.7 % in the Pacific and 21.7 % in the Caribbean Sea. The ratio of coccolith carbonate in the Pliocene samples shows mean values around 26 % in the Pacific and 14 % in the Caribbean Sea.

6.3.3 Species abundances Fig. 6.3-1A-D(3)

All samples show a predominance of *Reticulofenestra* spp. Other important species at Site 1241 are *Florisphaera profunda*, *Sphenolithus abies*, *Discoaster* spp., *Calcidiscus* spp., *Umbilicosphaera* spp., *Coccolithus pelagicus* and *Helicosphaera* spp. At Site 1000, *Florisphaera profunda* is quite abundant, as well as *Sphenolithus abies*, *Discoaster* spp. and *Rhabdosphaera clavigera*. Another important group is *Umbilicosphaera* spp., whereas *Calcidiscus* spp., *Coccolithus pelagicus*, *Helicosphaera* spp., *Syracosphaera* spp. and *Scyphosphaera apsteinii* are of minor importance. In the Pliocene, up to one forth of the assemblages are represented by the Lower Photic Zone taxa (LPZ), *Florisphaera profunda* and *Gladiolithus flabellatus*. Further contributors to the assemblage are *Umbilicosphaera* spp., *Calcidiscus* spp., *Helicosphaera* spp. and *Syracosphaera* spp.. *F. profunda* and (negligible) *G. flabellatus* together with *S. abies*, *Discoaster* spp., *Rhabdosphaera clavigera* and *Discosphaera tubifera* were grouped as Low Productivity Indicator Taxa (LPI) (see chapter 3, Appendix A2-2).

6.3.3.1 Biogenic Bloom interval, Pacific Site 1241 Fig. 6.3-1A(3)

Reticulofenestrids

Relative abundances of *Reticulofenestra* vary from 41.7 to 85.6 % (mean 70 %). The general trend shows a pronounced shift towards lower values in the younger part, at about 6.2 Ma. The small-sized *D. productus/R. minuta*-group shows abundances from 4.1 to 72.4 %. The generally high values, (> 40 %), drop towards values (< 10 %) at 5.92 Ma. The *R. haquii/R. minutula*-group shows fluctuating values with an overall increasing trend. *R. pseudoumbilicus* medium shows highest values prior to the end of the paracme of *R. pseudoumbilicus* at 7.1 Ma, but never reaches significant abundances, neither does *R. pseudoumbilicus*. This largest reticulofenestrid species never exceeds abundances of 2 %.

Low Productivity Indicators

The taxa of the lower photic zone (LPZ), *S. abies* and *Discoaster* spp. hold values from 7.4 to 39.1 %. LPZ taxa show strongly fluctuating abundances around a mean value of 9.3 % (2.3-

24.8 %. The values of *S. abies* gently increase from around 5 % (until 6.61 Ma) up to 25 % (5.7 Ma). *Discoaster* spp. range over the complete interval, they show small peaks in abundances up to 8 %, but no noticeable trends.

Others

All remaining species occur with 3.6-29.6 %, of which *Coccolithus* spp. reaches mean values of 5.5 % (1.1-26.2 %), *Umbilicosphaera* spp. 3 % (max. 14.7 %), *C. pelagicus* 0.9 % (max. 4.1 %) and *Helicosphaera* spp. 0.57 % (max. 2.4 %).

6.3.3.2 Biogenic Bloom interval, Caribbean Site 1000 Fig. 6.3-1B(3)

Reticulofenestrids

Abundances of *Reticulofenestra* spp. vary between 30.4 and 73 % (mean 52.2 %). Low values (< 50 %) are only observable in the middle part of the interval between 6.95 and 5.88 Ma. The *D. productus/R. minuta*-group shows highly fluctuating values between 18.3 % and 55.7 %. The S-shaped trend shows higher values between 6.95 and 6.5 Ma and again from 5.85 Ma onwards. The abundances of the *R. haquii/R. minutula*-group range from 2.7 % to 31.5 %. A decreasing trend towards lowest values at 6.78 Ma is followed by a slight increase of values similar to previous ones. The *R. pseudoumbilicus* (including the medium form) generally occurs in low frequency, below 7 %. Abundances of reticulofenestrids are in average two-fold higher in the older than in the younger part.

Low Productivity Indicators

F. profunda, S. abies, *Discoaster* spp. and *R. clavigera* exhibit abundances of 18.6-54 %. Their record shows lower values in the older part, and higher, more fluctuating values in the younger part. This trend follows the abundance patterns of *F. profunda* with values between 12.4 and 41.9 % with *S. abies* (3.4-15.8 %), *Discoaster* spp. (max 4.4 %) and *R. clavigera* (max 3 %).

Umbilicosphaera

U. jafari and *U. rotula* show abundances between 2.6 and 17.5 %. The values show a stepwise decrease with higher values before 6.95 Ma, and lowest values from 6.14Ma onward.

Others

All remaining species build 0.5–13.3 % of the total assemblage, of which *Calcidiscus* spp. and *Helicosphaera* spp. show the highest values but each never exceed 3 %. *Syracosphaera* spp., *Pontosphaera* spp. and *S. apsteinii* hold negligible values, *Syacosphaera* spp. show a single strong peak around 6.42 Ma.

6.3.3.3 Final Closure interval, Pacific Site 1241 Fig. 6.3-1C(3)

Reticulofenestrids

Reticulofenestra spp. contribute with 58.8 % of the coccolithophorid assemblage. Abundances start with 46 % in the oldest part. After a slight increase towards maximum values of up to 76 % at 3.385 Ma, abundances drop continuously below the mean value. *D. productus/R. minuta* dominate the reticulofenestrids with 17.5–48.5 %. *R. haquii/R. minutula* occur with 2-16.6 % and *R. pseudoumbilicus* shows values of 4–21.4 %.

Small *Gephyrocaspa* spp. occur, but in negligible quantities (< 2.5 %).

Low Productivity Indicators

The low productivity indicators *F. profunda, S. abies* and *Discoaster* spp. together build around 25.6 % of the assemblage. The dominant species in this group is *F. profunda* with abundances between 12.9 and 35 %. *S. abies* has high abundances up to 11.5 % just before its extinction at 3.636 Ma (chapter 4). *Discoaster* spp. are negligible.

Umbilicosphaera spp.

The portion of *U. jafari* and *U. rotula* is smaller than 2.2 % over the entire interval.

Others

Other coccoliths make up 5.9–21.2 % of the assemblage. Most abundant are *Calcidiscus* spp. (4.6–17.1 %), followed by *Helicosphaera* spp. (max. 1.9 %) and *Syracosphaera* spp. (max. 4.1 %). *C. pelagicus* is almost absent, except for minor peaks at 3.64, 3.55, 3.43 and 3.41 Ma.

6.3.3.4 Final Closure interval, Caribbean Site 1000 Fig. 6.3-1D(3)

Reticulofenestrids

Reticulofenestra spp. reach abundances between 26.8–57.5 %, (mean 40.5 %). With values between 15.3 and 48.6 % the *D. productus/R. minuta*-group shows highest abundances within the reticulofenestrids. The *R. haquii/R. minutula*-group appears with 2.9–25.2 %. *R. pseudoumbilicus* was not found in the Caribbean assemblage. The small *Gephyrocapsa* spp. occurs with abundances up to 16.4 %, with a strong decreasing trend towards younger ages.

Low Productivity Indicators

Represented species are *F. profunda, R. clavigera* as well as *Discoaster* spp., *S. abies,* and *D. tubifera* whereas the latter gain scarcely attention due to negligible abundances. The entire group supplies a mean of 22 % to the entire assemblage. *F. profunda* shows abundances between 3 and 35.8 %, *R. clavigera* makes up at least for 3.4 %. Following the abundances of *F. profunda*, the portion to the coccolith assemblage decreases after 3.38 Ma.

Umbilicosphaera spp.

With up to 33.1 % *U. jafari* shows high abundances, and together with *U. rotula*, the group accounts for 13.7–33.7 % of the assemblage. Abundances increase towards the younger part of the interval.

Others

Additional species are *C. pelagicus*, *Helicosphaera* spp., *Pontosphaera* spp. and *S. apsteinii*. Together, they build 2–10.7 % of the assemblage with more or less equal ratios.

6.3.4 Species mass Fig. 6.3-1A-D(4)

Main contributors to coccolith carbonate are *Reticulofenestra* spp., *Florisphaera profunda*, *Rhabdosphaera clavigera, Calcidiscus* spp., *Coccolithus pelagicus*, *Helicosphaera* spp. *Umbilicosphaera* spp., *Pontosphaera* spp., and *Scyphosphaera apsteinii*. Their contribution to bulk coccolith carbonate was calculated to be 67.9–99.3 % at Site 1241 and 80.2–99.6 % at Site 1000.

6.3.4.1 Biogenic Bloom interval, Pacific Site 1241 Fig. 6.3-1A(4)

Reticulofenestrids

The reticulofenestrids contribute a carbonate mass of 19.4–70.3 % to bulk sediment (mean 41.21 %). Highest values occurred in the older, lower values in the younger part of the time interval. The small *D. productus/R. minuta*-group forms 0.5-33.8 %, the *R. haquii/R. minutula*-group makes up 6.1–56.6 %, the *R. pseudoumbilicus* medium contributes a maximum of 46.3 %, *R. pseudoumbilicus* constitutes never more than 10.8 %.

Low Productivity Indicators

Within this group mass estimation was only possible for *F. profunda* because there are no shape factor calculations available for *S. abies* and *Discoaster* spp.. *F. profunda* builds a negligible amount of 0.3–4.8 % of coccolith carbonate.

Others

Even though this group is of minor importance for the abundance record, they are of utmost significance for the carbonate budget. These remaining coccoliths together contribute a mass of 14–68.8 % to the entire coccolith carbonate. *Calcidiscus* spp. build up a mass of 9–51.6 %, *C. pelagicus* 1–31.2 %, and *Helicosphaera* spp. 2.1–30.5 % within the coccolith carbonate. *C. pelagicus* dominates over *Helicosphaera* spp. in the older part, in contrast to the younger part, where *Calcidiscus* spp. show a homogenous distribution over the entire record.

6.3.4.2 Biogenic Bloom interval, Caribbean Site 1000 Fig. 6.3-1B(4)

Reticulofenestrids

The reticulofenestrids build a carbonate mass with mean values of 37.9 % (6.3-72.1 %). Average values increase from 30 %, to 50 % starting at 6.09 Ma. The small *D. productus/R. minuta*-group makes up 4.5–26.8 %, the *R. haquii/R. minutula*-group forms 3.1–40.6 % and *R. pseudoumbilicus* (including the medium-sized form) produced up to 21.4 %.

Low Productivity Indicators

Due to lack of shape factors for *S. abies* and *Discoaster* spp., mass estimations for low productivity indicators were only possible for *F. profunda* and *R. clavigera*. The latter produced together up to 25 % of all coccolith carbonate.

Contribution of *F. profunda* to carbonate mass varies between 1 and 11.8 %. *R. clavigera* builds 1.2 to 22.2 % of the carbonate produced by coccoliths.

Umbilicosphaera

Umbilicosphaera spp. contribute relatively constant1.1-2.2 % to coccolith carbonate.

Others

Together, *Calcidiscus* spp., *C. pelagicus*, *Helicosphaera* spp., *S. apsteinii* and *Pontosphaera* spp. constitute up to 39.4 % of the entire coccolith carbonate. *Calcidiscus* spp. make up to 28.5 %, *C. pelagicus* reaches a maximum of 9.4 % and *Pontosphaera* spp. up to 9.2 % of the mass. The quite rare abundant but massive *S. apsteinii* builds exceptional peaks up to 28.7 % at 6.8, 6.74, 6,46, 6.22 and 6.26 Ma. *Helicosphaera* spp. show high masses over the entire interval varying between 3.2 and 33.3 %.

6.3.4.3 Final Closure interval, Pacific Site 1241 Fig. 6.3-1C(4)

Reticulofenestrids

Reticulofenestra spp. build in average 37 % (17.5-57.6 %) of the coccolith carbonate. *D. productus/R. minuta* contribute with 1.3–8.6 %, followed by *R. haquii/R. minutula* with 0.9–7.5 % and *R. pseudoumbilicus* with 8.6–47.7 %. The few small *Gephyrocapsa* add a maximum of 0.3 %.

Low Productivity Indicators

F. profunda contributes a maximum of 8.6 % to coccolith carbonate.

Umbilicosphaera spp.

Umbilicosphaera spp. reach maximum values of 8.9 % in carbonate production.

Others

Together, *Calcidiscus* spp., *C. pelagicus*, *Helicosphaera* spp. and *Syracosphaera* spp. build up to 64 % of the carbonate mass. *C. pelagicus* and *Syracosphaera* spp. are negligible due to low abundances or minute masses, respectively. On the other hand, *Calcidiscus* spp. produce between 19–56 % and *Helicosphaera* spp. up to 29 % of the coccolith mass.

6.3.4.4 Final Closure interval, Caribbean Site 1000 Fig. 6.3-1D(4)

Reticulofenestrids

Reticulofenestra spp. build up between 8.5–29.6 %, whereas the smaller *D. productus/R. minuta*-group contributes 2.4–15.3 %, the *R. haquii/R. minutula*-group 3.6–20.4 %. The mass of small *Gephyrocapsa* never exceeds 1 %.

Low Productivity Indicators

F. profunda shows values between 0.7 and 9.2 %, *R. clavigera* together with *D. tubifera* contribute up to 6.8 % to coccolith carbonate mass.

Umbilicosphaera spp.

U. jafari and *U. rotula* contribute with 9.1–54.5 % to the carbonate mass.

Others

Calcidiscus spp. shows small peaks up to 16.3 %, *C. pelagicus* rarely contributes small amounts with maxima of 4.7 %. *Helicosphaera* spp. builds 3–34.6 % of the coccolith carbonate, *Pontosphaera* spp. up to 24.6 % and *S. apsteinii* up to 32.7 %.

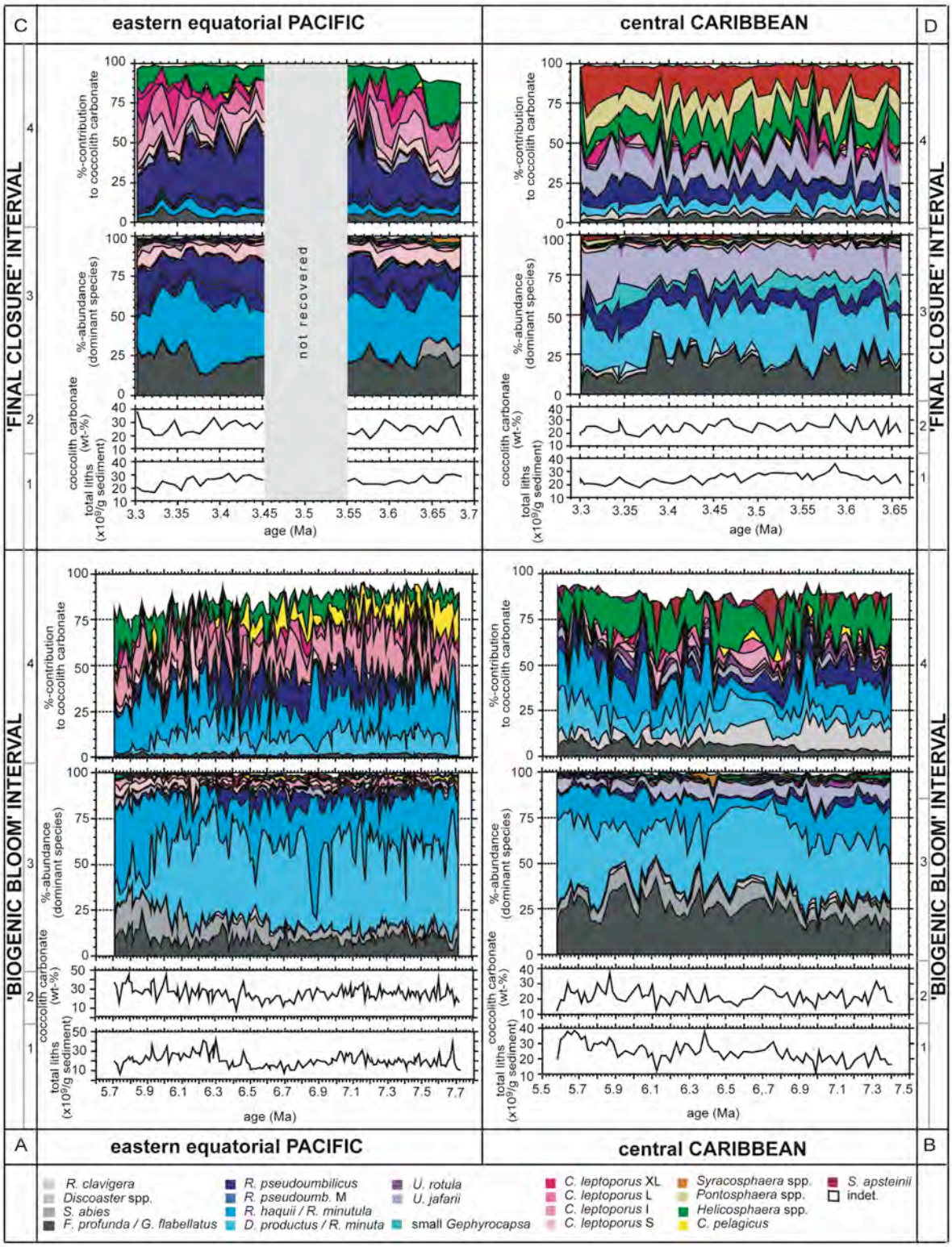

Fig. 6.3-1 Absolute and relative coccolith values of ODP Sites 1241 and 1000 during Biogenic Bloom and Final Closure interval.
A: Site 1241, BBP Interval, B: Site 1000, BBC Interval, C: Site 1241, FCP Interval, D: Site 1000, FCC Interval
1: absolute numbers of nannofossil liths, 2: relative nannofossil carbonate content, 3: relative abundance of dominant nannofossil species, 4: relative contribution of dominant species to nannofossil carbonate.

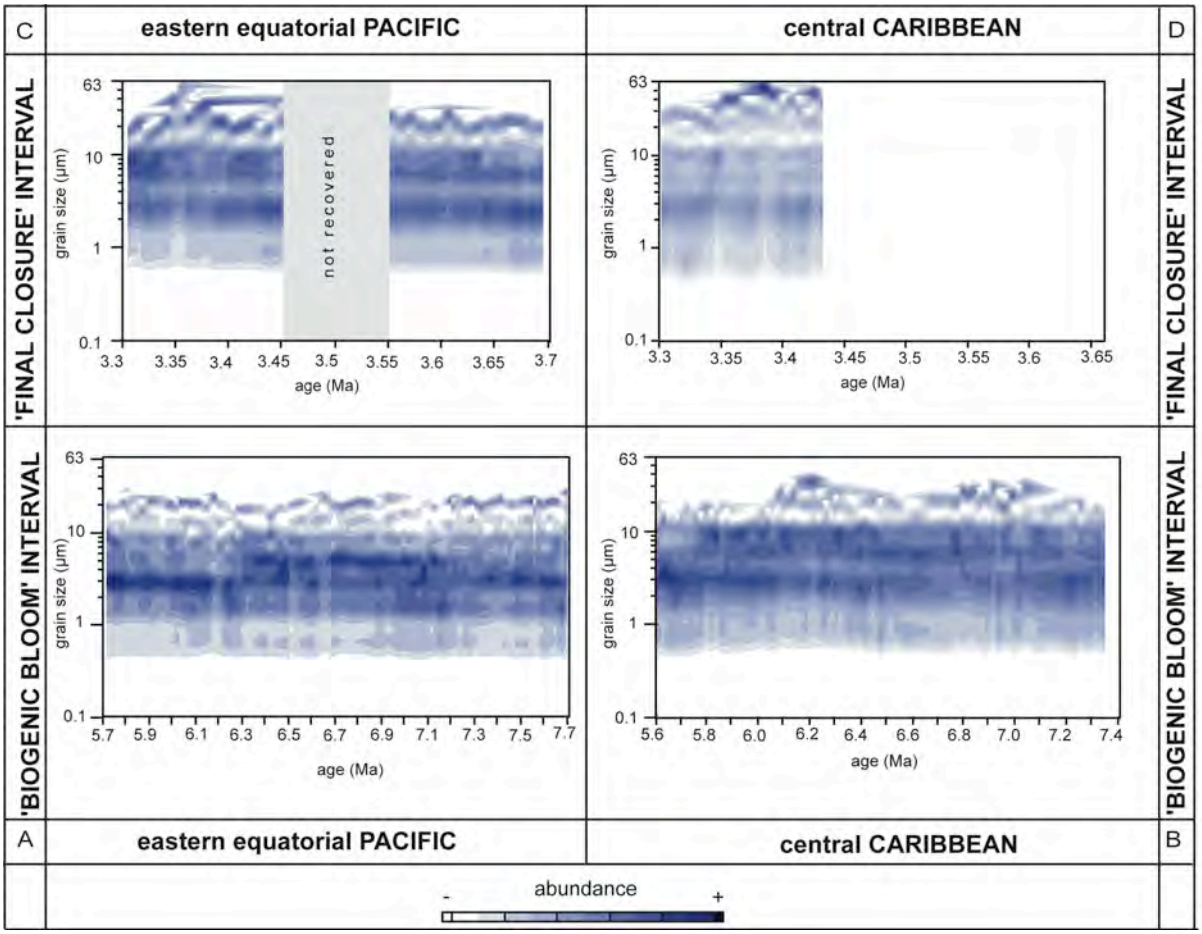

Fig. 6.3-2 Grain size distribution of fine fraction determined by LALLS of ODP Sites 1241 and 1000 during Biogenic Bloom and Final Closure interval. Logarhithmic presentation of grain size abundances.
A: Site 1241, BBP Interval, B: Site 1000, BBC Interval, C: Site 1241, FCP Interval, D: Site 1000, FCC Interval.

6.3.5 Grain size

Grain size distribution Fig. 6.3-2

The Biogenic Bloom interval shows a polymodal grain size distribution with a clear peak around 3 µm at Site 1241, and distinct peaks around 3 and around 7 µm at Site 1000. Range of grain sizes in the late Miocene is from 0.5 to 12 µm, with highest abundances between 1.5 and 7 µm at Site 1241 and between 1.5 and 11 µm at Site 1000.

A distinct tripartition of grain sizes occurs in late Miocene samples of Site 1241. The oldest part (7.72-7.31 Ma) and the youngest part (6.32-5.71 Ma) show a strong peak in abundance around 3 µm. This is in contrast to the middle part (6.96-6.32 Ma) showing a wide distribution of high values ranging from 3 to 6 µm (maximum at 5 µm).

At Site 1000, a development towards higher amounts of finer grain sizes is as follows: The oldest part shows high ranges of grain sizes from 1.2 to 10.5 µm until 6.8 Ma. Maximum grain sizes in that interval are around 3 and 6 µm. Until 6.65 Ma grain sizes around 3 µm loose dominance. Amounts of 3 µm grain size increase until 5.76 Ma. The youngest part between 5.75 and 5.6 Ma shows high values between 3 and 5µm but lacks big grain sizes.

The grain size distributions of the Final Closure Interval at Site 1241 and 1000 show a homogeneous pattern over the entire interval with maximum values around 3 µm. Generally, high values are present between 1.3 and 11 µm. Site 1241 shows abundance maxima at 3 and 6 µm, grain sizes between 12 and 70 µm include several peaks of higher abundances. Due to analytical problems, we did not analyse the entire record of the Final Closure Interval of Site 1000. However, the few samples support the data of the assemblage composition, which also indicate no significant changes in grain size.

Sediment fractions Fig. 6.3-3A-D(1)

All samples show low abundances of sand and predominance of silt. In the late Miocene sediment record, sand has mean values of 2.2 % at Site 1241 and mean values of 19 % at Site 1000. Fine silt dominates within the silt fraction (mean values around 68 % at both sites). At both sites, fine silt has high abundances around 55 % and coarse silt around 12 %, and clay fraction shows mean values of 30 %.

In the Pliocene samples, sand content is around 9 % in the Pacific and 27 % in the Caribbean Sea. Silt is dominant (mean values around 71 % at both sites), with coarse silt values around 21 % / 26 % and fine silt values around 51 % / 44 %, and clay with mean values around 27 % / 29 %.

Coccolith Carbonate Index Fig. 6.3-3A-D(2)

The fine silt fraction shows a strong dominance over both, the coarse silt fraction and the clay fraction in all samples. The CCI-fine (dominance of coccolith fraction against clay fraction) is constant over the entire interval. Values of CCI-coarse (dominance of coccolith fraction against foraminiferal and biosilicious fossil fragments) fluctuate strongly.

6.3.6 Accumulation Rates Fig. 6.3-3A-D(3)

6.3.6.1 Biogenic Bloom interval, Pacific Site 1241 Fig. 6.3-3A(3)

Mass accumulation rates (MARs) vary around 4.2 g/cm^2/ka and display an increase after 6.67 Ma. Due to high carbonate contents, the same trend is found for carbonate MARs, with values around 3.3 g/cm^2/ka. Non-carbonate MARs show negligible amounts of 0.9 g/cm^2/ka. Values of nannofossil ARs vary around 89 × 10^9/cm^2/ka, with lower amounts in the older and increasingly higher amounts in the younger part of the interval, beginning at 6.67 Ma. The 'high productivity indicator' -group with mainly *Reticulofenestra* spp. traces that trend, with lower values around 57 × 10^9/cm^2/ka before, and higher values around 77 × 10^9/cm^2/ka after 6.67 Ma. Generally, low amounts of the 'low productivity indicator' -group (around 10 × 10^9/cm^2/ka) increase after 6.67 Ma (around 26 × 10^9/cm^2/ka).

6.3.6.2 Biogenic Bloom interval, Caribbean Site 1000 Fig. 6.3-3B(3)

Mass accumulation rates strongly fluctuate around 5.7 g/cm^2/ka. Stepwise increases and decreases result in minimum values around 3 g/cm^2/ka at 7.96 Ma and 7.1 Ma, with

interjacent maximum values of up to 9 g/cm²/ka. Lowest values of 2 g/cm²/ka exist at 6.7 Ma. Values increase again gradually, with one distinct minimum of 2 g/cm²/ka at 6.0 Ma. Carbonate MARs follow the same trend, since non-carbonate ARs are negligible. Nannofossil ARs vary around 133 × 10^9/cm²/ka, clearly tracing the bulk MARs course. The 'high productivity indicator' -group of *Reticulofenestra* spp. shows only one distinct minimum at 6.12 Ma reaching values around 20 × 10^9/cm²/ka. Values are generally high around 82 × 10^9/cm²/ka. General lower amounts of the 'low productivity indicator' -group (around 48 × 10^9/cm²/ka) follow an inverse trend compared to bulk MARs, with minima at 7.0 Ma, 6.4 Ma and 5.8 Ma and maxima at 6.7 Ma and 5.98 Ma.

6.3.6.3 Final Closure interval, Pacific Site 1241 Fig. 6.3-3C(3)

All accumulation rates are constant over the entire interval. Mass accumulation rates vary minimal around 3 g/cm²/ka, carbonate accumulation rates vary around 2.45 g/cm²/ka, and non-carbonate accumulation rates show values around 0.6 g/cm²/ka. Nannofossil accumulation rates are around 77 × 10^9/cm²/ka, with a decrease in values towards 3.3 Ma.

6.3.6.4 Final Closure interval, Caribbean Site 1000 Fig. 6.3-3D(3)

Mass accumulation rates show values around 5 g/cm²/ka, carbonate accumulation rates are around 4.4 g/cm²/ka and non-carbonate accumulation rates around 0.5 g/cm²/ka. Nannofossil accumulation is around 74 × 10^9liths/cm²/ka with a continuous decrease in values until 3.3 Ma.

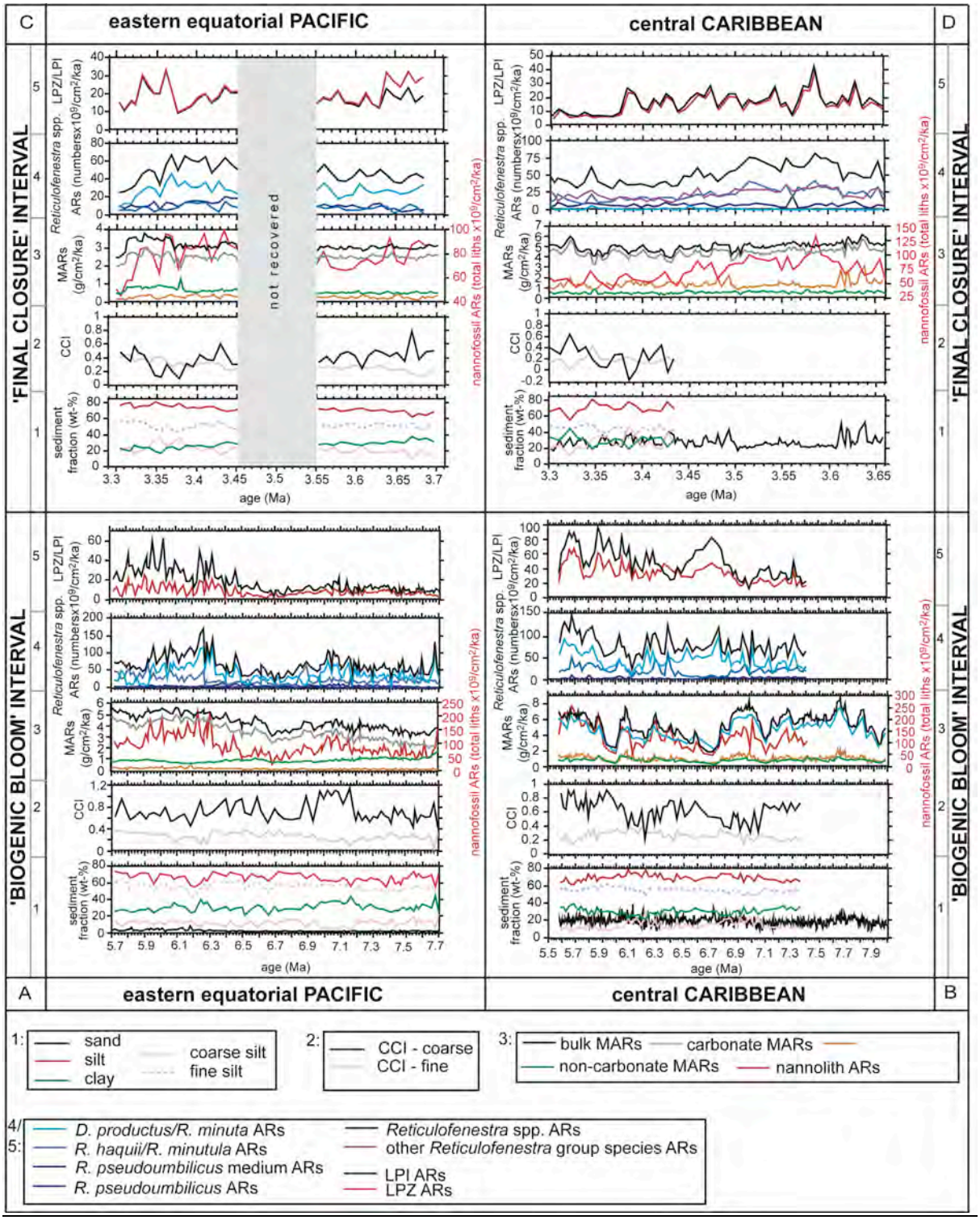

Fig.6.3-3 Grain size distribution and accumulation rates of ODP Sites 1241 and 1000 during Biogenic Bloom and Final Closure interval.
A: Site 1241, BBP Interval, B: Site 1000, BBC Interval, C: Site 1241, FCP Interval, D: Site 1000, FCC Interval
1: sediment fractions, 2: coccolith carbonate Index, 3: mass accumulation rates, 4: reticulofenestrid accumulation rates, 5: lower photic zone / low productivity indicator species accumualtion rates.

6.4 Discussion

6.4.1 Coccolith Carbonate Contribution

Estimation of coccolith contribution to the carbonate budget is relatively difficult. Several approaches have been applied for estimating coccolith calcite fluxes (Beaufort, 2002). Besides the indirect measurement of the coccolith carbonate content using image analysis (Beaufort and Dollfus, 2004; Beaufort, 2005), absolute abundances of coccoliths multiplied by an estimated coccolith weight is the current and approved method. This coccolith weight is based on either an average placolith (Honjo, 1976) or on species-specific coccolith weight depending on its geometry (Beaufort and Heussner, 1999; Young and Ziveri, 2000). In order to test a possible link between changes in general carbonate accumulation rate and primary productivity and/or ecology-/evolution- induced changes in species-specific carbonate production of coccoliths, possible errors have to be discussed. Fact is, that coccolith-carbonate flux calculations can only provide an estimate for the real value.

6.4.1.1 Mass calculations

Beaufort et al. (2007) proposed from sediment trap samples, that the weight of coccoliths did not change significantly over depth. They concluded that the weight of coccoliths in sediments can be considered to present their original weight on a coccosphere (Beaufort et al., 2007). However, the calculation of coccolith mass encounters difficulties. According to Young and Ziveri (2000), substantial errors of up to 50 % in the calculations of coccolith volume are inevitable. These authors discussed several uncertainties in volume calculation. (1) Besides the inaccuracy in the geometric coccolith model, (2) the choice of values for the calculation is important: for maximum accuracy the mean volume should be calculated rather than the volume of mean linear size, otherwise the volume would be undercalculated. (3) Allometric growth is another uncertainty. The increase in number of elements with size does not change the cross-section profile needed for the volume calculation (Young, 1989), but the question is still whether or not coccolith height and elements thickness increase proportional to coccolith length. (4) The greatest potential errors compared to any other source are due to size variations, which have much greater effect than shape variation in controlling coccolith volume (Young and Ziveri, 2000, Fig. 6.4-1). The importance of size measurements for coccolith carbonate flux estimates was described by Baumann (2004). He postulated that a slight difference in size of species could result in an up to a three-fold variability in carbonate mass contribution, where some species are much more variable in size and thus more important to calibrate (*C. leptoporus*, *G. oceanica*, *S. pulchra*) compared to morphometrically stable species (*E. huxleyi*, *H. carteri*). Since the sum of carbonate fluxes of the individual species is used for the estimation of total coccolith carbonate fluxes this value varies by approximately 50-60 % (Baumann, 2004).

Our results clearly underline the importance of size measurements. Within our data we achieved enormous differences in total coccolith carbonate mass between calculations based on minimum or maximum sizes, respectively (Table, Appendix A3.2). Total carbonate fluxes show 0.3 to 13.5 fold variations depending on size measurements. Herein, *Calcidiscus* spp. and *C. pelagicus* are of prime importance due to high shape factors, and thus high carbonate contribution, compared to others such as *Syracosphaera* spp. and *F. profunda*. We carried out discrete size measurements with SEM on important species in 165 samples. These data were used for calculation of species-specific carbonate masses.

6.4.1.2 Size variabilites and consequences

Intraspecific morphological groups display ecological and/or genetic differences. Morphological variations within several coccolithophorid species have been reported (e.g. Bollmann, 1997; Knappertsbusch et al., 1997; Quinn et al., 2004; Quinn et al., 2005). Geisen et al. (2002) proposed that morphological differences represent discrete taxa (see chapter 5). This has subsequently been confirmed by culture experiments (Quinn et al., 2003) and molecular genetic analyses, where Sáez et al. (2003) demonstrated, that morphological differences within certain morphotypes are indeed related to sibling species. Geisen et al. (2004) provided evidence that coccolith morphology is stable if tested under different ecological parameters, and hence is under strong genetic control and not ecophenotypic in nature.

However, high intraspecific variability in coccolith weight is likely to affect the accuracy of the calculation (Beaufort, 2005). To balance spatial differences, no mean species mass should be applied for different locations. General variations of species-specific coccolith carbonate after Young and Ziveri (2000) are given in Fig. 6.4-1.

The calcareous nannoplankton assemblages at Sites 1241 and 1000 are characterised by relatively high species diversity and by a high abundance of cosmopolitan taxa, such as the *D. productus/R. minuta*-group, the *R. haquii/R. minutula*-group and *R. pseudoumbilicus*, as well as abundant temperate to subtropical genera such as *Calcidiscus*, *Helicosphaera*, *Umbilicosphaera*, *Sphenolithus* or *Discoaster*.

The deep dweller *Florisphaera profunda* is also a common species in all samples. Its abundances are highest in the Caribbean Sea and additionally common on both sides of the isthmus in the younger FC interval. With its simple non-ornamented polygonal plates, the nannoliths posses easily measurable morphological characters (Baumann and Sprengel, 2000). Mean length of *F. profunda* varies between 1.9 µm in the BBP and 3.7 µm in the FCC interval, mean masses show values between 0.7-5.6 pg per individual specimen. Nannoliths are generally larger in the Caribbean Sea than in the Pacific with increasing sizes in the younger part. Thus, largest mass variations occur in the FCC interval, with values up to 16.64 pg/individual specimen. But altogether, *F. profunda* provides a nearly negligible contribution to the coccolith mass.

Coccoliths of the genus *Reticulofenestra* are the numerically most important taxa in the late Miocene to mid-Pliocene. Abundances in our samples reach up to 85 %, whereupon their predominance is particularly pronounced in the late Miocene tropical Pacific. Site 1241 shows in general higher abundances in *Reticulofenestra*, whereas at Site 1000 this genus looses its dominance with respect to *Umbilicosphaera.* The mean size within all groups of reticulofenestrids stays more or less constant over both, location and age. Due to their definition based on size, the different groups of *Reticulofenestra* offer a distinct range of coccolith length (e.g. 3-5 µm for *R. haquii / R. minutula* group), which in itself contains a huge error for volume calculation. To note is the small *D. productus/R. minuta*-group, which shows up to 33-fold variabilities in volume estimates for min and max sizes, respectively, but negligible mean amounts of 1.75–2.06 pg per individual specimen. With extant mass variations with a coefficient of 4.25, *R. pseudoumbilicus* medium holds 2.8-fold variabilities and the large *R. pseudoumbilicus* shows values of × 1.1–2.5. Due to the importance of size in the volume formula, the mean masses grow exponentially. The small-sized groups exhibit 1.75–2.06 and 7.27–8.87 pg/individual specimen; the large *R. pseudoumbilicus* contributes 21.23–26.78 and 48.35–65.79 pg/individual specimen respectively. A decrease in carbonate mass built by reticulofenestrids is observable over time due to extinction of *Reticulofenestra pseudoumbilicus* and the larger abundances of the smallest *D. productus/R. minuta* group in the Pliocene samples.

Calcidiscus shows a constant but subordinate record in our samples. Greatest abundances were reached in the Pacific, especially in the younger mid-Pliocene interval. For estimation of masses, individual coccoliths of *Calcidiscus* were clustered into four different morphotypes following Knappertsbusch (2000) and Quinn et al. (2004) (Appendix A2.3). Differences in *Calcidiscus* size correspond to an approximately > 100–fold variability in volume estimates for that genus. The variability within these species is still enormous, 3–7.5 times for *C. leptoporus* S, 4 times for *C. leptoporus* I, 1.9 times for *C. leptoporus* L and around 1–1.7 times for *C. leptoporus* XL. Mean contribution to carbonate mass increases with size from 10.8 to 291.1 pg for one individual specimen. Their constant record around 5.5 % in abundance causes a mean contribution to coccolith carbonate of 28.5 % in the late Miocene tropical Pacific assemblage. In the mid-Pliocene, *Calcidiscus* spp. show average abundances of 11 % and build up a carbonate mass around 36.4 %. Their importance in the Caribbean Sea is minor, but their produced carbonate still may reach up to 28.5 % in individual samples.

C. pelagicus shows absolute negligible abundances. In the late Miocene tropical Pacific, the low abundances smaller than 1 % result in a coccolith weight of up to 31 % due to the massive construction and large size of that species. *C. pelagicus* only occurs in the older part of that interval. After 6.46 Ma nearly no carbonate produced by *C. pelagicus* is detected. Size ranges may result in a nearly 8-fold mass variability in the BBP samples.

Helicosphaera shows low abundances in all samples (< 3 %), but, due to the large sizes and shape factor, it makes enormous contributions to coccolith carbonate with maximum values

around 30 % in all four intervals. The mean sizes are larger in the late Miocene, nevertheless mass variabilities occur in all samples with magnitudes between 4.6 and 7.7. Especially in the BBP samples, an increase in mass of *Helicosphaera* spp. leads to dominance over *C. pelagicus* after 6.46 Ma. The other records show more constant values.

Detailed information on carbonate masses of discussed and other selected species is given in Table A3-3 in the Appendix A3.

A detailed morphometric analysis with variations in sizes of *Reticulofenestra* and *Calcidiscus* is given in chapter 5.

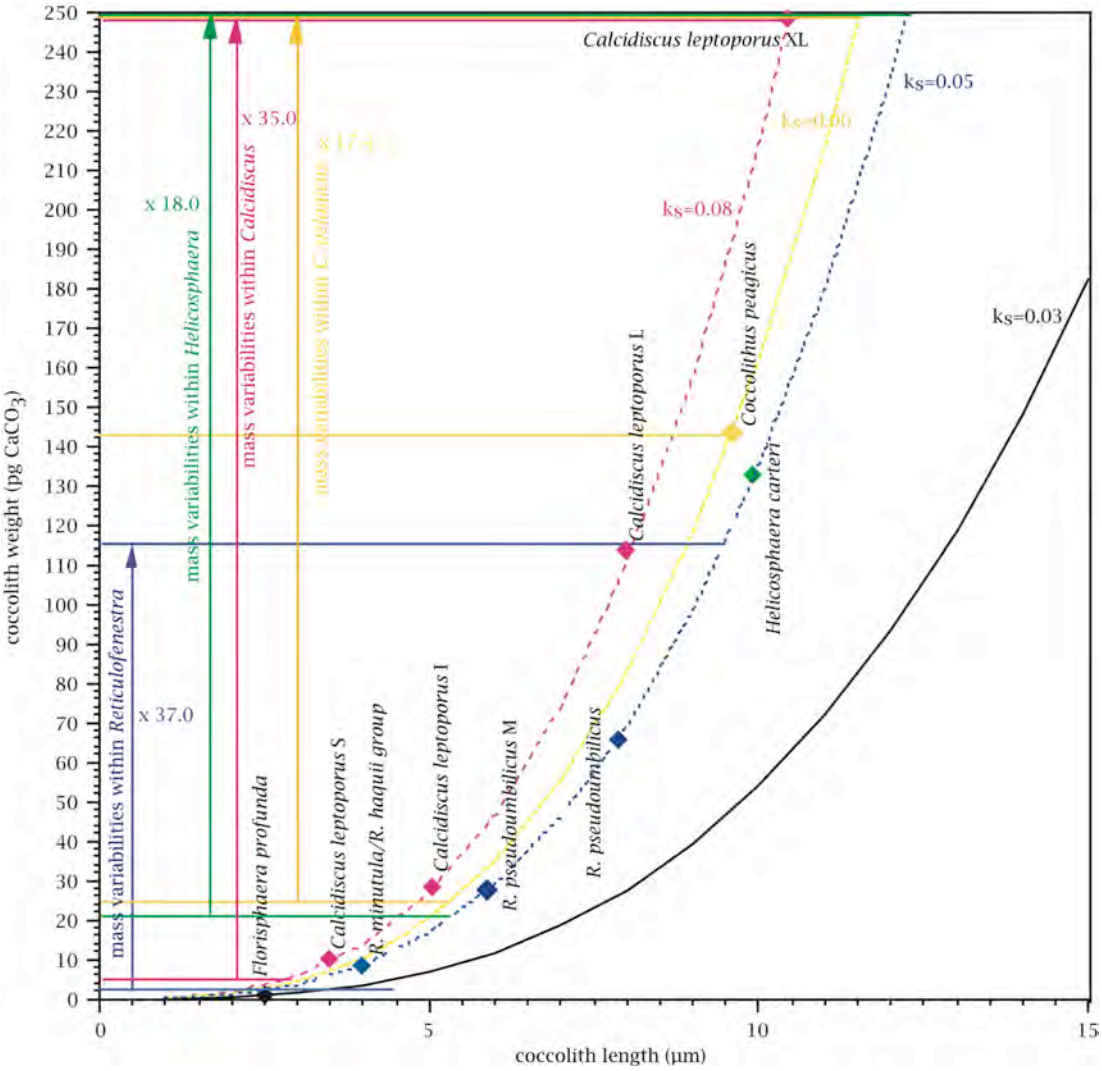

Fig. 6.4-1 Species specific coccolith carbonate, curves represent shape factors k(s), squares identify mean sizes of species in this study, arrows show possible mass variability within individual taxa. Modified from Young and Ziveri (2000).

6.4.1.3 Coccolith carbonate and importance of grain size analysis

As described in chapter 6.3.2, carbonate built from coccoliths is relatively low in all samples and never exceeds 50 % (Fig. 6.3-1A-D(2)). In search for the other 50 % it must be considered, that this value has been calculated from the crucial and critical 'coccolith volume'. But since the carbonate content is extremely high, especially in the high productive samples of the Biogenic Bloom interval, and the sand content is negligibly low in all samples (Fig. 6.4-2A-B(5,6)), the main producers of these sediments are represented by the bulk carbonate of the fine fraction – the coccolithophores. The results of the grain size analysis thus provide important information on the predominance of the biogenous constituents; hence we used the particle size distribution as relative quantification of individual particles. There are no other possible carbonate producers in our samples than coccolithophores. Therefore we re-emphasise, that calculations of coccolith carbonate are limited by methodological errors and hence can only provide a rough estimate for the real value. Thus, grain size analysis is an important tool in understanding the quantification of carbonate budgets of the fine fraction, especially of samples with dominantly high carbonate and significantly low sand content.

6.4.1.4 Grain sizes

Besides the determination of total accumulation of coccoliths (SEM), the determination of grain size distribution is of prime importance for the quantification of the carbonate budgets.

The sediment composition analysis (Fig. 6.3-3A-D(1)) gives a first idea of the dominant fraction, which, in all samples, is the fine silt. With evidence from SEM investigations, we defined two groups out of the fine silt fraction in order to point out the dominance of coccoliths in the silt fraction, the 2-10 µm group and the 10-63 µm group. The 'Coccolith Carbonate Index' (Fig. 6.3-3A-D(2)) is used to show the dominance of the 2–10 µm group. This group is represented almost exclusively by coccoliths. Especially in the Biogenic Bloom interval the 2–10 µm fraction is highly dominant over the 10–63 µm fraction ('CCI – coarse'), which is represented by foraminiferal detritus, juvenile foraminifers and mainly diatom frustules. The Final Closure interval also shows dominance of the coccolith fraction, but not as pronounced as in the Biogenic Bloom interval. Same is true for the 'CCI–fine', the ratio between the coccolith fraction and the fraction < 2 µm, representing unidentifiable particles. It is persistently low in all samples, especially the Biogenic Bloom samples, implying the constantly minor role of that 'detrital' fraction.

It is obvious that there is a relation between grain size and assemblage composition (Figs. 6.3-1 and Figs. 6.3-2). Grain size variations in our samples trace distinct floral shifts, albeit it is not comprehensible (chapter 7; Goossens, 2008). Laser diffraction is a useful tool to measure temporal or spatial trends in particle size characteristics (Blott and Pye, 2006). Floral changes within the fine fraction are easily detectable, especially prior to time-

consuming assemblage investigations, and additionally, to better understand the various reasons for changes in accumulation rates (see chapter 7.).

Variations in the grain size of calcareous compounds might be influenced by water chemistry, ecology/evolution and production rates of certain biogenic components (Henrich et al., 2003). Variations of the sand percentages of the carbonate fraction are often used as a proxy to reconstruct either changes in carbonate dissolution or differences in carbonate accumulation between foraminifers and calcareous nannoplankton (e.g. Peterson and Prell, 1985). In deep-sea carbonates, decreasing sand content is often interpreted to indicate increasing dissolution (Berger et al., 1982; Bickert et al., 1997; Stuut et al., 2002a; Gröger et al., 2003a; Gröger et al., 2003b). Especially, changes in the ratio between nannofossil placoliths and foraminiferal shells are regarded as the primary mechanism that could change the relative portion of the coarse fraction (Dittert et al., 1999 and references therein).

Sand content is negligibly low in our samples, especially in the Pacific site over both intervals. Due to the influence of the bank-derived neritic carbonates, the Caribbean Sea shows generally higher, but still unimportant sand contents. Sand MARs do not seem to influence accumulation patterns and coccolith (fine silt) dominance (Fig. 6.3-3A-D(1,2)). Dissolution is of minor importance due to the shallow depth of Site 1241 (2027 m) compared to lysocline depth of 3600 m (Lyle et al., 1995). Same is true for the Caribbean Site 1000.

6.4.2 Spatial and temporal correlation – Biogenic Bloom and closing history of the Isthmus of Panama

6.4.2.1 Fluxes

The consideration of nannofossil accumulation rates has been established as a useful tool for palaeoproductivity reconstructions in regions where coccolithophores are major primary and export producers and biogenic carbonate preservation throughout the whole interval is relatively good (Lototskaya et al., 1998).

The Interval of the Biogenic Bloom at Site 1241 shows distinct accumulation patterns (Fig. 6.3-3A(3)). A first rise in bulk MARs between 7.7 and 6.67 Ma is associated with minima around 3.3 g/cm^2/ka and maxima around 4 g/cm^2/ka. After that, the values increase further to about 5.5 g/cm^2/ka. The investigated time interval from 7.7 to 5.7 Ma at this site thus displays a 1.67 times increase in accumulation rates. Since the non-carbonate fraction plays a minor role, that increase in accumulation is only due to carbonate sedimentation. But herein, sand contents are negligible (around 2 wt-%, Fig. 6.3-3A(1)). The coccolith sedimentation rates trace the bulk and carbonate MARs, with a first increase from mean values around 60 to 90 × 10^9/cm^2/ka until 6.67 Ma, followed by a further increase to values around 150 × 10^9/cm^2/ka. The nannolith accumulation thus experiences a 2.5 fold increase, isolated values increase about 9.2 times. This dominant rise of nannofossil accumulation in comparison to the bulk mass accumulation rates in the eastern equatorial Pacific supports

the suggestion of Diester-Haass et al. (2005) that the Biogenic Bloom is primarily made by coccolithophores.

In the Caribbean Sea the Biogenic Bloom interval shows different patterns in the MAR compared to the eastern equatorial Pacific (Fig. 6.3-3B(3)): starting at 7.8 Ma, high values around 6.2 g/cm^2/ka drops to a minimum of 2.8 g/cm^2/ka at 6.7 Ma and increase with mean values of 4.6 g/cm^2/ka to max of 7.6 g/cm^2/ka until 6 Ma. Afterwards, values are around 5.9 g/cm^2/ka. This implies a 2.2 fold decrease until 6.7 Ma followed by a 2-fold increase until 5.6 Ma. The coccolith sedimentation rates trace the bulk MARs, both showing a depletion at 6.7 Ma and 6 Ma. Mean values of around 120 × 10^{9}liths/cm^2/ka decrease to 110 × 10^{9}liths/cm^2/ka in between these two minima, and increase again to 198 × 10^{9}liths/cm^2/ka. Coccoliths thus experienced a 1.8 fold increase during that time interval.

A comparison between the Pacific and the Caribbean sites (Fig. 6.4-2A(1)) indicates different amounts of accumulation on both sides of the Panamanian Isthmus, but accordance in the general characteristics of the patterns. The Pacific site shows lower mass accumulation rates than the Caribbean site. However, at both locations, the Biogenic Bloom seems not to be one single event of increased accumulation rates but the result of a complex process with coincidently fluctuating accumulation patterns. Both sites display a partition into two intervals separated by a distinct minimum in all accumulation rates at 6.7 Ma. The first section is marked by a two-step variation in mass accumulation with lower amplitudes in the Pacific than the Caribbean site. The nannofossil accumulation rate shows same patterns as MARs and has nearly equal rates and reduplicative values at both locations. A flattening in minima accumulation rates within that first interval appears around 7.18 Ma, with a 1.3-fold decrease in values at Site 1241 and a 3.5-fold decrease in values Site 1000. Both sites correlate again in the minimum accumulation at 6.7 Ma. Afterwards, the strong 1.8-fold increase in mass accumulation at the Pacific is paralleled by a more than 6-fold increase in nannofossil accumulation. The Caribbean Sea exhibits a two-fold increase in both, mass and nannofossil accumulation rates with 1.5 to 3-fold increase in values. This is intersected by a decrease at around 5.99 Ma. The absolute abundances, and thus accumulation rates, of the high-productivity indicator species *Reticulofenestra* spp. (Fig. 6.3-3A-B(4)) follow the nannofossil accumulation rates at both sites. The high-productivity indicators loose dominance for the benefit of the low productivity indicator group (Fig. 6.4-2A(3,4).

The complex nature of the Biogenic Bloom event is visible at both sides of the Panamanian Isthmus. The accumulation patterns do not reinforce the Biogenic Bloom as one single event as maybe assumed after consideration of floral changes, but as two successive, complex incidents.

As expected, the 'Final Closure' phase does not show any appreciable changes in mass -, carbonate -, and non-carbonate accumulation rates on both sides of the Panamanian Isthmus

(Fig. 6.3-3C-D(3)). Generally, depleted mass values and nannofossil accumulation rates are apparent in all Pliocene samples compared to the Biogenic Bloom. The central Caribbean Sea shows higher values than the eastern equatorial Pacific.

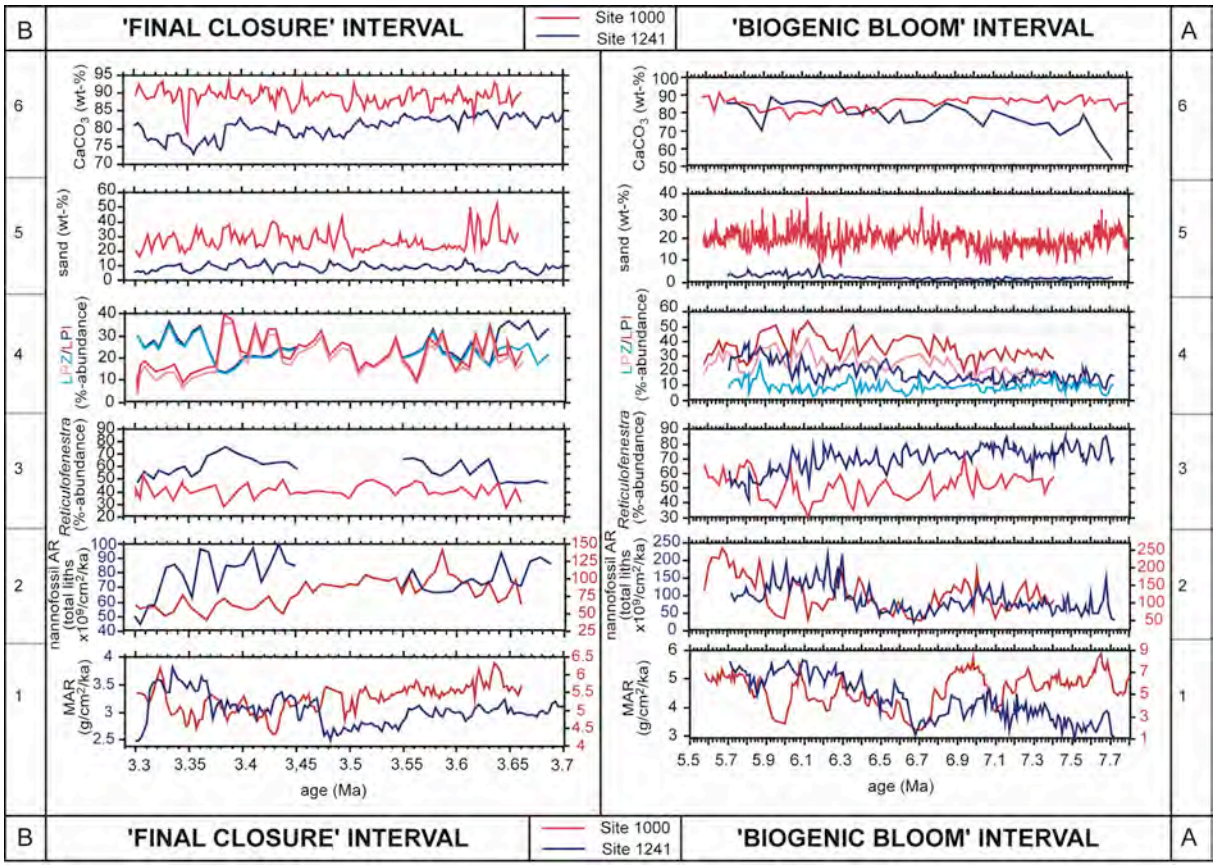

Fig. 6.4-2 Correlation between eastern equatorial Pacific ODP Site 1241 (blue), central Caribbean ODP Site 1000 (red) during late Miocene Biogenic Bloom and Pliocene Final Closure Interval:
A: Biogenic Bloom interval, B: Final Closure Interval
1: bulk MARs (g/cm²/ka), 2: nannofossil ARs (total liths x10⁹/g/cm²/ka), 3: realtive abundance of *Reticulofenestra* spp., 4: relative abundance of LPZ (lower photic zone) and LPI (lower productivity indicator) species, 5: sand content (wt-%), 6: $CaCO_3$ content (wt-%).

6.4.2.2 Ecology

The late Miocene to Pliocene calcareous nannofossil assemblages at Sites 1241 and 1000 show a typical open-marine species composition, with high diversities. Seven taxa/species dominate the assemblages, *Florisphaera profunda*, *Sphenolithus abies, Reticulofenestra*, *Umbilicosphaera*, *Coccolithus pelagicus*, *Calcidiscus leptoporus* and *Helicosphaera.*

As mentioned above, general distribution patterns of coccolithophorid assemblages (Fig. 6.3-1A-D(3)) around the Panamanian Isthmus show predominance of *Reticulofenestra* spp., with higher abundances of reticulofenestrids in the eastern equatorial Pacific than in the Caribbean Sea. Reticulofenestrids still present the majority of the coccolith assemblages in the Pliocene at both locations, but they have lost their absolute predominance, especially at the Caribbean site. Reticulofenestrids are typical representatives of r-selective eutrophic opportunists, which are typical for unstable environments, such as tropical, nutrient-rich upwelling settings (Okada and Honjo, 1973), and periods of high fertility (Biekart, 1989; Wade and Bown, 2006). Their usefulness as an indicator of palaeoproductivity has been established, since Okada (2000) proposed a generally reversed stratigraphic trend of 'small placoliths' (thus *Reticulofenestra*) compared to that of *F. profunda.* The same pattern is obvious in our samples (Fig. 6.4-3). Thus, the Lower Photic Zone Taxa generally show higher abundances in the Caribbean Sea, as well as in the younger Pliocene interval. *F. profunda* provides a robust transfer function for palaeoproductivity estimates, as abundances are inversely related to intensity of upwelling and turbidity (Ahagon et al., 1993; Jordan and Kleijne, 1994; Jordan, 1996; Ziveri and Thunell, 2000). Abundance patterns of *Umbilicosphera* show similar trends to that of the LPZ taxa. They play a more important role in the Caribbean Sea and here are even more dominant in the Pliocene. Umbilicospheres are a reliable marker of oligotrophic conditions (Okada and McIntyre, 1979; Grideau, 1992; Roth, 1994), with a possible affinity to hypersaline conditions, with no response to changed nutrient levels (Wade and Bown, 2006; Flores et al., 2005).

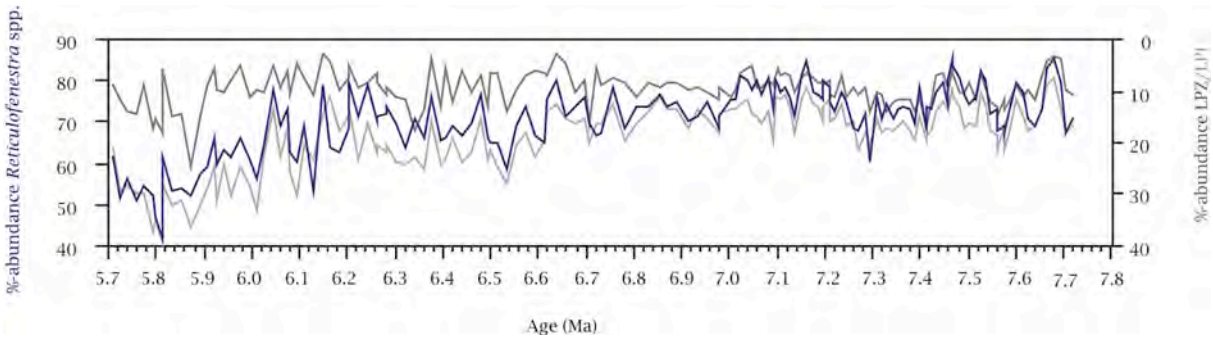

Fig. 6.4-3 Invers relation between abundances of *Reticulofenestra* spp. (blue line) and Lower Photic Zone taxa (dark grey line), Low Productivity Indicator (light grey line) of Site 1241.

C. leptoporus has generally higher abundances in the Pacific samples. *C. leptoporus* is cosmopolitan (McIntyre and Bé, 1976; Geitzenauer et al., 1998) and its distribution seems to be controlled by warm and oligotrophic conditions (e.g. Ziveri et al., 2000; Flores et al., 2003; Hagino and Okada, 2006). Highest fluxes of *C. leptoporus* have been associated with low to intermediate nutrient concentrations and high coccolithophorid productivity (Flores et al., 2003). Similarities in abundances between *C. leptoporus* and *Helicosphaera*, as observed by Ziveri et al., 1995, Ziveri and Thunell, 2000, Ziveri et al., 2000, and Flores et al., 2003, are also obvious in our samples, although the latter taxon has higher abundances in the central Caribbean Sea than in the eastern equatorial Pacific. *Helicosphaera* species seem to thrive in shallow, eutrophic, warm environments, but *H. carteri* has also been documented in sediments from eutrophic, hyposaline waters (Giraudeau, 1992; Flores et al., 2005). Opposite patterns to that of *C. pelagicus* were described for *Helicosphaera* by Flores et al., 2003. Same is noticable in the Miocene samples of Site 1241, where *Helicosphaera* gains dominance due to decreasing values of *C. pelagicus*. *C. pelagicus*, however, appears only in the latter samples, in all other observed intervals, this species has negligible abundances. *C. pelagicus* is known to prefer cold and eutrophic conditions, but its relation with increased productivity has been discussed contradictory (e.g. Cachao and Moita, 1995; Filippelli et al., 2003; Boeckel and Baumann, 2004; Flores et al., 2005).

The latest Miocene presents hydrographical conditions in which an open Panamanian Gateway allowed exchange of surface water masses. However, an emerging sill had already formed a significant deep interoceanic biogeographic barrier (Collins et al., 1996) with sill depths between 200 and 500 m (Keller et al., 1989; Duque-Caro, 1990; Chaisson and Ravelo, 2000; Jain et al., 2007). During that time interval, Site 1241 was located close to the Equatorial Divergence Zone and the South Equatorial Current (Fig. 1.2.1.2-2), which suggests cooler sea-surface temperatures (SST) and higher sea-surface salinities (SSS) than today (Mix et al., 2003). Furthermore, the thermocline and nutricline would have been shallower in the past, resulting in higher sea-surface nutrient concentrations and primary productivity.

Relatively high abundances of *C. pelagicus* support these colder SST at Site 1241 during the late Miocene, whereas high-nutrient conditions of the equatorial upwelling are exploited through high abundances of typical r-selective reticulofenestrids. Due to free surface water circulation at this time, high nutrient water masses flew from the Pacific into the Caribbean Sea, and enabled reticulofenestrids to thrive at both sides of the Panamanian Seaway. Abundances of the LPZ taxa are higher at Site 1000, indicating stronger stratification. Additionally, the lack of *C. pelagicus* and presence of *Umbilicosphaera* point to warmer, more oligotrophic and maybe more saline conditions in the Caribbean Sea even before the closure of the seaway. High abundances of *C. leptoporus* restricted to the Pacific, could point to the high coccolithophorid productivity at that site. On the other hand, the increase in the Low Productivity Indicator species *S. abies,* staring around 6.0 Ma in late Miocene at

Site 1241 at the expense of reticulofenestrids, could underline the onset towards decreasing productivity and more oligotrophic conditions in the Pliocene.

Apart from these differences in abundances, calcareous nannoplankton assemblages of the late Miocene are quite similar in diversity and species composition on both sides of the Panamanian Seaway. However, during the late Pliocene interval views obvious differences in coccolith assemblage compositions around the Isthmus of Panama. During this interval, there is no longer exchange of surface water masses between the Pacific and the Caribbean Sea (e.g. Haug and Tiedemann, 1998; chapter 1.2.1.2). While diversity has not changed significantly at Site 1241, Site 1000 faces new warm-water species, such as *Syracosphaera* spp. or *Scyphosphaera apsteinii,* possibly pointing at increased SSTs. Umbilicospheres gain importance during the Pliocene on both sides of the Panamanian Isthmus, but mainly in the Caribbean Sea they build an important part of the nannofossil assemblage. Lack of water mass exchange from the Pacific towards the Caribbean Sea and pronounced increase in SSS (e.g. Haug et al., 2001; chapter 1.2.1.2) in the Caribbean Sea could support the hypothesis of *Umbilicosphaera* to flourish under high saline conditions. Reticulofenestrids are still the main component in both assemblages. LPZ taxa show high frequencies on both sides, however, they gain higher importance in the Pacific compared to the late Miocene. This strongly indicates the decrease in upwelling intensity at this particular site, which may be due to the tectonically induced change in the position of Site 1241 on the Cocos Plate away from the equator. This could trigger both, a decrease of turbidity and increase in stratification due to changing current systems.

6.4.2.3 Closure of the Panamanian Seaway

The fundamental changes in ocean circulation associated with the Neogene closure of the Panamanian Seaway strongly affect nutrient distributions and marine productivity. Recent modelling studies by Schneider & Schmittner (2006) document shifts in nutrient distributions associated with reorganisations of ocean circulation and marine productivity patterns. The model describes strongest regional impact of the closing Panamanian Seaway on the net primary production in the eastern equatorial Pacific. Model results show a more than 3-fold increase of primary production from the deep-sill stadium to the fully closed Panamanian Isthmus, due to restriction of nutrient-enriched outflow, thus leading to increased productivity in the tropical Pacific. In contrast, the reduced inflow of high nutrient sub-surface water from the Pacific decreased biological productivity in the Atlantic (Schneider and Schmittner, 2006). Proxy records largely support the relation of palaeoproductivity trends to the Neogene closure of the Panamanian Seaway. These are (1) the increasing and eastward shifts in Pacific mass accumulation rates of $CaCO_3$ (Lyle, 2003) and opal (Farrell et al., 1995b) as well as (2) changes in foraminiferal species composition towards low productivity indicators in the North Atlantic (Bartoli et al., 2005), (3) decreasing $\delta^{13}C$ from benthic foraminifers in the Panama Basin (ODP site 677, Mix et al.,

1995), (4) divergence of Atlantic-Pacific benthic $\delta^{13}C$ (Jain and Collins, 2007), and (5) relative sand fraction values (Haug and Tiedemann, 1998; Haug et al., 2001; Steph et al., 2005). The gradual constriction and final closure of the Panamanian Seaway resulted in higher nutrient concentrations in the deep Panama basin (Mix et al., 1995) together with enhanced flux of organic material (Schneider and Schmittner, 2006), as well as a gradual decrease in Caribbean palaeoproductivity, consistent with reduced current velocity and seasonality of photodetrital input (Jain and Collins, 2007).

Our data underline the relation between changes in marine palaeoproductivity of calcareous nannoplankton and the closure of the Panamanian Seaway. During open-Isthmus conditions in the late Miocene, MARs are higher in the Caribbean Sea than in the Pacific, mainly due to neritic carbonate delivered from adjacent carbonate banks. This also explains the higher sand and high carbonate contents at Site 1000. Amounts of nannofossil ARs are conform during that time interval on both sides of the Panamanian Seaway. They are conspicuously high with dominance of r-selective taxa, indicating the influence and connection of Pacific high-productivity waters into the Caribbean Sea. The high productivity indicator *Reticulofenestra* predominates in Pacific samples, whereas opponent LPZ taxa play a minor role, pointing to the high nutrient concentration and dominance of r-selective species at Site 1241. High nutrient waters flow into the Caribbean Sea and allow these species to flourish, although higher abundances of LPZ taxa clearly point to strong oligotrophic conditions during that in general high-productivity interval at Site 1000. This supports Jain et al. (2007), who proposed that Caribbean palaeoproductivities never reached an eutrophic threshold value during the Neogene. The presence of *Umbilicosphaera* at Site 1000 possibly refers to higher saline conditions in the Caribbean Sea, whereas the presence of *C. pelagicus* at Site 1241 indicates colder temperatures due to proximity to Equatorial Divergence.

Our Pliocene samples support changes due to closed Panamanian Seaway conditions. Due to interrupted surface water communication, two distinct settings developed. Still, MARs and sand contents are higher in the Caribbean Sea due to bank-derived material. Nannofossil ARs, however, are higher, and more fluctuating in the Caribbean Sea. But we observe a general decrease in coccolith productivity at both sides of the Isthmus of Panama towards the Pliocene. Reticulofenestrids are still dominant at both sites, but increase in LPZ taxa clearly underlines the oligotrophic conditions at Site 1241. Changing coccolithophore ecology after the closure of the seaway seems also to be reflected in a decrease in the relative contribution of *F. profunda* at Site 1000. However, coccolith accumulation rates are by far lower in the Pliocene, which might be a result of short-lived seasonal productivity events in an overall oligotrophic regime. Increased abundances of Umbilicospheres in the Caribbean Sea may indicate an elevation of salinities.

6.5 Conclusions

Our results indicate an increase in carbonate accumulation on both sides of the Panamanian Seaway during the Biogenic Bloom interval, reflecting an increase in nannoplankton productivity. The discrepancy in timing and duration of enhanced productivity between the Sites 1241 and 1000 clarifies the complexity of that event (Diester Haass et al., 2005). Use of grain size analysis gives insight in assemblage changes and the resulting changes in mass accumulation rates. The complex nature of the Biogenic Bloom interval appears to consist of two subsequent events of increased accumulation rates intersected at 6.7 Ma at both sites (chapter 7). This distinct minimum at 6.7 Ma in all accumulation rates (bulk mass, carbonate, nannofossils, single nannofossil species) could point to a superimposed forcing mechanism that controls accumulation patterns, like a general decrease in productivity or enhanced dissolution. Its relation to palaeoceanographic changes (chapter 8) will be discussed in chapter 9.

A comparatively much higher increase in coccolith accumulation rates than the general MARs supports the primary coccolithophorid response to the Biogenic Bloom event. Additionally, an increase in coccolith size may contribute to elevated coccolith ARs (discussed in chapter 7).

High pre-closure productivity is followed by lower MARs during closed-seaway conditions, as well as lowered coccolith ARs, which strongly decrease. A decrease in r-selective species and an increase in K-selective ones, however, point at typical oligotrophic conditions. Interrupted exchange of surface water masses led to a development of discrete nannofossil assemblages after the closure, which might point to higher stratification at Site 1241 and increased SSTs and SSS at Site 1000. An increase in productivity due to the closure of the Panamanian Seaway in the eastern equatorial Pacific was not observed, which may be superimposed by the tectonical induced drift of that particular site away from the equator and the preceding strongly elevated productivity due to the Biogenic Bloom.

CHAPTER 7 GRAIN SIZES

SEDIMENTOLOGICAL GRAIN SIZE ANALYSIS AS A PROXY IN MICROPALAEONTOLOGY – THE COCCOLITHOPHORID ASSEMBLAGE DURING THE LATE MIOCENE TO PLIOCENE BIOGENIC BLOOM INTERVAL IN THE EASTERN EQUATORIAL PACIFIC

(This chapter is a manuscript in preparation for Marine Geology. Minor text modifications have been made.)

7.1 Introduction

Coccolithophores are the most productive calcifying organisms on Earth today (e.g. Rost and Riebesell, 2004). Together with planktonic foraminifers, they produce the largest reservoir of carbonate rocks. This comparatively young group of haptophyte algae first appeared in the fossil record during the late Triassic (Bown et al., 2004) and gained dominance as the major contributor to pelagic deep-sea sedimentation in the Cretaceous. Several major evolutionary steps in the development of these primary producers have forced further changes in the carbon cycle, favouring the deep sea as a site of carbonate deposition (Hay, 2004). This shift of carbonate sedimentation from shallow shelves to the deep sea, with it´s creation of a responsive deep-sea sedimentary sink of $CaCO_3$, had major impact on the global carbon cycle and stability of Earth´s climate (Ridgwell and Zeebe, 2005). In general, the regional accumulation patterns are variably affected by the changing balance between productivity and dissolution and by physical processes (Peterson et al., 1992). However, very little is known about the evolutionary induced changes in carbonate sedimentation due to variations in marine calcareous plankton body sizes.

Since carbonate production in open-ocean conditions is mainly restricted to planktonic foraminifers and coccolithophores, grain size analyses provide a potential tool for quantification and evaluation of processes that contribute to spatial and temporal variations in the composition of biogenic carbonates. The distribution of grain sizes is widely used in palaeoceanography as a palaeoenvironmental proxy (Stuut et al., 2002b; Warner and Domack, 2002; Weltje and Prins, 2003; Le Roux and Rojas, 2007) for reconstruction of palaeocurrent vigour estimations of deep-sea bottom currents (McCave et al., 1995a; 1995b; Bianchi et al., 1999; McCave and Hall, 2006; McCave et al., 2006). Particle size analysis also helps to improve the characterisation of biogenic deposits. It is a powerful tool to detect and quantify compositional and textural changes of sediments (Aiello and Kellet, 2006). Variations in the grain size of calcareous compounds might be influenced by ecology and production rates of certain biogenic constituents and by dissolution and fragmentation due to sensibility to deep-water chemistry. In order to interpret the signal of particle size distribution, McCave et al. (1995b) proposed size-differentiated subfractions of deep-sea carbonates to range around a threshold value of 10 µm due to both coccoliths and foraminiferal fragments. Hay (2004) pointed out the use of the 'sand-silt-clay' ratio from calcium carbonate-rich sediments, where 'sand' means tests of planktic foraminifers, 'silt'

are test fragments of planktic foraminifers and some large calcareous nannoplankton remains, and 'clay' is essentially the calcareous nannoplankton component. Aiello and Kellet (2006) determined different size classes of sediment grains of very fine-grained sediments that represent the common biogenic components: tests and frustule fragments (10-100 µm), fecal pellets (> 50 µm), radiolarians (40-100 µm), juvenile foraminifers (40-50 µm), pennate (10-20 µm) and centric diatoms (20-50 µm), and coccoliths (2-10 µm).

Major evolutionary events in calcareous nannoplankton (e.g. Bown et al., 2004) are reflected in the average test size (Aubry et al., 2005). Thus, Aubry et al. (2005) implied that size history parallels diversity history in Mesozoic coccolithophores. Besides well known examples like the Cretaceous-Paleogene Boundary (Schmidt et al., 2004a; Bralower et al., 2006), less apparent events in Earth history could feature variations in grain size composition of the carbonate fraction of pelagic sediments due to assemblage changes. The well known size reduction in calcareous plankton at the Cretaceous-Palaeogene Boundary (Schmidt et al., 2004b; Bernaola and Monechi, 2007) is the result of a major global extinction; other evolutionary and ecological events could likely produce similar patterns. Such an example for drastic variations in the pelagic carbonate deposition is known from the late Miocene to Pliocene, which is characterized by prominent changes in carbonate accumulation rates between 12 and 5 Ma in all low latitude sites (Peterson et al., 1992; e.g. Berger et al., 1993; Mix et al., 2003b). These variations in carbonate accumulation rate are associated with the so called 'Carbonate Crash' and the 'Biogenic Bloom' (Farrell et al., 1995b; Lyle et al., 1995), which are thought to be influenced by changes in deep-water circulation, shoaling of the CCD, and shallow- to deep-sea fractionation (Peterson et al., 1992; Farrell et al., 1995b; Lyle et al., 1995; Roth et al., 2000; Lyle, 2003), or, respectively, an increase in palaeoproductivity (Dickens and Owen, 1999; Hermoyian and Owen, 2001; Diester-Haass et al., 2004). Aiello and Kellet (2006) detected grain size variations during that time interval. They identified the dominant large particles of the 'Carbonate Crash' as mainly formed by biosilicious components and, conversely, the smallest grain sizes deposited during the late Miocene to Pliocene 'Biogenic Bloom' as coccolith oozes.

In this paper, we claim that the determination of grain size distribution is a useful tool to detect micropalaeontological assemblage changes within the important coccolith carbonate fine fraction. It is used to interpret grain size changes within the context of ecologically or evolutionary induced changes of the nannoplankton assemblage. Thus, distinct floral shifts are supposed to be reflected in the particle size distribution. To test this hypothesis, we investigated the particle size distribution in late Miocene to Pliocene samples from eastern equatorial Pacific ODP Site 1241. Grain size distribution of the predominantly very fine-grained coccolith carbonate was compared with the floral composition during that interval of enhanced biogenic accumulation.

7.2 Grain size analysis

A variety of approaches exists to separate particles through thermal, chemical or mechanical parameters, e.g. adsorption, crystallisation, drying, solubility, boiling- or melting temperature, density (sedimentation, decanting, flotation), size (filtration, sieving), magnetism, or electrical charge. Traditionally used techniques for the determination of grain sizes are mechanical separations such as settling, Andreasen pipette, decanting, centrifugal sedimentation, and sieving (Irani and Callis, 1963). Since these technologies are time consuming and relatively imprecise, three analytical methods, especially for particle size analysis of the very fine-grained sediments, based on electrical (Coulter Counter), transport (SediGraph) or optical (Laser Particle Sizer) properties, became widely accepted within the last years. Their accuracy and application range are still under discussion since different techniques are likely to produce different results for identical samples (McCave and Syvitski, 1991; Syvitski et al., 1991b; Webb, 2000; Ferraris et al., 2002; Blott and Pye, 2006; Flemming, 2007; Goossens, 2008). Since different properties are measured, data are not comparable between Coulter Counter (electrical resistance pulse), Sedigraph (settling velocity) and Laser Particle Sizer (laser diffraction) (Syvitski et al., 1991b; McCave et al., 2006). Particle size determinations, especially in sediments, will always differ due to the imperfect sphericity of particles and heterogeneity of particle densities und thus neither of the three analytical methods shows 'true' results (Konert and Vandenberghe, 1997). There is no such thing as a 'perfect' method (Goossens, 2008).

These instruments are based on fundamentally different principles discussed in detail elsewhere (e.g. Syvitski et al., 1991a; Goossens, 2008). To note briefly: The Coulter Counter instruments operate on the principle of electro-resistant particle counting. It measures the number and volume of particles suspended in an electrically conductive liquid (Stein, 1985). The Sedigraph particle analyser determines the equilibrium velocities of particles settling through a liquid medium under influence of gravity by x-ray absorption. Stokes law relates these velocities to particle diameters for spherical particles (Singer et al., 1988; Webb and Orr, 1997). The Laser Particle Sizer is based on the system of low-angle laser light scattering (LALLS), i.e., the diffraction of scattered light caused by particles passing through a laser beam.

Besides these differences in physical principles, other issues are of prime importance for grain size analysis as discussed by Goossens (2008), such as the physical properties of the particles, the type of information a technique produces and the definition of grain-size.

7.2.1. Choice of methods

Each technique for particle size analysis measures different properties of the same material. Thus, differences between the measurements have a methodological origin. In all three methods, the shape of the particles is of prime importance since every technique defines the size of a particle in a different way. Sieve analysis provides a measure of the

width of the particle (measurement of the b-axis), whereas the settling (=pipette) analysis defines an equivalent spherical diameter (ESD='Stokes-diameter') for every particle of any shape. The laser diffraction reveals the disc diameters in volume-% depending on the orientation of particles or the detector geometry.

The limitation of electro-resistant particle counting of the Coulter Counter, as explained by McCave and Syvitzki (1991), is that it measures only a fairly narrow range of grain size on a single pass through the gadget. Bianchi et al. (1999) demonstrated that the use of volume-ESD (equivalent spherical diameter) with the Coulter Counter is especially useful for sediments with less than 5 % fine silt. Settling is strongly dependent on homogeneity of the analysed material, as well as the shape of the particle. It is expected to underestimate the nominal diameter of a sediment grain (Lane, 1938), because of the higher hydrodynamic resistance of nonspherical particles, which align perpendicular to highest stress when allowed to settle freely (Frenz et al., 2005). McCave et al. (2006) in turn elucidated the progressively higher underestimation of the sortable silt fraction (10-63 µm) by the Sedigraph due to change in absorption of the x-ray beam by particles of different mineralogical composition. However, for triaxial, platy particles, Matthews (1991) calculated a reduction of the terminal velocity of up to 40 % compared to their nominal equivalent and thus, the application of the settling methodology results in grain sizes that tend to be smaller than the actual particle sizes (Murray, 2002). Measurements of coccolith sizes using the settling methodology were done by Frenz et al. (2005). They detected coccolith plates to settle with slower velocities than spheres with the same diameter (ESD) and inferred that coccoliths with a nominal diameter of < 4 µm are strongly depleted in silt and enriched in clay fraction. For placolith species (e.g. *C. leptoporus*) they observed their nominal diameter to be about twice as large as their equivalent spherical diameters. Konert and Vandenberghe (1997) did a series of tests for interpretation of laser grain size analysis with respect to other methodologies. For certified material (glass spheres and certified reference material), the accuracy and reproducibility of the laser diffraction are very good. Their results for terrestrial soil suggest an offset towards larger diameters, which gets smaller with increasing particle size. That discrepancy has been explained by the anisometric shape of particles (Lehmann et al., 2004). Diffracted light distribution responds to the major and intermediate axes of particles that are primarily platy in the clay and fine silt fraction (Konert and Vandenberghe, 1997). Therefore, clays and fine silts are recorded as coarser particles by laser compared to settling, hence an underestimation of clay fraction occurs if a Laser Particle Sizer is used. Likewise, other authors revealed that laser diffraction underestimates the amount of clay particles by 20-70 % with respect to the clay content determined from pipette (= settling) analysis (McCave et al., 1986; Loizeau et al., 1994). Pabst et al. (2000), showed that small particles < 2 µm (ESD, settling diameter) exhibit disc diameters of 3-5 µm and larger when analysed by laser diffractometry. Pabst et al. (2000) studied systematic differences in the measurement of particle size distributions of kaolins

and clays by both, sedimentation and laser light scattering method. They proposed a physically justified modification of Stokes law, based on utilisation of a shape factor for the oblate, platy-like particles. They found that with the use of the modified Stokes law, the corrected sedimentation data come very close to light scattering data. Lehmann et al. (2004) observed the shape factor to change with grain size making it impossible to convert sedimentation to laser diffraction data or vice versa by using a single conversion factor. They postulated the shape factor to become smaller for larger grain sizes, supporting the 'underestimation' results of the small-sized fraction evaluated by laser diffraction (Konert and Vandenberghe, 1997). Blott and Pye (2006) demonstrated significant differences between laser diffraction analysis and dry sieving of natural sediments due to effects of particle shape, but also due to the way in which the computer software interprets the light scattering data to calculate the most likely size distribution. The importance of the adopted post-processing procedure for particle-size distribution is demonstrated by Flemming (2007). He pointed out that the computation of textural parameters from bi- or multimodal size distributions produce erroneous results.

The choice of analytical methodology for grain size determination depends on the objective target (Syvitski et al. 1991). For palaeocurrent speed estimations it is indispensable to respect the sedimentological 'dynamical' behaviour of particles and thus neglect grain sizes < 10 µm due to their cohesive behaviour (McCave et al., 1995b). In this case, size is a way of expressing sedimentation velocity and the 'sedimentation' size (i.e. ESD, 'Stokes diameter') may be more valuable than the size determined by light scattering, thus two particles that settle with the same velocity (therefore have the same Stokes size) can scatter light differently (therefore have different Mie/Fraunhofer sizes, see below) (Webb, 2000). An oblate, plate-like particle with a Stokes diameter of 2 µm, may have a length of 10 µm and a thickness of 0.4 µm. Herein the 2 µm are of interest for palaeocurrent investigations (dynamical grain size), whereas the 10 µm are of interest for micropalaeontological analyses (maximum grain size). The volume-equivalent sphere of that particle has a diameter of about 3.9 µm (see Konert and Vandenberghe, 1997). Thus, the platy particles are detected in different grain size fractions depending on the chosen method. Whereas the settling method is controlled by sedimentological parameters, the laser scattering method depends on the technical parameters specified by the construction of the Laser Sizer (W. Mutter, Fritsch GmbH, Technical Director, pers. com.) (Berthold et al., 2006). In the case of anisometric particles, 'particle size' is not even uniquely defined (Pabst et al., 2006) and interpretations have to be done carefully.

Based on the arguments above, the use of a Laser Particle Sizer appears to be the most suitable technique for the interpretation of carbonate fine-fraction for comparison with nannoplankton assemblages.

7.2.2 Low-Angle Laser Light Scattering

For evaluation of scattered laser information, two main diffraction theories are typically used. The Mie theory uses light scattering energy as a function of particle size and observation angle (Wedd, 2003), hence absorption and refraction indices of sample and medium have to be considered. The Fraunhofer theory approximates particle size from extinction efficiency (scattering + absorption) and assumes a constant extinction coefficient for all particles (Sperazza et al., 2004). The intensity and distribution of diffracted light around the central beam can be related to particle size, assuming spherical geometry. The range of validity for this method is limited on the low end to particle diameters a few times greater than the wavelength of the incident light for particles (e.g., Agrawal et al., 1991). The advantage in using the Fraunhofer diffraction is that this model does not take the optical properties into account (Wedd, 2003; ™FRITSCH, Instruction manual analysette 22), thus the interpretation is not dependent on the absorptive or refractive properties of the material (Ferraris et al., 2002). Extinction and hence the scattering is very weak for tiny particles and particularly weak below 0.2 µm. Following this, the Mie theory continues to report the presence of the sub-0.2 µm material. Sperazza et al. (2004), who worked with Mie parameters, observed extraordinary bimodal distributions for sediments in the < 10 µm size fraction, if absorption settings are near zero (clear), probably because of sub-optimal diffraction by particles with a diameter similar in size to the laser wavelength. The Fraunhofer approximation disregards small scattering contribution relative to the rest of the light energy and in this instance fails to report any quantity of particles less than 0.2 µm (Wedd, 2003). The appearance of 'ghost' particles is interpreted by Ferraris et al. (2002) as virtual particles in the range < 1 µm, produced as an artefact of refractive dispersion of light within transparent particles. The refracted light is registered at large scattering angles as anomalous diffraction, and is therefore interpreted by the Fraunhofer analysis as being produced by very small particles (Ferraris et al., 2002).

7.3 Material and methods

ODP Site 1241 was recovered during Leg 202 at 5°50´N 86°26´W in the Guatemala Basin on the north flank of Cocos Ridge at 2027 m water depth (Mix, Tiedemann, Blum et al., 2003a) Tectonic backtracking of today´s position on the Cocos Ridge places Site 1241 southwestwards to about 4°N 87°10´W at 3 Ma; 1.5°N, 89°30´W at 7.5 Ma (Pisias et al., 1995).

Sieving analysis resulted in a mean sand content of the samples of around 3 wt-%, carbonate content was determined around 80 wt-% (http://iodp.tamu.edu/janusweb/links/links_all.shtml). Thus, the analysed sediments represent nannofossil oozes. SEM investigation confirmed this assumption. Silicious and foraminiferal detritus occur only in the size class larger than nannofossils (> 12 µm) and are rare. Preservation of calcareous nannofossils is excellent. In our samples this is notably indicated by existence of delicate structures of placoliths and even holococcoliths.

All sediment samples were freeze-dried prior to examination. In order to disaggregate the carbonate-rich sediment, sonification proved to be the most effective tool. For nannofossil abundance analysis, tests of non-destructive dispersing support the work of Bairbakhish et al. (1999) that coccolith breakage in ultrasonic bath (in our test up to 60 min) is negligible. Associated with grain size measurements, however, sonification has to be applied carefully, since fragmentation of larger fragile microfossil tests may create new, smaller particles. As result of sonification experiments, we chose a sonification time of 30 s as best balance between avoidance of formation of aggregates and prevention of fragmentation of delicate foraminifera tests. Since organic carbon content in the samples is low (< 0.4 wt- %, Mix et al., 2003b) binding of grains and forming of particle aggregates due to organic carbon are negligible and, therefore, treatment of the samples with organic solvents was avoided. Cohesive behaviour due to clay was not perceived.

Determination of absolute and relative coccolith abundances was carried out with Scanning Electron Microscopy (SEM) on a total of 149 samples. For sample preparation the filtration technique described by Andruleit (1996) was used. SEM investigation was performed with a ™CamScan 44 at 5000 x magnification. Taxonomic identification follows Farinacci (1969), Jordan and Kleijne (1994), Perch-Nielsen (1985b), Young (1998) and Young et al. (2003).

Particle size analysis by laser diffraction was carried out at IFM-GEOMAR, Kiel using the ™FRITSCH analysette 22 NanoTec Laser Particle Sizer (Fritsch GmbH, Idar Oberstein, Germany). No separate sample preparation was necessary prior to measurements, since complete dispersion can be achieved by applying the built-in ultrasonification unit. The NanoTec Laser Particle Sizer works with a HeNe-Laser (wavelength λ=655 nm) and measures particles with a convergent laser beam (reversed Fourier-Optic) and model-independent evaluation by Fraunhofer theory (Pabst et al., 2000; Gregorova et al., 2006), which we used as standard report of the scattered light information due to its advantages for homogeneity of samples. Thus, our analysis used foreward-scattered light falling on the photosensitive sensor rings, enabling screening of a particle size range from 0.1-2000 µm. To increase resolution, we selected multiple measurements with a measuring range of 204 channels with 200 scans each. In order to exclude measuring artefacts, after initial tests all adjustable parameters concerning sample treatment during measurement (volumetric flow rate, stirrer speed and ultrasonics) were kept constant for all measurements. The entire system of the ™FRITSCH analysette 22 NanoTec works with distilled water. Turbulent flow through the measuring cell guarantees a statistical distribution of particles (pers. com. C. Berthold); reproducibility of Laser Particle Sizer measurements is assessed as high. For grain size analyses, measurements were made on a total of 74 samples (every second of SEM-samples), on which assemblage counts were conducted.

The age model for the late Miocene to Pliocene Interval in the tropical east Pacific Site 1241 (unpublished, see chapter1.1.3.4) is based on tuning high frequency variations in GRA density and benthic $\delta^{13}C$ to the orbital solution of Laskar et al. (1993), and benthic and

planktonic $\delta^{18}O$ records. This astronomically derived age model is in agreement with the most recent astronomical polarity time scale (Lisiecki and Raymo, 2005) and other recent orbitally tuned age models (Site 1237, R. Tiedemann, unpublished data).

7.4 Results

7.4.1 Assemblage composition

The mid-Neogene assemblages of the eastern equatorial Pacific Site 1241 show a strong predominance of reticulofenestrid coccoliths. Other dominant species are *Florisphaera profunda*, *Sphenolithus abies*, *Discoaster* spp., *Calcidiscus* spp., *Umbilicosphaera* spp., *Coccolithus pelagicus,* and *Helicosphaera* spp. (Fig. 7.4-1).

Taxa of the lower photic zone (LPZ), *Florisphaera profunda* and *Gladiolithus flabellatus*, show strongly fluctuating abundances between 2.3 and 24.8 % with a mean value of 9 % and lowest values between 7 and 5.9 Ma. Abundances of *Sphenolithus abies* strongly increase from about 5 % at 6.6 Ma to 25 % at 6 Ma. *Discoaster* spp. show low abundances over the entire interval, with a slight increase and small peaks in abundances up to 6 % around 6.4 Ma. The observable trend of an increase in abundances of the low productivity indicators (LPI = LPZ + *Discoaster* spp. + *S. abies*) is coincident with a dramatic decrease of reticulofenestrids.

The relative abundances of *Reticulofenestra* vary from 41.7-85.6 % with an average value of 70 %. The general trend shows a pronounced shift towards lower values in the younger part, reaching minimum values at 5.9 Ma. The small-sized *Dictyococcites productus / Reticulofenestra minuta* group shows abundances from 4.1-72.4 %. The generally high values (~ 50 %) show a decrease starting at 6.3 Ma towards lowest values below 10 % after 6.0 Ma. Abundances of the *Reticulofenestra haquii / Reticulofenestra minutula* group fluctuate around 20 % with an overall trend towards higher values in the younger part after 6.3 Ma. *Reticulofenestra pseudoumbilicus* Medium shows a strong increase in abundance between 7.55 and 6.3 Ma. *Reticulofenestra pseudoumbilicus* never reaches significant values.

Other placoliths exhibit abundances of 3.6-29.6 %, whereas *Calcidiscus* spp. reach mean values around 5.5 % (1.1-26.2 %), *Umbilicosphaera* spp. 3 % (max. 14.7 %), *Coccolithus pelagicus* 0.9 % (max. 4.1 %) and *Helicosphaera* spp. 0.57 % (max. 2.4 %). Here, occurrences of *C. pelagicus* and *Helicosphaera* spp. correlate inversely, with high abundances of *C. pelagicus* during the late Miocene samples and *Helicosphaera* spp. in the Pliocene sediments.

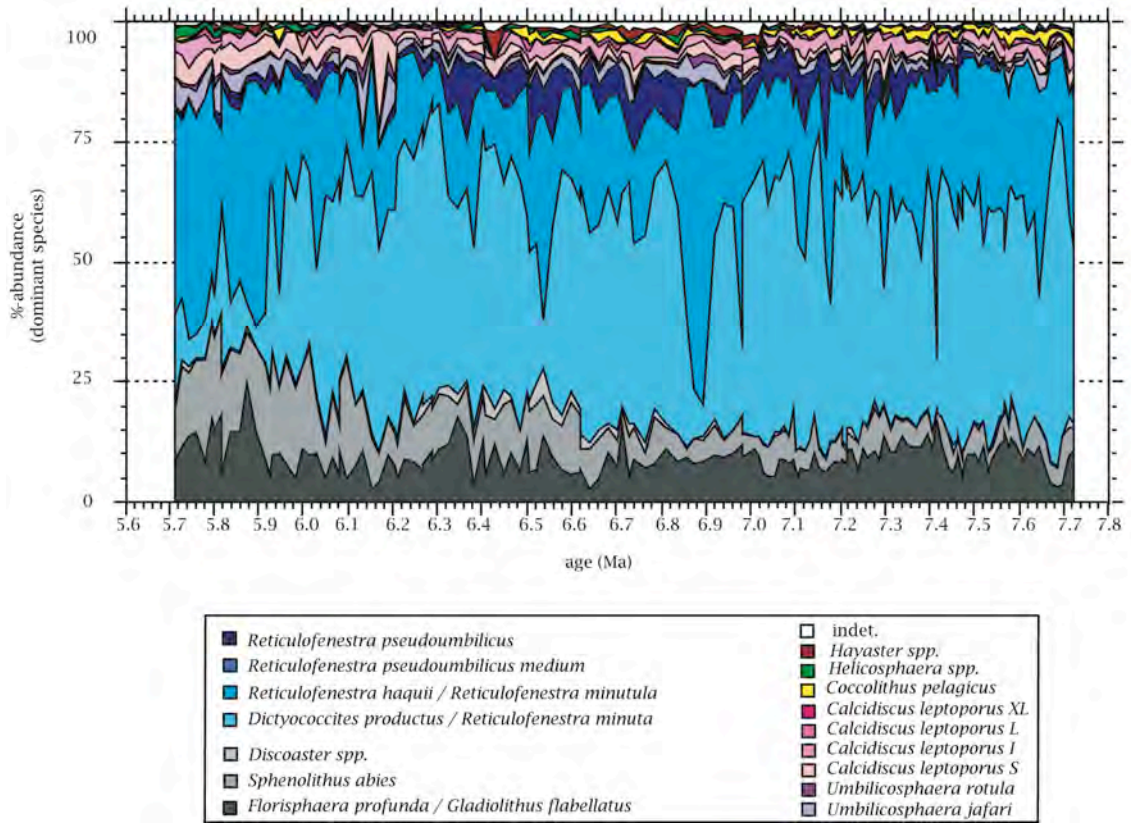

Fig. 7.4.1-1 Site 1241: Calcareous nannoplankton assemblage composition.

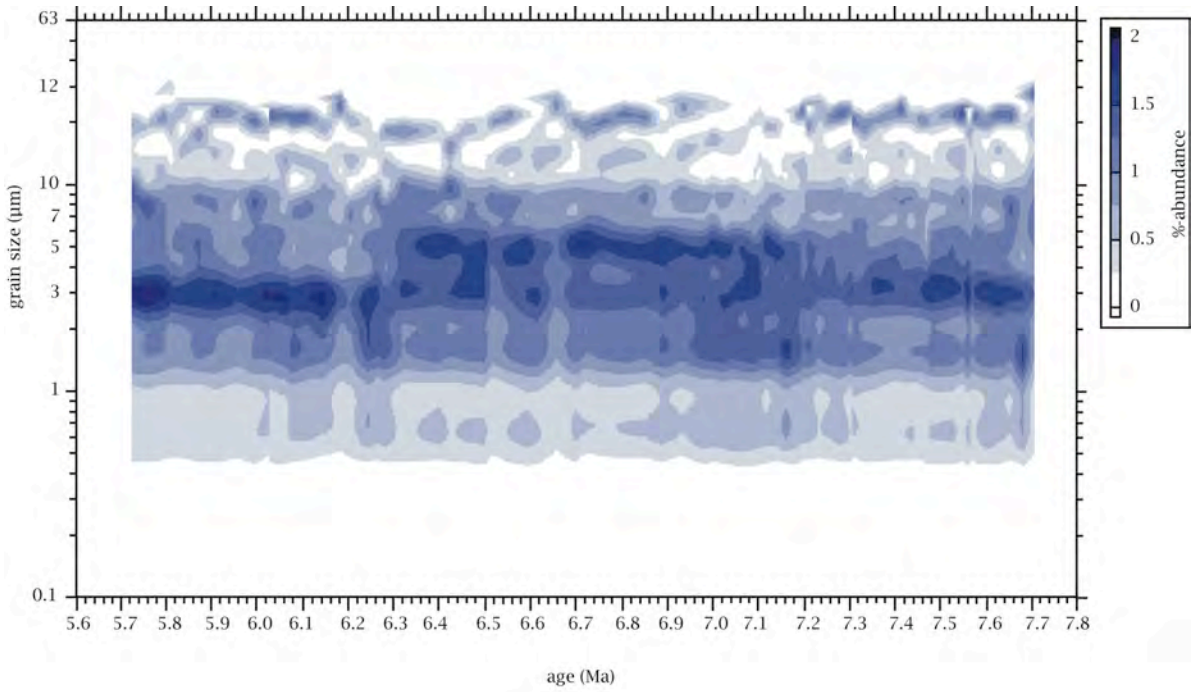

Fig. 7.4.2-1 Site 1241: Grain size distribution measured by LALLS.

7.4.2. Granulometry

According to the texture of the bulk sediment of the late Miocene to Pliocene Site 1241 (Fig. 7.5-2), clay and silt fractions show moderate amplitudes with an inverse relation. Values of clay range around 30 wt- %, silt content ranges between 55 and 75 wt- %, whereas sand content is extremely low. Within the silt fraction, the fine silt (2-10 µm), represented by coccoliths, builds the main part. Sand fraction in Laser measurements show few distinct peaks, which are not supported by the sieving results (here values are constantly around 2 wt- % sand).

Laser particle size analysis (Fig. 7.4.2-1) shows polymodal grain size distribution, with clear peaks around 3 µm in all samples. The total range of grain sizes is from 0.5 to 12 µm, whereas highest abundances are between 1.5 and 7 µm.

Analysis of particle sizes shows three distinct phases of grain size evolution in the record. The oldest part from around 7.7 Ma to 7.2 Ma as well as the youngest part from 6.3 Ma to 5.72 Ma show a strong peak of abundance around 3µm whereas the middle part, from 7.2 to 6.3 Ma shows a wide distribution of maximum values between 3 and 6 µm with an absolute maximum at 5 µm.

7.5 Discussion

7.5.1 Preservation

Henrich et al. (2003) summarized the state of preservation of carbonate particles in marine environments to depend on various factors, including dissolution, pCO_2 and CO_3^{2-} concentrations in the water masses, sedimentation rates, carbon rain ratio, diagenetic regime in pore water, as well as over all size, wall thickness, crystal size, surface texture and porosity of the particles. Thus, variations in the grain size of calcareous compounds might be influenced by sensibility to water chemistry, ecology/evolution and production rates of certain biogenic components.

Variations of sand percentages in the carbonate fraction are used as a proxy to reconstruct either changes in carbonate dissolution or differences in carbonate accumulation between foraminifers and calcareous nannoplankton (e.g. Peterson and Prell, 1985). In deep-sea carbonates, decreasing sand content is often interpreted as increasing dissolution (Berger et al., 1982; Bickert et al., 1997; Stuut et al., 2002b; Gröger et al., 2003a; 2003b), however, according to Henrich et al. (2003) conventional calcite dissolution proxies produce incorrect and misleading results due to dilution with non-carbonate particles, downslope re-suspension, lateral advection and winnowing of sediments by bottom currents, as well as changes in ecology of carbonate producers. Especially changes in the ratio between nannofossil placoliths and foraminiferal shells are regarded as the primary mechanism that could change the relative portion of the coarse fraction (Dittert et al., 1999 and references therein). Since our late Miocene sediments at Site 1241 never contain more than 8 wt- % sand and possess extremely high carbonate contents around 80 %, the results of the grain size

distribution provide important information about the predominance of the biogenic constituents. The dominance of finest grain sizes (1-10 µm) suggests calcareous nannoplankton to be the most important carbonate producer in the Miocene eastern equatorial Pacific with negligible contribution of foraminifers. Foraminifers are rare, but well preserved, and no substantial amount of fragments is observed.

The great resistance of coccoliths to dissolution (Hay, 1970) is generally attributed to an organic coating (McIntyre and McIntyre, 1971) or to the accelerated transport via sinking faecal pellets (Honjo, 1975). However, in contrast to planktic foraminifers, dissolution of coccoliths appears not to be related to a restricted depth range but to phylogeny (Hay, 2004). Importance of a size-dependent preservation-potential threshold of 3 µm for coccoliths is highlighted by Young et al. (2005). They argued that subtle changes in coccolith size-frequency through time could result in significant changes in observed diversity, independent of any change in actual diversity, especially if large numbers of coccoliths shifted above or below the 3-µm preservation-potential threshold. Additionally, Beaufort et al (2007) indicated the absence of dissolution of coccoliths between the photic zone and the lysocline. Anyway, the relatively shallow depth of 2027 m, in comparison with the depth of the East Pacific lysocline at 3600 m Lyle et al. (1995), indicates carbonate dissolution to be of minor importance at Site 1241. Even though biodiversity estimations of calcareous nannoplankton may particularly be biased by preservation (Young et al., 2005), their excellent preservation in our samples makes them a useful tool for the use of grain size analyses.

7.5.2 Texture of sediments

A posed challenge is the representative quantification of the coarse fraction in a fine-fraction dominated sediment. In our samples, the sand-fraction measured by laser diffraction is negligible except for a few single peaks, most of which are represented by one single measure point. Since these peaks are not traced in the distribution of the sand-fraction determined by sieving, it is questionable if this is a problem of the methodology, due to small amount of material measured, or if it might be due to building of aggregates. The small amount of material (100 mg) needed for the analysis with the analysette 22 would explain peaks in the sand-fraction, if, by accident one / few sand grains are measured, and conversion of values into volume-% of the ™FRITSCH software would overestimate this value.

The correlation of sediment fractions suggests the formation of aggregates by an inverse relation between the grain size classes. Thus, as shown in Fig. 7.5.2-1, peaks in sand are compensated by clay and fine silt, not by coarse silt. This supports the cohesive behaviour of fine sediments < 10 µm as defined by McCave et al. (1995b). Since the traditional method of quantification of sand gives amounts < 5 wt-% sand in our samples, we recalculated texture values given by the laser normed on fine fraction for further plots (Fig. 7.5.2-2A). This way,

we ignore the small amount of sortable silt (McCave et al., 1995b) and clay -sized material that behaves cohesive. Also, these critical sand values have not been observed in SEM measurements.

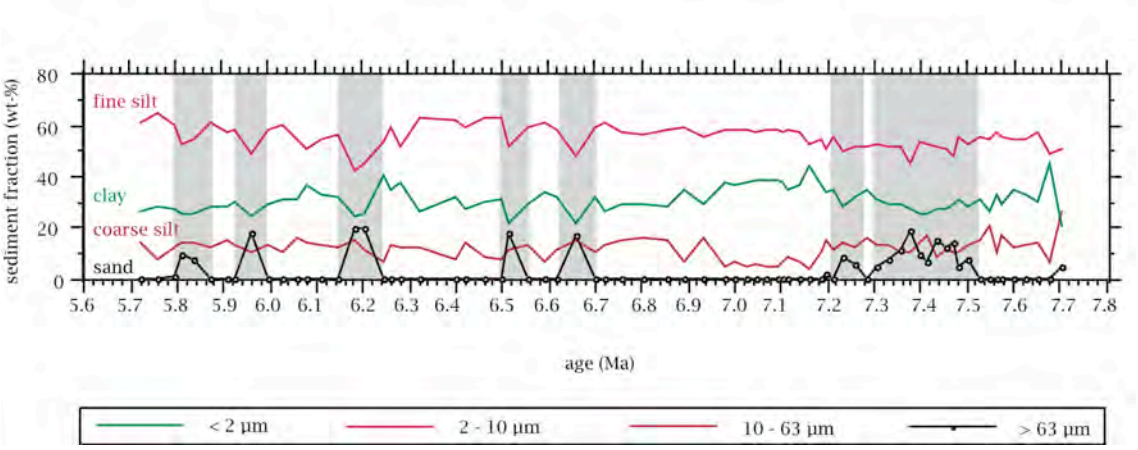

Fig. 7.5.2-1 Site 1241: Sediment fractions measured by LALLS.

7.5.2.1. Biogenic Bloom at Site 1241 and marine plankton body size

Since silt is the dominating grain size in our sediments, we defined two size classes within the silt-fraction, between the coccolith-fraction and the foraminiferal plus biosilicious fossil fragments. Fraction A was defined as 2-10 µm, fraction B as 10-63 µm (after Robinson and McCave, 1994). As applied by Stuut et al. (2002a), we used a log-ratio of the relative abundances of the two fractions A and B to relate coccolith abundances against other fragments. This relation between fine and coarse silt, the 'coccolith-carbonate-index' (CCI), is presented in Figure 7.5.2-1B. The CCI shows strong predominance of fine silt, starting with highest values at 7.2 Ma, followed by strongly fluctuating values from at 6.94 Ma onward and strong incursions of values occurring at 6.67 Ma and 6.19 Ma.

This trend of strongly increased dominance of fine silt at 7.2 Ma with following constant high values is supported by an increase in grain size maxima in the silt fraction (Fig. 7.5.2-2C) as well as by the increase in MARs and nannofossil ARs (Fig. 7.5.2-2D).

Inferred from the grain size distribution at Site 1241 it is evident, that an increase in coccolith dominance (CCI) appeared as well as an increase in coccolith size at 7.2 Ma. This is supported by increased nannofossil accumulation rates, but surprisingly accumulation values drop back again (until 6.68 Ma) during that interval of dominance of fine silt and largest grain sizes (7.2-6.2 Ma).

McCave et al. (1995b) showed the coccolith carbonate to be directly related to productivity at pelagic sites above the lysocline. The elevated CCI-values in our samples point to an increase in coccolith productivity during the Biogenic Bloom interval. Additionally, the increase in maximum grain sizes is verified by a change in the assemblage composition, where larger coccolith species appear and become more abundant (notably

R. pseudoumbilicus M). Their disappearance is similarly affirmed by a change in the grain size distribution towards dominance of smaller particles after 6.3 Ma.

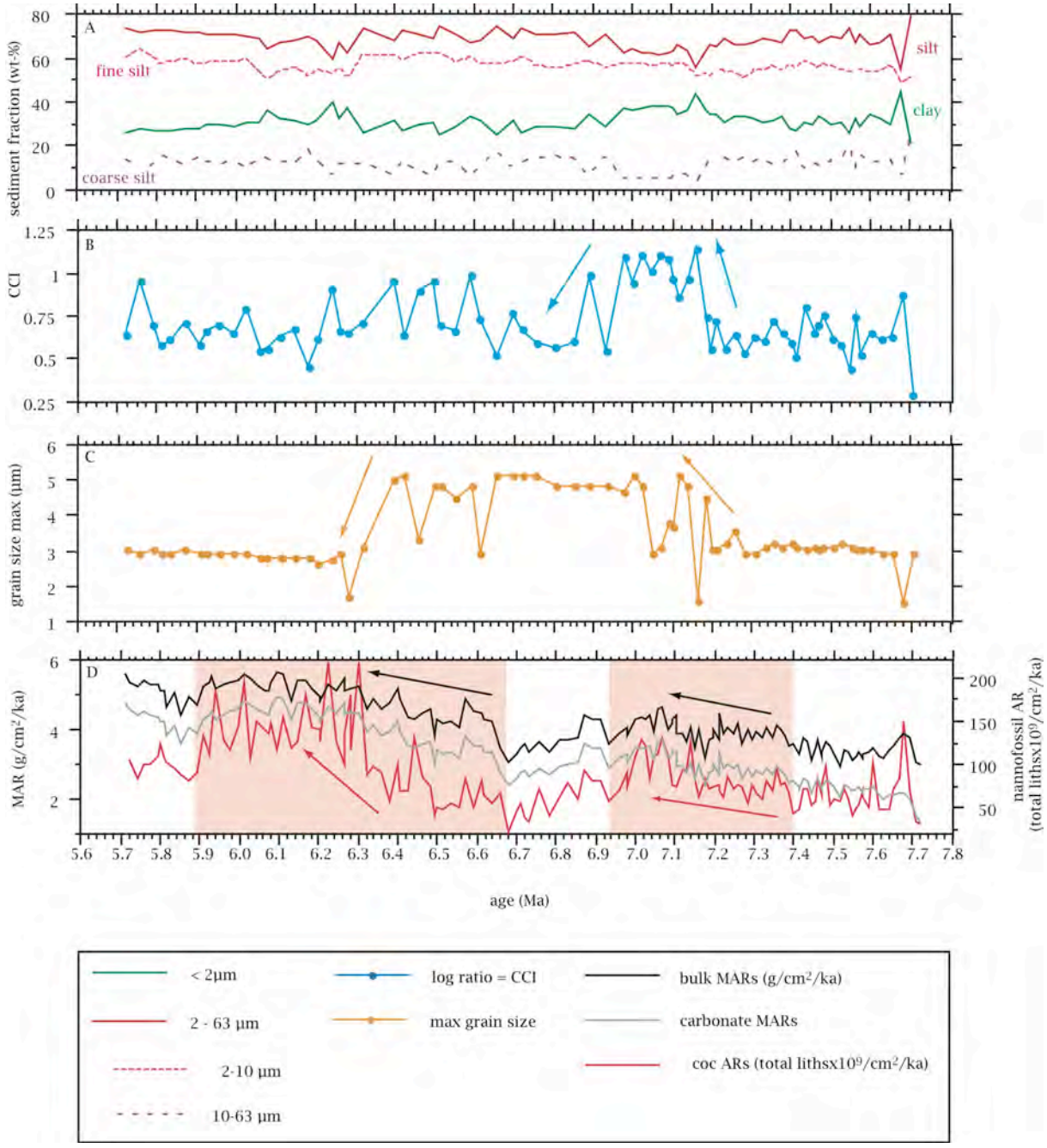

Fig. 7.5.2-2 Site 1241: A: sediment fractions measured by LALLS, B: calculated 'coccolith-carbonate-index', C: grain size maxima within fine-fraction, D: mass accumulation rates: bulk MARs, carbonate MARs and nannofossil accumulation rates.

Floral composition and grain size analyses point to the importance of nannofossils with respect to carbonate accumulation patterns in the Biogenic Bloom interval. The observed patterns suggest a 'dual-model' of the Biogenic Bloom interval at eastern equatorial Pacific Site 1241. A slight rise in MARs is favoured by an increase in coccolith dominance as well as an increase of maximum grain sizes, i.e. larger species. Regarding the %-contribution of

different species to coccolith carbonate (Young and Ziveri, 2000; Baumann, 2004) larger species contribute a comparatively greater amount of carbonate compared to small species. For this reason these large species (e.g. *R. pseudoumbilicus* M) play a dominant role during that first interval of the Biogenic Bloom but loose importance after 6.3 Ma. Although the numerical dominance of nannofossils stays constant, it is obvious, that the second, and drastic increase in coccolith accumulation between 6.68 and 5.9 Ma is due to an ecologically induced increases in productivity.

7.5.3 Micropalaeontology

In order to use grain size analysis as a proxy for changes in nannofossil composition one has to keep in mind, that assemblage composition only describes the nannofossil content of the sample, whereas laser grain size measurements reflect the whole grain size spectrum within a sample.

In order to assess the entire grain size spectrum at the SEM we did a series of size measurements of all particles using measurements of a- and b- axes of platy particles. A comparison of both data sets is given in Fig. 7.5.3-1. The figure shows that smallest grain sizes are underestimated by LALLS compared to SEM. Thus, these results strongly support the conclusions of Konert and Vandenberghe (1997), Lehmann et al. (2004) and Papst et al. (2000) that laser diffraction underestimates the amount of smallest grain sizes. Peaks in larger grain sizes in the laser measurements may appear due to the methodological problem, that data are converted to volume- % by the software of the ™FRITSCH analysette 22. Thus, linear correlation between the volume- %-distribution of laser grain size measurements with SEM-length measurements of sediment particles is questionable. The question is still unsolved, what information may be contained in a grain-size frequency distribution. It is fact that different methods of grain-size analysis, when applied to the same material, produce incongruent textural data (Flemming, 2007).

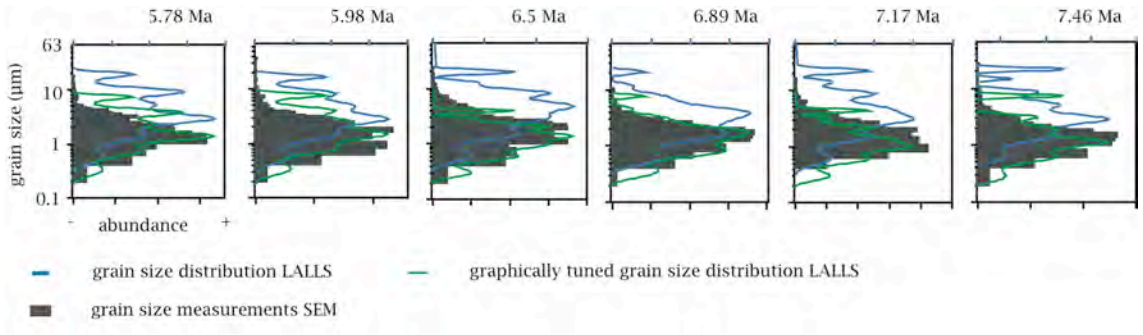

Fig. 7.5.3-1 Site 1241: 'Correlation' between grain size distribution determined by LALLS and SEM.

Our data prove that there is a relation between grain size and assemblage composition. Even if the results of the LALLS have to be taken carefully, grain size variations trace distinct floral shifts in the Biogenic Bloom interval at Site 1241. This underlines the statement of

Blott and Pye (2006), that laser diffraction analysis of a sediment record is sufficient to establish spatial or temporal trends in particle size characteristics.

Our results, however confirm that particle-size distribution is not only depending on the method, but also on the adopted post-processing procedure (computer software interpreting the light scattering data). An arbitrary arrangement of nannofossil assemblages into certain grain size classes does not fully allow a correlation of the 'relative' abundances of both datasets, i.e. the micropalaeontological and the sedimentological grain size distributions. This underlines the complexity of problems by converting data received by different methods into comparable values (Lehmann et al., 2004).

7.6 Conclusions and summary

Our data support that grain size analysis with laser diffraction is a useful tool to easily detect floral changes within the fine fraction of pelagic carbonates. Interpretation of particle size distribution given by LALLS has methodological problems, which also depend and can be reduced by on the adopted post-processing procedure (computational procedures; Blott and Pye, 2006; Flemming, 2007).

The late Miocene Biogenic Bloom at Site 1241 is characterised by a 2.5-fold increase in the total carbonate accumulation rate. However, the nannofossil accumulation rates show an up to 8-fold increase and therefore highlight the importance of coccolithophores as the primary carbonate source for the bloom. This supports the data observed by Diester-Haass et al. (2005) for the Biogenic Bloom interval in the Atlantic.

We are able to classify the Biogenic Bloom in the eastern equatorial Pacific to be not only generated by one single cause, but to be the result of two subsequent changes: (1) an increase in grain sizes within the fine fraction followed by (2) an increase in coccolith accumulation rates. Thus, the investigated time interval reveals distinct shifts in the nannofossil assemblages, in grain size distribution, and in carbonate accumulation. The first increase in carbonate accumulation rates occurs between 7.4 Ma and 7 Ma. During this initial increase, grain sizes and coccolith assemblage both indicate a boom of rather large species (particularly important is *R. pseudoumbilicus* M), whereas the coccolith accumulation rate increased only slightly. Thus, the increase in carbonate accumulation is caused mainly by the increase of coccolith size. At 6.7 Ma accumulation rates started to increase rigorously and reached maximum values between 6.3 and 5.9 Ma. Here, the most prominent shift in grain size and assemblages is observed, indicated by smaller species and thus smaller grain sizes. However, MARs remain unexpectedly high, which is the result of dramatic increase in coccolith accumulation rates.

This clearly indicates that both, evolution- induced size changes and ecology- induced increases in productivity, contribute to enhanced carbonate accumulation rates. It seems, that the increase in productivity had a stronger impact on the carbonate budget than size of species. The Biogenic Bloom seems to be solely a coccolithophorid bloom at Site 1241.

CHAPTER 8 STABLE CARBON AND OXYGEN ISOTOPES OF FINE-FRACTION

Stable carbon and oxygen isotopes ($\delta^{13}C$ and $\delta^{18}O$) of the bulk fine-fraction (< 63 µm) of deep-sea carbonates have been widely used to investigate past changes in oceanic productivity and shallow mixed-layer temperatures (e.g. Anderson and Cole, 1975; Margolis et al., 1975; Shackleton et al., 1993; Williams and Bralower, 1995; Shackleton and Hall, 1995d; Shackleton and Hall, 1997). This technique is particularly useful for pelagic nannofossil oozes and chalk, which contain little or no unaltered planktonic foraminifers or are indurated or cemented (Margolis et al., 1975; Zachos et al., 1989). Additionally, sample processing is easy and fast and allows a more rapid assay than does treatment of foraminifers. Culture and field studies document the value of the stable isotope signal of coccoliths for palaeoceanographic studies (Dudley et al., 1980; Goodney et al., 1980; Dudley et al., 1986; Dudley and Nelson, 1989; Paull and Balch, 1994; Liu et al., 2002). Since individual coccoliths are too small to be routinely separated (Paull and Thierstein, 1987), however, the isotope measurement of the bulk fine-fraction in coccolith-dominated sediments is still a standard method for stable isotope analyses (e.g. Bains et al., 1999).

8.1 Composition and preservation of bulk fine-fraction

Pre-requisite for the use of the bulk fine-fraction for isotope analyses is that contamination by other carbonate particles that may mask the primary nannofossil isotope signal is minimal. Therefore, detailed examination of sample composition is necessary. This was done with the late Miocene to Pliocene sediments of Sites 1241 and 1000 using SEM (Chapter 2.2 and following). This guaranteed that contribution of non-coccolith carbonate particles, such as fragments and juvenile tests of foraminifers and secondary, diagenetically precipitated calcite is negligible. Here, the inspection of the degree of preservation of coccoliths was turned out to be optimal.

Due to the fact, that all samples are almost exclusively composed of nannofossils with absolutely negligible contribution of other calcareous bioclastic fragments (restricted to the fraction larger than 20 µm), the fraction smaller than 20 µm was chosen for bulk isotope analyses (see Fig. 8.1-1). Mainly pennate and centric diatom frustules, some rare silicoflagellate, dinoflagellate cysts and foraminiferal test fragments present the > 20 µm -fraction, whereas the < 20 µm -fraction is exclusively composed by nannofossils, except some few (mainly opal) test fragments, and unidentifiable detritus, the latter represented in grain sizes smaller 1 µm (see chapter 8.2.3). Due to influence of surrounding carbonate platforms, sediments of Site 1000 contain aragonitic needles in the grain size fraction smaller than 1 µm (Plate 5, Appendix A1-5).

In addition laser grain size measurements support the constancy of samples composition (see chapter 6).

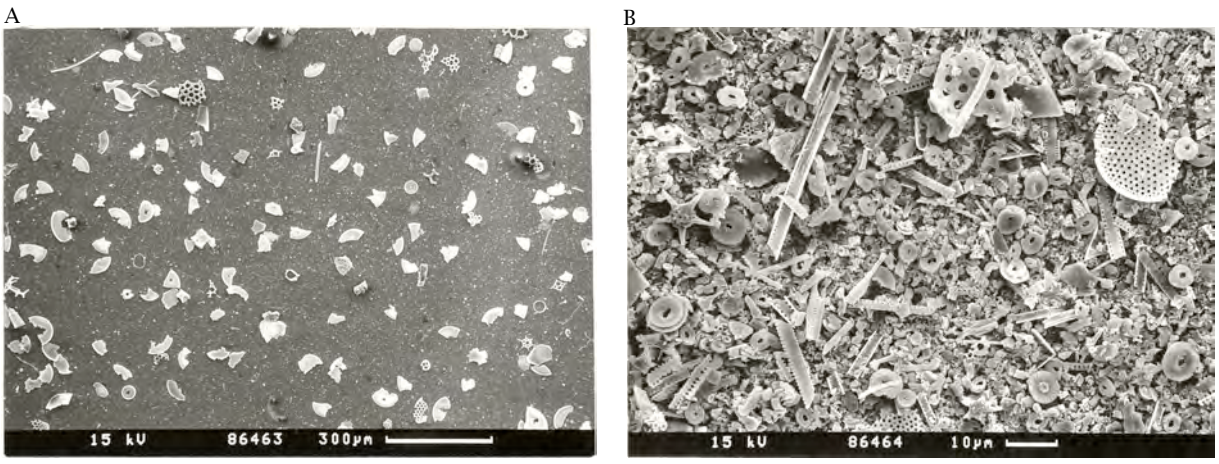

Fig. 8.1-1 SEM photomicrographs of wet-sieved bulk sample material, (sample BBP 56; see Appendix 3-1)
A: > 20 µm, represented mainly by pennate and centric diatom frustules, rarely silicoflagellate, dinoflagellate or foraminiferal test fragments;
B: < 20 µm, 'coccolith' fraction, used for stable oxygen and carbon isotope analyses.

8.2 Quasi-monospecific stable isotopes of the fine-fraction

Stable isotope analysis of the bulk fine-fraction provides advantages over the traditional approach with foraminifers, but several uncertainties made authors doubt their utility as a palaeoceanographic indicator (Paull and Thierstein 1987, 1990; Shackleton and Hall 1997; Ennyu et al., 2003). Discrepancies and offsets in downcore isotope trends and differences between isotopic composition of bulk fine-fraction carbonate and shallow-dwelling planktonic foraminifers are reported from various locations and time intervals. This raised questions concerning the reliability of polyspecific fine-fraction carbonate for isotope analyses, and which of the presumed near-surface indicators represent most accurately the surface water conditions (e.g. Anderson and Steinmetz, 1981; Paull and Thierstein, 1990; Mead et al., 1991; Broecker and Woodruff, 1992; Shackleton and Hall, 1997). The stable isotopic composition of tests of planktonic organisms is affected not only by the depth habitat but also by the seasonal timing of calcite production near the surface. Furthermore, their hydrographic signals are potentially masked by non-equilibrium isotopic fractionation upon precipitation of carbonate skeletons (Ennyu & Arthur 2004). Additionally, the bulk fine-fraction isotope approach can be complicated by various factors. These are (1) diagenetic overprint and/or (2) contribution of non-coccolith carbonate particles to the fine-fraction as well as (3) floral composition variations. The species-specific isotopic non-equilibrium fractionation (Dudley et al., 1980; Dudley et al., 1986; Paull and Thierstein, 1987; Mead et al., 1991) may raise momentous modifications in the isotope ratios of the polyspecific assemblage, potentially masking the signals of oceanic variability. In order to interpret changes in the isotope record of the bulk sediment it is necessary to assess the mix of species that builds this fraction and to evaluate the contribution of species-specific isotope signals to the bulk signal. An approach to separate quasi-monospecific samples is needed to

evaluate influences of these factors and the reliability of the use of bulk fine-fraction for stable isotope analysis.

8.2.1 Biological fractionation

Culture studies of coccolithophores have proved that biological fractionation takes place during the formation of calcium carbonate (e.g. Ennyu and Arthur, 2004). Non-equilibrium effects appear to reflect changing ecological and physiological responses of the organisms (Stoll and Schrag, 2000; Ziveri et al., 2000). The oxygen isotopic composition is influenced by growth rate, and shows a definite temperature dependence that closely parallels that of equilibrium precipitation of calcium carbonate (Dudley and Goodney, 1979). Oligotrophic settings, however, minimize the effect of growth rate on coccolithophorid isotopic disequilibrium (Goodney et al., 1980). The disequilibrium is approximately constant for a given species, but pronounced differences exist between different species. In-vitro studies of Dudley et al. (1980, 1986) have shown that the so called 'vital effects' in oxygen isotopic composition of coccolithophorid species reach up to 3.5 ‰ between different species. Culture experiments of Ziveri et al. (2003), confirmed a large oxygen isotopic fractionation among different species. Additionally, they calculated a range of 5 ‰ of carbon isotopic fractionation of coccolith calcite (Ziveri et al., 2003). Within a single species, vital effects are constant within 1 ‰ and do not vary with cell physiology (Ziveri et al., 2003). This constancy of vital effects suggests that coccolith stable isotopes will provide a reliable proxy for reconstructions of temperature and seawater chemistry, as long as monospecific fractions are used or species-specific correction factors are considered, if changes in polyspecific assemblage composition occur.

8.2.2 Methodology of size class separation

In order to achieve quasi-monospecific sub-samples, all methodologies to separate individual coccolith species are based on Stokes´ law, using the relationship between size and density of the particle and parameters of the carrier liquid. Thus, the species-specific size of coccoliths is used for separating into different grain size classes, assuming that a definite grain size class presents a certain coccolith species. Previous workers have attempted to separate different fractions of the fine carbonate using repeated decanting (e.g. Paull and Thierstein, 1987) or a combination of decanting with density-stratified settling columns (Stoll and Ziveri, 2002), or with filtration, respectively (Minoletti et al., 2001).

A detailed knowledge of sample composition is indispensable for size separation. For samples of this study, investigation with a Laser Particle Sizer was used to distinguish the size classes (see Chapter 6). Detailed observation with SEM was added in order to interpret the composition of different grain size classes. From this, six fractions depending on the assemblage composition have been defined as follows: < 1 µm, 1-3 µm, 3-5 µm, 5-8 µm, 8-11 µm and 11-20 µm.

After wet-sieving with tap water, the fine-fraction < 20 µm was separated into the chosen subfractions using a Sigma 301K centrifuge. Depending on physical and geometrical parameters, the settling time against speed frequency was calculated with the program Seditools 1.1.2 (available free on web: http://www.geologie.uni-frankfurt.de/Staff/ Homepages/Petschick/SediTools/ SediToolsE.html, Fig. 8.2.2-1). Centrifuge parameters are given in Tab. 8.2.2-1, a detailed protocol for centrifuging subfractions is specified in Tab. 8.2.2-2.

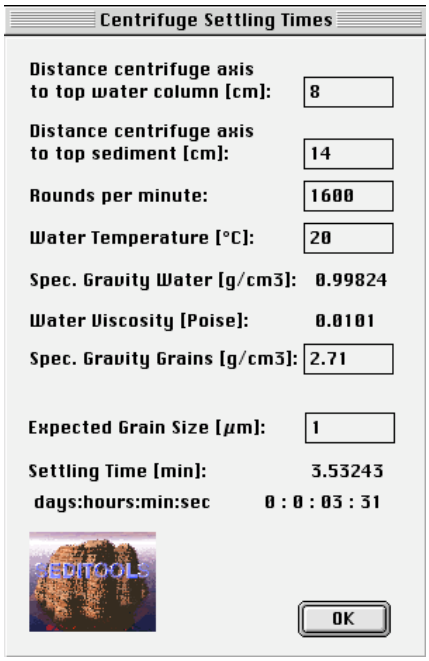

Fig. 8.2.2-1 Screenshot of Seditools 1.1.2. showing calculation of centrifuge settling times with needed parameters.

Supernatant represents the smaller fraction of the defined size class used for isotope analysis. Deposit consists of a mixture of grain sizes that are used for ongoing sample processing (Fig. 8.2.2-2).

Subfraction material was concentrated by removing the supernatant tap water by high-speed-centrifugation with a ™Eppendorf MiniSpin plus. Samples were then transferred into isotope analyser container and dried in the oven at around 40˚C.

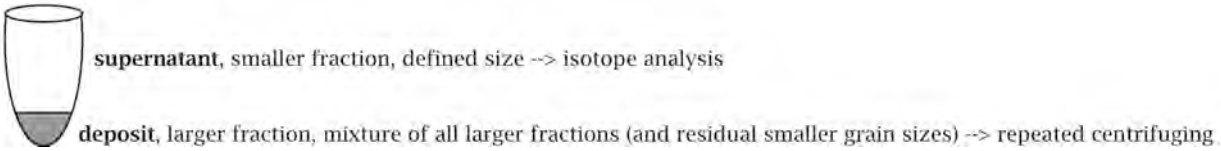

Fig. 8.2.2-2 Schematic representation of centrifuge breaker with supernatant fraction, that is to pipette off and used for analyses. Deposit is used for ongoing centrifugal processing.

Tab. 8.2.2-1 Centrifuge parameters

SIGMA 301K centrifuge	
Centrifuge beaker	20 ml, 10 cm height
Distance centrifuge axis to top water column	8 cm
Distance centrifuge axis to top sediment	14 cm
Water temperature	20 ˚C
Sample material	wet-sieved carbonate < 20 µm

Tab. 8.2.2-2 Protocol for centrifuging subfractions

Step	Grain size	Speed	Time	Supernatant	Deposit
1)	1 µm	1600 rpm	3 min 31 s	< 1µm	> 1 µm
2)	3 µm	600 rpm	2 min 47 s	1-3 µm	> 3 µm
3)	5 µm	400 rpm	2 min 15 s	3-5 µm	> 5 µm
4)	8 µm	200 rpm	3 min 31 s	5-8 µm	> 8 µm
5)	11 µm	200 rpm	2 min 15 s	8-11 µm	11-20 µm

8.2.3 Results and discussion of species-specific stable isotope values

Splitting of the bulk fine-fraction resulted in six subfractions represented in plates A1-5 to 8 (Appendix A1). The smallest fraction < 1 µm is presented by unidentifiable detritus (plate 5), fraction 1-3 µm is dominated by small reticulofenestrids (plate 6), fraction 3-5 µm possesses mainly reticulofenestrids and some few small *C. leptoporus* (plate 7), fraction 5-8 µm is composed of large reticulofenestrids, *C. leptoporus* and *Helicosphaera* spp. (plate 7), fraction 8-11 µm consists of *C. leptoporus, C. pelagicus* and *Helicosphaera* spp. and some other biogenic fragments (plate 8), fraction 11-20 µm is composed of different coccoliths and mainly other biogenic fragments. The latter, however, is to disregard, because this fraction is a mixture of all supernatant and pipetted (smaller) fractions of previous processing steps. Thus, this 'trash'-fraction is useless for interpretation of species-specific isotope values. This is proven by its unsorted particle composition (SEM, Appendix A1-8(D)) as well as the varying isotope signal (Fig. 8.2.3-1).

The isotopic composition of the subfractions (Fig. 8.2.3-1) follows along a linear trend of increasing $\delta^{18}O$ with increasing $\delta^{13}C$. An arrangement into isotopically heavy and light groups seems possible for both, $\delta^{13}C$ and $\delta^{18}O$. The small subfractions < 1 µm and 1-3 µm always offer heavy values. The larger subfractions 5-8 µm and 8-11 µm possess lighter values. The signal of the bulk fine-fraction < 20 µm is always heavier than that of the subfractions. Analogue patterns have also been observed for $\delta^{18}O$ by Dudley et al. (1986), who defined isotopically heavy and light groups with respect to equilibrium of different coccolith species grown in culture. They proposed large species (like *C. leptoporus*) to be depleted and small species (like *E. huxleyi*) to be enriched in their isotope signal compared to equilibrium.

The signal of the bulk fine-fraction is mainly represented by the smallest fractions < 1 µm and 1-3 µm (Fig. 8.2.3-1). The composition of bulk fine-fraction treated with pure ethanol is always heavier than that treated with tap water. This pattern is explicable by partial dissolution of these smallest fractions < 1 µm and 1-3 µm, and thus result in slightly depleted values of sample material treated with tap water. Therefore, ongoing treatment for bulk fine-fraction < 20 µm was carried out with pure ethanol.

The question remains, to what extent the isotopic composition of the bulk fine-fraction is represented by coccoliths, since the signal is also loaded by the fraction < 1 µm. But what is obvious is that the offset between the isotopic composition of different subfractions and the bulk fine-fraction is constant (Tab. 8.2.3-1). Because of that the bulk isotope signal of samples from Sites 1241 and 1000 were interpreted as real 'coccolith' signal.

These typical patterns of species-specific vital effects help to understand the bulk signal, although it seems reasonable to remove the < 1 µm-fraction as long as it is not sure, to what extent it influences the sample composition (see chapter 9).

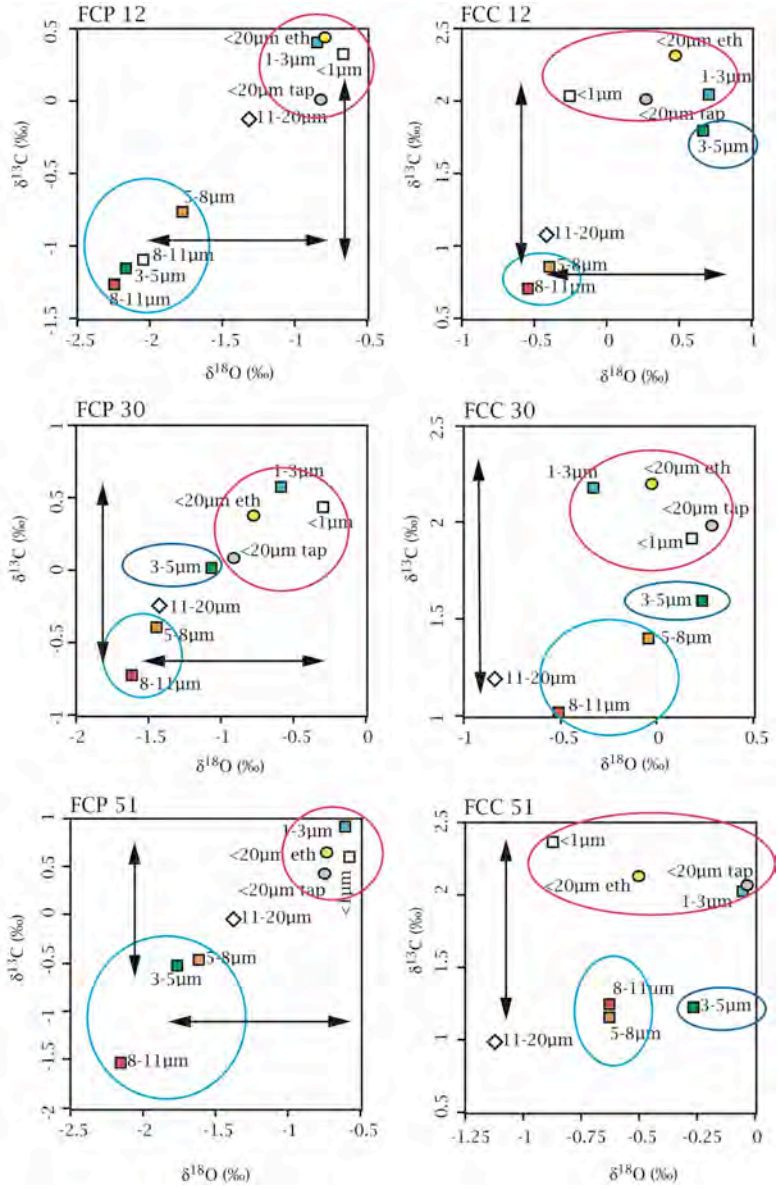

Fig. 8.2.3-1 Stable carbon and oxygen isotope values of subfractions. Circles mark bulk fine-fraction, yellow circles represent samples treated with pure ethanol, grey circles represent samples treated with tap water. Subfractions are marked by squares, diamonds represent the 'trash'-fraction. Left graphs show results for Pliocene Site 1241 (FCP - labels), right graphs shows results for Pliocene Site 1000 (FCC-labels). The isotopically heavy group is marked by purple circles, the isotopically light group is marked by light blue circle. Arrows indicate the ± 1 ‰-difference between the groups (see Tab. 8.2.3-1).

Tab. 8.2.3-1 ‰-deviation of stable isotopic composition of subfractions and bulk fine-fraction treated with tap water from the bulk fine-fraction treated with ethanol.

fractions	<20 tap		< 1 µm		1-3 µm		3-5 µm		5-8 µm		8-11 µm	
sample	$\delta^{13}C$	$\delta^{18}O$	$\delta^{13}C$	$\delta^{18}O$	$\delta^{13}C$	$\delta^{18}O$	$\delta^{13}C$	$\delta^{18}O$	$\delta^{13}C$	$\delta^{18}O$	$\delta^{13}C$	$\delta^{18}O$
FCC 12	-0.30	-0.21	-0.29	-0.74	-0.27	0.23	-0.52	0.18	-1.47	-0.87	-1.61	-1.03
FCC 30	-0.21	0.31	-0.28	0.21	-0.01	-0.30	-0.60	0.26	-0.79	-0.02	-1.17	-0.49
FCC 51	-0.06	0.46	0.25	-0.38	-0.09	0.44	-0.89	0.23	-0.97	-0.13	-0.88	-0.14
FCP 12	-0.43	0.01	-0.11	0.17	-0.03	-0.01	-1.59	-1.33	-1.22	-0.91	-1.70	-1.41
FCP 30	-0.31	-0.13	0.05	0.47	0.20	0.18	-0.36	-0.30	-0.77	-0.68	-1.11	-0.85
FCP 51	-0.22	0.00	-0.04	0.16	0.27	0.14	-1.17	-1.03	-1.10	-0.87	-2.17	-1.42
max deviation	±0.26	±0.46	±0.29	±0.74	±0.27	±0.44	±1.59	±1.33	±1.47	±0.91	±2.17	±1.42

8.3 Bulk fine-fraction stable isotope record of the late Miocene to Pliocene of Sites 1241 and 1000

8.3.1 Reliability of bulk fine-fraction stable isotope signal

Standard interpretations of overall trends in fine-fraction and coexisting surface-dwelling planktonic foraminiferal isotope profiles show systematic differences. $\delta^{13}C$ values are clearly depleted in the fine-fraction, whereas $\delta^{18}O$ values parallel or show slightly higher amplitudes than the corresponding foraminiferal record (e.g. Shackleton and Hall, 1997; Goodney et al., 1980; Ennyu et al., 2002; Liu et al., 2002). Margolis et al. (1975) pioneered the potential use of calcareous nannofossil isotopic compositions by comparing Cenozoic trends in bulk fine-fraction (< 44 µm) and planktonic foraminiferal stable isotopes. They found a variable relationship in $\delta^{13}C$ and roughly equivalent values in $\delta^{18}O$. Anderson and Cole (1975) found systematic covariance and Anderson and Steinmetz (1981) affirmed the coccolith record as a more reliable indicator of temperature and $\delta^{18}O$ changes in surface seawater. They suggested selective dissolution or deep calcification (gametogenetic calcite; Bé, 1980) to alter planktonic foraminiferal (*G. sacculifer*) oxygen isotopic composition. Goodney et al. (1980) found a relationship between increasing planktonic foraminiferal $\delta^{13}C$ and decreasing $\delta^{13}C$ of calcareous nannoplankton. They suggested that changing rates of primary productivity influenced this increased gradient between them. Incorporation of ^{13}C- depleted respiratory carbon in the coccolith intracellular fluid pool would result in precipitation of ^{13}C- depleted coccolith calcite (Goodney et al., 1980; cf. chapter 1.2.3). Ennyu et al. (2002) pointed on the bias of coccolith calcite to be not representative of an annual mean due to the seasonal timing of the dominant nannoplankton production depending on the prevailing climatic regime (Ennyu and Arthur, 2002). However, they found a good correspondence between fine-fraction records (< 63 µm) with deep-dwelling foraminifers, but no good correlation with surface-dwelling foraminiferal species. Ennyu et al. (2002) interpreted these isotopic discrepancies as resulting primarily from season of calcification, as well as possible biological fractionation. Finally, isotopic differences between bulk fine-fraction and planktonic foraminifers may likely reflect changes in the averaged biological fractionation, characterizing the mix of organisms making up the bulk.

The isotopic composition of late Miocene Site 1241 supports the well known systematic differences with depleted bulk fine-fraction $\delta^{13}C$ values compared to the planktonic foraminiferal record of *G. sacculifer* (Fig. 8.3.1-1). $\delta^{18}O$ values of the bulk fine-fraction are heavier than the corresponding foraminiferal record (Fig. 8.3.1-2). But both bulk fine-fraction records parallel the trends of planktonic foraminifers, even though foraminifers show higher amplitudes. The minimum of the Late Miocene Carbon Shift in foraminifers (6.55 Ma) is traced by the bulk fine-fraction, but values of the latter further decrease until 5.81 Ma (see also chapter 8.3.2).

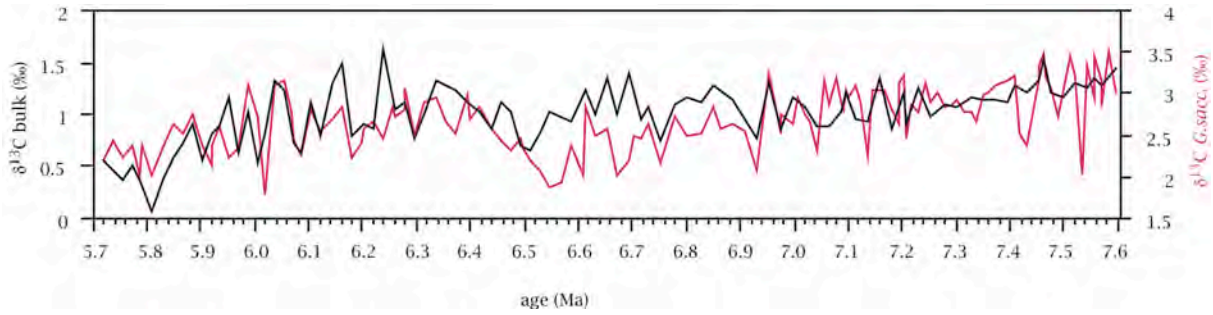

Fig. 8.3.1-1 Site 1241: Correlation between trends of stable-carbon isotope records of bulk fine-fraction (black line) and *G. sacculifer* (pink line).

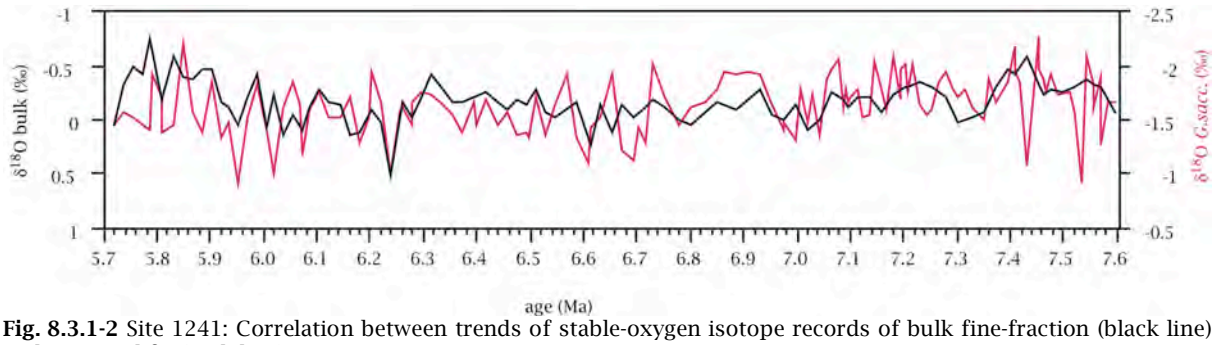

Fig. 8.3.1-2 Site 1241: Correlation between trends of stable-oxygen isotope records of bulk fine-fraction (black line) and *G. sacculifer* (pink line).

Changes in isotopic composition of the coccolith bulk fine-fraction point to real changes in isotopic composition of ambient water masses, not to changes of the isotopic composition due to variations in assemblage composition. This is supported by Williams and Bralower (1995), who found only little relationship between assemblage- and fine-fraction stable isotopic fluctuations. In the records of Sites 1241 and 1000, changes in floral and isotopic composition parallel imposingly. At both sites, variations in abundances of the high-productivity species *Reticulofenestra* correlate with fluctuations in $\delta^{13}C$ (Figs. 8.3.1-3 and 8.3.1-4).

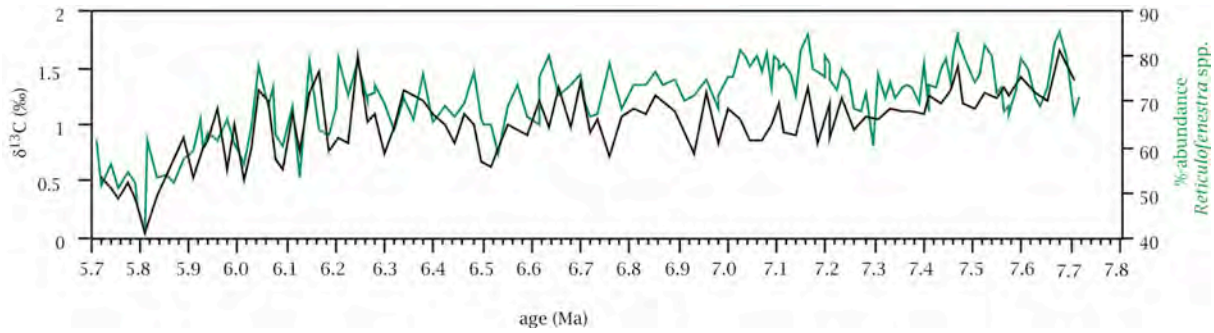

Fig. 8.3.1-3 Site 1241: Correlation between trends of bulk fine-fraction stable-carbon isotope record (black line) and reticulofenestrid abundance (green line).

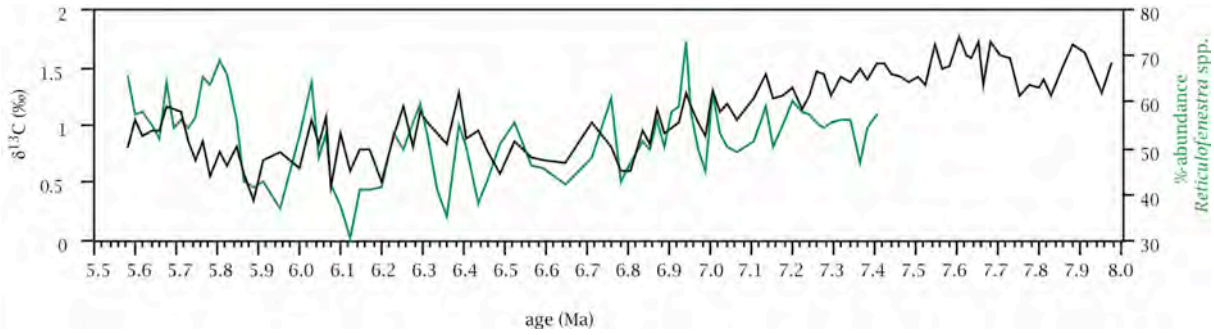

Fig. 8.3.1-4 Site 1000: Correlation between trends of bulk fine-fraction stable-carbon isotope record (black line) and reticulofenestrid abundance (green line).

8.3.2 The Late Miocene Carbon Shift

A rapid global negative shift in $\delta^{13}C$ occurs during the late Miocene magnetic chron C3AR as described in detail in chapter 1.2.1.2. At Sites 1241 and 1000 (Fig. 8.3.2-1), the isotope excursion is pronounced in all records: bulk fine-fraction (Sites 1241 and 1000) as well as planktonic and benthic foraminifers (Site 1241, see chapter 2.5). In order to correlate timing and characteristics of that event, reference data were used of ODP Site 926 (equatorial Atlantic, Shackleton and Hall, 1997) and ODP Site 1237 (south-eastern Pacific, Tiedemann, unpublished data).

The orbitally tuned stable isotope record of the bulk fine-fraction of the Late Miocene Carbon Shift at Site 926 (Fig. 8.3.2-1(A)) coincides well with both, the $\delta^{13}C$ record of Site 1000 (Fig. 8.3.2-1(B)), and Site 1241 (Fig. 8.3.2-1(C)). The long-term trend of $\delta^{13}C$ of bulk fine-fraction reveals a decrease in $\delta^{13}C$ values of around 1.0 ‰ in all three records. This trend is reflected as a stepwise decrease at all sites. A point of minimum values occurs at around 6.5 Ma at Sites 1241 and 1000. Absolute minima, indicating the end of the Late Miocene Carbon Shift, occur at around 5.9 Ma in the Atlantic and at 5.81 Ma in the eastern equatorial Pacific. The isotopic composition of the planktonic foraminifer *G. sacculifer* at Site 1241 shows heavier $\delta^{13}C$ values compared to bulk fine-fraction, with a decrease from around 3.5 ‰ to 2 ‰. The minimum value occurs at 6.55 Ma (Fig. 8.3.2-1(D)) but it seems that another reversal of values appears at 5.8 Ma. The benthic record of that site shows a fast depletion of stable carbon isotopic composition towards a minimum at 6.88 Ma (Fig. 8.3.2-1(E)). Correlation with the benthic foraminiferal isotope record of Site 1237 (Tiedemann, unpublished data) fits well, whereas Site 1237 shows the lowest value slightly earlier, namely at 6.75 Ma (Fig. 8.3.2-1(F)). Both benthic isotope records also propose a possible reversal point towards heavier values at around 5.8 Ma.

By comparison of records of bulk fine-fractions (i.e. calcareous nannoplankton), planktonic foraminifers and benthic foraminifers, the end of the decrease in $\delta^{13}C$ values of the Late Miocene Carbon Shift offers an offset in timing. This offset occurs between the different fossil groups, not within one group.

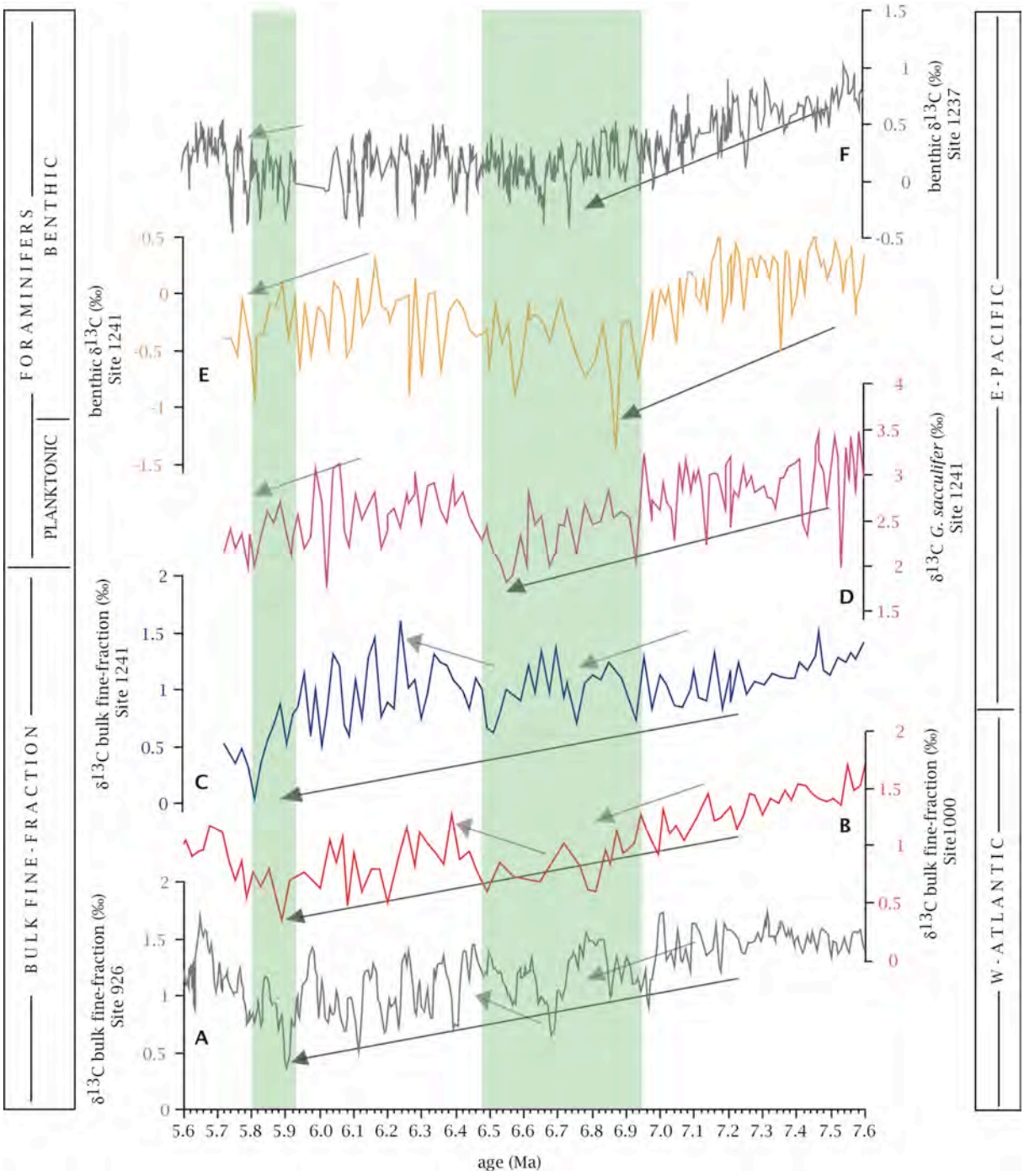

Fig. 8.3.2-1 The Late Miocene carbon shift- $\delta^{13}C$-records of bulk fine-fraction, planktonic foraminifers and benthic foraminifers of locations in the W-Atlantic and E-Pacific. A: bulk fine-fraction, Site 926 (Shackleton and Hall, 1997). B: bulk fine-fraction, Site 1000 (this study). C: bulk fine-fraction, Site 1241 (this study). D: planktonic foraminifers, Site 1241 (this study). E: benthic foraminifers, Site 1241 (this study). F: benthic foraminifers, Site 1237 (Tiedemann, pers. com). Green bars mark periods of lowest values.

8.3.3 Possible effects of the Panamanian Seaway Closure on the stable isotope signal

In the late Miocene, the Pacific and Caribbean isotope records show a corresponding trend of the bulk fine-fraction stable isotopic composition. In the Pliocene, however, the isotope records of Sites 1241 and 1000 apparently show an opposite trend in both, the stable carbon and stable oxygen (Figs. 8.3.3-1,2). The values of the eastern equatorial Pacific pursue the Miocene trends: Carbon values remain isotopically light after the late Miocene $\delta^{13}C$ decrease;

the oxygen isotope record is constant over the entire interval of the late Miocene to Pliocene. The central Caribbean record, however, shows increasing values of stable carbon and oxygen isotopes during the Pliocene.

The oxygen isotope record of the bulk fine-fraction clearly traces the patterns of planktonic foraminifer *G. sacculifer*, described by Steph (2005). Strong accordance of isotope signals between Site 1241 and Site 1000 occurs prior to the closure of the Panamanian Seaway (Figs. 8.3.3-1,2). Divergence between the records starts at around 4.2 Ma, with distinct increases in foraminiferal and nannofossil $\delta^{18}O$, indicating the pronounced salinity increase in the Caribbean as described in chapter 1.2.1.1. The foraminiferal carbon isotope signal is identical at both sites after the closure, whereas the nannofossil $\delta^{13}C$ increases conspicuously in the Caribbean site.

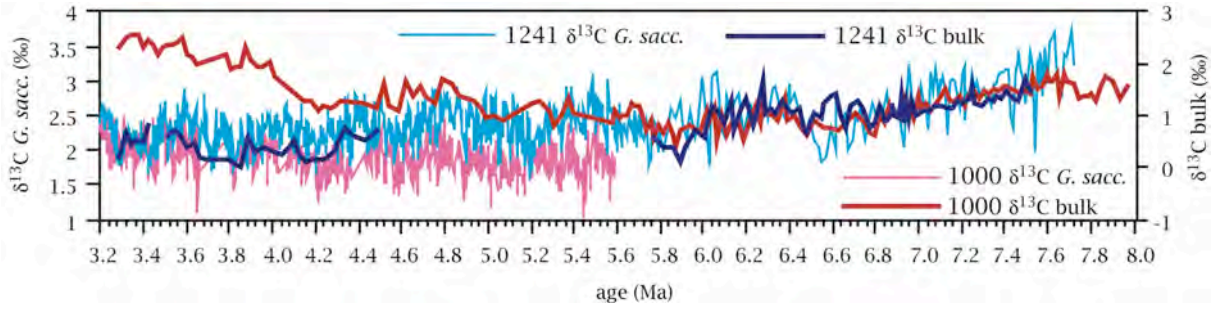

Fig. 8.3.3-1 Correlation between trends of stable-carbon isotope record of Sites 1241 (blue) and 1000 (red), *G. sacculifer* (bright colours, thin lines) vs bulk fine-fraction (dark colours, thick lines).

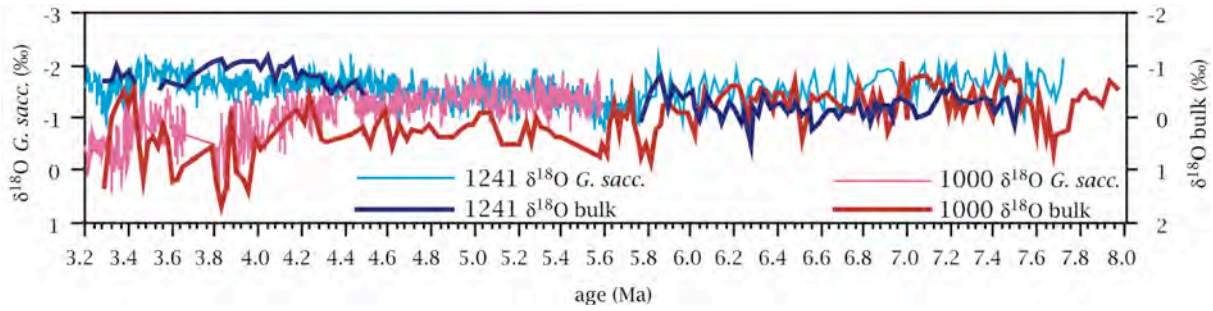

Fig. 8.3.3-2 Correlation between trends of stable-oxygen isotope record of Sites 1241 (blue) and 1000 (red), *G. sacculifer* (bright colours, thin lines) vs bulk fine-fraction (dark colours, thick lines).

8.4 Discussion and conclusions

The isotope analysis of quasi-monospecific subfractions of the bulk fine-fraction resulted in distinct patterns: (1) coccoliths can be grouped in isotopically heavy and light groups depending on size. Large coccoliths (e.g. *C. leptoporus*, *Helicosphaera* spp.) possess lighter values and small coccoliths (e.g. *R. minuta*, *R. minutula*) possess heavier values in both, stable oxygen and stable carbon composition; (2) the bulk fine-fraction (< 20 µm) is represented by the smallest subfractions, < 3 µm (within ± 0.5 ‰); (3) the offset in stable isotopic composition between the larger coccolith subfractions and bulk fine-fraction is constant (± 1 ‰), regardless of the absolute isotope value and age of the investigated

samples; (4) samples treated with tap water posses slightly depleted isotope values due to dissolution of finest material.

It is obvious that in the bulk fine-fraction (< 20 µm) provides a reliable coccolith isotope signature, since the majority of the coccolith carbonate is derived from this size fraction (chapters 6 and 7). However, one should be cautious with interpretation of bulk fine-fraction stable isotopes, when the contribution from larger coccoliths increases substantially. This requires a detailed analysis of grain-size and coccolith assemblage composition when bulk fine fraction stable isotopes are used (chapter 9). The analogy in the amplitude of foraminiferal and nannofossil isotope records, however, clearly underlines the reliability of the bulk fine-fraction signature in the samples of Sites 1241 and 1000.

The oxygen isotope records of bulk fine-fractions at Sites 1241 and 1000 show the same trend as the observed foraminiferal isotopic signal (Steph, 2005). It indicates divergence between the signals at both sites after 4.2 Ma, accounting separation of both ocean basins with the distinct salinity increase in the Caribbean. The carbon isotope record, however, offers unchanged foraminiferal values before and after the closure at both sites, whereas the bulk fine-fraction signal clearly deviates and increases in the Caribbean.

The large divergence between the stable carbon isotope signal of *G. sacculifer* and the bulk fine-fraction and within the bulk fine-fraction from both sides of the gateway after 4.2 Ma (Fig. 8.3.3-1) may be related to following factors:

(1) The stable carbon isotope record of *G. sacculifer* does not deviate from the fine-fraction signal in the tropical eastern Pacific. In the Caribbean Sea, however, the large difference in carbon isotopic composition requires, that the signal is either (a) incorporated at different seasons, and/or (b) from different water masses. Thus, the discrepancy between coccolith to foraminiferal $\delta^{13}C$ values seems to be most likely the result of changing coccolithophore ecology after the closure of the Panamanian Seaway, which is reflected in the decrease in the relative contribution of *F. profunda* at Site 1000 (cf. Fig 6.3-1). This indicates that coccolithophore productivity increased when the closure of the Panamanian Seaway proceeded and the Caribbean Sea became more saline (Fig. 8.4-1). This, at the first glance, seems to be ad odds with the general assumption, that the Caribbean Sea became more oligotrophic after the closure. However, the coccolith accumulation rates are by far lower in the Pliocene compared to the late Miocene in the Caribbean Sea (chapter 6, cf. Fig. 6.3-3), which might be the result of short-lived seasonal productivity events in an overall oligotrophic regime.

Additionally, the similarity of coccolith and foraminiferal signals during the Biogenic Bloom interval seems to exclude the incorporation of a different isotopic signature of both plankton groups during high-productive intervals.

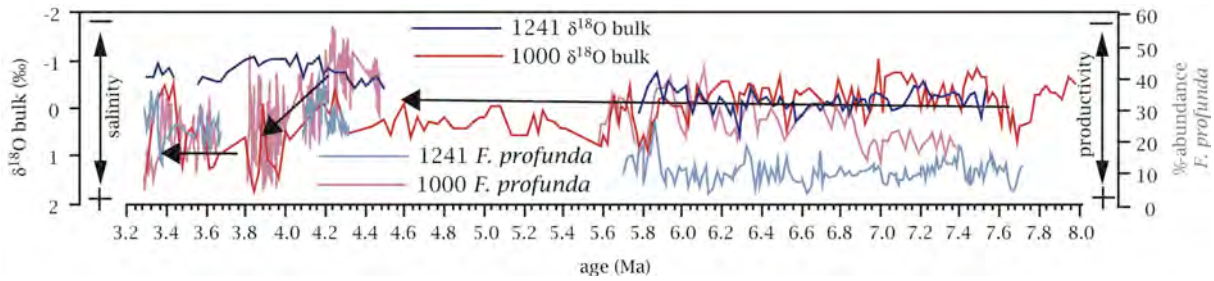

Fig. 8.4-1 Correlation between bulk fine-fraction stable-oxygen isotope records (thick lines) and relative abundances of *F. profunda* (thin lines) at Sites 1241 (blue colours) and 1000 (red colours). Arrows underline the steadiness with open-isthmus conditions and apparent changes in the post-closure interval, in both, salinity and productivity.

(2) An alternative interpretation of the carbon isotopic signal might be drawn, if it is assumed that a substantial part of the fine-fraction is derived from other sources than coccolith carbonate. The most likely mechanism is the shedding of platform carbonates from the nearby Pedro Bank on the Nicaraguan Rise. Platform-derived material at the Central Caribbean Site 1000 is apparently increasing after 4.2 Ma, indicated by the aragonite content of the bulk sediment (up to 60%, Groeneveld et al., 2008). Aragonitic-rich sediments have relatively positive $\delta^{13}C$ values (Fig. 8.4-2(A)) due to the photosynthetic activity of their main producers like *Halimeda* (Swart, 2008). Mixing of shallow-water carbonates with pelagic materials would thus result in an increased carbon isotope signature of bulk sediment. Swart (2008) recently published carbon isotope records of bulk periplatform sediments over the past 10 million years. He found globally synchronous changes in $\delta^{13}C$ towards heavier values (Fig. 8.4-2(B)) during the late Miocene to Pliocene, which seem to be unrelated to globally open-oceanic decreasing trend in $\delta^{13}C$. Swart (2008) suggested the increase of $\delta^{13}C$ of platform margin sediments is caused by addition of aragonite-rich sediments to pelagic carbonates.

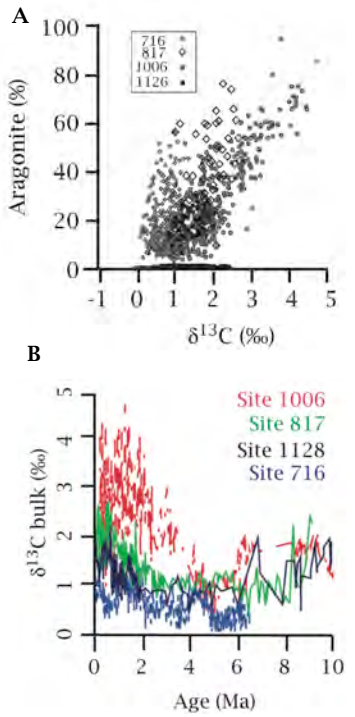

Fig. 8.4-2 A: Positive correlation between $\delta^{13}C$ and aragonite contents from periplatfom carbonates studied by Swart (2008). B: Bulk carbon isotopic records of different ODP Sites. Modified from Swart (2008).

This hypothesis is clearly supported by the data of Site 1000 (Fig. 8.4-3), where aragonite content strongly increases after 4.2 Ma and clearly traces the positive carbon isotope shift. Possible reasons for the enhanced growth of global periplatform sediments in the late Miocene are still to elucidate (Swart and Eberli, 2005; Swart, 2008).

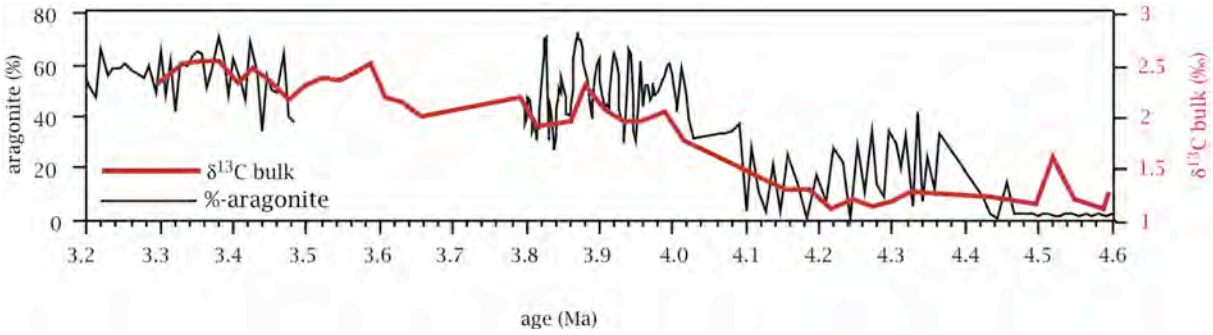

Fig. 8.4-3 Correlation between trends of bulk fine-fraction stable-carbon isotope records (red line) and aragonite contents (black line, data kindly provided by J. Groeneveld) of Site 1000.

There is no doubt about the long-term trend of positive correlation between aragonite contents and $\delta^{13}C$ values (Fig. 8.4-3). Regarded in detail, however, Groeneveld et al. (2008) found a negative correlation between variations in aragonite diagenesis and abundances of *F. profunda* (Fig. 8.4-4). They postulated an increase in aragonite dissolution to reflect increased surface water productivity. The amplitudes of both signals of these short-term variations are nearly parallel. As known from Groeneveld et al. (2008), diagenetic overprint as crystalline overgrowth on foraminiferal tests between 4.5 and 3.8 Ma is a problem at Site 1000. Implications on potentially affected $\delta^{18}O$ values are not yet clear, but good correlations of benthic $\delta^{18}O$ with those of ODP Site 925 and 999 challenge the reliability of the primary signal of the planktonic $\delta^{18}O$ record (Greoneveld et al., 2008; Steph, 2005). The effect of diagenesis would result in increasing $\delta^{18}O$ amplitudes (Groeneveld et al., 2008). Swart and Eberli (2005), however, found only a small initial increase in the $\delta^{18}O$ of the pore fluids.

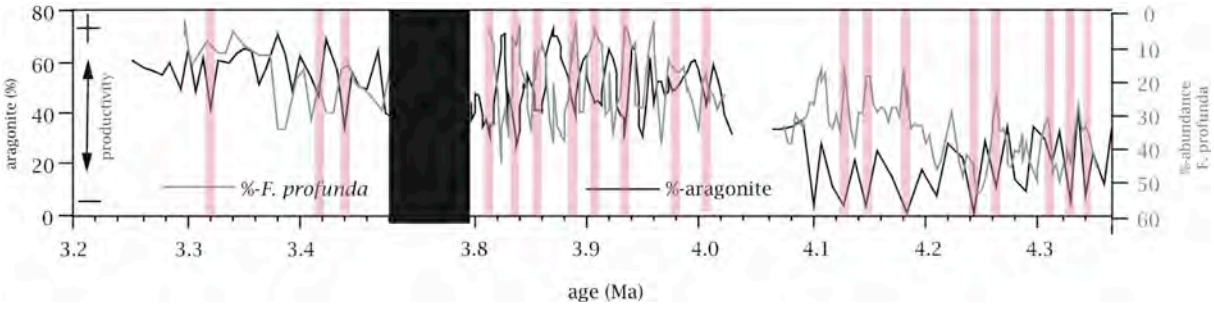

Fig. 8.4-4 Correlation between relative abundances of *F. profunda* (grey line) and aragonite contents (black line, data kindly provided by J. Groeneveld) of Site 1000. Red bars present intervals of negative correlations between aragonite dissolution and surface water productivity.

To explicitly decipher the diagenetic effect on the $\delta^{13}C$ values of bulk fine-fraction, it is necessary to determine the composition of all sub-samples of Site 1000 in detail. As shown in plates 5-8 (A1-5-8) all related subfractions contain aragonitic needles (A1-5(A-F), A1-6(B,C,D,F), A1-7(B,D)). Carbon isotopic composition of all subfractions of samples of Site 1000 is indeed 1 to 1.5 ‰ heavier compared to corresponding material of Site 1241 (Fig. 8.2.3-1). As discussed above, the offset between different subfractions is constant. Since

this is also true for subfractions of sediments from Site 1000, the contamination and influence of the isotope signature due to bank-derived aragonite is even more obvious.

Thus, the discrepancy between foraminiferal and bulk fine-fraction isotope records excludes ecology as driving force for changing the carbon isotopic composition. The $\delta^{13}C$ record of the bulk fine-fraction of Site 1000 is clearly influenced by transported material from surrounding carbonate banks after 4.2 Ma. Measurement of quasi-monospecific samples clearly supported, that a correction factor for excluding the aragonite-signal of altered Caribbean sediments, depending on its mass balance, would result in a decrease of $\delta^{13}C$ values of around 1 to 1.5 ‰ to similar Pacific bulk- and foraminiferal values. Since aragonite needles of different sizes are present in all subfractions we must conclude that stable carbon isotope records from sites with substantial contributions of platform-derived carbonates are not suitable for paleoceanographic interpretations.

CHAPTER 9 SYNTHESIS

The restriction in throughflow and closure of a gateway system has a strong influence on the evolution of large-scale oceanic provinces with different chemical and physical properties. These affect the distribution and productivity of planktonic organisms that thrive within their surface waters. There is a strong link between environmental forcing and changes in plankton evolution, and hence their biogeography and productivity. Several different environmental factors may force evolutionary change like changes in water temperature, global latitudinal gradients in the physical environment, water column stratification, and nutrient supply. Generally, changing climatic conditions caused reorganisation of the ecosystem with increased (or decreased) competitive pressure by different species for the same niche. Otherwise, selective biological pressure could force events in the biosphere.

Related to the closure of the Panamanian Seaway, this study distinguishes different modes of evolution as well as species dispersal within the nannofossil community on both sides of the emerging isthmus. Extrinsic factors, like the continental barrier or changes in surface water circulation, are not sufficient to explain the high degree of synchrony of nannofossil bioevents (Tab. 4.3-1), thus intrinsic factors or a large-scale mechanism, like changes in the global carbon cycle, are needed to trigger synchronous evolution within geographically separated coccolithophores. Distinct evolutionary patterns of assemblage-dominating r-selective reticulofenestrids become apparent in intrageneric and intraspecific morphometry (Fig. 5.4.1-2). Size changes occur in dependence to their preferred ecological niche, and thus depend on extrinsic factors related to (palaeo-) ecology and palaeoceanography. These patterns are clearly traced within the grain size distribution (Fig. 6.3-2). A link between evolution-induced changes and palaeoproductivity is given by biodiversity and species-specific carbonate production (Fig. 6.3-1) as well as accumulation rate changes (Fig. 6.3-3). Coccolith geochemistry interacts with evolutionary patterns as well as changes in biogeography and palaeoproductivity (Figs. 8.3.3-1/2). The coccolith carbon isotope signature traces changes in the global carbon cycle, a possible extrinsic trigger on evolution and production, since photosynthesis and calcification of coccolithophores are intimately linked to changes in the oceanic dissolved inorganic carbon input. However, the advection of bank-produced aragonite in the Caribbean resulted in a shift in bulk fine-fraction carbon isotope values, which was not related to changes in the cocclithophore ecology. This needs to be taken into account in all settings where bank-derived aragonite is present in substantial amounts.

Coccolith evolution and ecology provide feedback mechanisms on morphometry, biostratigraphy, palaeoproductivity and grain size distribution, as well as on the isotope signature. Here, coccolith morphology takes an important position within the interaction of the set objectives. Small adjustments within coccolith size will have strong impact on all observed parameters. The late Miocene Biogenic Bloom interval demonstrates this

phenomenon. Site 1241 offers distinct morphological patterns of coccolith size variations, which seem to affect accumulation patterns and isotopic composition. Ecological changes, however, as well as palaeoproductivity may act as a positive or negative feedback on the carbonate accumulation rate.

Morphometrical patterns within the reticulofenestrids at Site 1241 (chapter 5, splitting into intervals BBP-A, -B, -C; Fig. 5.4.1-2) are perfectly traced by the general grain size distribution (chapter 7; Fig. 7.4.2-1). Conspicuous changes occur at 7.3 Ma and 6.3 Ma (Fig. 5.4.1-4). The interval within these time points is characterized by a change in the assemblage composition (Fig. 7.4.1-1) towards increased numbers of larger species (*R. pseudoumbilicus* M), which is also traced in the grain size distribution (Figs. 7.4.2-1; 7.5.2-2(C)). MARs and cocARs (Fig. 7.5.2-2(D)) are marked by distinct changes within mentioned time points to a distinct minimum at 6.7 Ma. A first maximum in accumulation rates between 7.4 and 7.0 Ma appears due to that increase in coccolith sizes. The cause for the second and major increase in accumulation rates between 6.7 and 5.9 Ma, however, is a dramatic increase in coccolith accumulation rates, that is an increase in the number of (even smaller) coccoliths.

At Site 1000, the same temporal patterns occur as at Site 1241, where accumulation rate maxima also change around 6.7 Ma (Fig. 6.3-3(B3). However, coccolith size variations at this site (Fig. 5.4.1-5) are not that obvious and occur with a temporal offset compared to Site 1241 due to different ecological tolerances (see chapter 5.4). Yet, assemblage composition (Fig. 6.3-1(B3)) clearly points to an interval of ecological change with increases in abundance of *F. profunda* between 6.9 and 5.8 Ma, which indicates decreased productivity in the upper photic zone.

The influence of coccolith size is also quite apparent in stable carbon and oxygen isotopic composition patterns (chapter 8). The definition of isotopically light and heavy groups of quasi monospecific coccolith subgroups is also based on coccolith size. The question arises, to what extend a change in assemblage composition, thus a change in size, will affect the isotope signal of the bulk fine-fraction. The detailed look into the carbon isotopic composition in Fig. 8.3.2-1 offers a slight but constant offset between the carbon isotope signal of the bulk fine-fraction and planktonic foraminifer *G. sacculifer* between 6.9 and 6.5 Ma at Site 1241. The composition of bulk fine-fraction offers systematically heavier values compared to the preceding and following intervals. Could this be the result of the species-specific vital effect of the changed nannofossil assemblage composition observed between 7.3 and 6.3 Ma? Based on the grading in isotopically light and heavy groups, an increase in large coccoliths would result in a depleted isotope record - but compared to the foraminiferal record, values of nannofossils are getting even heavier. And since these existing larger coccolith specimens produce a statistically irrelevant amount of carbonate (Fig. 6.3-1(A4)), one could exclude the species-specific isotope fractionation as reason for changed values of the bulk fine-fraction signal. As proposed above (cf. Fig. 7.5.2-2(D)), palaeoproductivity changed between around 6.9 and 6.5 Ma at Site 1241, with a decrease in

mass and nannofossil accumulation rates and a distinct minimum in accumulation at 6.7 Ma. May changes in palaeoproductivity have such a strong impact on the nannofossil isotope signal as already proposed by Goodney et al. (1980) or does it simply reflect the global changes in the carbon cycle, because the same trends are also observed in the benthos?

The late Miocene Biogenic Bloom interval at the investigated sites is characterized by a two-step increase in accumulation rates, accounted for by (1) an increase in coccolith sizes and (2) an increase in coccolith productivity. The isotopic composition of that interval offers a distinct negative shift in carbon isotope values. A period of lower values (Fig. 8.3.2-1, green bar) clearly underlines the interval of minima in accumulation rates between 6.9 and 6.5 Ma, and thus confirms a minimum in palaeoproductivity at both sites. Since coccolith size had no influence on the bulk fine-fraction signal, large coccoliths appear due to changes in ecological parameters like enhanced nutrient supply or indicate selective preservation of coccolith carbonate. But since no parameter points to increased dissolution during that interval (Fig. 6.4-2(A5,6), one could ask why large specimens of r-selective coccolithophores thrive during an interval of decreased nannofossil productivity. Thus the ecological shift, which favours the growth of large coccolithophores is not necessarily associated with enhanced coccolithophore accumulation rates.

The Late Miocene Carbon Shift (chapter 8.3.2) may possibly refer to an increase in productivity until 6.9 Ma in the eastern equatorial Pacific (benthic signal, Sites 1241 and 1237, Fig. 8.3.2-1), which is also debated in recent discussions (e.g. Diester-Haass et al., 2006). The coinciding decrease in all planktonic values, however, is not explainable related to increased productivity. Additionally, accumulation patterns and assemblage composition clearly point to decreased productivity in surface waters between 6.9 and 6.5 Ma. The global perturbation in the carbonate budget needs other mechanisms to explain the depletion of the isotopic composition of dissolved inorganic carbon than solely productivity changes (see chapter 1.2.1.2).

CHAPTER 10 SUMMARY AND CONCLUSIONS

This thesis distinguished the influence of the closure of the Panamanian Seaway on coccolithophorid evolution, biogeography and palaeoproductivity and evaluated the response of coccolithophores to fundamentally changing palaeoceanographic patterns.

- **Biostratigraphy**

- Several nannofossil bioevents have been observed within the late Miocene to Pliocene intervals in the eastern equatorial Pacific and the central Caribbean:
  - Global events (T paracme *R. pseudoumbilicus*, FOs and LOs *R. calicis*, *S. abies*) and
  - Local events (LO *R. rotaria*)
  - Conspicuous synchrony in nannofossil bioevents between the Pacific and the Caribbean Sea points to more large-scale mechanisms controlled by intrinsic and/or extrinsic factors triggering coccolithophorid evolution

→ **Negative** evidence for the influence of Panamanian Seaway Closure on coccolithophorid evolution

- **Morphometry**

- Intrageneric size variations of *Reticulofenestra* spp.
- Intraspecific size variations of *Reticulofenestra* spp.
- Distinctive patterns:
  - Reticulofenestrids prefer the more eutrophic conditions in the eastern equatorial Pacific:
    - Largest coccolith sizes dominate during slightly eutrophic conditions in the late Miocene Pacific
    - Size increase and longer duration of the dominance of large species in the Pacific
  - Dominance of small coccolith sizes in oligotrophic environments
  - Gradual size variations seem to be ecology-induced; punctual changes seem to be evolution- induced
  - Ecology triggers evolution
  - No general size decrease within the late Miocene interval
    ATTENTION - this signal may be superimposed by small coccolith sizes having dominated during the preceding high palaeoproductivity Biogenic Bloom interval
  - Circulation-induced drift of large coccolithophore species from the eastern equatorial Pacific towards the central Caribbean Sea during open-gateway conditions
  - Development of in-situ coccolithophorid communities differing between the eastern equatorial Pacific and the Caribbean Sea during closed-gateway conditions

→ **Positive** evidence for the influence of the Panamanian Seaway Closure on coccolithophorid morphometric patterns

Assemblages and Palaeoproductivity

- Distinctive coccolith assemblages between the eastern equatorial Pacific and the central Caribbean, as well as between the late Miocene and the Pliocene intervals
- Coccolithophorid assemblages trace ecological patterns
  - r-selective reticulofenestrids prefer the eastern equatorial Pacific rather than the central Caribbean Sea
  - K-selective lower photic zone taxa indicate more oligotrophic conditions in the central Caribbean Sea
- Sediment accumulation at both sites is almost exclusively controlled by coccoliths
- Large species produce considerably higher amounts of carbonate than small ones
- small coccolithophores can increase accumulation rates due to their large quantities

→ the Biogenic Bloom is a coccolithophorid bloom

- Changes in productivity with closed-gateway conditions:
  - Increase of oligotrophic conditions at eastern equatorial Pacific due to higher stratification (increase in the relative abundance of *F. profunda*)
  - Higher sea surface temperatures and sea surface salinities at central Caribbean Sea
  - Decreased coccolithophore productivity in the eastern equatorial Pacific
    ATTENTION - the signal may be superimposed by:
    - the preceding Biogenic Bloom interval,
    - the steady rise in distance from the equatorial divergence because of plate tectonic movements, or
    - a switch from a carbonate-dominated to a silica-dominated regime
  - Decreased coccolithophore producitivity in the central Caribbean Sea
    ATTENTION - though a single-proxy approach of abundances of *F. profunda* (indicating an increase in productivity) is misleading, the following arguments point towards a lowered coccolithophore productivity:
    - Total assemblage composition indicates strong oligotrophic conditions
    - Strong decrease in coccolith accumulation rates indicates decreased productivity
    - Methodological error: Comparison between different time intervals is hampered by different time resolution (cf. Biogenic Bloom Interval: 2 Ma; Final Closure Interval: 0.4 Ma) and differences in species composition (comparison of relative abundances)
    - Possibly a seasonal pulse in productivity is preserved in sedimentary record

→ **Positive** evidence for the influence of the Panamanian Seaway Closure on coccolithophorid palaeoproductivity patterns

Grain size distribution

- Two possible causes can be distinguished to explain the Biogenic Bloom event in the eastern equatorial Pacific:
  (1) Increase in coccolith sizes (7.4-7.0 Ma)
  (2) Increase in coccolith accumulation rates (6.7-5.9 Ma), coupled with decrease in coccolith sizes

→ Quantity of coccoliths is of higher importance for mass accumulation than is increase in coccolith sizes

o Stable isotope composition of bulk fine-fraction

- Coccolith species are distinguished into isotopically heavy and light groups depending on their size
- Bulk signal is represented by the smallest subgroups
- Reliability of the bulk fine-fraction signal is confirmed by the constant offset between the individual subgroups and the bulk fine-fraction
- Bulk signal parallels that of planktonic foraminifers, with systematically lighter values in carbon and heavier values in oxygen isotopic composition
- The Late Miocene Carbon Shift occurs in both the eastern equatorial Pacific and the central Caribbean Sea
- Advection of bank-derived aragonite after 4.2 Ma affects the carbon isotope signature of the bulk fine-fraction but leaves the oxygen isotope signal unaffected
- No conspicuous changes of carbon and oxygen isotopic composition in eastern equatorial Pacific due the closure of the seaway
- Divergence of oxygen isotope values of the bulk fine-fraction between eastern equatorial Pacific and central Caribbean Sea started at around 4.2 Ma, and indicates the initiation of the modern salinity contrast between the eastern equatorial Pacific and the Caribbean

→ **Positive** evidence for the influence of the Panamanian Seaway Closure on hydrographical divergence between the eastern equatorial Pacific and the central Caribbena Sea

The multi-proxy approach followed in this study clearly proves the great potential of coccoliths as a palaeoceanographic tool. Evaluation of the influence of the closure of the Panamanian Seaway on evolution, biogeography and palaeoproductivity of coccolithophores emphasises the complexity of feedback mechanisms between palaeoceanography and marine biota. High-resolution work on coccolithophore biostratigraphy, morphometry, ecology and geochemistry detects and exposes interactions between environmental forcing and evolutionary change.

Herein, the role of coccolith biometry occupies a central position to highlight the role of coccoliths for accumulation patterns. Also, the improvement of the understanding of the bulk fine-fraction stable isotopic signal has revealed coccoliths as a reliable geochemical tool. Together with other proxies, coccoliths contribute fundamentally to the understanding of important mechanisms triggering global climate and biota as response to changed palaeoceanographic conditions.

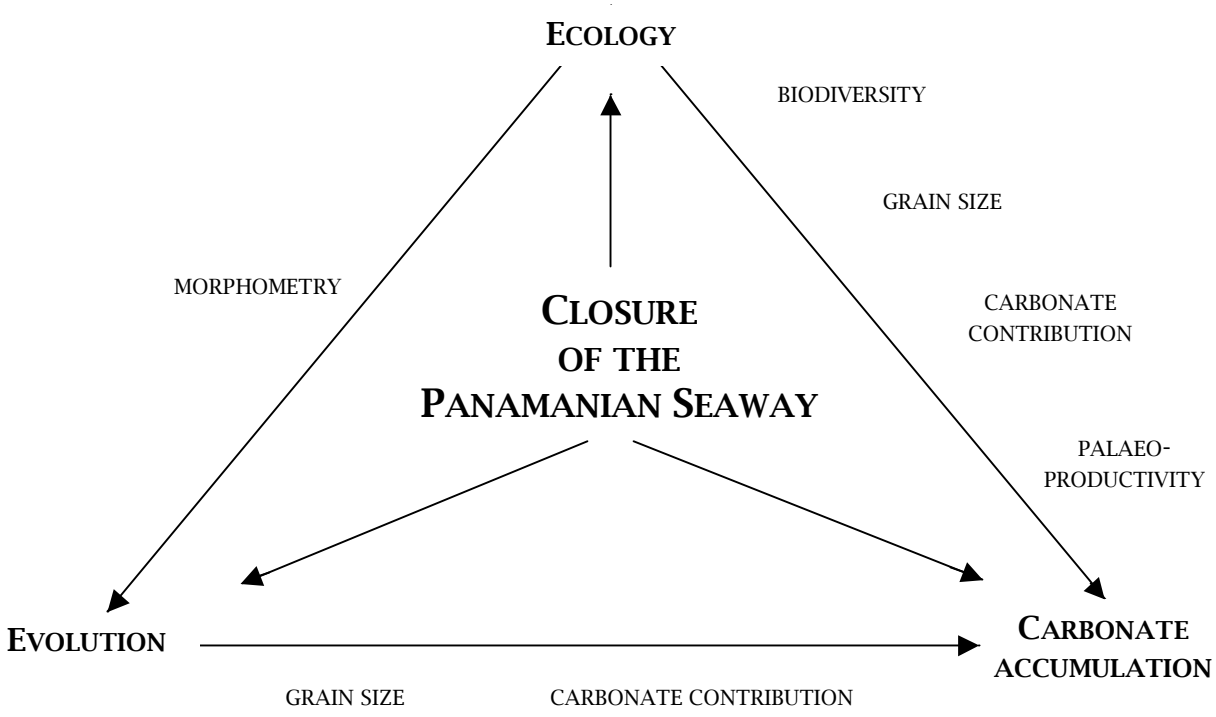

Fig. 10 Summary of impact and complexity of interactions due to the closure of the Panamanian Seaway on coccolithophores.

CONFERENCE CONTRIBUTIONS AND PRESENTATIONS

PROPER Course1: Proxies used in Paleoceanography
Vrije Universiteit Amsterdam / Royal NIOZ Texel, Netherlands
June 03–12, 2004
Talk: Lezius, J.: Contribution of coccoliths to the late Miocene to Pliocene biogenic bloom in the eastern equatorial Pacific
International Conference of Paleoceanography VIII, Biarritz, France
September 05-10, 2004
Poster: Kinkel, H., Lezius, J., Steph, S., Sturm, A., Tiedemann, R.: Contribution of coccoliths to the late Miocene – early Pliocene biogenic bloom in the eastern equatorial Pacific
Evaluation of Research Unit by German Research Foundation, Kiel, Germany
May 31, 2005
Poster: Lezius, J., Kinkel, H., Andersen, N.: Stable –carbon and – oxygen isotopes in coccolith carbonate – preliminary results of fine fraction separation techniques
Foraminifera and Nannofossil Groups Joint Spring Meeting 2005, Southampton Oceanography Centre, United Kingdom
June 16-17, 2005
Poster: Lezius, J., Kinkel, H., Andersen, N.: Coccolith evolution and stable isotopes during the Late Miocene / Early Pliocene Biogenic Bloom in the Eastern Equatorial Pacific
ECOLMAS course: Organism-based proxies in paleoceanography
University of Bremen, Germany
July 11-13, 2005
Talk: Lezius, J. Kinkel, H., Andersen, N.: Coccolith evolution and stable isotopes
Urbino Summer School in Paleoclimatology-The Cenozoic Record of Paleoclimate Change Urbino, Italy
July 25 – August 5, 2005
Poster: Lezius, J., Kinkel, H., Andersen, N.: Fine-fraction stable isotopes during the Late Miocene / Early Pliocene Biogenic Bloom in the Eastern Equatorial Pacific
Biogeochemical Controls on Palaeoceanographic Proxies, Conference of the Geological Society, London, United Kingdom
October 3-4, 2005
Poster: Lezius, J., Kinkel, H., Andersen, N.: Neogene stable isotopes in coccolith carbonate
Foraminifera and Nannofossil Groups Joint Spring Meeting 2006, University of Liverpool, United Kingdom
May 25-26, 2006
Poster: Lezius, J., Crudeli, D., Kinkel, H.: Impact of Panama uplift on nannofossil evolution
76. Jahrestagung der Paläontologischen Gesellschaft, Paläontologie zwischen Land und Meer, University of Kiel, Germany
August 28-30, 2006
Talk: Lezius, J., Kinkel, H.: The uplift of Panama – The coccolith side of the story: biodiversity
Poster: Lezius, J., Crudeli, D., Kinkel, H.: Impact of Panama uplift on nannofossil evolution
INA 11 - International Nannoplankton Association, Lincoln, Nebraska, USA
September 24-30, 2006
Talk: Lezius, J., Kinkel, H., Crudeli, D., Andersen, N., Flores, J.-A.: The uplift of Panama – The coccolith side of the story

REFERENCES

Agrawal, Y.C., McCave, I.N., Riley, J.B. and M., S.J.P., 1991. Laser diffraction size analysis. In: J.P.M. Syvitski (Editor), Principles, methods, and application of particle size analysis. Cambridge University Press, Cambridge - New York - Port Chester - Melbourne - Sydney, pp. 119-128.

Ahagon, N., Tanaka, Y. and Ujiie, H., 1993. Florisphaera profunda, a possible nannoplankton indicator of late Quaternary changes in sea-water turbidity at the northwestern margin of the Pacific. Marine Micropaleontology, 22(3): 255-273.

Aharon, P., Goldstein, S.L., Wheeler, C.W. and Jacobson, G., 1993. Sea-level events in the South Pacific linked with the Messinian salinity crisis. Geology, 21(9): 771-775.

Aiello, I.W. and Kellet, K., 2006. Sedimentology of open-ocean biogenic sediments from ODP Leg 201 Eastern Equatorial Pacific (Sites 1225 and 1226). Proceedings of the Ocean Drilling Program, Scientific Results, 201: doi:10.2973/odp.proc.sr.201.102.2006.

Alroy, J., 1998. Cope's Rule and the Dynamics of Body Mass Evolution in North American Fossil Mammals. Science, 280: 731-734.

Anderson, T.F. and Cole, S.A., 1975. The stable isotope geochemistry of marine coccoliths; a preliminary comparison with planktonic foraminifera. Journal of Foraminiferal Research, 5(3): 188-192.

Anderson, T.F. and Steinmetz, J.C., 1981. Isotopic and biostratigraphical records of calcareous nannofossils in a Pleistocene core. Nature, 294: 741-744.

Andruleit, H., 1996. A filtration technique for quantitative studies of coccoliths. Micropaleontology, 42(4): 403-406.

Andruleit, H.A., von Rad, U., Bruns, A. and Ittekkot, V., 2000. Coccolithophore fluxes from sediment traps in the northeastern Arabian Sea off Pakistan. Marine Micropaleontology, 38(3-4): 308.

Archer, D.E., 1991. Equatorial Pacific calcite preservation cycles: production or dissolution? Paleoceanography, 6(5): 561-571.

Archer, D.E., 1996. An atlas of the distribution of calcium carbonate in sediments of the deep sea. Global Biogeochemical Cycles, 10(1): 159-174.

Armstrong, R.A., Lee, C., Hedges, J.I., Honjo, S. and Wakeham, S.G., 2002. A new, mechanistic model for organic carbon fluxes in the ocean based on the quantitative association of POC with ballast minerals. Deep Sea Research Part II: Topical Studies in Oceanography
The US JGOFS Synthesis and Modeling Project: Phase 1, 49(1-3): 219-236.

Arnold, A.J., Kelly, D.C. and Parker, W.C., 1995. Causality and Cope´s rule: evidence from planktonic foraminifera. Journal of Paleontology, 69(2): 203-210.

Aubry, M.P., Bord, D., Beaufort, L., Kahn, A. and Boyd, S., 2005. Trends in size changes in the coccolithophorids, calcareous nannoplankton, during the Mesozoic: A pilot study. Micropaleontology, 51(4): 309-318.

Backman, J., E. and Hermelin, J.O.R., 1986. Morphometry of the Eocene nannofossil Reticulofenestra umbilicus lineage and its biochronological consequences. Palaegeography, Palaeoclimatology, Palaeoecology, 57(1): 103-116.

Backman, J. and Raffi, I., 1997. Calibration of Miocene nannofossil events to orbitally tuned cyclostratigraphies from Ceara Rise. Proceedings of the Ocean Drilling Program, Scientific Results, 154: 83-99.

Backman, J. and Shackleton, N.J., 1983. Quantitative biochronology of Pliocene and Early Pleistocene calcareous nannofossils from the Atlantic, Indian and Pacific oceans. Marine Micropaleontology, 8(2): 141-170.

Bains, S., Corfield, R.M. and Norris, R.D., 1999. Mechanisms of Climate Warming at the End of the Paleocene. Science, 285(5428): 724-727.

Bairbakhish, A.N., Bollmann, J., Sprengel, C. and Thierstein, H.R., 1999. Disintegration of aggregates and coccospheres in sediment trap samples. Marine Micropaleontology, 37(2): 219-223.

Bartoli, G. et al., 2005. Final closure of Panama and the onset of northern hemisphere glaciation. Earth and Planetary Science Letters, 237(1-2): 33-44.

Baumann, K.-H., 2004. Importance of size measurements for coccolith carbonate flux estimates. Micropaleontology, 50(1): 35-43.

Baumann, K.-H., Andruleit, H., Böckel, B., Geisen, M. and Kinkel, H., 2005. The significance of extant coccolithophores as indicators of ocean water masses, surface water temperature, and palaeoproductivity: a review. Paläontologische Zeitschrift, 79(1): 93-112.

Baumann, K.-H., Böckel, B. and Frenz, M., 2004. Coccolith contribution to South Atlantic carbonate sedimentation. In: H.R. Thierstein and J.R. Young (Editors), Coccolithophores. From Molecular Processes to Global Impact. Springer-Verlag Berlin Heidelberg, pp. 367-402.

Baumann, K.-H. and Sprengel, C., 2000. Morphological variations of selected coccolith species in a sediment trap north of the Canary Islands. Journal of Nannoplankton Research, 22(3): 185-193.

Baumgartner, P.O., 1987. Age and genesis of Tethyan Jurrasic radiolarites. Eclogae Geologicae Helvetiae, 80(831-879).

Bé, A.W.H., 1980. Gametogenetic calcification in a spinose planktonic foraminifer, *Globigerinoides sacculifer* (Brady). Marine Micropaleontology, 5: 283-310.

Beaufort, L., 2002. Geographic variability of individual coccolith weight in the Indian and Pacific Oceans. Journal of Nannoplankton Research, 24(2): 70.

Beaufort, L., 2005. Weight estimates of coccoliths using the optical properties (birefringence) of calcite. Micropaleontology, 51(4): 289-298.

Beaufort, L., de Garidel-Thoron, T., Mix, A.C. and Pisias, N.G., 2001. ENSO-like Forcing on Oceanic Primary Production During the Late Pleistocene. Science, 293(5539): 2440-2444.

Beaufort, L. and Dollfus, D., 2004. Automatic recognition of coccoliths by dynamical neural networks. Marine Micropaleontology, 51(1-2): 57-73.

Beaufort, L. and Heussner, S., 1999. Coccolithophorids on the continental slope of the Bay of Biscay - production, transport and contribution to mass fluxes. Deep Sea Research Part II: Topical Studies in Oceanography, 46(10): 2147-2174.

Beaufort, L. et al., 1997. Insolation Cycles as a Major Control of Equatorial Indian Ocean Primary Production. Science, 278(5342): 1451-1454.

Bender, M.L. and Keigwin, L.D., Jr., 1979. Speculations about the upper Miocene change in abyssal Pacific dissolved bicarbonate delta (super 13) C. Earth and Planetary Science Letters, 45(2): 383-393.
Berger, W., H., Fischer, K., Lai, C. and Wu, G., 1987. Ocean productivity and organic carbon flux. Part 1. Overview and maps of primary productivity and export production. University of California, San Diego.
Berger, W.H., Bonneau, M.C. and Parker, F.L., 1982. Foraminifera on the deep-sea floor; lysocline and dissolution rate. Oceanologica Acta, 5(2): 249-258.
Berger, W.H., Leckie, R.M., Janecek, T.R., Stax, R. and Takayama, T., 1993. Neogene carbonate sedimentation on Ontong Java Plateau; highlights and open questions. Proceedings of the Ocean Drilling Program, Scientific Results, 130: 711-744.
Berger, W.H. and Wefer, G., 1996. Central Themes of South Atlantic Circulation. In: G. Wefer, W.H. Berger, G. Siedler and D.J. Webb (Editors), The South Atlantic - Present and Past Circulatinon. Springer-Verlag, Berlin, Heidelberg, pp. 1-11.
Bernaola, G. and Monechi, S., 2007. Calcareous nannofossil extinction and survivorship across the Cretaceous-Paleogene boundary at Walvis Ridge (ODP Hole 1262C, South Atlantic Ocean). Palaeogeography, Palaeoclimatology, Palaeoecology Cretaceous-Paleogene Boundary Events, 255(1-2): 132-156.
Berthold, C., Pabst, W. and Nickel, K.G., 2006. Influence of detector geometries of common laser diffractometers on the apparent particle size distribution of strongly anisometric particles, The Fifth World Congress on Particle Technology (WCPT-5), pp. 1-6.
Bianchi, G.G., Hall, I.R., McCave, I.N. and Joseph, L., 1999. Measurement of the sortable silt current speed proxy using the Sedigraph 5100 and Coulter multisizer IIe; precision and accuracy. Sedimentology, 46(6): 1001-1014.
Bickert, T., Cordes, R. and Wefer, R., 1997. Late Pliocene to Mid-Pleistocene (2.6-1.0 M.Y.) Carbonate dissolution in the Western Equatorial Atlantic: Results of Leg154, Ceara Rise. Proceedings of the Ocean Drilling Program, Scientific Results, 154: 229-237.
Bickert, T., Haug, G.H. and Tiedemann, R., 2004. Late Neogene benthic stable iotope record of Ocean Drilling Program Site 999: Implications for Caribbean paleoceanography, organic carbon burial, and the Messinian Salinity Crisis. Paleoceanography, 19: PA1023, doi:10.1029/2002PA000799.
Biekart, J.W., 1989. The distribution of calcareous nannoplankton in late Quaternary sediments collected by the Snellius II Expedition in some southeast Indonesian basins. Proc. K. Ned. Akad. Wet, 92(2): 77-141.
Billard, C. and Inouye, I., 2004. What is new in coccolithophore biology? In: H.R. Thierstein and J.R. Young (Editors), Coccolithophores. From Molecular Processes to Global Impact. Springer-Verlag Berlin Heidelberg, pp. 1-29.
Billups, K., 2002. Late Miocene through early Pliocene deep water circulation and climate change viewed from the sub-Antarctic South Atlantic. Palaeogeography, Palaeoclimatology, Palaeoecology, 185(3-4): 287-307.
Billups, K., Ravelo, A.C., Zachos, J.C. and Norris, R.D., 1999. Link between oceanic heat transport, thermohaline circulation, and the Intertropical Convergence Zone in the early Pliocene Atlantic. Geology, 27(4): 319-322.
Blott, S.J. and Pye, K., 2006. Particle size distribution analysis of sand-sized particles by laser diffraction: an experimental investigation of instrument sensitivity and the effects of particle shape. Sedimentology, 53(3): 671-685.
Blum, P., 1997. Physical Properties Handbook: A guide to shipboard measurement of physical properties of deep-sea cores. ODP Tech. Note, 26.
Boeckel, B. and Baumann, K.-H., 2004. Distribution of coccoliths in surface sediments of the south-eastern South Atlantic Ocean: ecology, preservation and carbonate contribution. Marine Micropaleontology, 51(3-4): 301-320.
Bolli, H.M., Saunders, J.B. and Perch-Nielsen, K., 1985. Plankton Stratigraphy. Cambridge Earth Science Series. Cambridge University Press, Cambridge.
Bollmann, J., 1997. Morphology and biogeography of *Gephyrocapsa* coccoliths in Holocene sediments. Marine Micropaleontology, 29: 319-350.
Bollmann, J., Henderiks, J. and Brabec, B., 2002. Global Calibration of *Gephyrocapsa* coccolith abundance in holocene sediments for paleotemperature assessment. Paleoceanography, 17(0).
Bown, P., 2005. Selective calcareous nannoplankton survivorship at the Cretaceaus-Tertiary boundary. Geology, 33(8): 653-656.
Bown, P.R. et al., 1998. Calcareous Nannofossil Biostratigraphy. British Micropalaeontological Society Publications Series. Kluwer Academic Publishers, Dordrecht, Boston, London, 314 pp.
Bown, P.R., Lees, J.A. and Young, J.R., 2004. Calcareous nannoplankton evolution and diversity through time. In: H.R. Thierstein and J.R. Young (Editors), Coccolithophores. From Molecular Processes to Global Impact. Springer-Verlag Berlin Heidelberg, pp. 481-508.
Bown, P.R. and Young, J.R., 1998. Introduction. In: P.R. Bown (Editor), Calcareous Nannofossil Biostratigraphy. Kluwer Academic, Dordrecht, pp. 1-15.
Braga, J.C. and Martin, J.M., 1996. Geometries of reef advance in response to relative sea-level changes in a Messinian (uppermost Miocene) fringing reef (Cariatiz reef, Sorbas Basin, SE Spain). Sedimentary Geology, 107(1-2): 61-81.
Bralower, T., J., Bown Paul, R. and Siesser, W., 1991. Significance of Upper Triassic nannofossils from Southern Hemisphere (ODP Leg 122, Wombat Plateau, NW Australia). Marine Micropaleontology, 17: 119-154.
Bralower, T.J., 2002. Evidence of surface water oligotrophy during the Paleocene-Eocene thermal maximum: nannofossil assemblage data from Ocean Drilling Program Site 690, Maud Rise, Weddell Sea. Paleoceanography, 17(2): 1-13.
Bralower, T.J., Geleskie, S., Arthur, M.A. and Eccles, L., 2006. Quantification of Plankton Size and Flux Changes across the Cretaceous/Paleocene Extinction. International Nannoplankton Association, Program with Abstracts(11): 20.
Brand, L.E., 1994. Physiological ecology of marine coccolithophores. In: A. Winter and W. Siesser (Editors), Coccolithophores. Cambridge University Press, Cambridge, pp. 39-49.
Brassell, S.C., Eglinton, G., Marlowe, I.T., Pflaumann, U. and Sarnthein, M., 1986. Molecular stratigraphy: a new tool for climatic assessment. 320(6058): 129-133.
Broecker, W., S. and Denton, G., H., 1989. The role of ocean-atmosphere reorganizations in glacial cycles. Geochimica et Cosmochimica Acta, 53(10): 2465-2501.

Broerse, A.T.C., Ziveri, P., van Hinte, J.E. and Honjo, S., 2000. Coccolithophore export production, species composition, and coccolith-CaCO3 fluxes in the NE Atlantic (34[deg]N 21[deg]W and 48[deg]N 21[deg]W). Deep Sea Research Part II: Topical Studies in Oceanography, 47(9-11): 1877-1905.

Brown, J.H. and Maurer, B.A., 1986. Body size, ecological dominance and Cope's rule. 324(6094): 248-250.

Brownlee, C. and Taylor, A., 2004. Calcification in coccolithophores: A cellular perspective. In: H.R. Thierstein and J.R. Young (Editors), Coccolithophores. From Molecular Processes to Global Impact. Springer-Verlag Berlin Heidelberg, pp. 31-49.

Brummer, G.J.A. and van Eijden, A.J.M., 1992. "Blue-ocean" paleoproductivity estimates from pelagic carbonate mass accumulation rates. Marine Micropaleontology, 19: 99-117.

Buitenhuis, E.T., de Baar, H.J.W. and Veldhuis, M.J.W., 1999. Photosynthesis and Calcification by Emiliana huxleyi (Prymnesiophyceae) as a function of inorganic carbon species. Journal of Phycology, 35(5): 949-959.

Burky, A.J., 1971. Biomass turnover, respiration and interpopulation variation in the stream limpet, Fgrrissa rivularis (Say). Ecological Monographs, 41: 235-251.

Cachao, M. and Moita, M.T., 1995. Coccolithus pelagicus, a sort of productivity proxy?
In: 6th International Nannoplankton Association conference; programme and abstracts. Journal of Nannoplankton Research, 17(2): 50-51.

Cachao, M. and Moita, M.T., 2000. Coccolithus pelagicus, a productivity proxy related to moderate fronts off Western Iberia. In: Nannoplankton ecology and palaeoecology. Marine Micropaleontology, 39(1-4): 131-155.

Cerling, T.E., 1997. Late Cenozoic vegetation change, atmospheric CO_2 and tectonics. In: W. Ruddiman (Editor), Tectonic uplift and climate change. Plenum Press New York, pp. Pages 313-327 1997.

Cerling, T.E. et al., 1997. Global vegetation change through the Miocene/Pliocene boundary. Nature, 389: 153-158.

Cerling, T.E., Wang, Y. and Quade, J., 1993. Expansion of C4 ecosystems as an indicator of global ecological change in the late Miocene. Nature, 361: 344-345.

Chaisson, W.P. and Ravelo, A.C., 2000. Pliocene development of the east-west hydrographic gradient in the equatorial Pacific. Paleoceanography, 15(5): 497-505.

Chapman, M.R. and Chepstow, L.A., 1997. Late Pliocene climatic change and the global extinction of the discoasters; an independent assessment using oxygen isotope records. Palaeogeography, Palaeoclimatology, Palaeoecology, 134(1-4): 109-125.

Charlson, R.J., Lovelock, J.E., Andreae, M.O. and Warren, S.G., 1987. Oceanic phytoplankton, atmospheric sulphur, cloud albedo and climate. Nature, 326(6114): 655-661.

Chepstow-Lusty, A., Backman, J. and Shackleton, N.J., 1989. Comparison of upper Pliocene *Discoaster* abundance variations from North Atlantic Sites 552, 607, 659 and 662: further evidnce for marine plankton responding to orbital forcing. Proceedings of the Ocean Drilling Program - Scientific Results, 108: 121-141.

Chisholm, S.W., 1991. Phytoplankton size. In: P.G. Falkowski and A.D. Woodhead (Editors), Primary Productivity and Biogeochemical Cycles in the Sea. Environmental Science Research. Plenum Press, New York, pp. 213-237.

Coates, A.G., Aubry, M.-P., Berggren, W.A., Collins, L.S. and Kunk, M., 2003. Early Neogene history of the Central American arc from Bocas del Toro, western Panama. Geological Society of America Bulletin, 115(3): 271-287.

Coates, A.G. et al., 1992. Closure of the Isthmus of Panama; the near-shore marine record of Costa Rica and western Panama. Geological Society of America Bulletin, 104(7): 814-828.

Coates, A.G. and Obando, J.A., 1996. The geologic evolution of the Central American Isthmus. In: J.B.C. Jackson, A.F. Budd and A.G. Coates (Editors), Evolution and environment in tropical America, pp. 21-56.

Collins, L., S., Coates Anthony, G., Berggren William, A., Aubry Marie, P. and Zhang, J., 1996. The late Miocene Panama Isthmian strait. Geology, 29(8): 687-690.

Colmenero-Hidalgo, E., Flores, J.-A. and Sierro, F.J., 2002. Biometry of Emiliania huxleyi and its biostratigraphic significance in the eastern north atlantic ocean and western mediterranean sea in the last 20 000 years. Marine Micropaleontology, 886: 1-17.

Colmenero-Hidalgo, E. et al., 2004. Ocean surface water response to short-term climate changes revealed by coccolithophores from the Gulf of Cadiz (NE Atlantic) and Alboran Sea (W Mediterranean). Palaeogeography, Palaeoclimatology, Palaeoecology, 205(3-4): 317-336.

Cooke, S. and Rohling, E.J., 2001. Stable Isotopes in Foraminiferal Carbonate. Southampton Oceanography Centre Internal Document, 72: 56 pp.

Cortese, G., Gersonde, R., Hillenbrand, C.-D. and Kuhn, G., 2004. Opal sedimentation shifts in the World Ocean over the last 15 Myr. Earth and Planetary Science Letters, 224(3-4): 509-527.

Cros, L., Kleijne, A., Billard, C. and Young, J., R., 2000. New examples of holococcolith-heterococcolith combination coccospheres and their impleications for coccolithophorid biology. Marine Micropaleontology, 39: 1-34.

Crudeli, D., 2005. Early Pliocene evolution of coccolithophores in the Caribbean Sea: Taxonomy, Biostratigraphy, Paleoecology and Paleoceanography, Christian-Albrechts-Universität zu Kiel.

De Vargas, C., Saez, A.G., Medlin, L.K. and Thierstein, H.R., 2004. *Super-Species* in the calcareous plankton. In: H.R. Thierstein and J.R. Young (Editors), Coccolithophores. From Molecular Processes to Global Impact. Springer-Verlag Berlin Heidelberg, pp. 271-298.

Delaney, M.L. and Boyle, E.A., 1987. Cd/Ca in late Miocene benthic foraminifera and changes in the global organic carbon budget. 330(6144): 156-159.

Delaney, M.L. and Filippelli, G.M., 1994. An apparent contradiction in the role of phosphorus in Cenozoic chemical mass balances for the world ocean. Paleoceanography, 9(4): 513-527.

Dennison, J.M. and Hay, W.W., 1967. Estimating the needed sampling area for subaquatic ecologic studies. Journal of Paleontology, 41(3): 706-708.

Di Nocera, S. and Scandone, P., 1977. Triassic nannoplankton limestones of deep basin origin in the Central Mediterranean region. Palaegeography, Palaeoclimatology, Palaeoecology, 21: 101-111.

Dickens, G., R. and Owen, R.M., 1994. Late Miocene-early Pliocene manganese redirection in the central Indian Ocean; expansion of the intermediate water oxygen minimum zone. Paleoceanography, 9(1): 169-181.

Dickens, G.R. and Owen, R.M., 1999. The latest Miocene-early Pliocene biogenic bloom; a revised Indian Ocean perspective, In: Aspects of geology, geophysics and paleoceanography of the Indian Ocean; selected papers. Marine Geology, 161(1): 75-91.

Diester Haass, L., Billups, K. and Emeis, K.C., 2005. In search of the late Miocene-early Pliocene "biogenic bloom" in the Atlantic Ocean (Ocean Drilling Program Sites 982, 925, and 1088). Paleoceanography, 20: 1-13.
Diester-Haass, L., Billups, K. and Emeis, K.C., 2005. In search of the late Miocene-early Pliocene "biogenic bloom" in the Atlantic Ocean (Ocean Drilling Program Sites 982, 925, and 1088). Paleoceanography, 20: 1-13.
Diester-Haass, L., Meyers, P.A. and Bickert, T., 2004. Carbonate crash and biogenic bloom in the late Miocene: Evidence from ODP Sites 1085, 1086, and 1087 in the Cape Basin, southeast Atlantic Ocean. Paleoceanography, 19(PA1007): doi:10.1029/2003PA000933.
Dittert, N. et al., 1999. Carbonate dissolution in the deep sea: Methods, quantification and paleoceanographic application. In: G. Fischer and G. Wefer (Editors), Proxies in paleoceanography. Springer-Verlag, Berlin Heidelberg, pp. 255-284.
Dowsett, H.J. et al., 1999. Middle Pliocene paleoenvironmental reconstruction. PRISM2, U.S. Geol. Surv. Open File Rep., 99-535: 13pp.
Dowsett, H.J. et al., 1992. Micropaleontological Evidence for Increased Meridional Heat Transport in the North Atlantic Ocean During the Pliocene. Science, 258: 1133-1135.
Driever, B.W.M., 1988. Calcareous nannofossil biostratigraphy and paleoenvironmental interpretation of the Mediterranean Pliocene. Utrecht Micropaleontological Bulletins, 39, Utrecht, 245 pp.
Driscoll, N.W. and Haug, G.H., 1998. A Short Circuit in Thermohaline Circulation: A Cause for Northern Hemisphere Glaciation? Science, 282(5388): 436-438.
Droxler, A.W. et al., 1992. Late middle (?) Miocene segmentation of an Eocene-early Miocene carbonate megabank on the northern Nicaragua Rise tied to the tectonic activity at the North America/Caribbean plate boundary zone. EOS, 43(73): 299.
Droxler, A.W., Morse, J.W., Glaser, K.S., Haddad, G.A. and Baker, P.A., 1991. Surface sediment carbonate mineralogy and water column chemistry: Nicaragua Rise versus the Bahamas. Marine Geology, 100: 277-289.
Dudley, W.C., Blackwelder, P., Brand, L., Duplessy, J.C. and Haq, B.U., 1986. Stable isotopic composition of coccoliths. In: Stable isotopic and biogeographic clues in oceanography and paleoceanography. Marine Micropaleontology, 10(1-3): 1-8.
Dudley, W.C., Duplessy, J.C., Blackwelder, P.L., Brand, L.E. and Guillard, R.R.L., 1980. Coccoliths in Pleistocene-Holocene nannofossil assemblages. Nature, 285: 222-223.
Dudley, W.C. and Goodney, D.E., 1979. Oxygen isotope content of coccoliths grown in culture. Deep Sea Research, 26A: 495-503.
Dudley, W.C. and Nelson, C.S., 1989. Quaternary surface-water stable isotope signal from calcareous nannofossils at DSDP Site 593, southern Tasman Sea. Marine Micropaleontology, 13(4): 353-373.
Dudley, W.C. and Nelson, C.S., 1994. The influence of non-equilibrium isotope fractionation on the Quaternary calcareous nannofossil stable isotope signal in the southwest Pacific Ocean, DSDP Site 594. Marine Micropaleontology, 24: 3-27.
Duque-Caro, H., 1990. Neogene stratigraphy, paleoceanography and paleobiogeography in northwest South America and the evolution of the Panama Seaway. paleogeography, paleoclimatology, paleoecology, 77: 203-234.
Edvardsen, B. et al., 2000. Phylogenetic reconstruction of the Haptophyta inferred from 18S ribosomal DNA sequences and available morphological data. Phycologia, 38: 149-155.
Eldredge, N. and Gould, S.J., 1988. Punctuated equilibrium prevails. 332(6161): 211-212.
Eldredge, N. et al., 2005. The Dynamics of evolutionary stasis. Paleobiology, 31(2): 133-145.
Ennyu, A. and Arthur, M.A., 2004. Data Report: oxygen and carbon stable isotope records of the Miocene calcareous Microfossils from ODP Leg 189 Sites 1170 (South Tasman Rise) and 1172 (East Tasman Plateau). Proceedings of the Ocean Drilling Program, Scientific Results, 189: 1-12.
Falkowski, P.G. and Oliver, M.J., 2007. Mix and match: how climate selects phytoplankton. 5(10): 813-819.
Farinacci, A., 1969. Catalogue of Calcareous Nannofossils. Edizioni Tecnoscienza, Roma.
Farrell, J.W., Murray, D.W., McKenna, V.S. and Ravelo, A.C., 1995a. Upper ocean temperature and nutrient contrasts inferred from Pleistocene planktonic foraminifer delta (super 18) O and delta (super 13) C in the eastern Equatorial Pacific. Proceedings of the Ocean Drilling Program, Scientific Results, 138: 289-319.
Farrell, J.W. et al., 1995b. Late Neogene sedimentation patterns in the eastern Equatorial Pacific Ocean. ODP Sci. Res., 138: 717-756.
Ferraris, C.F., Hackley, V.A., Avilés, A.I. and Buchanan, C.E.J., 2002. Analysis of the ASTM Round-Robin Test on Particle Size Distribution of Portland Cement: Phase I., National Institute of Standards and Technology - Technology Administration, U.S. Department of Commerce.
Filippelli, G.M. and Delaney, M.L., 1994. The oceanic phosphorus cycle and continental weathering during the Neogene. Paleoceanography, 9(5): 643-652.
Filippelli, G.M. et al., 2003. A sediment-nutrient-oxygen feedback responsible for productivity variations in Late Miocene sapropel sequences of the western Mediterranean. Palaeogeography, Palaeoclimatology, Palaeoecology, 190: 335-348.
Finkel, Z.V., Katz, M.E., Wright, J.D., Schofield, O.M.E. and Falkowski, P.G., 2005. Climatically driven macroevolutionary patterns in the size of marine diatoms over the Cenozoic. PNAS, 102(25): 8927-8932.
Finkel, Z.V. et al., 2007. A universal driver of macroevolutionary change in the size of marine phytoplankton over the Cenozoic 10.1073/pnas.0709381104. Proceedings of the National Academy of Sciences, 104(51): 20416-20420.
Flemming, B.W., 2007. The influence of grain-size analysis methods and sediment mixing on curve shapes and textural parameters: Implications for sediment trend analysis. Sedimentary Geology, 202(3): 425-435.
Flores, J., Abel, Marino, M., Sierro, F.J., Hodell, D.A. and Charles, C.D., 2003. Calcareous plankton dissolution pattern and coccolithophore assemblages during the last 600 kyr at ODP Site 1089 (Cape Basin, South Atlantic); paleoceanographic implications. Palaeogeography, Palaeoclimatology, Palaeoecology, 196(3-4): 409-426.
Flores, J.-A. et al., 2005. Surface water dynamics and phytoplankton communities during deposition of cyclic late Messinian sapropel sequences in the western Mediterranean. Marine Micropaleontology, 56(1-2): 50-79.
Frenz, M., Baumann, K.-H., Boeckel, B., Höppner, R. and Henrich, R., 2005. Quantification of foraminifer and coccolith carbonate in South Atlantic surface sediments by means of carbonate grain-size distributions. Journal of Sedimentary Research, 75(3): 464-475.
Fritsch, Instruction Manual, Analysette22. http://www.fritsch.de/data/manuals/hb_222xxx_0001_e.pdf.

Gartner, S., Chow, J. and Stanton, R.J., Jr., 1987. Late Neogene paleoceanography of the eastern Caribbean, the Gulf of Mexico, and the eastern Equatorial Pacific. Marine Micropaleontology, 12(3): 255-304.
Gartner, S.J., 1969. Correlation of Neogene planktonic foraminifer and calcareous nannofossil zones. Transactions - Gulf Coast Association of Geological Societies, 19: 585-599.
Geisen, M. et al., 2002. Life-cycle associations involving pairs of holococcolithophorid species: intraspecific variation or cryptic speciation? Eur. J. Phycol., 37: 531-550.
Geisen, M. et al., 2004. Species level variation in coccolithophores. In: H.R. Thierstein and J.R. Young (Editors), Coccolithophores. From Molecular Processes to Global Impact. Springer-Verlag Berlin Heidelberg, pp. 327-366.
Geitzenauer, K.R., Roche, M.B. and McIntyre, A., 1976. Modern pacific coccolithophore assemblages: derivation and application to Late Pleistocene paleotemperature analysis. In: Cline, R. M. and Hays, J. D., Editors. Investigations of Late Quaternary Paleoceanography and Paleoclimatology. Geological Society of America (GSA), 145: 423-428.
Geitzenauer, K.R., Roche, M.B. and McIntyre, A., 1977. Coccolith biogeography from North Atlantic and Pacific surface sediments. Oceanic Micropaleontology, 2: 973-1008.
Gibbs, S.J., Young, J.R., Bralower, T.J. and Shackleton, N.J., 2005. Nannofossil evolutionary events in the mid-Pliocene: an assessment of the degree of synchrony in the extinctions of Reticulofenestra pseudoumbilicus and Sphenolithus abies. Palaeogeography, Palaeoclimatology, Palaeoecology, 217(1-2): 155-172.
Giraudeau, J., 1992. Distribution of Recent nannofossils beneath the Benguela System; Southwest African continental margin. Marine Geology, 108(2): 219-237.
Goodney, D.E., Margolis, S.V., Dudley, W.C., Kroopnick, P. and Williams, D.F., 1980. Oxygen and carbon isotopes of Recent calcareous nannofossils as paleoceanographic indicators. Marine Micropaleontology, 5(1): 31-42.
Goossens, D., 2008. Techniques to measure grain-size distributions of loamy sediments: a comparative study of ten instruments for wet analysis
doi:10.1111/j.1365-3091.2007.00893.x. Sedimentology, 55(1): 65-96.
Grant, K.M. and Dickens, G.R., 2002. Coupled productivity and carbon isotope records in the Southwest Pacific Ocean during the late Miocene-early Pliocene biogenic bloom. Palaeogeography, Palaeoclimatology, Palaeoecology, 187(1-2): 61-82.
Gregorova, E., Pabst, W. and Bohacenko, I., 2006. Characterization next term of different starch types for their application in ceramic processing. Journal of the European Ceramic Society, 26: 1301-1309.
Groeneveld, J., 2005. Effect of the Pliocene closure of the Panamanian Gateway on Caribbean and east Pacific sea surface temperatures and salinities by applying combined Mg/Ca and $\partial^{18}O$ measurements (5.6-2.2 Ma). Kummulative Dissertation Thesis, Christian-Albrechts-Universität Kiel, Kiel, 81 pp.
Groeneveld, J. et al., 2008. Foraminiferal Mg/Ca increase in the Caribbean during the Pliocene: Western Atlantic Warm Pool formation, salinity influence, or diagenetic overprint? G3: Geochemistry, Geophysics, Geosystems, 9(Q01P23).
Gröger, M., Henrich, R. and Bickert, T., 2003a. Glacial-interglacial variability in lower North Atlantic deep water: inference from silt grain-size analysis and carbonate preservation in the western equatorial Atlantic. Marine Geology, 201(4): 321-332.
Gröger, M., Henrich, R. and Bickert, T., 2003b. Variability of silt grain size and planktonic foraminiferal preservation in Plio/Pleistocene sediments from the western equatorial Atlantic and Caribbean. Marine Geology, 201(4): 307-320.
Gupta, A.K., Singh, R.K., Joseph, S. and Thomas, E., 2004. Indian Ocean high-productivity event (10-8 Ma); linked to global cooling or to the initiation of the Indian monsoons? Geology, 32(9): 753-756.
Hagino, K. and Okada, H., 2004. Floral Response of Coccolithophores to Progressive Oligotrophication in the South Equatorial Current, Pacific Ocean. In: M. Shiyomi and e. al. (Editors), Global Environmental Change in the Ocean and on Land. Terrapub.
Hagino, K. and Okada, H., 2006. Intra- and infra-specific morphological variation in selected coccolithophore species in the equatorial and subequatorial Pacific Ocean. Marine Micropaleontology, 58: 184-206.
Haq, B.U. and Lohmann, G.P., 1976. Early Cenozoic calcareous nannoplankton biogeography of the Atlantic Ocean. Marine Micropaleontology, 1(2): 119-194.
Hart, M.B., 2003. In search for the origin of the planktic Foraminifera. J. Geol. Soc., 160: 341-343.
Haug, G.H., Hughen, K.A., Sigman, D.M., Peterson, L.C. and Röhl, U., 2001a. Southward migration of the intertropical convergence zone through the holocene. Science, 293: 1304-1308.
Haug, G.H. and Tiedemann, R., 1998. Effect of the formation of the Isthmus of Panama on Atlantic Ocean thermohaline circulation. Nature, 393: 673-676.
Haug, G.H., Tiedemann, R., Zahn, R. and Ravelo, A.C., 2001b. Role of Panama uplift on oceanic freshwater balance. Geology, 29(3): 207-210.
Hay, W.W., 1970. Calcareous Nannofossils from Cores Recovered on Leg 4. In: R.G. Bader, E.D. Gerard and e. al. (Editors), Init. Repts. DSDP, pp. 455-502.
Hay, W.W., 2004. Carbonate fluxes and calcareous nannoplankton. In: H.R. Thierstein and J.R. Young (Editors), Coccolithophores. From Molecular Processes to Global Impact. Springer-Verlag Berlin Heidelberg, pp. 509-528.
Hays, J.D., Imbrie, J. and Shackleton, N.J., 1976. Variations in the Earth's Orbit: Pacemaker of the Ice Ages 10.1126/science.194.4270.1121. Science, 194(4270): 1121-1132.
Henderiks, J., 2008a. Coccolithophore size rules -- Reconstructing ancient cell geometry and cellular calcite quota from fossil coccoliths. Marine Micropaleontology, 67(1-2): 143-154.
Henderiks, J., 2008b. Late Miocene coccolithophore (r)evolution. Geophys Research Abstracts, 10.
Henderiks, J. and Pagani, M., 2008. Correction to “Refining ancient carbon dioxide estimates: Significance of coccolithophore cell size for alkenone-based pCO2 records”. Paleoceanography, 23(PA2206).
Henderiks, J. and Renaud, S., 2004. Coccolith size increase of *Calcidiscuc leptoporus* offshore Morocco during the last Glacial Maximum: an expression of enhaced glacial productivity? Journal of Nannoplankton Research, 26(1): 1-12.
Henrich, R., Baumann, K.-H., Gerhardt, S., Gröger, M. and Volbers, A., 2003. Carbonate Preservation in Deep and Intermediate Water Masses in the South Atlantic: Evaluation and Geological Record (a Review). In: G. Wefer, S. Mulitza and V. Ratmeyer (Editors), The South Atlantic in the Late Quaternary: Reconstruction of Material Budgets and Current Systems. Springer-Verlag Berlin Heidelberg New York Tokyo, pp. 645-670.

Hermoyian, C.S. and Owen, R.M., 2001. Late Miocene-early Pliocene biogenic bloom; evidence from low-productivity regions of the Indian and Atlantic Oceans. Paleoceanography, 16(1): 95-100.
Hibberd, D.J., 1976. The ultrastructure and taxonomy of the Crysophyceae and Prymnesiophyceae (Haptophyceae): a survey with some new observations on the ultrastrucutre of the Chrysophyceae. Botanical Journal of the Linnean Society, 72: 55-80.
Hilgen, F.J., Abdul Aziz, H., Krijgsman, W., Raffi, I. and Turco, E., 2003. Integrated stratigraphy and astronomical tuning of the Serravallian and lower Tortonian at Monte dei Corvi (Middle-Upper Miocene, northern Italy). Palaeogeography, Palaeoclimatology, Palaeoecology, 199(3-4): 229-264.
Hilgen, F.J. et al., 1999. Present status of the astronomical (polarity) time-scale for the Mediterranean Late Neogene. Phil. Trans. Roy. Soc. of Lond. A, 357: 1931-1947.
Hilgen, F.J. et al., 1995. Extending the astronomical (polarity) time scale into the Miocene. Earth and Planetary Science Letters, 136(3-4): 495-510.
Hills, S.J. and Thierstein, H.R., 1989. Plio-Pleistocene calcareous plankton biochronology. Marine Micropaleontology Plankton Biochronology, 14(1-3): 67-96.
Hodell, D.A., Benson, R.H., Kent, D.V., Boersma, A. and Rakic-El Bied, K., 1994. Magnetostratigraphic, biostratigraphic, and stable isotope stratigraphy of an Upper Miocene drill core from the Salé Briqueterie (northwestern Morocco): A high-resolution chronology for the Messinian stage. Paleoceanography, 9(6): 835-855.
Hodell, D.A., Curtis, J.H., Sierro, F.J. and Raymo, M.E., 2001. Correlation of late Miocene to early Pliocene sequences between the Mediterranean and North Atlantic. Paleoceanography, 16(2): 164-178.
Hodell, D.A., Müller, D.W., Ciesielski, P.F. and Mead, G.A., 1991c. Synthesis of oxygen and carbon isotopic results from Site 704: Implications for major climatic-geochemical transitions during the late Neogene. Proceedings of the Ocean Drilling Program, Scientific Results, 114: 475-480.
Hoernle, K. et al., 2002. Missing history (16-71 Ma) of the Galapagos hotspot; implications for the tectonic and biological evolution of the Americas. Geology, 30(9): 795-798.
Holligan, P.M., 1991. Do marine Phytoplankton influence global climate? In: P.G. Falkowski and A.D. Woodhead (Editors), Primary Productivity and Biogeochemical Cycles in the Sea. Environmental Science Research. Plenum Press, New York, pp. 487-501.
Hone, D.W.E. and Benton, M.J., 2005. The evolution of large size: how does Cope's Rule work? Trends in Ecology & Evolution, 20(1): 4-6.
Honjo, S., 1975. Dissolution of suspended coccoliths in the deep-sea water column and sedimentation of coccolith ooze. Special Publications - Cushman Foundation for Foraminiferal Research, Dissolution of deep-sea carbonates, 13: 114-120.
Honjo, S., 1976. Coccoliths: Production, Transportation and Sedimentation. Marine Micropaleontology, 1: 65-79.
Honjo, S., 1996. Fluxes of particles to the interior of the open oceans. In: V. Ittekkot, Schäfer, P., Honjo, S., Depetris, P.J. (Editor), Particle FLux in the Ocean. Wiley, New York.
Hoorn, C., Ohja, T. and Quade, J., 2000. Palynological evidence for vegetation development and climatic change in the sub-Himalayan zone (Neogene, central Nepal). Palaeogeography, Palaeoclimatology, Palaeoecology, 163(3-4): 133-161.
Hsü, K.J., Ryan, W.B.F. and Cita, M.B., 1973. Late Miocene Desiccation of the Mediterranean. 242(5395): 240-244.
Huesing, S.K., Hilgen, F.J., Abdul Aziz, H. and Krijgsman, W., 2007. Completing the Neogene geological time scale between 8.5 and 12.5†Ma. Earth and Planetary Science Letters, 253(3-4): 340-358.
Hunt, G. and Roy, K., 2006. Climate change, body size evolution, and Cope's Rule in deep-sea ostracodes. PNAS, 103(5): 1347-1352.
Imbrie, J. and Imbrie, J.Z., 1980. Modeling the Climatic Response to Orbital Variations 10.1126/science.207.4434.943. Science, 207(4434): 943-953.
Irani, R.R. and Callis, C.F., 1963. Particle Size: Measurement, Interpretation and Application. John Wiley & Sons, Inc., New York, London, 165 pp.
Jablonski, D., 1997. Body-size evolution in Cretaceous molluscs and the status of Cope's rule. 385(6613): 250-252.
Jafar, A.S., 1983. Significance of Late Triassic calcareous Nannoplankton from Austria and Southern Germany. Neues Jahrbuch für Geologie und Paläontologie, Abhandlungen, 166: 218-256.
Jain, S. and Collins, L.S., 2007. Trends in Caribbean Paleoproductivity related to the Neogene closure of the Central American Seaway. Marine Micropaleontology.
Jain, S., Collins, L.S. and Hayek, L.-A.C., 2007. Relationship of benthic foraminiferal diversity to paleoproductivity in the Neogene Caribbean. Palaeogeography, Palaeoclimatology, Palaeoecology, 255(3-4): 223-245.
Jansen, E. and Sjoholm, J., 1991. Reconstruction of glaciation over the past 6 Myr from ice-borne deposits in the Norwegian Sea. Nature, 349(6310): 600-603.
Jasper, J.P. and Hayes, J.M., 1990. A carbon isotope record of CO2 levels during the late Quaternary. Nature, 347(6292): 462-464.
Jiang, S., Wise Sherwood, W.J. and Wang, Y., 2007. Cause of the middle/late Miocene carbonate crash: dissolution or low productivity? In: D.A.H. Teagle, Wilson, D.S., Acton, G.D., and Vanko, D.A. ((Editor), Proc. ODP, Sci. Results, 206: College Station, TX (Ocean Drilling Program),.
Jiang, S. and Wise, S.W., Jr., 2007. Upper Cenozoic calcareous nannofossil biostratigraphy and inferred sedimentation, ODP Leg 206, East Pacific Rise. In: D.A.H. Teagle, Wilson, D.S., Acton, G.D., and Vanko, D.A. (Editor), Proc. ODP, Sci. Results, 206: College Station, TX (Ocean Drilling Program),.
Jordan, R.W. and Kleijne, A., 1994. A classification system for living coccolithophores. In: A. Winter and W.G. Siesser (Editors), Coccolithophores. Cambridge University Press, pp. 83-105.
Jordan, R.W. and Winter, A., 2000. Assemblages of coccolithophorids and other living microplankton off the coast of Puerto Rico during January-May 1995. Marine Micropaleontology, 39(1-4): 113-130.
Jordan, R.W., Zhao, M., Eglinnton, G. and Weaver, P.P.E., 1996. Coccolith and alkenone stratigraphy and paleoceanography at an upwelling site off NW Africa (ODP 658C) during the last 130,000 years. In: A. Moguilevsky and R. Whatley (Editors), Microfossils and Oceanic Environments. Aberystwyth Press, University of Wales, pp. 111-130.
Kameo, K., 2002. Late Pliocene Caribbean surface water dynamics and climatic changes based on calcareous nannofossil records. Palaeogeography, Palaeoclimatology, Palaeoecology, 179(3-4): 211-226.

Kameo, K. and Bralower, T., J., 2000. Neogene calcareous nannofossil biostratigraphy of sites 998, 999, and 1000, Caribbean Sea. Proceedings of the Ocean Drilling Program, Scientific Results, 165: 3-17.
Kameo, K. and Sato, T., 2000. Biogeography of Neogene calcareous nannofossils in the Caribbean and the eastern Equatorial Pacific; floral response to the emergence of the Isthmus of Panama. Marine Micropaleontology, 39(1-4): 201-218.
Keeling, C.D., Chin, J.F.S. and Whorf, T.P., 1996. Increased activity of northern vegetation inferred from atmospheric CO2 measurements. 382(6587): 146-149.
Keeling, C.D., Whorf, T.P., Wahlen, M. and van der Plichtt, J., 1995. Interannual extremes in the rate of rise of atmospheric carbon dioxide since 1980. 375(6533): 666-670.
Keigwin, L., 1982a. Isotopic paleoceanography of the Caribbean and East Pacific; role of Panama Uplift in late Neogene time. Science, 217(4557): 350-353.
Keigwin, L.D., Jr., 1982b. Stable isotope stratigraphy and paleoceanography of sites 502 and 503. Initial Reports of the Deep Sea Drilling Project, 68: 445-453.
Keigwin, L.D., Jr. and Shackleton, N.J., 1980. Uppermost Miocene carbon isotope stratigraphy of a piston core in the equatorial Pacific. Nature, 284: 613-614.
Keigwin, L.D.J., 1978. Pliocene closing of the Isthmus of Panama, based on biostratigraphic evidence from nearby Pacific Ocean and Caribbean Sea cores. Geology, 6: 630-634.
Keigwin, L.D.J., 1979. Late Cenozoic stable isotope stratigraphy and paleoceanography of DSDP sites from the east equatorial and central North Pacific Ocean. Earth and Planetary Science Letters, 45(2): 361-382.
Keller, G. and Barron John, A., 1993. Paleoceanogrphic implications of Miocene deep-sea hiatuses. Geol. Soc. Am. Bull., 94: 590-613.
Keller, G., Zenker, C.E. and Stone, S.M., 1989. Late neogene history of the Pacific-Caribbean gateway. Journal of South American Earth Sciences, 2(1): 73-108.
Kennett, J., P., 1982. Marine Geology. Englewood Cliffs,, New Jersey.
King, T.A., Ellis Jr., W.G., Murray, D.W., Shackleton, N.J. and Harris, S.E., 1997. Miocene evolution of carbonate sedimentation at the Ceara Rise; a multivariate data/ proxy approach. Proceedings of the Ocean Drilling Program, Scientific Results, 154: 349-365.
Kinkel, H., Baumann, K.-H. and Cepek, M., 2000. Coccolithophores in the equatorial Atlantic Ocean: response to seasonal and Late Quaternary surface water variability. Marine Micropaleontology, 39(1-4): 87-112.
Klaas, C.M. and Archer, D.E., 2002. Association of sinking organic matter with various types of mineral ballast in the deep sea: Implications for the rain ratio. Global Biogeoch. Cycles, 16(4).
Klocker, A., Prange, M. and Schulz, M., 2005. Testing the influence of the Central American Seaway on orbitally forced Northern Hemisphere glaciation. Geophysical Research Letters, 32: doi:10.1029/2004GL021564.
Knappertsbusch, M., 2000. Morphologic evolution of the coccolithophorid Calcidiscus leptoporus from the early Miocene to Recent. Journal of Paleontology, 74(4): 712-730.
Knappertsbusch, M. and Brummer, G.J.A., 1995. A sediment trap investigation of sinking coccolithophorids in the North Atlantic. Deep-Sea Research Part I: Oceanographic Research Papers, 42(7): 1083-1109.
Knappertsbusch, M., Cortes, M.Y. and Thierstein, H.R., 1997. Morphologic variability of the coccolithophorid Calcidiscus leptoporus in the plankton, surface sediments and from the Early Pleistocene. Marine Micropaleontology, 30(4): 293-317.
Konert, M. and Vandenberghe, J., 1997. Comparison of laser grain size analysis with pipette and sieve analysis; a solution for the underestimation of the clay fraction. Sedimentology, 44(3): 523-535.
Krammer, R., Baumann, K.-H. and Henrich, R., 2006. Middle to late Miocene fluctuations in the incipient Benguela Upwelling System revealed by calcareous nannofossil assemblages (ODP Site 1085A). Palaeogeography, Palaeoclimatology, Palaeoecology, 230(3-4): 319-334.
Krijgsman, W., Hilgen, F.J., Raffi, I., Sierro, F.J. and Wilson, D.S., 1999. Chronology, causes and progression of the Messinian salinity crisis. Nature, 400: 652-655.
Kroon, D., Steens Tineke, N.F. and Troelstra Simon, R., 1991. Onset of monsoonal related upwelling in the western Arabian Sea as revealed by planktonic foraminifers. Proceedings of the Ocean Drilling Program, Scientific Results, 117: 257-263.
Lane, E.W., 1938. Notes on the formation of sand. Trans. Am. Geophys. Union, 19: 505-508.
Langer, G., 2005. Calcification of selected coccolithophore species: strontium partitioning, calcium isotope fractionation and dependence on seawater carbonate chemistry. Dissertation Thesis, Universität Bremen, Bremen, 162 pp.
Laskar, J., 1999. The limits of Earth orbital calculations for geological time-scale use. Phil. Trans. Roy. Soc. of Lond. A, 357: 1735-1759.
Laskar, J., Joutel, F. and Boudin, F., 1993. Orbital, precessional, and insolation quantities for the Earth from -20 MYR to +10 MYR. Astronomy and Astrophysics, 270(1-2): 522-533.
Laws, E.A., Popp, B.N. and Bidigare, R.R., 2001. Controls on the molecular distribution and carbon isotopic composition of alkenones in certain haptophyte algae. Geochemistry, Geophysics, Geosystems, 2: 2000GC000057.
Le Roux, J.P. and Rojas, E.M., 2007. Sediment transport patterns determined from grain size parameters: Overview and state of the art. Sedimentary Geology From Particle Size to Sediment Dynamics, 202(3): 473-488.
Lear, C.H., Rosenthal, Y. and Wright, J.D., 2003. The closing of a seaway; ocean water masses and global climate change. Earth and Planetary Science Letters, 210(3-4): 425-436.
Lehmann, M., Berthold, C., Pabst, W., Gregorova, E. and Nickel, K.G., 2004. Particle Size and Shape Characterization of Kaolins - Comparison of Settling Methods and Laser Diffraction. Key Engineering Materials, 264-268: 1378-1390.
Li, B. et al., 2004. South China Sea surface water evolution over the last 12 Myr: A south-north comparison from Ocean Drilling Program Sites 1143 and 1146. Paleoceanography, 19: doi:10.1029/2003PA000906.
Lisiecki, L.E. and Raymo, M.E., 2005. A Pliocene-Pleistocene stack of 57 globally distributed benthic $\delta^{18}O$ records. Paleoceanography, 20(PA1003): doi:10.1029/2004PA001071.
Liu, Z. and Herbert, T.D., 2004. High-latitude influence on the eastern equatorial Pacific climate in the early Pleistocene epoch. Nature, 427(6976): 720-723.
Liu, C., Cheng, X., Zhu, Y., Tian, J. and Xia, P., 2002. Oxygen and carbon isotope records of calcareous nannofossils for the past 1 Ma in the southern South CHina Sea. Chinese Science Bulletin, 47(10).

Lohmann, G.P. and Carlson, J.J., 1981. Oceanographic Significance of Pacific Late Miocene Calcareous Nannoplankton. Marine Micropaleontology, 6: 553-579.
Loizeau, J.L., Arbouille, D., Santiago, S. and Vernet, J.P., 1994. Evaluation of a wide range laser diffraction grain size analyser for use with sediments. Sedimentology, 41(2): 353-361.
Lototskaya, A., Ziveri, P., Ganssen Gerald, M. and van Hinte Jan, E., 1998. Calcareous nannofloral response to Termination II at 45 degrees N, 25 degrees W (Northeast Atlantic). Marine Micropaleontology, 34(1-2): 47-70.
Lourens, L.J., Hilgen, F., Laskar, J., Shackleton Nicholas, J. and Wilson, D.S., 2004. The Neogene Period. Geological Time Scale. Cambridge University Press, 409-440 pp.
Loutit, T.S. and Keigwin, J., L. D., 1982. Stable isotopic evidence for latest Miocene sea-level fall in the Mediterranean region. Nature, 300: 163-166.
Loutit, T.S., Kennett James, P. and Savin, S.M., 1983. Miocene equatorial and Southwest Pacific paleoceanography from stable isotope evidence. Marine Micropaleontology, 8(3): 215-233.
Loutit, T.S. and Kennett, J.P., 1979. Application of carbon isotope stratigraphy to late Miocene shallow marine sediments, New Zealand. Science, 204(4398): 1196-1199.
Lundelius, E.L. et al., 1987. The North American Quaternary Sequence. In: M. Woodburne (Editor), Cenozoic Mammals of North America. University of California Press.
Lunt, D., Valdes, P., Haywood, A. and Rutt, I., 2008. Closure of the Panama Seaway during the Pliocene: implications for climate and Northern Hemisphere glaciation. Climate Dynamics, 30(1): 1-18.
Lyle, M., 2003. Neogene carbonate burial in the Pacific Ocean. Paleoceanography, 18(3): 1059, doi: 10.1029/2002PA000777.
Lyle, M., Dadey Kathleen, A. and Farrell John, W., 1995. The late Miocene (11-8 Ma) eastern Pacific carbonate crash; evidence for reorganization of deep-water circulation by the closure of the Panama Gateway. Proceedings of the Ocean Drilling Program, Scientific Results, 138: 821-838.
MacArthur, R.H. and Wilson, E.O., 1967. The Theory of Island Biogeography. Acta Biotheoretica, 50: 133-136.
Maier-Reimer, E., Mikolajewicz, U. and Crowley, T.J., 1990. Ocean general circulation model sensitivitiy experiment with an open Central American isthmus. Paleoceanography, 5(3): 349-366.
Malin, G., Turner, S.M. and Liss, P.S., 1992. Sulfur: The plankton/climate connection. Journal of Phycology, 28(5): 590-597.
Manton, I. and Oates, K., 1980. Polycrater galapagensis gen. et sp. nov., a putative coccolithophorid from the Galapagos Islands with an unusual aragonitic periplast. Br. Phycol. J., 15: 95-103.
Margolis, S.V., Kroopnick, P.M., Goodney, D.E., Dudley, W.C. and Mahoney, M.E., 1975. Oxygen and carbon isotopes fron calcareous nannofossils as paleoceanographic indicators. Science, 189(4202): 555-557.
Marshall, L.G., Webb, S.D., Sepkoski, J.J. and Raup, D.M., 1982. Mammalian evolution and the Great American Interchange. Science, 215(4538): 1351-1357.
Martin, R.E., 1995. Cyclic and secular variation in microfossil biomineralization - cluess to the biogeochemical evolution of Phanerozoic oceans. Global and Planetary Change, 11: 1-23.
Martini, E. and Worsley, T., 1970. Standard Neogene calcareous nannoplankton zonation. Nature, 226: 560-561.
Matthews, M.D., 1991. The effect of grain shape and density on size measurement. In: J.P.M. Syvitski (Editor), Principles, methods and application of particle size analysis. Cambridge University Press, Cambridge - New York - Port Chester - Melbourne - Sydney, pp. 22-33.
Mattioli, E., Pittet, B., Young, J.R. and Bown, P.R., 2004. Biometric analysis of Pliensbachian-Toarcian (Lower Jurassic) coccoliths of the family Biscutaceae: intra- and interspecific variability versus palaeoenvironmental influence. Marine Micropaleontology, 52(1-4): 5-27.
McCave, I.N., 1975. Vertical flux of particles in the ocean. Deep Sea Research and Oceanographic Abstracts, 22(7): 491-502.
McCave, I.N., Bryant, R.J., Cook, H.F. and Coughanowr, C.A., 1986. Evaluation of a laser-diffraction-size analyzer for use with natural sediments. Journal of Sedimentary Petrology, 56(4): 561-564.
McCave, I.N. and Hall, I.R., 2006. Size sorting in marine muds: Processes, pitfalls, and prospects for paleoflow-speed proxies. Geochemistry, Geophysics, Geosystems, 7(10): doi:10.1029/2006GC001284.
McCave, I.N., Hall, I.R. and Bianchi, G.G., 2006. Laser vs. settling velocity - differences in silt grain size measurements: estimation of palaeocurrent vigour. Sedimentology, 53: 919-928.
McCave, I.N., Manighetti, B. and Beveridge , N.A.S., 1995a. Circulation in the glacial North Atlantic inferred from grain-size measurements. Nature, 374(6518): 149-152.
McCave, I.N., Manighetti, B. and Robinson, S.G., 1995b. Sortable silt and fine sediment size/ composition slicing; parameters for palaeocurrent speed and palaeoceanography. Paleoceanography, 10(3): 593-610.
McCave, I.N. and Syvitski, J.P.M., 1991. Principles and methods of geological particle size analysis. In: J.P.M. Syvitski (Editor), Principles, methods and application of particle size analysis. Cambridge University Press, Cambridge - New York - Port Chester - Mebourne - Sydney, pp. 3-21.
McDougall, K., 1996. Benthic foraminiferal response to the emergence of the Isthmus of Panama and coincident paleoceanographic changes. Marine Micropaleontology, 28(2): 133-169.
McIntyre, A., Be Allan, W.H. and Roche Michael, B., 1970. Modern Pacific Coccolithophorida; a paleontological thermometer. Transactions of the New York Academy of Sciences, 32(6): 720-731.
McIntyre, A. and Bé, A.W.H., 1967. Modern Coccolithophoridae of the Atlantic Ocean - I. Placoliths and Cyrtoliths. Deep-Sea Research, 14: 561-597.
McIntyre, A. and McIntyre, R., 1971. Coccolith concentrations and differential solution in oceanic sediments. In: B.M. Funnell and W.R. Riedel (Editors), The Micropaleontology of Oceans. Cambridge Univ. Press, London, pp. 253– 261.
McKenzie, J.A., Hodell, D.A., Mueller, P.A. and Mueller, D.W., 1988. Application of strontium isotopes to late Miocene-early Pliocene stratigraphy. Geology, 16(11): 1022-1025.
Mead, G., A., Hodell David, A., Muller Daniel, W. and Ciesielski Paul, F., 1991. Fine-fraction carbonate oxygen and carbon isotope results from Site 704; implications for movement of the polar front during the late Pliocene. Proceedings of the Ocean Drilling Program, Scientific Results, 114: 437-458.
Meschede, M. and Frisch, W., 1998. A plate-tectonic model for the Mesozoic and early Cenozoic history of the Caribbean Plate. Tectonophysics, 296(2-4): 269-291.

Mikolajewicz, U., Maier-Reimer, E., Crowley, T.J. and Kim, K.-Y., 1993. Effect of Drake and Panamanian gateways on the circulation of an ocean model. Paleoceanography, 8(4): 409-426.
Miller, K.G., Wright, J.D. and Fairbanks, R.G., 1991. Unlocking the ice house: Oligocene-Miocene oxygen isotopes, eustasy, and margin erosion. Journal of Geophysical Research, 96(B4): 6829-6848.
Milliman, J.D., 1993. Production and accumulation of calcium carbonate in the ocean: Budget of a nonsteady state. Global Biogeochemical Cycles, 7(4): 927-957.
Minoletti, F., Gardin, S., Nicot, E., Renard, M. and Spezzaferri, S., 2001. Mise au point d'un protocole experimental de separation granulometrique d'assemblages de nannofossiles calcaires; applications paleoecologiques et geochimiques. Bulletin de la Societe Geologique de France, 172(4): 437-446.
Mitchell, T.P. and Wallace, J.M., 1992. The annual cycle of equatorial convection and sea surface temperature. Journal of Climate, 5: 1140-1156.
Mix, A., Tiedemann, R., Blum, P. and al., e., 2003a. Site 1241 - Shipboard Scientific Party. Proceedings of the Ocean Drilling Program, Initial Reports, 202.
Mix, A.C. et al., 2003b. Leg 202 summary. Proceedings of the Ocean Drilling Program, Part A: Initial Reports, 202: Ms 202IR-101.
Molfino , B. and McIntyre, A., 1990. Nutricline Variation in the equatorial Atlantic coincident with the Younger Dryas. Paleoceanography, 5(6): 997-1008.
Molfino, B. and McIntyre, A., 1990. Precessional Forcing of Nutricline Dynamics in the Equatorial Atlantic. Science, 249: 766-769.
Molnar, P., 2005. Mio-Pliocene Growth of the Tibetan Plateau and Evolution of East Asian Climate. Palaeontologia Electronica, 8(1).
Molnar, P., 2008. Closing of the Central American Seaway and the Ice Age: A critical review. Paleoceanography, 23(PA2201).
Mudelsee, M. and Raymo, M.E., 2005. Slow dynamics of the Northern Hemisphere glaciation. Paleoceanography, 20: PA4022, doi:10.1029/2005PA001153.
Müller, D.W., Hodell, D.A. and Ciesielski, P.F., 1991. Late Miocene to earliest Pliocene (9.8-4.5 MA) paleoceanography of the subantarctic Southeast Atlantic: stable isotopic, sedimentologic, and microfossil evidence. Proceedings of the Ocean Drilling Program, Scientific Results, 114: 459-474.
Murray, M.R., 2002. Is laser particle size determination possible for carbonate-rich lake sediments? Journal of Paleolimnology, 27(2): 173-183.
Negri, A., Giunta, S., Hilgen, F., Krijgsman, W. and Vai, G.B., 1999. Calcareous nannofossil biostratigraphy of the M. del Casino section (Northern Apennines, Italy) and paleoceanographic conditions at times of late Miocene sapropel formation. Marine Micropaleontology, 36(1): 13-30.
Negri, A. and Villa, G., 2000. Calcareous nannofossil biostratigraphy, biochronology and paleoecology at the Tortonian/ Messinian boundary of the Faneromeni section (Crete). Palaeogeography, Palaeoclimatology, Palaeoecology, 156(3-4): 195-209.
Nimer, N., Dixon, G.K. and Merrett, M.J., 1992. Utilization of inorganic carbon by the coccolithophorid Emiliania huxleyi (Lohmann) Kamtner. New Phytologist, 120: 153-158.
Nimer, N., Iglesias-Rodriguez, M.D. and Merrett, M.J., 1997. Bicarbonate utilization by marine phytoplankton species. J. Phycol., 33: 6265-631.
Nimer, N. and Merrett, M.J., 1995. Calcification rates in relation to carbon dioxide release, photosynthetic carbon fixation and oxygen evolution in emiliania huxleyi. bulletin de l´insitute Oceanographique (monaco)(14): 337-42.
Nisancioglu, K.H., Raymo, M.E. and Stone, P.H., 2003. Reorganization of Miocene deep water circulation in response to the shoaling of the Central American Seaway. Paleoceanography, 18(1): doi:10.1029/2002PA000767.
Njestgaard, J.C., Gismervik, I. and Solberg, P.T., 1996. Feeding and reproduction by Calanus finmarchicus, and microzooplankton grazing during mesocosm blooms of diatoms and the coccolithophore *Emiliania huxleyi*.
Norris, R.D., 1991. Biased extinction and evolutionary trends. Paleobiology, 17(4): 388-399.
Nürnberg, D., Bijma, J. and Hemleben, C., 1996. Assessing the reliability of magnesium in foraminiferal calcite as a proxy for water mass temperatures. Geochimica et Cosmochimica Acta, 60(5): 803-814.
Okada, H., 2000. 33. Neogene and quarternary calcareous nannofossils from the blake ridge, sites 994, 995 and 997. Proceedings of the ocean drilling program, Scientific results, 164: 331-341.
Okada, H. and Bukry, D., 1980. Supplementary modification and introduction of code numbers to the low-latitude coccolith biostratigraphic zonation (Bukry, 1973; 1975). Marine Micropaleontology, 5(3): 321-325.
Okada, H. and Honjo, S., 1973. The distribution of oceanic coccolithophorids in the Pacific. Deep - Sea - Research, 20: 355-374.
Okada, H. and McIntyre, A., 1977. Modern coccolithophores of the Pacific and North Atlantic Oceans. Micropaleontology, 23(1): 1-55.
Okada, H. and McIntyre, A., 1979. Seasonal distribution of modern coccolithophores in the western North Atlantic Ocean. Marine Biology, 54: 319-328.
Pabst, W., Berthold, C. and Gregorova, E., 2006. Size and shape characterization of polydisperse short-fiber systems. Journal of the European Ceramic Society, 26: 1121-1130.
Pabst, W., Kunes, K., Havrda, J.K. and Gregorova, E., 2000. A note on particle size analyses of kaolins and clays. Journal of the European Ceramic Society, 20: 1429-1437.
Pagani, M., Arthur, M.A. and Freeman, K.H., 2000. Variations in Miocene phytoplankton growth rates in the Southwest Atlantic; evidence for changes in ocean circulation. Paleoceanography, 15(5): 486-496.
Pagani, M., Freeman Katherine, H. and Arthur Michael, A., 1999. Late Miocene atmospheric CO_2 concentrations and the expansion of C_4 grasses. Science, 285(5429): 876-879.
Pagani, M., Zachos, J.C., Freeman, K.H., Tipple, B. and Bohaty, S., 2005. Marked Decline in Atmospheric Carbon Dioxide Concentrations During the Paleogene. Science, 309(5734): 600-603.
Paull, C.-K. and Thierstein, H.-R., 1990. Comparison of fine fraction with monospecific foraminiferal stable isotopic stratigraphies from pelagic carbonates across the last glacial termination. Marine Micropaleontology, 16(3-4): 207-217.
Paull, C.K. and Balch, W.M., 1994. Oxygen isotopic disequilibrium in coccolith carbonate from phytoplankton blooms. Deep Sea Research Part I: Oceanographic Research Papers, 41(1): 223-228.

Paull, C.K. and Thierstein, H.R., 1987. Stable isotopic fractionation among particles in Quaternary coccolith-sized deep-sea sediments. Paleoceanography, 2(4): 423-429.
Paytan, A., Kastner, M. and Chavez, F.P., 1996. Glacial to interglacial fluctuations in productivity in the equatorial Pacific as indicated by marine barite. Science, 274: 1355-1357.
Perch-Nielsen, K., 1985a. Cenozoic calcareous nannofossils. In: H.M. Bolli, J.B. Saunder and K. Perch-Nielsen (Editors), Plankton Stratigraphy. Press Syndicate of the University of Cambridge, Cambridge, pp. 427-553.
Perch-Nielsen, K., 1985b. Mesozoic calcareous nannofossils. In: H.M. Bolli, J.B. Saunder and K. Perch-Nielsen (Editors), Plankton Stratigraphy. Press Syndicate of the University of Cambridge, Cambridge, pp. 329-426.
Peters, R.H., 1983. The ecological implications of body size. Cambridge Studies in ecology. Cambridge University Press, 329 pp.
Peterson, L.C., Murray, D.W., Ehrmann, W.U. and Hempel, P., 1992. Cenozoic Carbonate Accumulation and Compensation Depth Changes in the Indian Ocean, Synthesis of Results from Scientific Drilling in the Ocean. Geophysical Monograph. American Geophysical Union, pp. 311-333.
Peterson, L.C. and Prell, W.L., 1985. Carbonate dissolution in Recent sediments of the eastern equatorial Indian Ocean: Preservation patterns and carbonate loss above the lysocline. Marine Geology, 64(3-4): 290.
Pienaar, R.N., 1994. Ultrastructure and calcification of coccolithophores. In: A. Winter and W.G. Siesser (Editors), Coccolithophores. Cambridge University Press, pp. 13-37.
Pisias, N.G., Mayer, L.A. and Mix, A.C., 1995. Paleoceanography of the eastern equatorial Pacific during the Neogene: Synthesis of Leg 138 Drilling Results. Proceedings of the Ocean Drilling Program, Scientific Results, 138: 5-21.
Popp, B.N. et al., 1998. Effect of phytoplankton cell geometry on carbon isotopic fractionation. Geochimica et Cosmochimica Acta, 62(1): 69-77.
Porter, S.M., 2007. Seawater Chemistry and Early Carbonate Biomineralization 10.1126/science.1137284. Science, 316(5829): 1302-.
Prahl, F. et al., 2000. Status of alkenone paleothermometer calibration: Report from Working Group 3. Geochemistry, Geophysics, Geosystems, 1: 2000GC000058.
Prange, M. and Schulz, M., 2004. A coastal upwelling seesaw in the Atlantic Ocean as a result of the closure of the Central American Seaway. Geophysical Research Letters, 31: L17207, doi:10.1029/2004GL020073.
Prell, W.L. and Kutzbach, J.E., 1992. Sensitivity of the Indian monsoon to forcing parameters and implications for its evolution. Nature, 360: 647-652.
Qiang, X.K., Li, Z.X., Powell, C.M. and Zheng, H.B., 2001. Magnetostratigraphic record of the late Miocene onset of the East Asian monsoon, and Pliocene uplift of northern Tibet. Earth and Planetary Science Letters, 187(1-2): 83-93.
Quinn, P., Thierstein, H.R., Brand, L.E. and Winter, A., 2003. Experimental evidence for the species character of *Calcidiscus leptoporus* morphotypes. Journal of Paleontology, 77(5): 825-830.
Quinn, P.S., Cortes, M.Y. and Bollmann, J., 2005. Morphological variation in the deep ocean-dwelling coccolithophore *Florisphaera profunda* (Haptophyta). Eur. J. Phycol., 40(1): 123-133.
Quinn, P.S. et al., 2004. Coccolithophorid biodiversity: evidence from the cosmopolitan species *Calcidiscus leptoporus*. In: H.R. Thierstein and J.R. Young (Editors), Coccolithophores. From Molecular Processes to Global Impact. Springer-Verlag Berlin Heidelberg, pp. 299-326.
Raffi, I., 1999. Precision and accuracy of nannofossil biostratigraphic correlation. Phil. Trans. Roy. Soc. of Lond. A, 357.
Raffi, I. et al., 2006. A review of calcareous nannofossil astrobiochronology encompassing the past 25 million years. Quaternary Science Reviews, 25(23-24): 3137.
Raffi, I., Backman, J. and Rio, D., 1998. Evolutionary trends of tropical calcareous nannofossils in the late Neogene. Marine Micropaleontology, 35(1-2): 17-41.
Raffi, I., Backman, J., Rio, D. and Shackleton, N.J., 1993. Plio-pleistocene nannofossil biostratigraphy and calibration to oxygen isotope stratigraphies from deep sea drilling project site 607 and ocean drilling program site 677. Paleoceanography, 8(3): 387-408.
Raffi, I. and Flores, J., Abel, 1995. Pleistocene through Miocene calcareous nannofossils from eastern Equatorial Pacific Ocean (Leg 138). Proceedings of the Ocean Drilling Program, Scientific Results, 138: 233-286.
Raffi, I., Rio, D., d Atri, A., Fornaciari, E. and Rocchetti, S., 1995. Quantitative distribution patterns and biomagnetostratigraphy of middle and late Miocene calcareous nannofossils from Equatorial Indian and Pacific oceans (legs 115, 130, and 138). Proceedings of the Ocean Drilling Program, Scientific Results, 138: 479-502.
Ravelo, A.C. and Andreasen, D.H., 2000. Enhanced circulation during a warm period. Geophysical Research Letters, 27(7): 1001-1004.
Ravelo, A.C., Andreasen, D.H., Lyle, M., Lyle, A.O. and Wara, M.W., 2004. Regional climate shifts caused by gradual global cooling in the Pliocene Epoch. Nature, 429: 263-267.
Raven, J.A., 1993. Limits on growth rates. Nature, 361: 209-210.
Rawson, J.D., Leadbeater, B.S.C. and Green, J.C., 1986. Calcium carbonate deposition in the motile (Crystallolithus) phase of C. pelagicus (Prymnesiophyceae). Br. Phycol. J., 21: 359-370.
Raymo, M., E., Ruddiman, W.F., Backman, J., Clement, B.M. and Martinson, D.G., 1989. Late Pliocene variation in Northern Hemisphere ice sheets and North Atlantic Deep Water circulation. Paleoceanography, 4(4): 413-446.
Raymo, M.E., 1994. The Himalayas, organic carbon burial, and climate in the Miocene. Paleoceanography, 9(3): 399-404.
Raymo, M.E., Grant, B., Horowitz, M. and Rau, G.H., 1996. Mid-Pliocene warmth: stronger greenhouse and stronger conveyor. Marine Micropaleontology, 27(1-4): 313-326.
Raymo, M.E. and Ruddiman, W.F., 1992. Tectonic forcing of late Cenozoic climate. Nature, 359: 117-122.
Raymo, M.E., Ruddiman, W.F. and Froelich, P.N., 1988. Influence of late Cenozoic mountain building on ocean geochemical cycles. Geology, 16(7): 649-653.
Reid, F.M.H., 1980. Coccolithophorids of the North Pacific Central Gyre with notes on their vertical and seasonal distribution. Micropaleontology, 26(2): 151-176.
Renaud, S. and Klaas, C., 2001. Seasonal variations in the morphology of the coccolithophore Calcidiscus leptoporus off Bermuda (N. Atlantic). J. Plankton Res., 23(8): 779-795.
Renaud, S., Ziveri, P. and Broerse, A.T.C., 2002. Geographical and seasonal differences in morphology and dynamics of the coccolithophore Calcidiscus leptoporus. Marine Micropaleontology, 46(3-4): 363-385.

Retallack, G., J., 2004. Late Miocene climate and life on land in Oregon within a context of Neogene global change. Palaeogeography, Palaeoclimatology, Palaeoecology, 214(1-2): 97-123.
Retallack, G.J., Tanaka, S. and Tate, T., 2002. Late Miocene advent of tall grassland paleosols in Oregon. Palaeogeography, Palaeoclimatology, Palaeoecology, 183(3-4): 329-354.
Ridgwell, A. and Zeebe, R.E., 2005. The role of the global carbonate cycle in the regulation and evolution of the Earth system. Earth and Planetary Science Letters, 234(3-4): 299-315.
Riebesell, U., Wolf-Gladrow, D.A. and Smetacek, V., 1993. Carbon dioxide limitation of marine phytoplankton growth rates. Nature, 361: 249-251.
Rio, D., Fornaciari, E. and Raffi, I., 1990. Late Oligocene through early Pleistocene calcareous nannofossils from western equatorial Indian Ocean (Leg 115). Proceedings of the Ocean Drilling Program, Scientific Results, 115: 175-235.
Robinson, S.G. and McCave, N., 1994. Orbital forcing of bottom-current enhanced sedimentation on Feni Drift, NE Atlantic, during the mid-Pleistocene. Paleoceanography, 9(6): 943-972.
Rost, B. and Riebesell, U., 2004. Coccolithophores and the biological pump: responses to environmental changes. In: H.R. Thierstein and J.R. Young (Editors), Coccolithophores. From Molecular Processes to Global Impact. Springer-Verlag Berlin Heidelberg, pp. 99-125.
Rost, B., Zondervan, I. and Riebesell, U., 2002. Light-dependent carbon isotope fractionation in the coccolithophorid *Emiliania huxleyi*. Limnol. Oceanogr., 47(1): 120-128.
Roth, J.M., Droxler, A.W. and Kameo, K., 2000. The Caribbean carbonate crash at the middle to late Miocene transition; linkage to the establishment of the modern global ocean conveyor. Proceedings of the Ocean Drilling Program, Scientific Results, 165: 249-273.
Roth, P.H., 1987. Mesozoic calcareous nannofossil evolution: relation to paleoceanographic events. Paleoceanography, 6: 601-611.
Roth, P.H., 1994. Distribution of coccoliths in oceanic sediments. In: A. Winter and W.G. Siesser (Editors), Coccolithophores. Cambridge University Press, pp. 199-218.
Roth, P.H. and Berger, W.H., 1975. Distribution and dissolution of coccoliths in the South and central Pacific. Special Publications - Cushman Foundation for Foraminiferal Research, Dissolution of deep-sea carbonates, 13: 87-113.
Ruddiman, W.F., 1998. Early uplift in Tibet. Nature, 394: 723-724.
Ruddiman, W.F. and Raymo, M.E., 1988. Northern Hemisphere climate régimes during the past 3 Ma: possible tectonic connections. Phil. Trans. Roy. Soc. of Lond. B, 318: 411-430.
Sáez, A.G. et al., 2003. Pseudo-cryptic speciation in coccolithophores. Proceedings of the National Academy of Sciences of the United States of America, 100(12): 7163-7168.
Samtleben, C., 1980. Die Evolution der Coccolithophoriden Gattung Gephyrocapsa nach Befunden im Atlantik. Paläontologische Zeitschrift, 54(1/2): 91-127.
Samtleben, C. and Bickert, T., 1990. Coccoliths in sediment traps from the Norwegian Sea. Marine Micropaleontology, 16(1-2): 39-64.
Samtleben, C. et al., 1995. Plankton in the Norwegian-Greenland Sea; from living communities to sediment assemblages; an actualistic approach. Geologische Rundschau, 84(1): 108-136.
Savin, S.M., Douglas, R.G. and Stehli, F.G., 1975. Tertiary marine paleotemperatures. Geological Society of America Bulletin 86; 11, Pages 1499-1510 1975.
Schiebel, R. et al., 2004. Distribution of diatoms, coccolithophores and planktic foraminifers along a trophic gradient during SW monsoon in the Arabian Sea. Marine Micropaleontology, 51(3-4): 345-371.
Schmidt, D.M., Lazarus, D., Young, J.R. and Kucera, M., 2006. Biogeography and evolution of body size in marine phytoplankton. Earth-Science Reviews, 78: 239-266.
Schmidt, D.N., Thierstein, H.R. and Bollmann, J., 2004a. The evolutionary history of size variation of planktic foraminiferal assemblages in the Cenozoic. Palaeogeography, Palaeoclimatology, Palaeoecology, 212(1-2): 159-180.
Schmidt, D.N., Thierstein, H.R., Bollmann, J. and Schiebel, R., 2004b. Abiotic Forcing of Plankton Evolution in the Cenozoic. Science, 303(5655): 207-210.
Schneider, B. and Schmittner, A., 2006. Simulating the impact of the Panamanian seaway closure on ocean circulation, marine productivity and nutrient cycling. Earth and Planetary Science Letters, 246(3-4): 367-380.
Schneider, R., 2001. Alkenone temperature and carbon isotope records: Temporal resolution, offsets, and regionality. Geochemistry, Geophysics, Geosystems, 2: 2000GC000060.
Schneidermann, N., 1977. Selective dissolution of recent coccoliths in the Atlantic Ocean. Oceanic Micropaleontology, 2: 1009-1053.
Schroeder, D.C. et al., 2005. A genetic marker to seperata Emiliania huyleyi (Prymnesiophyceae) morphotypes. Journal of Phycology, 41: 874-879.
Shackleton, N., J. and Crowhurst, S., 1997. Sediment fluxes based on an orbitally tuned time scale 5 Ma to 14 Ma, Site 926. Proceedings of the Ocean Drilling Program, Scientific Results, 154: 69-82.
Shackleton, N.J., Crowhurst, S., Hagelberg, T., Pisias, N.G. and Schneider, D.A., 1995a. A new late Neogene time scale; application to Leg 138 sites. Proceedings of the Ocean Drilling Program, Scientific Results, 138: 73-101.
Shackleton, N.J. and Hall, M.A., 1995d. Stable isotope records in bulk sediments (Leg 138). Proceedings of the Ocean Drilling Program, Scientific Results, 138: 797-805.
Shackleton, N.J. and Hall, M.A., 1997. The late Miocene stable isotope record, Site 926. Proceedings of the Ocean Drilling Program, Scientific Results, 154(367-373).
Shackleton, N.J., Hall, M.A. and Pate, D., 1995b. Pliocene stable isotope stratigraphy of Site 846. Proceedings of the Ocean Drilling Program, Scientific Results, 138: 337-355.
Shackleton, N.J., Hall, M.A., Pate, D., Meynadier, L. and Valet, P., 1993. High-resolution stable isotope stratigraphy from bulk sediment. Paleoceanography, 8(2): 141-148.
Shackleton, N.J. and Kennett, J.P., 1975a. Paleotemperatur history of the cenozoic and the initiation of antarctic glaciation: oxygen and carbon isotope analyses in DSDP sites 277, 279 and 281. Initial Reports of the Deep Sea Drilling Project, 29: 743-755.
Shackleton, N.J. and Kennett, J.P., 1975b. Paleotemperature history of the Cenozoic and the initiation of Antarctic glaciation; oxygen and carbon isotope analyses in DSDP sites 277, 279, and 281. Initial Reports of the Deep Sea Drilling Project, 29: 743-755.

Sheldon, P., 1990. Shaking up evolutionary patterns. 345(6278): 772.
Siegenthaler, U. and Sarmiento, J.L., 1993. Atmospheric carbon dioxide and the ocean. 365(6442): 119-125.
Sigurdsson, H. et al., 1997. Caribbean ocean history and the Cretaceous/ Tertiary boundary event. Proceedings of the Ocean Drilling Program, Part A: Initial Reports, 165.
Sikes, C.S. and Fabry, V.J., 1994. Photosynthesis, CaCO3 deposition, coccolithophorids, and the GLobal Carbon Cylce. In: N.E. Tolbert and J. Preiss (Editors), Regulation of Atmospheric CO2 and O2 by Photosynthetic Carbon Metabolism. Oxford University Press, New York, Oxford.
Simpson, D. et al., 1999. Inventorying emissions from nature in Europe. Journal of Geophysical Research, 104(D7): 8113-8152.
Singer, J.K. et al., 1988. An assessment of analytical techniques for the size analysis of fine-grained sediments. Journal of Sedimentary Petrology, 58(3): 534-543.
Smetacek, V., 2001. A watery arms race. Nature, 411(6839): 745.
Smith, F.A., Betancourt, J.L. and Brown, J.H., 1995. Evolution of Body Size in the Woodrat over the Past 25,000 Years of Climate Change 10.1126/science.270.5244.2012. Science, 270(5244): 2012-2014.
Spencer-Cervato, C., Thierstein, H., Lazarus, D. and Beckman, J.P., 1994. How synchronous are Neogene marine plankton events? Paleoceanography, 9: 739-763.
Sperazza, M., Moore, J.N. and Hendrix, M.S., 2004. High-resolution particle size analysis of naturally occurring very fine-grained sediment through laser diffractometry. Journal of Sedimentary Research, 74(5): 736-743.
Sprengel, C. et al., 2002. Modern coccolithophore and carbonate sedimentation along a productivity gradient in the Canary Islands region: seasonal export production and surface accumulation rates. Deep-Sea Research Part II: Topical Studies in Oceanography, 49(17): 3577-3598.
Stanley, S.M., 1973. An explanation for Cope´s Rule. Evolution, 27(1): 1-26.
Stein, R., 1985. Rapid grain size analyses of clay and silt fraction by Sedigraph 5000D: Comparison with Coulter Counter and Atterberg Methods. Journal of Sedimentary Petrology, 55(4): 590-615.
Steinmetz, J.C., 1991. Calcareous Nannoplankton Biocoenosis: Sediment Trap Studies in the Equatorial Atlantic, Central Pacific, and Panama Basin. In: S. Honjo (Editor), Ocean Biocoenosis Series. Woods Hole Oceanogr. Inst. Press, pp. 85.
Steinmetz, J.C., 1994. Sedimentation of coccolithophores. In: A. Winter and W.G. Siesser (Editors), Coccolithophores. Cambridge University Press, pp. 179-197.
Stenseth, N.C. and Maynard Smith, J., 1984. Coevolution in ecosystems: Red Queen evolution or stasis? Evolution, 38: 870-880.
Steph, S., 2005. Pliocene Stratigraphy and the Impact of Panama uplift on changes in Caribbean and Tropical East Pacific upper ocean stratification (6-2.5 Ma). Kumulative Dissertation Thesis, Christian-Albrechts-Universität Kiel, Kiel.
Steph, S., Tiedemann, R., Groenevald, J., Sturm, A. and Nürnberg, D., 2006a. Pilocene Changes in Tropical East Pacific Upper Ocean Stratification: Response to Tropical Gateways? Proc. ODP, Sci. Results, 202: 1–51.
Steph, S. et al., 2006b. Changes in the Caribbean surface hydrography during Pliocene shoaling of the Central American Seaway. Paleoceanography, 21: 1-51.
Stoll, H.M. and Schrag, D.P., 2000. Coccolith Sr/Ca as a new indicator of coccolithophorid calcification and growth rate. Geochemistry, Geophysics, Geosystems, 1: 1999GC000015.
Stoll, H.M. and Ziveri, P., 2002. Separation of monospecific and restricted coccolith assemblages from sediments using differential settling velocity. Marine Micropaleontology, 46(1-2): 209-221.
Stoll, H.M. and Ziveri, P., 2004. Coccolithophorid-based geochemical paleoproxies. In: H.R. Thierstein and J.R. Young (Editors), Coccolithophores. From Molecular Processes to Global Impact. Springer-Verlag Berlin Heidelberg, pp. 529-562.
Stuut, J.-B.W. et al., 2002a. A 300-kyr record of aridity and wind strength in southwestern Africa: inferences from grain-size distributions of sediments on Walvis Ridge, SE Atlantic. Marine Geology, 180(1-4): 221-233.
Stuut, J.B., W., Prins, M.A. and Jansen, J.H.F., 2002b. Fast reconnaissance of carbonate dissolution based on the size distribution of calcareous ooze on Walvis Ridge, SE Atlantic Ocean. Marine Geology, 190(3-4): 581-589.
Suc, J.P. and Bessais, E., 1990. Perennite d'un climat thermo-xeric en Sicile avant, pendant, apres la crise de salinite messinienne. C. R. Acad. Sci. Ser. II, 310: 1701-1707.
Suess, E., 1980. Particulate organic carbon flux in the oceans; surface productivity and oxygen utilization. Nature, 288: 260-263.
Swart, P.K., 2008. Global synchronous changes in the carbon isotopic composition of carbonate sediments unrelated to changes in the global carbon cycle. PNAS, 105(37): 13741-13745.
Swart, P.K. and Eberli, G., 2005. The nature of the [delta]13C of periplatform sediments: Implications for stratigraphy and the global carbon cycle. Sedimentary Geology, Sedimentology in the 21st Century - A Tribute to Wolfgang Schlager, 175(1-4): 115-129.
Syvitski, J.P.M. et al., 1991a. Principles, methods and application of particle size analysis. Cambridge University Press, Cambridge - New York - Port Chester - Melbourne - Sydney, 363 pp.
Syvitski, J.P.M., LeBlanc, K., William, G. and Asprey, K.W., 1991b. Interlaboratory, interinstrument calibration experiment. In: J.P.M. Syvitski (Editor), Principles, methods and application of particle size analysis. Cambridge University Press, Cambridge - New York - Port Chester - Melbourne - Sydney, pp. 174-193.
Takayama, T., 1993. Notes on Neogene calcareous nannofossil biostratigraphy of the Ontong Java Plateau and size variations of Reticulofenestra coccoliths. Proceedings of the Ocean Drilling Program, Scientific Results, 130: 179-229.
Theodoridis, S., 1984. Calcareous nannofossil biozonation of the Miocene and revision of the helicoliths and discoasters. Utrecht Micropaleontological Bulletins, 32.
Tiedemann, R. and Franz, S.O., 1997. Deep-water circulation, chemistry, and terrigenous sediment supply in the Equatorial Atlantic during the Pliocene, 3.3-2.6 Ma and 5-4.5 Ma. Proceedings of the Ocean Drilling Program, Scientific Results, 154: 299-318.
Tiedemann, R., Sturm, A., Steph, S., Lund, S.P. and Stoner, J.S., 2007. Astronomically calibrated time-scales from 6–2.5 Ma and benthic isotope Stratigraphies of Sites 1236, 1237, 1239 and 1241. Proc. ODP, Sci. Results, 202: 1–69.

Tremolada, F. and Young, J., R., 2002. Volume calculation of Cretaceous calcareous nannofossils. Journal of Nannoplankton Research 24; 3, Pages 199-202 2002.
Van der Wal, P., Kempers, R. and Veldhuis, M., 1995. Production and downward flux of organic matter and calcite in a North Sea bloom of the coccolithophore Emiliania huxleyi. Marine Ecology Progress Series, 126: 247-265.
Vazquez, A. et al., 2000. Precession-related sapropelites of the Messinian Sorbas Basin (South Spain); paleoenvironmental significance. Palaeogeography, Palaeoclimatology, Palaeoecology, 158(3-4): 353-370.
Vincent, E. and Berger, W.H., 1985. Carbon dioxide and polar cooling in the Miocene: the monterey hypothesis. In: E.T. Sundquist and W.S. Broecker (Editors), The carbon cycle and atmospheric CO_2: Natural variations archean to present. Geophysical Monograph 32, Washington, DC, pp. 455-468.
Vincent, E., Killingley John, S. and Berger Wolfgang, H., 1980. The Magnetic Epoch-6 carbon shift; a change in the ocean's $^{13}C/^{12}C$ ratio 6.2 million years ago. Marine Micropaleontology, 5(2): 185-203.
Wade, B.S. and Bown, P.R., 2006. Calcareous nannofossils in extreme environments: The Messinian Salinity Crisis, Polemi Basin, Cyprus. Palaeogeography, Palaeoclimatology, Palaeoecology, 233(3-4): 271-286.
Wallace, J.M. et al., 1998. On the structure and evolution of ENSO-related climate variability in the tropical Pacific: Lessons from Toga. J. Geophys. Res., 103: 14241-14259.
Warner, N., R. and Domack, E., W., 2002. Millennial- to decadal-scale paleoenvironmental change during the Holocene in the Palmer Deep, Antarctica, as recorded to particle size analysis. Paleoceanography, 17(3): 8004, doi:10.1029/2000PA000602.
Webb, P. and Orr, C., 1997. Analytical Methods in Fine Particle Technology. ch. 3. Norcross, GA: Micromeritics Instrument Corporation.
Webb, P.A., 2000. Interpretation of Particle Size Reported by Different Analytical Techniques. Micromeritics.
Webb, S.D., 1985. Late Cenozoic mammal dispersals between the Americas. In: F.G. Stehli and S.D. Webb (Editors), The Great American Biotic Interchange. Plenum Press, New York, pp. 357-386.
Webb, S.D., 1991. Ecogeography and the great American interchange. Paleobiology, 17(3): 266-280.
Webb, S.D., Hulbert, R.C. and Lambert, W.D., 1995. Climatic implications of large-herbivore distributions in the Miocene of North America. In: E. Vrba (Editor), Paleoclimate and evolution, with emphasis on human origins. Yale University.
Webb, S.D. and Rancy, A., 1996. Late Cenozoic evolution of the neotropical mammal fauna. In: B.C. Jackson Jeremy, A.F. Budd and A.G. Coates (Editors), Evolution and environment in tropical America, pp. 335-358.
Wedd, M.W., 2003. Determination of Particle Size Distribution using Laser Diffraction. Educ. Reso. f. Part. Techn.
Wei, W., 1993. Calibration of upper Pliocene - lower Pleistocene nannofossil events with oxygen isotope stratigraphy. Paleoceanography, 8(1): 85-99.
Wei, W. and Wise, J.S.W., 1989. Paleogene calcareous nannofossil magnetobiochronology: Results from South Atlantic DSDP Site 516. Marine Micropaleontology
Plankton Biochronology, 14(1-3): 119-152.
Wells, M.L., Vallis, G.K. and Silver, E.A., 1999. Tectonic processes in Papua New Guinea and past productivity in the eastern equatorial Pacific Ocean. 398(6728): 601-604.
Weltje, G.J. and Prins, M.A., 2003. Muddled or mixed? Inferring palaeoclimate from size distributions of deep-sea clastics. Sedimentary Geology
Climate Impact on Sedimentary Systems, 162(1-2): 39-62.
Westbroek, P. et al., 1993. A model system approach to biological climate forcing; the example of Emiliania huxleyi, Ocean carbon cycle and climate change; a selection of papers presented at the Seventh biennial meeting of the European Union of Geosciences, Interdisciplinary Union symposium (IUS 5). Elsevier, Amsterdam, Netherlands, pp. 27-46.
Westbroek, P., Young, J.R. and Linschooten, K., 1989. Coccolith Production (Biomineralization) in the Marine Alga *Emiliania huxleyi*. J. Protozool., 36(4): 368-373.
Westerhold, T., Bickert, T. and Rohl, U., 2005. Middle to late Miocene oxygen isotope stratigraphy of ODP site 1085 (SE Atlantic): new constrains on Miocene climate variability and sea-level fluctuations. Palaeogeography, Palaeoclimatology, Palaeoecology, 217(3-4): 205-222.
Williams, J.R. and Bralower, T.J., 1995. Nannofossil assemblages, fine fraction stable isotopes, and the paleoceanography of the Valanginian-Barremian (Early Cretaceous) North Sea Basin. Paleoceanography, 10(4): 815-840.
Winter, A., Jordan, R.W. and Roth, P.H., 1994. Biogeography of living coccolithophores in ocean waters. In: A. Winter and W.G. Siesser (Editors), Coccolithophores. Cambridge University Press, pp. 161-177.
Winter, A., Rost, B., Hilbrecht, H. and Elbrächter, M., 2002. Vertical and horizontal distribution of coccolithophores in the Caribbean Sea. Geo-Marine Letters, 22: 150-161.
Winter, A. and Siesser, W.G., 1994. Atlas of living coccolithophores. In: A. Winter and W.G. Siesser (Editors), Coccolithophores. Cambridge University Press, pp. 107-159.
Wolfe, G., Steinke, M. and Kirst, G.O., 1997. Grazing-activated chemical defence in a unicellular marine alga. Nature, 387: 894-897.
Wood, R.A., Grotzinger, J.P. and Dickson, J.A.D., 2002. Proterozoic Modular Biomineralized Metazoan from the Nama Group, Namibia 10.1126/science.1071599. Science, 296(5577): 2383-2386.
Woodruff, F., 1989. Miocene Deepwater Oceanography. Paleoceanography, 4(1): 87-140.
Wright, J.D. and Miller, K.G., 1996. Control of North Atlantic Deep Water circulation by the Greenland-Scotland Ridge. Paleoceanography, 11(2): 157-170.
Wüst, G., 1964. Stratification and Circulation in the Antillean-Caribbean Basin, Part 1: Spreading and Mixing of the Water Types with an Oceanic Atlas. Columbia University Press, London and New York.
Young, J. et al., 2003. A guide to extant coccolithophore taxonomy. Journal of Nannoplankton Research Special Issue 1, 125 pp.
Young, J., R., 1989. Observations on heterococcolith rim structure and its relationship to developmental processes. In: A. Crux Jason and S.E. van Heck (Editors), Nannofossils and their Biostratigraphic Applications. Ellis Horwood, Chichester, pp. 1-20.
Young, J., R., 1990. Size variation of Neogene *Reticulofenestra* coccoliths from Indian Ocean DSDP Cores. J. micropalaeontol., 9(1): 71-86.

Young, J.R., 1994. Functions of coccoliths. In: A. Winter and W.G. Siesser (Editors), Coccolithophores. Cambridge University Press, pp. 63-82.
Young, J.R., 1998. Neogene. In: P.R. Bown (Editor), Calcareous Nannofossil Biostratigraphy. Kluwer Academic, Dordrecht, pp. 304-322.
Young, J.R., Didymus, J.M., Bown, P.R., Prins, B. and Mann, S., 1992. Crystal assembly and phylogenetic evolution in heterococcoliths. Nature, 356: 516-518.
Young, J.R., Geisen, M. and Probert, M., 2005. A review of selected coccolithophore biology with implications for paleobiodiversity estimation. Micropaleontology, 51(4): 267-288.
Young, J.R., Geisen, M., Cros, L., Kleijne, A., probert, I., Sprengel, C., Ostergaard, J.B., 2003. A guide to extant coccolithophore taxonomy. Journal of Nannoplankton Research Special Issue, 1: 124pp.
Young, J.R. and Henriksen, K., 2003. Biomineralization Within Vesicles: The Calcite of Coccoliths. Reviews in Mineralogy and Geochemistry, 54(1): 189-215.
Young, J.R. and Ziveri, P., 2000. Calculation of coccolith volume and its use in calibration of carbonate flux estimates. Deep-Sea Research Part II: Topical Studies in Oceanography, 47(9-11): 1679-1700.
Zachos, J. et al., 2001a. Trends, rhythms, and aberrations in global climate 65 Ma to present. Science, 292(5517): 686-693.
Zachos, J.C., Arthur, M.A. and Dean, W.E., 1989. Geochemical evidence for suppression of pelagic marine productivity at the Cretaceous/Tertiary boundary. Nature, 337(6202): 61-64.
Zachos, J.C., Shackleton, N.J., Revenaugh, J.S., Palike, H. and Flower, B.P., 2001b. Climate Response to Orbital Forcing Across the Oligocene-Miocene Boundary. Science, 292(5515): 274-278.
Zeebe, R., E. and Westbroek, P., 2003. A simple model for the $CaCO_3$ saturation state of the ocean; the "Strangelove," the "Neritan," and the "Cretan" ocean. Geochemistry, Geophysics, Geosystems, 4(12): 1104, doi:10.1029/2003GC000538.
Ziegler, C.L., Murray, R., W., Plank, T. and Hemming, S.R., 2008. Sources of Fe to the equatorial Pacific Ocean from the Holocene to Miocene. Earth and Planetary Science Letter, 270(3-4): 258-270.
Zisheng, A., Kutzbach, J.E., Prell, W.L. and Porter, S.C., 2001. Evolution of Asian monsoons and phased uplift of the Himalaya-Tibetan plateau since Late Miocene times. Nature, 411: 62-66.
Ziveri, P., Baumann, K.-H., Bollmann, B. and Young, J., 2004. Biogeography of selected Holocene coccoliths in the Atlantic Ocean. In: H.R. Thierstein and Y.R. Young (Editors), Coccolithophores from molecular processes to global impact. Springer, Berlin, pp. 403-428.
Ziveri, P. et al., 2000. Present-day coccolith fluxes recorded in central eastern Mediterranean sediment traps and surface sediments. Palaeogeography, Palaeoclimatology, Palaeoecology, 158(3-4): 175-195.
Ziveri, P. et al., 2003. Stable isotope 'vital effects' in coccolith calcite. Earth and Planetary Science Letters, 210(1-2): 137-149.
Ziveri, P. and Thunell, R.C., 2000. Coccolithophore export production in Guaymas Basin, Gulf of California: response to climate forcing. Deep Sea Research Part II: Topical Studies in Oceanography, 47(9-11): 2073-2100.
Ziveri, P., Thunell, R.C. and Rio, D., 1995. Export production of coccolithophores in an upwelling region: Results from San Pedro Basin, Southern California Borderlands. Marine Micropaleontology, 24(3-4): 335-358.

DANKSAGUNG

Ohne die Hilfe und Unterstützung vieler freundlicher Menschen wäre diese Arbeit nicht möglich gewesen. Ihnen und Euch allen möchte ich an dieser Stelle Dankeschön sagen.

Frau Prof. Dr. Priska Schäfer danke ich dafür, daß sie mir ermöglicht hat, diese Promotion an der Universität Kiel durchzuführen. Besonders herzlich bedanke ich mich für die intensive Korrekturarbeit in den letzten Wochen. Ein weiterer Dank gilt PD Dr. Mara Weinelt, die sich zur Übernahme des Koreferats bereit erklärt hat. Des Weiteren danke ich dem Dekan Prof. Dr. Lutz Kipp und den Mitgliedern meiner Prüfungskommission: Prof. Dr. Ralph Schneider, PD Dr. Dirk Nürnberg, Prof. Dr. Martin Frank, Prof. Dr. Birgit Schneider und Prof. Dr. Wolfgang Kuhnt.

Das größte Dankeschön geht an Dr. Hanno Kinkel, für Betreuung und Unterstützung, sowie für zahlreiche Ratschläge, Hilfestellungen, Tipps und Tricks, die feine Arbeitsatmosphäre und eine richtig gute Zeit an der Uni.

Herrn Prof. Dr. Ralph Schneider danke ich ganz besonders für finanzielle Unterstützung und Möglichkeit der Mithilfe bei der Koordinierung sowie Teilnahme der Forschungsausfahrt M75.

Ich danke: • Dr. Torsten Bickert für das Astronomical Tuning des Biogenic Bloom Intervalls von Site 1000 • Prof. Dr. Ralf Tiedemann und Dr. Arne Sturm für die Erstellung des Altersmodells des Biogenic Bloom Intervalls von Site 1241 • ganz herzlich Dr. Silke Steph, Dr. Jeroen Groeneveld (Dank je wel!) und Dr. Daniela Crudeli (Grazie!) für die Überlassung von Daten des Final Closure Intervalls der Sites 1241 und 1000 • ganz besonders herzlich Frau Ute Schuldt für die warme Aufnahme im REM-Labor, sowie Einweisung, Unterstützung und Vertrauen bei der Arbeit, bis hin zur Erstellung sämtlicher Phototafeln und Beistand beim Drucken der Diss • Dr. Nils Andersen für die Messungen der stabilen Isotope der Fein- und Subfraktionen, sowie für Diskussion und Anregung bei der Interpretation der Daten • PD Dr. Dirk Nürnberg und Lulzim Haxhiaj für die Übernahme der Messung der stabilen Isotope der Foraminiferen von Site 1241 • Prof. Dr. John J. G. Reijmer und der ehemaligen Sedimentologie-Arbeitsgruppe am Geomar für die Möglichkeit der intensiven Nutzung der Analysette • Dr. Christoph Berthold, Dr. Willi Pabst und Wolfgang Mutter für Hilfe zum Verständnis von Korngrößenanalysen • Herrn Wolfgang Reimers für die Hilfe bei der Gefriertrocknung des Probenmaterials • Karin Kißling für die Überlassung der MiniSpin • Dr. Ilka Peeken für die Dauerleihgabe der Sigma301K • Günter Bresa für die Erstellung verschiedenster Test-Konstruktionen zur Splittung der Feinfraktion • herzlich Prof. Dr. José-Abel Flores und der Cocco-Arbeitsgruppe der Uni Salamanca: Les agradezco la amable acogida y la introducción al manejo de microscopio óptico • Dr. Ann Holbourn pour l´introduction á la taxomomie des foraminifèrs benthique • Dr. Sven Nielsen, Veronica Rhode, Ellen Traichel und Jens Wein für Korrekturarbeiten • Nabil Khélifi (Mercie beaucoup!) und v.a. Mathias Marquardt für die Nutzung verschiedenster Farb-Drucker • Veronica Rhode und Jan Riethdorf für anregende PalOz-Diskussionen, und • ganz besonders allen Hiwis: Janne Repschläger, Andreas David, Hendrik Lantzsch, Alina Kabuth, Harald Meyer, Jan Riethdorf und, vor allem, Sonja Reich - ohne Euch wären Genauigkeit und Ausführlichkeit durch die Produktion der immensen Datenmengen nicht möglich gewesen!

Ein großes Dankeschön an meine lieben Kollegen und Freunde an der Uni: den Arbeitsgruppen der Paläontologie, Paläoozeanographie und Mikropaläontologie, sowie allen “Ozeanpassagen”-Zugehörigen, ganz besonders auch den “guten Seelen” Bettina Kaste, Heidi Blaschek sowie Ute Schuldt, aber auch Frau Crnjar, Frau Schröder, Frau Stielow, Herrn Lenthföhr, sämtlichen Geomar-Leuten und Ex-Kollegen und natürlich allen, die sich gerne und stetig bei mir auf einen Kaffee-Klatsch eingefunden haben.

Meiner Familie und all meinen lieben Freunden kann ich nicht oft und tief genug danken für alles, was sie für mich getan und “erlitten“ haben. Ihr wart, seid und bleibt das Wichtigste überhaupt!
Zum Durchstehen dieser Zeit haben so viele tolle Menschen beigetragen, Euch allen danke ich von ganzem Herzen. Unabdingbar hierbei waren neben meinen Eltern ganz besonders Elias und Johannes, aber auch meine Sportmädels, der KMTV, meine “drei besten Freunde“ sowie mein “Personal Trainer“ Björn (checkcheck), das Ex-Viva, Andreas, Veronica (Tusen hjertelig takk!), und natürlich mein Tzschöckelchen. Mein innigster Dank geht an meine beste Freundin und tollste Frau auf der ganzen weiten Welt, Nikoleta (φιλεκι!).

Ganz besonders danke ich nochmals denen, die mich gerade in der Endphase so herzlich aufgefangen, und mich mit Geduld und Verständnis maßgeblich unterstützt haben: Johannes, Veronica, Christian und Hanno; für Beistand und Unterstützung bedanke ich mich auch bei Frau Schuldt.
Hier auch vielen Dank für alle Glückwünsche, guten Gedanken und Zusprüche der „letzten“ Wochen.

The samples for his study were provided by the Ocean Drilling Program (ODP).

Diese Arbeit wurde von der Deutschen Forschungsgemeinschaft (DFG) im Rahmen der Forschergruppe “Ocean Gateways“ finanziell unterstützt (Projekt FOR451/1-3).

LIST OF FIGURES

LIST OF TABLES

LIST OF APPENDICES

A1 TABLES 1 - 8

PLATE 1

PLATE 1 - LEGEND

A *Dictyococcites productus* (sample BBP 100)

B *Reticulofenestra minuta* (sample FCP 33)

C *Reticulofenestra haquii* (sample BBP 97)

D *Reticulofenestra minutula* (sample BBP 5)

E *Reticulofenestra pseudoumbilicus* M (sample BBP 23)

F *Reticulofenestra pseudoumbilicus* (sample BBP 3)

PLATE 1

Neogene *Reticulofenestra* coccoliths of Sites 1241 and 1000.

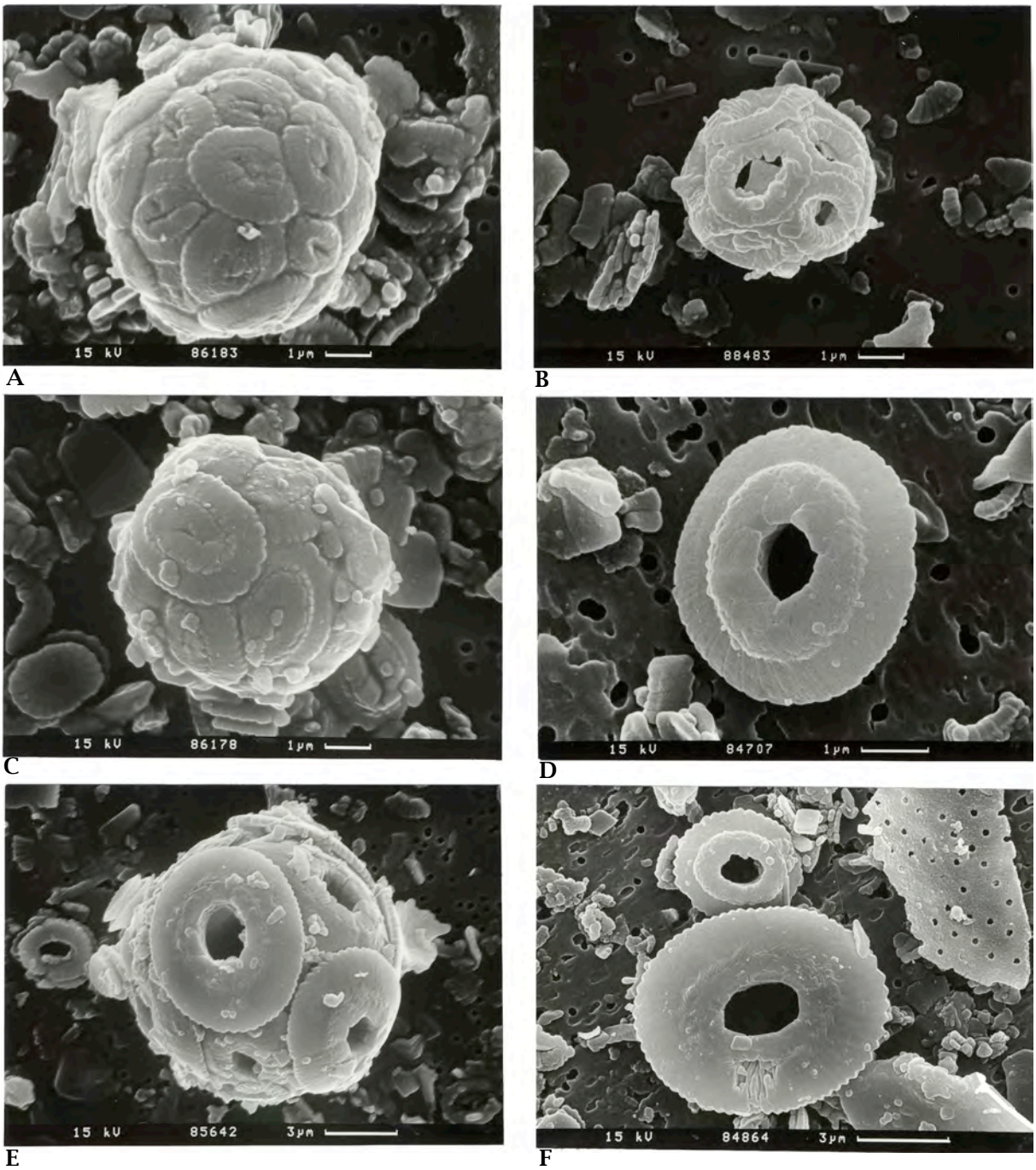

PLATE 2

PLATE 2 - LEGEND

A *Sphenolithus abies* (sample BBP 24)

B *Sphenolithus abies* (sample BBP 1)

C *Florisphaera profunda* (sample BBC 147)

D *Rhabdosphaera tubifera* (sample FCC 15)

E *Discosphaera tubifera* (sample FCC 102)

F *Discoaster sp. (quinueramus)* (sample BBP 53)

PLATE 2

Neogene nannoliths of Sites 1241 and 1000.

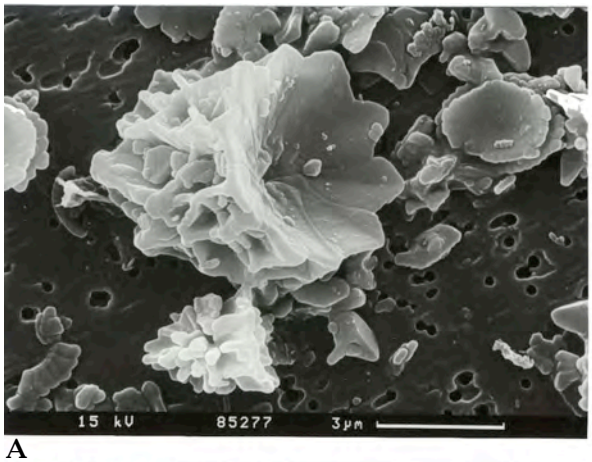

A

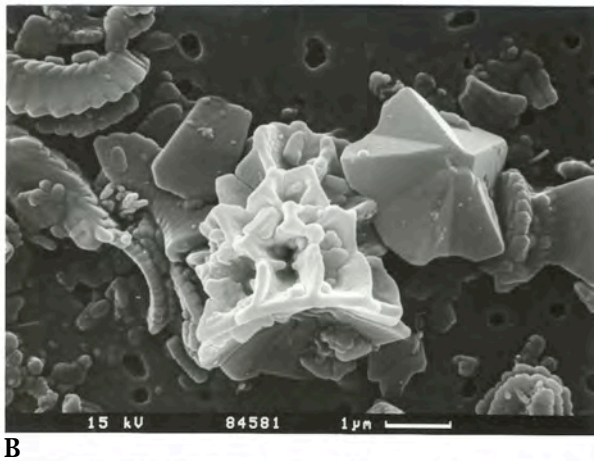

B

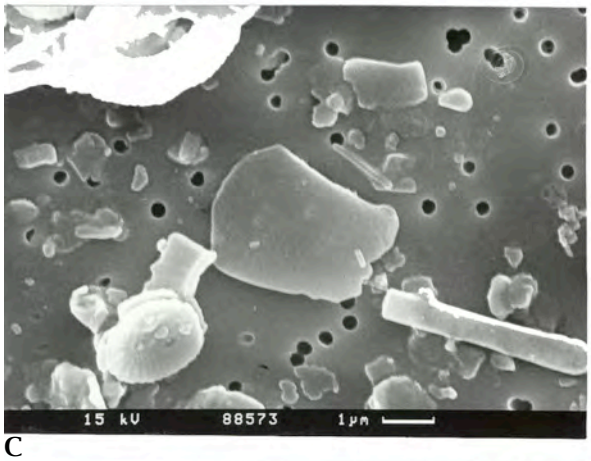

C

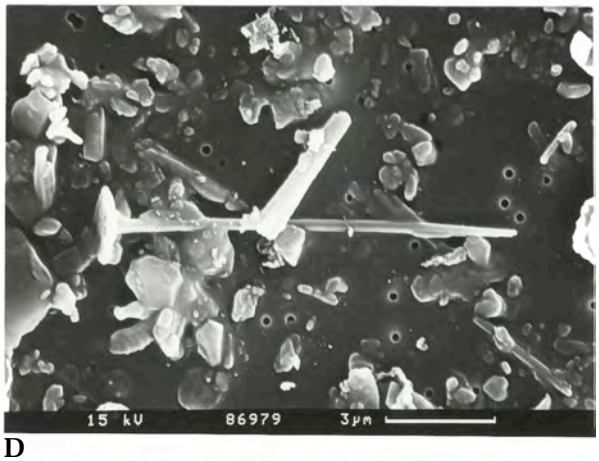

D

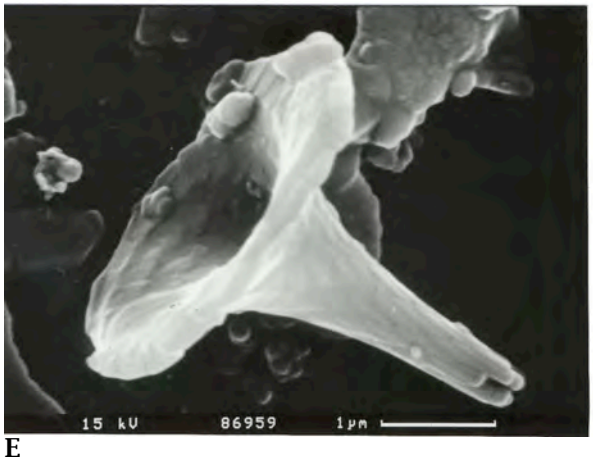

E

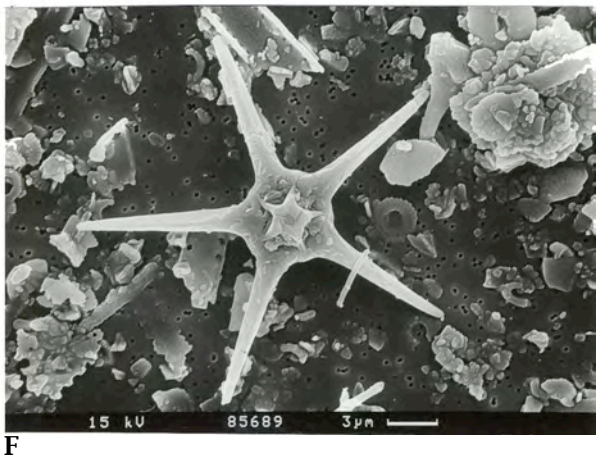

F

PLATE 3

PLATE 3 - LEGEND

A *Calcidiscus leptoporus* S, proximal and distal view (sample FCP 36)

B *Calcidiscus leptoporus* S, proximal view (sample FCC 66)

C *Calcidiscus leptoporus* I (sample FCP 36)

D *Calcidiscus leptoporus* I, proximal and distal view (sample BBP 7)

E *Calcidiscus leptoporus* XL (sample BBP 71)

F *Calcidiscus leptoporus* XL (sample BBP 138)

PLATE 3

Neogene *Calcidiscus* coccoliths of Sites 1241 and 1000.

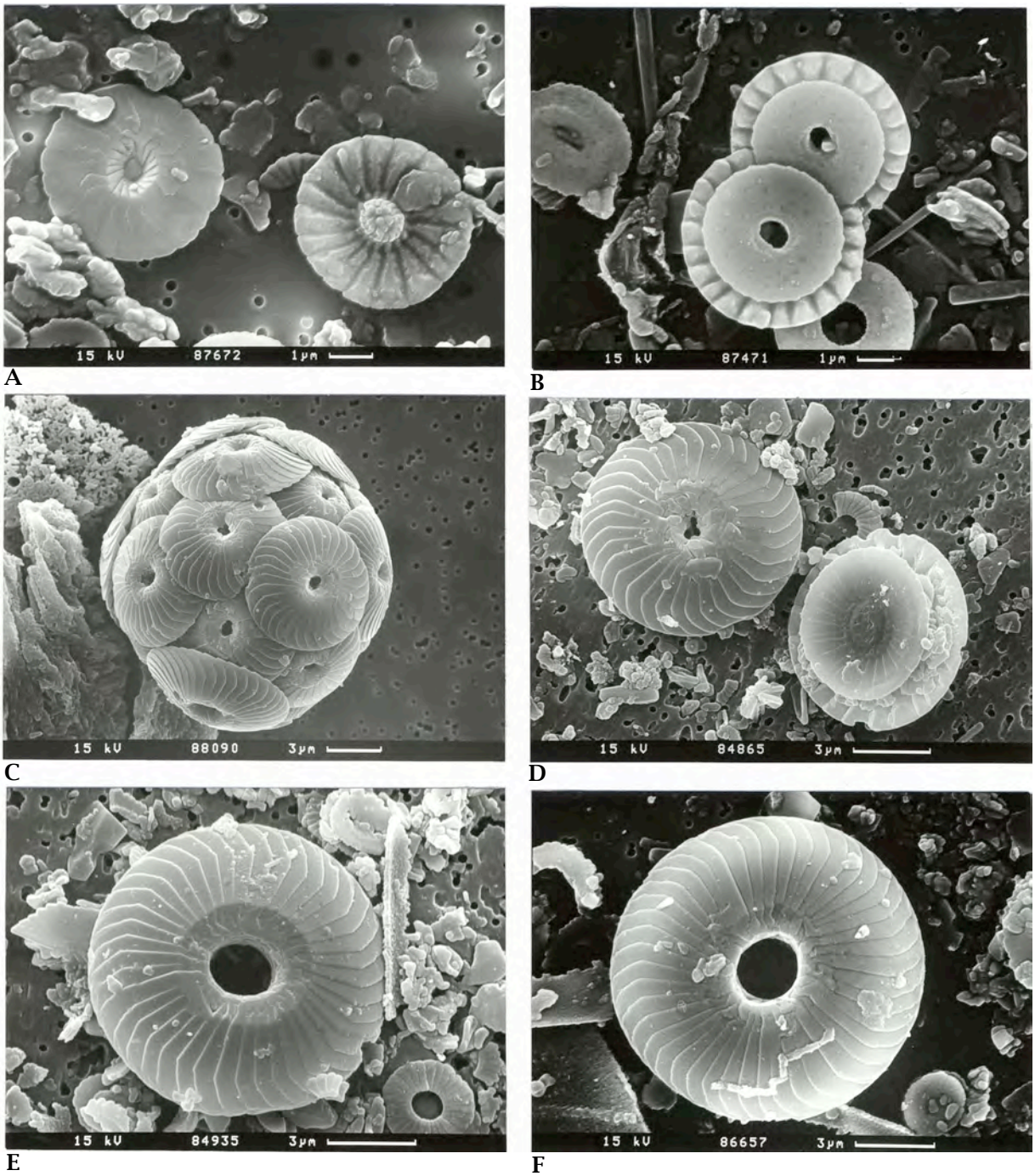

PLATE 4

PLATE 4 - LEGEND

A *Coccolithus pelagicus* (sample BBP 143)
B *Helicosphaera sp.* (sample BBP 4)
C *Pontosphaera sp.* (sample FCP 12)
D *Scyphosphaera apsteinii* (sample FCP 8)
E *Umbilicosphaera sp.* (sample FCC 57)
F *small Gephyrocapsa* (sample FCC 87)

PLATE 4

Neogene coccoliths of Sites 1241 and 1000.

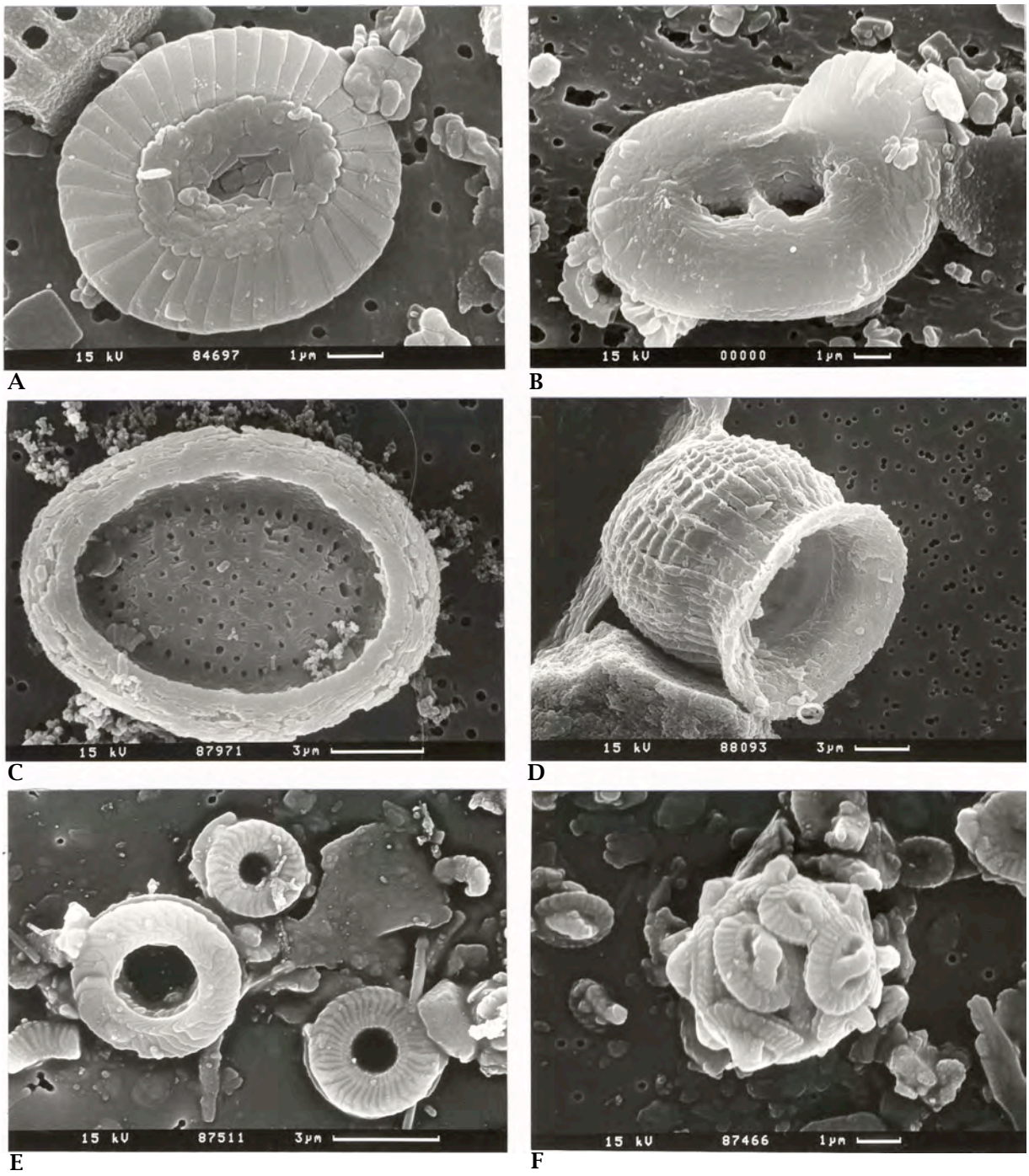

PLATE 5

PLATE 5 - LEGEND

Subfraction < 1 μm

A to F with increasing magnification, all samples from Pliocene Site 1000 (FCC).

PLATE 5

Subfraction < 1 µm.

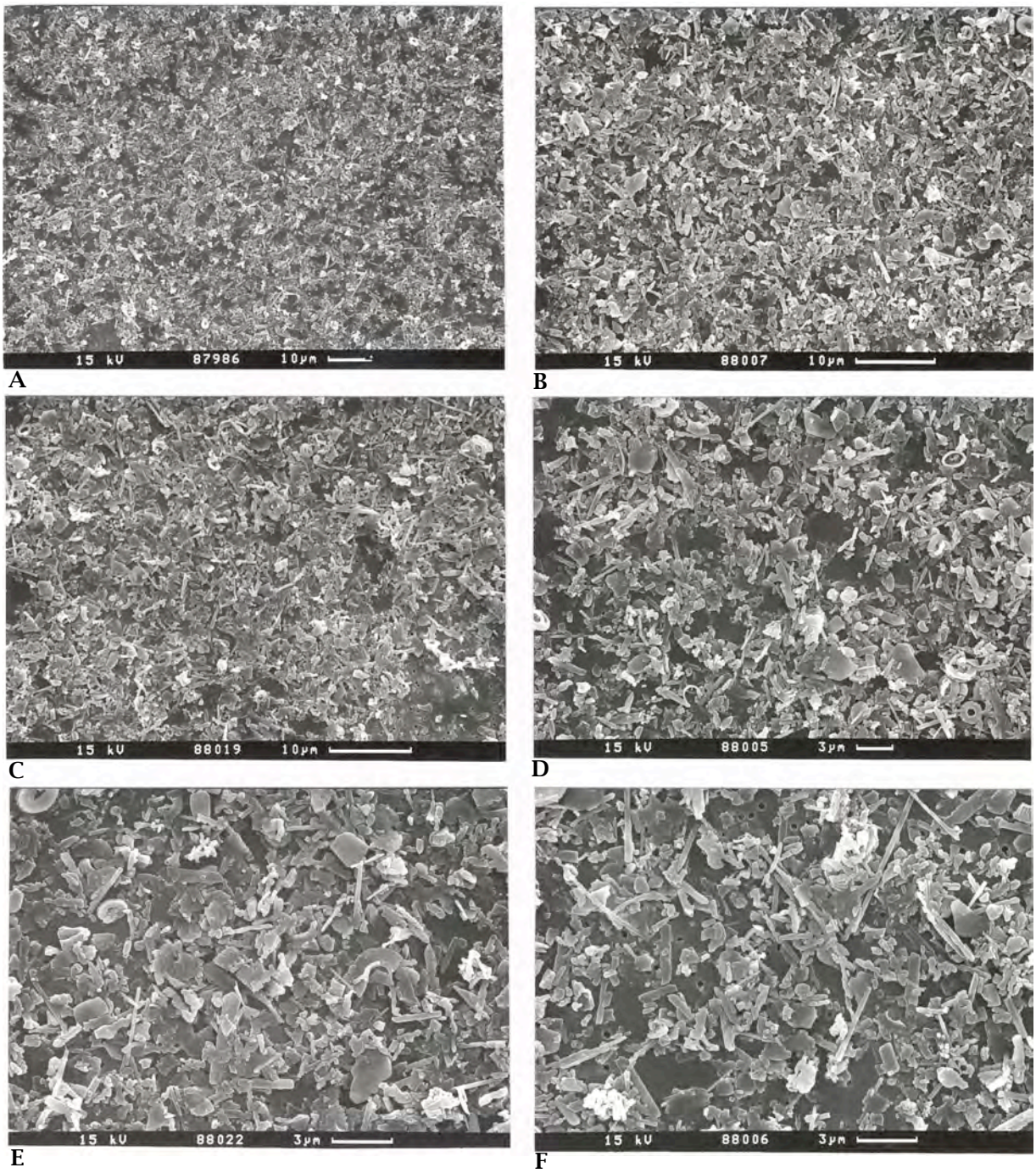

PLATE 6

PLATE 6 - LEGEND

Subfraction 1-3 µm

A to F with increasing magnification,

A FCP 51

B FCC 51

C FCC 51

D FCC 12

E FCP 51

F FCC 12

PLATE 6

Subfraction 1-3 µm.

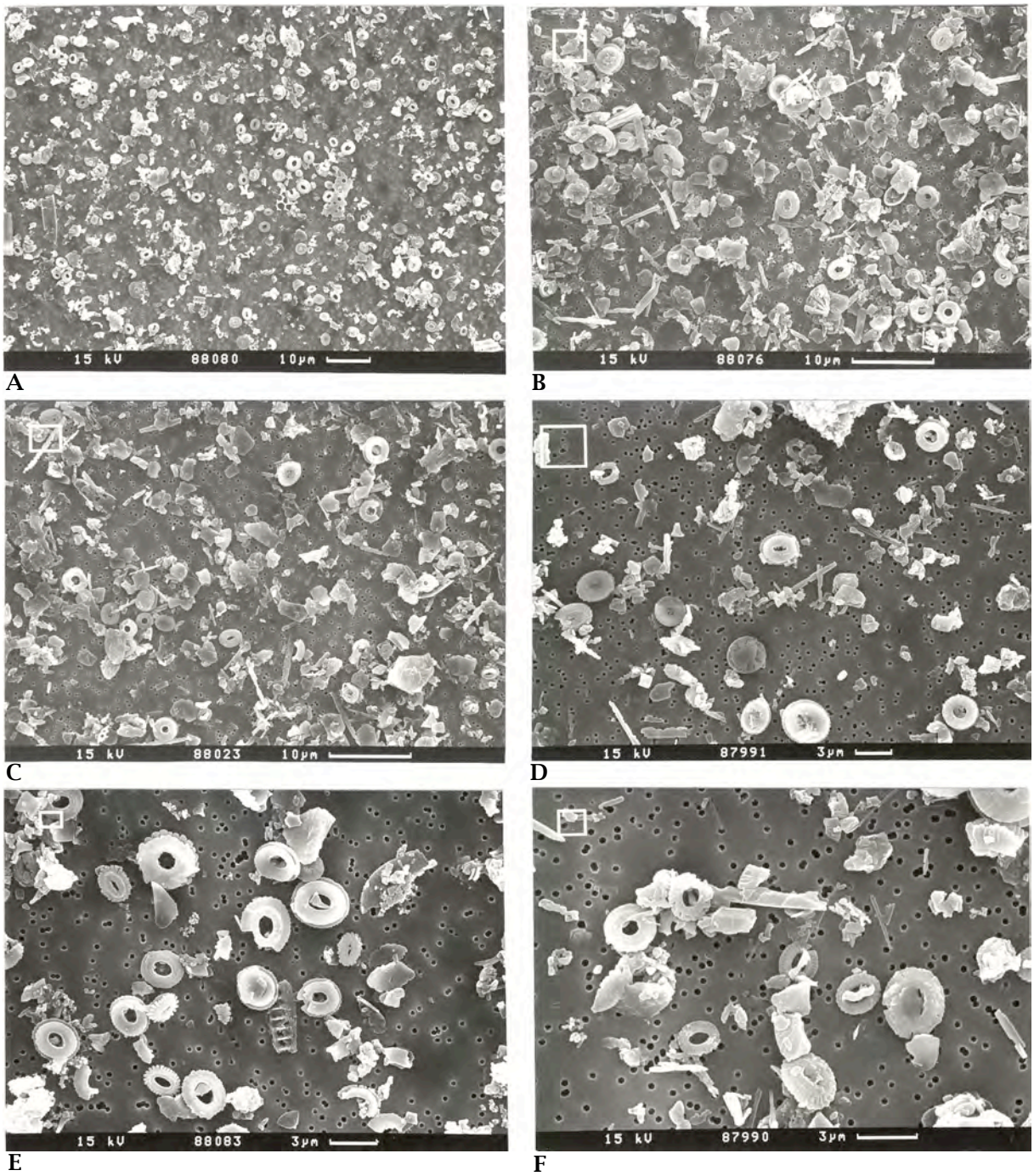

PLATE 7

PLATE 7 - LEGEND

Subfraction 3-5 µm

A FCP 51 (square = 5 µm)

B FCC 30 (square = 3 µm)

Subfraction 5-8 µm

C FCP 51 (square = 5 µm)

D FCC 30

PLATE 7

Subfraction 3-5 µm.

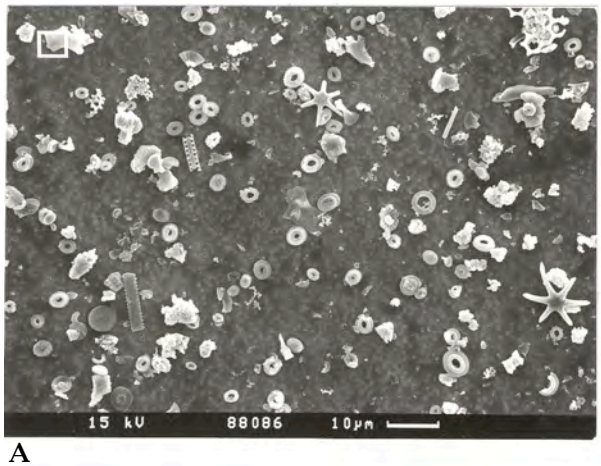

A

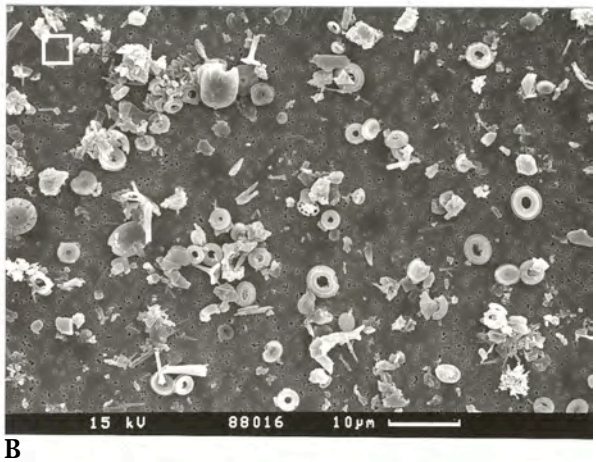

B

Subfraction 5-8 µm.

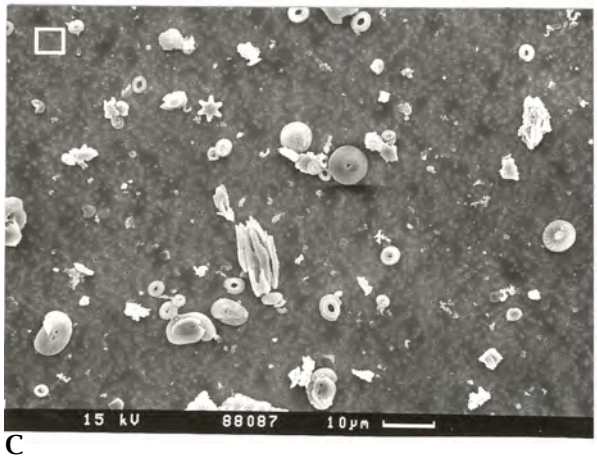

C

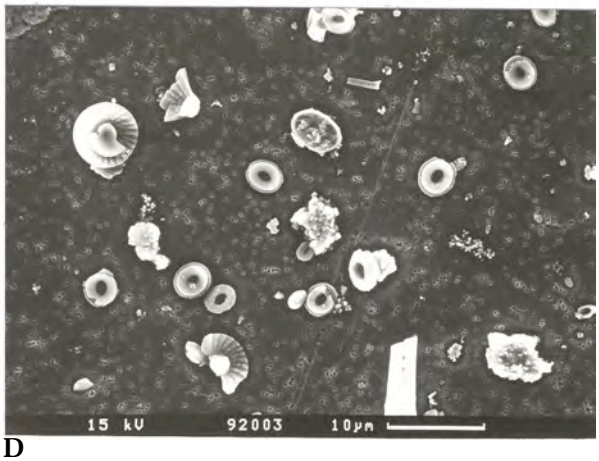

D

PLATE 8

PLATE 8 - LEGEND

Subfraction 8-11 µm

A FCP 12

B FCP 51 (square = 8 µm)

Subfraction 11-20 µm

C FCP 12

Subfraction > 20 µm

D FCP 12

PLATE 8

Subfraction 8-11 µm.

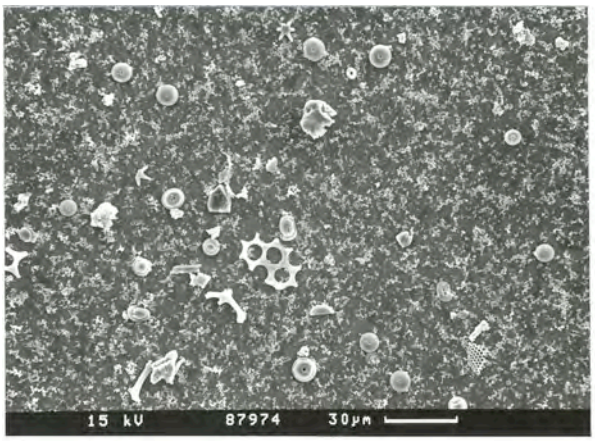

A

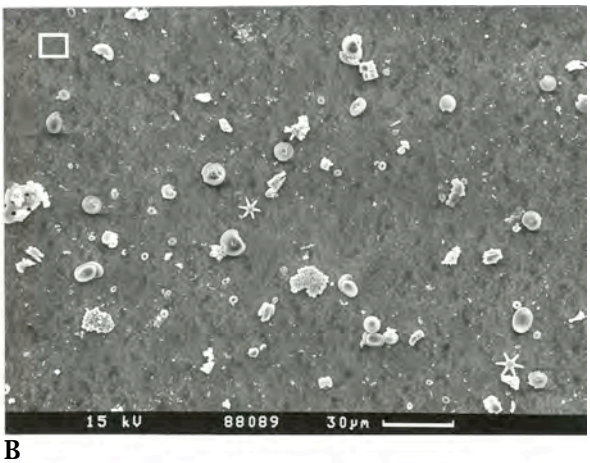

B

Subfractions 11-20 µm and > 20 µm.

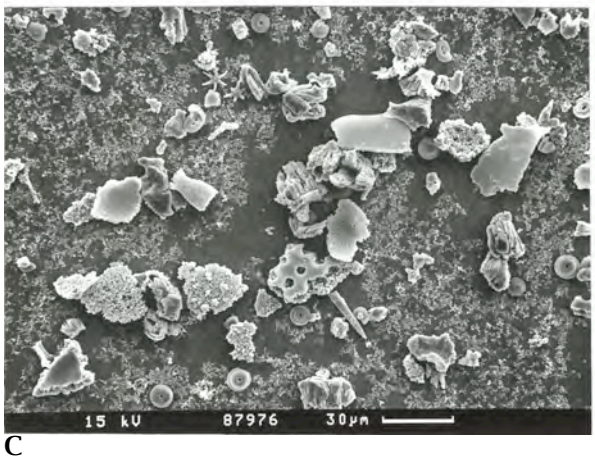

C

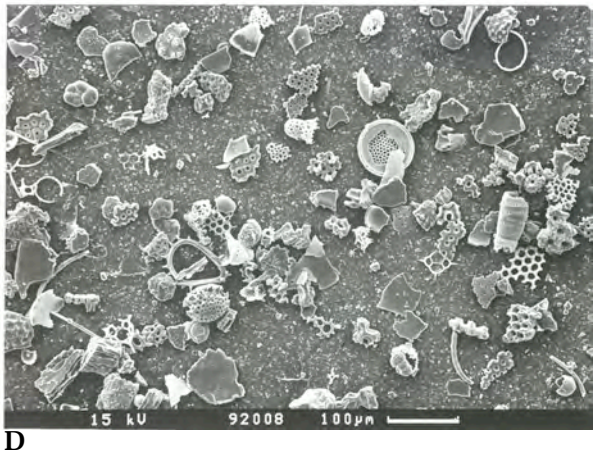

D

A2 TAXONOMY

A2-1 Systematic classification

Isochrysidales

NOELAERHABDACEAE
Dictyococcites Black, 1967
Reticulofenestra Hay, Mohler and Wade, 1966
R. minuta Roth, 1970
R. haquii Backman, 1978
R. minutula Haq and Berggren, 1978
R. pseudoumbilicus Gartner, 1969
Gephyrocapsa Kamtner, 1943

Coccosphaerales

COCCOLITHACEAE
Coccolithus pelagicus Schiller, 1930

CALCIDISCACEAE
Calcidiscus Kamptner, 1950
Hayaster perplexus Burky, 1973
Umbilicosphaera Lohmann, 1902
U. jafari Müller, 1974
U. rotula Kamptner, 1956

Zygodiscales

HELICOSPHAERACEAE
Helicosphaera Kamptner, 1954

PONTOSPHAERACEAE
Pontosphaera Lohmann, 1902
Scyphosphaera Lohmann, 1902

Syracosphaerales

SYRACOSPHAERACEAE
Syracosphaera Lohmann, 1902

CALCIOSOLENIAECEAE
Calciosolenia Gran, 1912

RHABDOSPHAERACEAE
Discosphaera tubifera Ostenfeld, 1900
Rhabdosphaera clavigera Murray and Blackman, 1898

Nannoliths

CERATOLITHACEAE
Ceratolithus Kamptner, 1950

Nannoliths incertae sedis
Florisphaera profunda Okada and Honjo, 1973
Gladiolithus flabellatus Jordan and Chamberlain, 1993
Sphenolithus abies Deflandre in Deflandre and Fert, 1954

A2-2 Notes for species identification, sediments of Sites 1241 and 1000

Reticulofenestra: Oval to subcircular placoliths with an open central area and an imbricated distal shield structure. Backman (1980) defined Neogene *Reticulofenestra* species in a detailed study and proposed the distinction of very small to small (< 3 µm, 3-5 µm, Young et al., 1997). *R. minuta* are forms smaller than 3 µm. Flores and Sierro (1989) deviated the nomenclature with the small Dictyococcites productus, with a coccolith size smaller than 3 µm and a solid central area. *R. haquii* and *R. minutula* measure 3-5 µm . Specimens are distinguished by the size of the central opening, whereas the length of the central opening of *R. haquii* with 1.0–1.5 µm (Backman, 1978) is larger than that of *R. minutula* (Perch-Nielsen, 1985) where the central depression is covered by a coarse grill with twisted bars. *R. haquii* is distinguished from *R. pseudoumbilicus* by its smaller size and by the central opening being considerably smaller than that of *R. pseudoumbilicus* (Backman, 1978). *R. pseudoumbilicus* has been variably defined by size (> 5 µm: Young, 1990, Gartner, 1992; > 7 µm: Gartner 1969, Rio et al., 1990, Young, 1998) and by distally opened central area (longer than 4.5 µm: Flores and Sierro, 1989).
In combination with given definitions, I grouped *D. productus* and *R. minuta* as smallest reticulofenestrids < 3 µm (with open or rather closed central area) and *R. haquii* and *R. minutula* as small reticulofenestrids 3-5 µm (with open or rather closed central area). I chose the *R. pseudoumbilicus* M (medium) as reticulofenestrid specimens with a length of 5-7 µm, whereas I defined *R. pseudoumbilicus* to be >7 µm (both with wide central opening).

Gephyrocapsa: Elliptical reticulofenestrids with a conjunct bar spanning the central opening. Kameo and Sato (2000) observed *Gephyrocapsa* specimens in Miocene to Pliocene samples as small, usually below 4 µm in diameter.
Likewise our samples only show these small specimens, which were identified after Crudeli (2005). Due to their low abundances in the samples, I grouped all *Gephyrocapsa* species to „small *Gephyrocapsa*".

Calcidiscus spp.: Four subdivisions were identified after Knappertsbusch (2000) and Quinn et al.(2004) depending on size and number of segments: *C. leptoporus* S (< 5 µm = *C. fuscus* (Janin, 1987), around 15 elements), *C. leptoporus* I (5-8 µm, around 20 elements), *C. leptoporus* L (8-10 µm, around 30 elements), *C. leptoporus* XL (> 10 µm, = *C. macintyrei* (Loeblich and Tappan, 1978), >40 elements).

Umbilicosphaera spp.: Following Young (1998) we defined *U. jafari* (Müller, 1974) as small, round placolith with narrow central area, diameter < 5 µm, and *U. rotula* (Kamtner, 1956) as form with wide central area and narrow rim, diameter > 5 µm.

LPI (low productivity indicator):
Lower Photic Zone Taxa (LPZ): group of *Florisphaera profunda* and *Gladiolithus flabellatus*
Low Productivity Indicator Taxa: group of LPZ, *Sphenolithus abies*, *Rhabdosphaera clavigera* and *Discosphaera tubifera*.

A3 DATA

Biogenic Bloom interval Pacific

No	Leg	Site	Hole	Core	T	Sec.	Top	Bot	Depth (mcd)	SEM-tub	sample	age (Ma)
1	202	1241	B	17	H	4	135	137	176.66	Probe fehlt	**BBP 1**	5.710
2	202	1241	A	18	H	3	25	27	177.4	JL1B/1241-BB-1-2	**BBP 2**	5.723
3	202	1241	A	18	H	3	125	127	178.4	1241-BB-12-3	**BBP 3**	5.741
4	202	1241	A	18	H	4	75	77	179.41	1241-BB-13-4	**BBP 4**	5.758
5	202	1241	A	18	H	5	25	27	180.42	1241-BB-2-5	**BBP 5**	5.776
6	202	1241	A	18	H	5	125	127	181.42	1241-BB-14-6	**BBP 6**	5.793
7	202	1241	B	18	H	1	25	27	181.64	1241-BB-15-7	**BBP 7**	5.797
8	202	1241	A	18	H	6	75	77	182.43	1241-BB-16-8	**BBP 8**	5.811
9	202	1241	B	18	H	1	125	127	182.64	1241-BB-17-9	**BBP 9**	5.815
10	202	1241	B	18	H	2	75	77	183.65	1241-BB-18-10	**BBP 10**	5.834
11	202	1241	B	18	H	3	25	27	184.65	1241-BB-19-11	**BBP 11**	5.853
12	202	1241	B	18	H	3	125	127	185.65	1241-BB-3-12	**BBP 12**	5.872
13	202	1241	B	18	H	4	75	77	186.66	JL2/1241-BB-20-13	**BBP 13**	5.891
14	202	1241	B	18	H	5	25	27	187.66	1241-BB-21-14	**BBP 14**	5.909
15	202	1241	A	19	H	3	75	77	188.45	1241-BB-22-15	**BBP 15**	5.923
16	202	1241	B	18	H	5	125	127	188.66	1241-BB-23-16	**BBP 16**	5.927
17	202	1241	A	19	H	4	25	27	189.46	1241-BB-24-17	**BBP 17**	5.941
18	202	1241	A	19	H	4	125	127	190.46	1241-BB-4-18	**BBP 18**	5.958
19	202	1241	A	19	H	5	75	77	191.47	1241-BB-25-19	**BBP 19**	5.976
20	202	1241	A	19	H	6	25	27	192.48	1241-BB-26-20	**BBP 20**	5.994
21	202	1241	A	19	H	6	125	127	193.48	1241-BB-27-21	**BBP 21**	6.012
22	202	1241	B	19	H	2	75	77	194.28	1241-BB-28-22	**BBP 22**	6.026
23	202	1241	B	19	H	3	25	27	195.29	1241-BB-29-23	**BBP 23**	6.044
24	202	1241	B	19	H	3	125	127	196.29	1241-BB-30-24	**BBP 24**	6.061
25	202	1241	A	20	H	1	125	127	197.03	JL3/1241-BB-31-25	**BBP 25**	6.074
26	202	1241	B	19	H	4	75	77	197.29	1241-BB-32-26	**BBP 26**	6.079
27	202	1241	A	20	H	2	75	77	198.04	1241-BB-33-27	**BBP 27**	6.092
28	202	1241	A	20	H	3	25	27	199.05	1241-BB-34-28	**BBP 28**	6.110
29	202	1241	A	20	H	3	125	127	200.05	1241-BB-5-29	**BBP 29**	6.128
30	202	1241	A	20	H	4	75	77	201.06	1241-BB-35-30	**BBP 30**	6.147
31	202	1241	A	20	H	5	25	27	202.07	1241-BB-36-31	**BBP 31**	6.165
32	202	1241	A	20	H	5	125	127	203.07	1241-BB-37-32	**BBP 32**	6.184
33	202	1241	A	20	H	6	75	77	204.08	1241-BB-38-33	**BBP 33**	6.202
34	202	1241	B	20	H	2	25	27	204.24	1241-BB-39-34	**BBP 34**	6.205
35	202	1241	B	20	H	2	125	127	205.24	1241-BB-40-35	**BBP 35**	6.224
36	202	1241	B	20	H	3	75	77	206.25	1241-BB-41-36	**BBP 36**	6.243
37	202	1241	B	20	H	4	25	27	207.26	JL4/1241-BB-42-37	**BBP 37**	6.263
38	202	1241	A	21	H	1	75	77	207.28	1241-BB-43-38	**BBP 38**	6.263
39	202	1241	B	20	H	4	125	127	208.26	1241-BB-44-39	**BBP 39**	6.282
40	202	1241	A	21	H	2	25	27	208.29	1241-BB-45-40	**BBP 40**	6.282
41	202	1241	A	21	H	2	125	127	209.29	1241-BB-46-41	**BBP 41**	6.301
42	202	1241	A	21	H	3	75	77	210.3	1241-BB-47-42	**BBP 42**	6.321
43	202	1241	A	21	H	4	25	27	211.31	1241-BB-48-43	**BBP 43**	6.340
44	202	1241	A	21	H	4	125	127	212.31	1241-BB-49-44	**BBP 44**	6.359
45	202	1241	A	21	H	5	75	77	213.32	1241-BB-50-45	**BBP 45**	6.378
46	202	1241	A	21	H	6	25	27	214.33	1241-BB-51-46	**BBP 46**	6.398
47	202	1241	B	21	H	2	75	77	214.64	1241-BB-52-47	**BBP 47**	6.404
48	202	1241	B	21	H	3	25	27	215.65	1241-BB-53-48	**BBP 48**	6.423
49	202	1241	B	21	H	3	125	127	216.65	1241-BB-54-49	**BBP 49**	6.442

No	Leg	Site	Hole	Core	T	Sec.	Top	Bot	Depth (mcd)	SEM-tub	sample	age (Ma)
50	202	1241	B	21	H	4	75	77	217.66	JL5/1241-BB-55-50	**BBP 50**	6.461
51	202	1241	B	21	H	5	25	27	218.67	1241-BB-56-51	**BBP 51**	6.481
52	202	1241	A	22	H	2	75	77	219.43	1241-BB-57-52	**BBP 52**	6.495
53	202	1241	B	21	H	5	125	127	219.67	1241-BB-58-53	**BBP 53**	6.500
54	202	1241	A	22	H	3	25	27	220.44	1241-BB-6-54	**BBP 54**	6.514
55	202	1241	A	22	H	3	125	127	221.44	1241-BB-59-55	**BBP 55**	6.534
56	202	1241	A	22	H	4	75	77	222.45	1241-BB-60-56	**BBP 56**	6.553
57	202	1241	A	22	H	5	25	27	223.46	1241-BB-61-57	**BBP 57**	6.572
58	202	1241	A	22	H	5	125	127	224.46	1241-BB-62-58	**BBP 58**	6.593
59	202	1241	A	22	H	6	75	77	225.46	1241-BB-63-59	**BBP 59**	6.613
60	202	1241	B	22	H	3	25	27	225.58	1241-BB-64-60	**BBP 60**	6.616
61	202	1241	B	22	H	3	125	127	226.58	1241-BB-65-61	**BBP 61**	6.636
62	202	1241	B	22	H	4	75	77	227.58	JL6B/1241-BB-66-62	**BBP 62**	6.657
63	202	1241	B	22	H	5	25	27	228.59	1241-BB-67-63	**BBP 63**	6.678
64	202	1241	B	22	H	5	125	127	229.59	1241-BB-68-64	**BBP 64**	6.698
65	202	1241	A	23	H	1	125	127	230.05	1241-BB-69-65	**BBP 65**	6.708
66	202	1241	B	22	H	6	75	77	230.6	1241-BB-70-66	**BBP 66**	6.721
67	202	1241	A	23	H	2	75	77	231.06	1241-BB-71-67	**BBP 67**	6.732
68	202	1241	A	23	H	3	25	27	232.07	1241-BB-72-68	**BBP 68**	6.757
69	202	1241	A	23	H	3	125	127	233.07	1241-BB-73-69	**BBP 69**	6.782
70	202	1241	A	23	H	4	75	77	234.08	1241-BB-74-70	**BBP 70**	6.806
71	202	1241	A	23	H	5	25	27	235.09	1241-BB-75-71	**BBP 71**	6.831
72	202	1241	A	23	H	5	125	127	236.09	1241-BB-76-72	**BBP 72**	6.853
73	202	1241	B	23	H	3	75	77	236.8	1241-BB-77-73	**BBP 73**	6.869
74	202	1241	B	23	H	4	25	27	237.8	JL7/1241-BB-78-74	**BBP 74**	6.891
75	202	1241	B	23	H	4	125	127	238.8	1241-BB-79-75	**BBP 75**	6.912
76	202	1241	B	23	H	5	75	77	239.8	1241-BB-80-76	**BBP 76**	6.934
77	202	1241	B	23	H	6	25	27	240.8	1241-BB-7-77	**BBP 77**	6.956
78	202	1241	B	23	H	6	125	127	241.8	1241-BB-81-78	**BBP 78**	6.979
79	202	1241	A	24	H	2	25	27	241.81	1241-BB-82-79	**BBP 79**	6.979
80	202	1241	A	24	H	2	125	127	242.81	1241-BB-83-80	**BBP 80**	7.002
81	202	1241	A	24	H	3	25	27	243.32	1241-BB-84-81	**BBP 81**	7.013
82	202	1241	A	24	H	3	75	77	243.82	1241-BB-85-82	**BBP 82**	7.024
83	202	1241	A	24	H	3	125	127	244.32	1241-BB-86-83	**BBP 83**	7.036
84	202	1241	A	24	H	4	25	27	244.83	1241-BB-87-84	**BBP 84**	7.047
85	202	1241	A	24	H	4	75	77	245.33	1241-BB-88-85	**BBP 85**	7.058
86	202	1241	A	24	H	4	125	127	245.83	1241-BB-89-86	**BBP 86**	7.069
87	202	1241	A	24	H	5	25	27	246.34	1241-BB-90-87	**BBP 87**	7.081
88	202	1241	A	24	H	5	75	77	246.84	1241-BB-91-88	**BBP 88**	7.091
89	202	1241	B	24	H	3	25	27	246.99	1241-BB-92-89	**BBP 89**	7.095
90	202	1241	A	24	H	5	125	127	247.34	JL8/1241-BB-93-90	**BBP 90**	7.102
91	202	1241	B	24	H	3	75	77	247.49	1241-BB-94-91	**BBP 91**	7.106
92	202	1241	B	24	H	3	125	127	247.99	1241-BB-95-92	**BBP 92**	7.117
93	202	1241	B	24	H	4	25	27	248.5	1241-BB-96-93	**BBP 93**	7.128
94	202	1241	B	24	H	4	75	77	249	1241-BB-97-94	**BBP 94**	7.139
95	202	1241	B	24	H	4	125	127	249.5	1241-BB-98-95	**BBP 95**	7.150
96	202	1241	B	24	H	5	25	27	250.02	1241-BB-8-96	**BBP 96**	7.162
97	202	1241	B	24	H	5	75	77	250.52	1241-BB-99-97	**BBP 97**	7.174
98	202	1241	B	24	H	5	125	127	251.02	1241-BB-100-98	**BBP 98**	7.186
99	202	1241	A	25	H	1	25	27	251.49	1241-BB-101-99	**BBP 99**	7.197

No	Leg	Site	Hole	Core	T	Sec.	Top	Bot	Depth (mcd)	SEM-tub	sample	age (Ma)
100	202	1241	B	24	H	6	25	27	251.52	1241-BB-102-100	**BBP 100**	7.198
101	202	1241	A	25	H	1	75	77	251.99	1241-BB-103-101	**BBP 101**	7.209
102	202	1241	B	24	H	6	75	77	252.02	1241-BB-104-102	**BBP 102**	7.210
103	202	1241	A	25	H	1	125	127	252.49	1241-BB-105-103	**BBP 103**	7.222
104	202	1241	A	25	H	2	25	27	253	1241-BB-106-104	**BBP 104**	7.234
105	202	1241	A	25	H	2	75	77	253.5	1241-BB-107-105	**BBP 105**	7.246
106	202	1241	A	25	H	2	125	127	254	1241-BB-108-106	**BBP 106**	7.258
107	202	1241	A	25	H	3	25	27	254.52	1241-BB-109-107	**BBP 107**	7.271
108	202	1241	A	25	H	3	75	77	255.02	1241-BB-9-108	**BBP 108**	7.283
109	202	1241	A	25	H	3	125	127	255.52	1241-BB-110-109	**BBP 109**	7.295
110	202	1241	A	25	H	4	25	27	256.03	1241-BB-111-110	**BBP 110**	7.308
111	202	1241	A	25	H	4	75	77	256.53	1241-BB-112-111	**BBP 111**	7.320
112	202	1241	A	25	H	4	125	127	257.03	1241-BB-113-112	**BBP 112**	7.332
113	202	1241	A	25	H	5	25	27	257.54	1241-BB-114-113	**BBP 113**	7.344
114	202	1241	A	25	H	5	75	77	258.04	1241-BB-115-114	**BBP 114**	7.355
115	202	1241	A	25	H	5	125	127	258.54	1241-BB-116-115	**BBP 115**	7.366
116	202	1241	A	25	H	6	25	27	259.06	1241-BB-117-116	**BBP 116**	7.378
117	202	1241	A	25	H	6	75	77	259.56	1241-BB-118-117	**BBP 117**	7.389
118	202	1241	A	25	H	6	125	127	260.06	1241-BB-10-118	**BBP 118**	7.400
119	202	1241	A	25	H	7	25	27	260.57	1241-BB-119-119	**BBP 119**	7.412
120	202	1241	B	25	H	5	25	27	260.62	1241-BB-120-120	**BBP 120**	7.413
121	202	1241	B	25	H	5	75	77	261.12	1241-BB-121-121	**BBP 121**	7.424
122	202	1241	B	25	H	5	125	127	261.62	1241-BB-122-122	**BBP 122**	7.435
123	202	1241	B	25	H	6	25	27	262.13	1241-BB-123-123	**BBP 123**	7.446
124	202	1241	B	25	H	6	75	77	262.63	1241-BB-124-124	**BBP 124**	7.458
125	202	1241	A	26	H	1	75	77	262.68	1241-BB-125-125	**BBP 125**	7.459
126	202	1241	B	25	H	6	125	127	263.13	1241-BB-126-126	**BBP 126**	7.469
127	202	1241	A	26	H	1	125	127	263.18	1241-BB-127-127	**BBP 127**	7.470
128	202	1241	A	26	H	2	25	27	263.69	1241-BB-128-128	**BBP 128**	7.481
129	202	1241	A	26	H	2	75	77	264.19	1241-BB-129-129	**BBP 129**	7.492
130	202	1241	A	26	H	2	125	127	264.69	1241-BB-130-130	**BBP 130**	7.504
131	202	1241	A	26	H	3	25	27	265.2	1241-BB-131-131	**BBP 131**	7.515
132	202	1241	A	26	H	3	75	77	265.7	1241-BB-132-132	**BBP 132**	7.526
133	202	1241	A	26	H	3	125	127	266.2	1241-BB-133-133	**BBP 133**	7.537
134	202	1241	A	26	H	4	25	27	266.71	1241-BB-134-134	**BBP 134**	7.549
135	202	1241	B	26	H	2	75	77	267.15	1241-BB-135-135	**BBP 135**	7.561
136	202	1241	A	26	H	4	75	77	267.21	1241-BB-136-136	**BBP 136**	7.562
137	202	1241	B	26	H	2	125	127	267.65	1241-BB-137-137	**BBP 137**	7.574
138	202	1241	A	26	H	4	125	127	267.71	1241-BB-138-138	**BBP 138**	7.575
139	202	1241	B	26	H	3	25	27	268.16	1241-BB-139-139	**BBP 139**	7.587
140	202	1241	B	26	H	3	75	77	268.66	1241-BB-140-140	**BBP 140**	7.601
141	202	1241	B	26	H	3	125	127	269.16	1241-BB-141-141	**BBP 141**	7.614
142	202	1241	B	26	H	4	25	27	269.67	1241-BB-142-142	**BBP 142**	7.627
143	202	1241	B	26	H	4	75	77	270.17	1241-BB-11-143	**BBP 143**	7.640
144	202	1241	B	26	H	4	125	127	270.67	1241-BB-143-144	**BBP 144**	7.654
145	202	1241	B	26	H	5	25	27	271.17	1241-BB-144-145	**BBP 145**	7.667
146	202	1241	B	26	H	5	75	77	271.67	1241-BB-145-146	**BBP 146**	7.680
147	202	1241	B	26	H	5	125	127	272.17	1241-BB-146-147	**BBP 147**	7.693
148	202	1241	B	26	H	6	25	27	272.67	1241-BB-147-148	**BBP 148**	7.706
149	202	1241	B	26	H	6	75	77	273.17	1241-BB-148-149	**BBP 149**	7.719

Biogenic Bloom interval Caribbean

No.	Leg	Site	Hole	Core	T	Sec.	Top	Bot	Depth (mbsf)	SEM-tub / sample	age (Ma)
1	165	1000	A	20	H	1	15	17	174.45	**BBC 1**	5.5840
2	165	1000	A	20	H	1	65	67	174.95	**BBC 2**	5.5932
3	165	1000	A	20	H	1	115	117	175.45	**BBC 3**	5.6025
4	165	1000	A	20	H	2	15	17	175.95	**BBC 4**	5.6118
5	165	1000	A	20	H	2	65	67	176.45	**BBC 5**	5.6210
6	165	1000	A	20	H	2	115	117	176.95	**BBC 6**	5.6303
7	165	1000	A	20	H	3	15	17	177.45	**BBC 7**	5.6396
8	165	1000	A	20	H	3	65	67	177.95	**BBC 8**	5.6488
9	165	1000	A	20	H	3	115	117	178.45	**BBC 9**	5.6581
10	165	1000	A	20	H	4	15	17	178.95	**BBC 10**	5.6674
11	165	1000	A	20	H	4	65	67	179.45	**BBC 11**	5.6766
12	165	1000	A	20	H	4	115	117	179.95	**BBC 12**	5.6859
13	165	1000	A	20	H	5	15	17	180.45	**BBC 13**	5.6951
14	165	1000	A	20	H	5	65	67	180.95	**BBC 14**	5.7044
15	165	1000	A	20	H	5	115	117	181.45	**BBC 15**	5.7137
16	165	1000	A	20	H	6	15	17	181.95	**BBC 16**	5.7229
17	165	1000	A	20	H	6	65	67	182.45	**BBC 17**	5.7321
18	165	1000	A	20	H	6	115	117	182.95	**BBC 18**	5.7410
19	165	1000	A	20	H	7	15	17	183.45	**BBC 19**	5.7497
20	165	1000	A	20	H	7	65	67	183.95	**BBC 20**	5.7584
21	165	1000	A	21	H	1	65	67	184.45	**BBC 21**	5.7671
22	165	1000	A	21	H	1	115	117	184.95	**BBC 22**	5.7759
23	165	1000	A	21	H	2	15	17	185.45	**BBC 23**	5.7848
24	165	1000	A	21	H	2	65	67	185.95	**BBC 24**	5.7942
25	165	1000	A	21	H	2	115	117	186.45	**BBC 25**	5.8039
26	165	1000	A	21	H	3	15	17	186.95	**BBC 26**	5.8147
27	165	1000	A	21	H	3	65	67	187.45	**BBC 27**	5.8258
28	165	1000	A	21	H	3	115	117	187.95	**BBC 28**	5.8379
29	165	1000	A	21	H	4	15	17	188.45	**BBC 29**	5.8496
30	165	1000	A	21	H	4	65	67	188.95	**BBC 30**	5.8589
31	165	1000	A	21	H	4	115	117	189.45	**BBC 31**	5.8679
32	165	1000	A	21	H	5	15	17	189.95	**BBC 32**	5.8773
33	165	1000	A	21	H	5	65	67	190.45	**BBC 33**	5.8870
34	165	1000	A	21	H	5	115	117	190.95	**BBC 34**	5.8988
35	165	1000	A	21	H	6	15	17	191.45	**BBC 35**	5.9120
36	165	1000	A	21	H	6	65	67	191.95	**BBC 36**	5.9323
37	165	1000	A	21	H	6	115	117	192.45	**BBC 37**	5.9540
38	165	1000	A	21	H	7	15	17	192.95	**BBC 38**	5.9774
39	165	1000	A	22	H	1	15	17	193.45	**BBC 39**	5.9998
40	165	1000	A	22	H	1	65	67	193.95	**BBC 40**	6.0146
41	165	1000	A	22	H	1	115	117	194.45	**BBC 41**	6.0276
42	165	1000	A	22	H	2	15	17	194.95	**BBC 42**	6.0370
43	165	1000	A	22	H	2	63	65	195.43	**BBC 43**	6.0459

No.	Leg	Site	Hole	Core	T	Sec.	Top	Bot	Depth (mbsf)	SEM-tub / sample	age (Ma)
44	165	1000	A	22	H	2	115	117	195.95	**BBC 44**	6.0552
45	165	1000	A	22	H	3	15	17	196.45	**BBC 45**	6.0644
46	165	1000	A	22	H	3	65	67	196.95	**BBC 46**	6.0721
47	165	1000	A	22	H	3	115	117	197.45	**BBC 47**	6.0799
48	165	1000	A	22	H	4	15	17	197.95	**BBC 48**	6.0892
49	165	1000	A	22	H	4	65	67	198.45	**BBC 49**	6.0991
50	165	1000	A	22	H	4	115	117	198.95	**BBC 50**	6.1108
51	165	1000	A	22	H	5	15	17	199.45	**BBC 51**	6.1229
52	165	1000	A	22	H	5	65	67	199.95	**BBC 52**	6.1354
53	165	1000	A	22	H	5	115	117	200.45	**BBC 53**	6.1479
54	165	1000	A	22	H	6	15	17	200.95	**BBC 54**	6.1606
55	165	1000	A	22	H	6	65	67	201.45	**BBC 55**	6.1732
56	165	1000	A	22	H	6	115	117	201.95	**BBC 56**	6.1856
57	165	1000	A	22	H	7	15	17	202.45	**BBC 57**	6.1984
58	165	1000	A	22	H	7	65	67	202.95	**BBC 58**	6.2142
59	165	1000	A	23	H	1	65	67	203.45	**BBC 59**	6.2299
60	165	1000	A	23	H	1	115	117	203.95	**BBC 60**	6.2424
61	165	1000	A	23	H	2	15	17	204.45	**BBC 61**	6.2541
62	165	1000	A	23	H	2	65	67	204.95	**BBC 62**	6.2651
63	165	1000	A	23	H	2	115	117	205.45	**BBC 63**	6.2756
64	165	1000	A	23	H	3	15	17	205.95	**BBC 64**	6.2842
65	165	1000	A	23	H	3	65	67	206.45	**BBC 65**	6.2927
66	165	1000	A	23	H	3	115	117	206.95	**BBC 66**	6.3028
67	165	1000	A	23	H	4	15	17	207.45	**BBC 67**	6.3132
68	165	1000	A	23	H	4	65	67	207.95	**BBC 68**	6.3245
69	165	1000	A	23	H	4	115	117	208.45	**BBC 69**	6.3360
70	165	1000	A	23	H	5	15	17	208.95	**BBC 70**	6.3485
71	165	1000	A	23	H	5	65	67	209.45	**BBC 71**	6.3611
72	165	1000	A	23	H	5	115	117	209.95	**BBC 72**	6.3739
73	165	1000	A	23	H	6	15	17	210.45	**BBC 73**	6.3864
74	165	1000	A	23	H	6	65	67	210.95	**BBC 74**	6.3968
75	165	1000	A	23	H	6	115	117	211.45	**BBC 75**	6.4074
76	165	1000	A	23	H	7	15	17	211.95	**BBC 76**	6.4216
77	165	1000	A	23	H	7	65	67	212.45	**BBC 77**	6.4360
78	165	1000	A	24	H	1	65	67	212.95	**BBC 78**	6.4480
79	165	1000	A	24	H	1	115	117	213.45	**BBC 79**	6.4602
80	165	1000	A	24	H	2	15	17	213.95	**BBC 80**	6.4749
81	165	1000	A	24	H	2	65	67	214.45	**BBC 81**	6.4904
82	165	1000	A	24	H	2	115	117	214.95	**BBC 82**	6.5078
83	165	1000	A	24	H	3	15	17	215.45	**BBC 83**	6.5259
84	165	1000	A	24	H	3	65	67	215.95	**BBC 84**	6.5472
85	165	1000	A	24	H	3	115	117	216.45	**BBC 85**	6.5679
86	165	1000	A	24	H	4	15	17	216.95	**BBC 86**	6.5820
87	165	1000	A	24	H	4	65	67	217.45	**BBC 87**	6.5965

No.	Leg	Site	Hole	Core	T	Sec.	Top	Bot	Depth (mbsf)	SEM-tub / sample	age (Ma)
88	165	1000	A	24	H	4	115	117	217.95	**BBC 88**	6.6194
89	165	1000	A	24	H	5	15	17	218.45	**BBC 89**	6.6450
90	165	1000	A	24	H	5	65	67	218.95	**BBC 90**	6.6782
91	165	1000	A	24	H	5	115	117	219.45	**BBC 91**	6.7114
92	165	1000	A	24	H	6	15	17	219.95	**BBC 92**	6.7373
93	165	1000	A	24	H	6	65	67	220.45	**BBC 93**	6.7601
94	165	1000	A	24	H	6	115	117	220.95	**BBC 94**	6.7724
95	165	1000	A	24	H	7	15	17	221.45	**BBC 95**	6.7832
96	165	1000	A	24	H	7	65	67	221.95	**BBC 96**	6.7952
97	165	1000	A	25	H	1	65	67	222.45	**BBC 97**	6.8077
98	165	1000	A	25	H	1	115	117	222.95	**BBC 98**	6.8210
99	165	1000	A	25	H	2	15	17	223.45	**BBC 99**	6.8340
100	165	1000	A	25	H	2	65	67	223.95	**BBC 100**	6.8438
101	165	1000	A	25	H	2	115	117	224.45	**BBC 101**	6.8530
102	165	1000	A	25	H	3	15	17	224.95	**BBC 102**	6.8621
103	165	1000	A	25	H	3	65	67	225.45	**BBC 103**	6.8711
104	165	1000	A	25	H	3	115	117	225.95	**BBC 104**	6.8796
105	165	1000	A	25	H	4	15	17	226.45	**BBC 105**	6.8881
106	165	1000	A	25	H	4	65	67	226.95	**BBC 106**	6.8966
107	165	1000	A	25	H	4	115	117	227.45	**BBC 107**	6.9051
108	165	1000	A	25	H	5	15	17	227.95	**BBC 108**	6.9136
109	165	1000	A	25	H	5	65	67	228.45	**BBC 109**	6.9220
110	165	1000	A	25	H	5	115	117	228.95	**BBC 110**	6.9305
111	165	1000	A	25	H	6	15	17	229.45	**BBC 111**	6.9390
112	165	1000	A	25	H	6	65	67	229.95	**BBC 112**	6.9475
113	165	1000	A	25	H	6	115	117	230.45	**BBC 113**	6.9560
114	165	1000	A	25	H	7	15	17	230.95	**BBC 114**	6.9644
115	165	1000	A	25	H	7	65	67	231.45	**BBC 115**	6.9729
116	165	1000	A	26	H	1	65	67	231.95	**BBC 116**	6.9813
117	165	1000	A	26	H	1	115	117	232.45	**BBC 117**	6.9898
118	165	1000	A	26	H	2	15	17	232.95	**BBC 118**	6.9982
119	165	1000	A	26	H	2	65	67	233.45	**BBC 119**	7.0066
120	165	1000	A	26	H	2	115	117	233.95	**BBC 120**	7.0150
121	165	1000	A	26	H	3	15	17	234.45	**BBC 121**	7.0237
122	165	1000	A	26	H	3	65	67	234.95	**BBC 122**	7.0338
123	165	1000	A	26	H	3	115	117	235.45	**BBC 123**	7.0442
124	165	1000	A	26	H	4	15	17	235.95	**BBC 124**	7.0555
125	165	1000	A	26	H	4	65	67	236.45	**BBC 125**	7.0678
126	165	1000	A	26	H	4	115	117	236.95	**BBC 126**	7.0854
127	165	1000	A	26	H	5	15	17	237.45	**BBC 127**	7.1036
128	165	1000	A	26	H	5	65	67	237.95	**BBC 128**	7.1197
129	165	1000	A	26	H	5	115	117	238.45	**BBC 129**	7.1348
130	165	1000	A	26	H	6	15	17	238.95	**BBC 130**	7.1455
131	165	1000	A	26	H	6	65	67	239.45	**BBC 131**	7.1556

No.	Leg	Site	Hole	Core	T	Sec.	Top	Bot	Depth (mbsf)	SEM-tub / sample	age (Ma)
132	165	1000	A	26	H	6	115	117	239.95	**BBC 132**	7.1663
133	165	1000	A	26	H	7	15	17	240.45	**BBC 133**	7.1773
134	165	1000	A	26	H	7	65	67	240.95	**BBC 134**	7.1896
135	165	1000	A	27	H	1	65	67	241.45	**BBC 135**	7.2017
136	165	1000	A	27	H	1	115	117	241.95	**BBC 136**	7.2117
137	165	1000	A	27	H	2	15	17	242.45	**BBC 137**	7.2213
138	165	1000	A	27	H	2	65	67	242.95	**BBC 138**	7.2309
139	165	1000	A	27	H	2	115	117	243.45	**BBC 139**	7.2404
140	165	1000	A	27	H	3	15	17	243.95	**BBC 140**	7.2493
141	165	1000	A	27	H	3	65	67	244.45	**BBC 141**	7.2581
142	165	1000	A	27	H	3	115	117	244.95	**BBC 142**	7.2668
143	165	1000	A	27	H	4	15	17	245.45	**BBC 143**	7.2758
144	165	1000	A	27	H	4	65	67	245.95	**BBC 144**	7.2860
145	165	1000	A	27	H	4	115	117	246.45	**BBC 145**	7.2966
146	165	1000	A	27	H	5	15	17	246.95	**BBC 146**	7.3083
147	165	1000	A	27	H	5	65	67	247.45	**BBC 147**	7.3200
148	165	1000	A	27	H	5	115	117	247.95	**BBC 148**	7.3316
149	165	1000	A	27	H	6	15	17	248.45	**BBC 149**	7.3429
150	165	1000	A	27	H	6	65	67	248.95	**BBC 150**	7.3533
151	165	1000	A	27	H	6	115	117	249.45	**BBC 151**	7.3636
152	165	1000	A	27	H	7	15	17	249.95	**BBC 152**	7.3739
153	165	1000	A	27	H	7	65	67	250.45	**BBC 153**	7.3841
154	165	1000	A	28	H	1	65	67	250.95	**BBC 154**	7.3937
155	165	1000	A	28	H	1	115	117	251.45	**BBC 155**	7.4032
156	165	1000	A	28	H	2	15	17	252.00	**BBC 156**	7.4130
157	165	1000	A	28	H	2	65	67	252.50	**BBC 157**	7.4228
158	165	1000	A	28	H	2	115	117	253.00	**BBC 158**	7.4327
159	165	1000	A	28	H	3	15	17	253.50	**BBC 159**	7.4426
160	165	1000	A	28	H	3	65	67	254.00	**BBC 160**	7.4528
161	165	1000	A	28	H	3	115	117	254.50	**BBC 161**	7.4631
162	165	1000	A	28	H	4	15	17	255.05	**BBC 162**	7.4739
163	165	1000	A	28	H	4	65	67	255.55	**BBC 163**	7.4847
164	165	1000	A	28	H	4	115	117	256.05	**BBC 164**	7.4951
165	165	1000	A	28	H	5	15	17	256.55	**BBC 165**	7.5055
166	165	1000	A	28	H	5	65	67	257.05	**BBC 166**	7.5158
167	165	1000	A	28	H	5	115	117	257.55	**BBC 167**	7.5259
168	165	1000	A	28	H	6	15	17	258.05	**BBC 168**	7.5353
169	165	1000	A	28	H	6	65	67	258.55	**BBC 169**	7.5448
170	165	1000	A	28	H	6	115	117	259.05	**BBC 170**	7.5550
171	165	1000	A	28	H	7	15	17	259.55	**BBC 171**	7.5653
172	165	1000	A	28	H	7	65	67	260.05	**BBC 172**	7.5753
173	165	1000	A	29	H	1	75	77	260.55	**BBC 173**	7.5852
174	165	1000	A	29	H	1	125	127	261.05	**BBC 174**	7.5951
175	165	1000	A	29	H	2	25	27	261.55	**BBC 175**	7.6047

No.	Leg	Site	Hole	Core	T	Sec.	Top	Bot	Depth (mbsf)	SEM-tub / sample	age (Ma)
176	165	1000	A	29	H	2	75	77	262.05	**BBC 176**	7.6135
177	165	1000	A	29	H	2	125	127	262.55	**BBC 177**	7.6220
178	165	1000	A	29	H	3	25	27	263.05	**BBC 178**	7.6294
179	165	1000	A	29	H	3	75	77	263.55	**BBC 179**	7.6367
180	165	1000	A	29	H	3	125	127	264.05	**BBC 180**	7.6440
181	165	1000	A	29	H	4	25	27	264.55	**BBC 181**	7.6513
182	165	1000	A	29	H	4	75	77	265.05	**BBC 182**	7.6593
183	165	1000	A	29	H	4	125	127	265.55	**BBC 183**	7.6674
184	165	1000	A	29	H	5	25	27	266.05	**BBC 184**	7.6761
185	165	1000	A	29	H	5	75	77	266.55	**BBC 185**	7.6849
186	165	1000	A	29	H	5	125	127	267.05	**BBC 186**	7.6947
187	165	1000	A	29	H	6	25	27	267.55	**BBC 187**	7.7049
188	165	1000	A	29	H	6	75	77	268.05	**BBC 188**	7.7168
189	165	1000	A	29	H	6	125	127	268.55	**BBC 189**	7.7290
190	165	1000	A	29	H	7	25	27	269.05	**BBC 190**	7.7412
191	165	1000	A	30	H	1	25	27	269.55	**BBC 191**	7.7534
192	165	1000	A	30	H	1	75	77	270.05	**BBC 192**	7.7655
193	165	1000	A	30	H	1	125	127	270.55	**BBC 193**	7.7774
194	165	1000	A	30	H	2	25	27	271.05	**BBC 194**	7.7876
195	165	1000	A	30	H	2	75	77	271.55	**BBC 195**	7.7972
196	165	1000	A	30	H	2	125	127	272.05	**BBC 196**	7.8057
197	165	1000	A	30	H	3	25	27	272.55	**BBC 197**	7.8140
198	165	1000	A	30	H	3	75	77	273.05	**BBC 198**	7.8222
199	165	1000	A	30	H	3	125	127	273.55	**BBC 199**	7.8313
200	165	1000	A	30	H	4	25	27	274.05	**BBC 200**	7.8449
201	165	1000	A	30	H	4	75	77	274.55	**BBC 201**	7.8590
202	165	1000	A	30	H	4	125	127	275.05	**BBC 202**	7.8712
203	165	1000	A	30	H	5	25	27	275.55	**BBC 203**	7.8832
204	165	1000	A	30	H	5	75	77	276.05	**BBC 204**	7.8967
205	165	1000	A	30	H	5	125	127	276.55	**BBC 205**	7.9113
206	165	1000	A	30	H	6	25	27	277.05	**BBC 206**	7.9321
207	165	1000	A	30	H	6	75	77	277.55	**BBC 207**	7.9528
208	165	1000	A	30	H	6	125	127	278.05	**BBC 208**	7.9663
209	165	1000	A	30	H	7	25	27	278.55	**BBC 209**	7.9786

Final Closure interval Pacific

No.	Leg	Site	Hole	Core	T	Sec.	Top	Bot	Depth (mcd)	SEM-tub / sample	age (Ma)
1	202	1241	C	5	H	6	80	82	83.37	**FCP 1**	3.3026
2	202	1241	C	5	H	6	90	92	83.47	**FCP 2**	3.3059
3	202	1241	A	9	H	3	50	52	83.55	**FCP 3**	3.3085
4	202	1241	A	9	H	3	60	62	83.65	**FCP 4**	3.3117
5	202	1241	A	9	H	3	70	72	83.75	**FCP 5**	3.315
6	202	1241	A	9	H	3	80	82	83.85	**FCP 6**	3.3174
7	202	1241	A	9	H	3	90	92	83.95	**FCP 7**	3.3198
8	202	1241	A	9	H	3	100	102	84.05	**FCP 8**	3.3222
9	202	1241	A	9	H	3	110	112	84.15	**FCP 9**	3.3246
10	202	1241	A	9	H	3	120	122	84.25	**FCP 10**	3.3271
11	202	1241	A	9	H	3	130	132	84.35	**FCP 11**	3.3294
12	202	1241	A	9	H	3	140	142	84.45	**FCP 12**	3.3319
13	202	1241	A	9	H	4	0	2	84.55	**FCP 13**	3.3343
14	202	1241	A	9	H	4	10	12	84.65	**FCP 14**	3.3367
15	202	1241	A	9	H	4	20	22	84.75	**FCP 15**	3.3391
16	202	1241	A	9	H	4	30	32	84.85	**FCP 16**	3.3415
17	202	1241	A	9	H	4	40	42	84.95	**FCP 17**	3.3439
18	202	1241	A	9	H	4	50	52	85.05	**FCP 18**	3.3463
19	202	1241	A	9	H	4	60	62	85.15	**FCP 19**	3.3487
20	202	1241	A	9	H	4	70	72	85.25	**FCP 20**	3.3511
21	202	1241	A	9	H	4	80	82	85.35	**FCP 21**	3.3536
22	202	1241	A	9	H	4	90	92	85.45	**FCP 22**	3.3559
23	202	1241	A	9	H	4	100	102	85.55	**FCP 23**	3.3584
24	202	1241	A	9	H	4	110	112	85.65	**FCP 24**	3.3608
25	202	1241	A	9	H	4	120	122	85.75	**FCP 25**	3.3632
26	202	1241	A	9	H	4	130	132	85.85	**FCP 26**	3.3656
27	202	1241	A	9	H	4	140	142	85.95	**FCP 27**	3.368
28	202	1241	A	9	H	5	0	2	86.05	**FCP 28**	3.3708
29	202	1241	A	9	H	5	10	12	86.15	**FCP 29**	3.3736
30	202	1241	A	9	H	5	20	22	86.25	**FCP 30**	3.3764
31	202	1241	A	9	H	5	30	32	86.35	**FCP 31**	3.3792
32	202	1241	A	9	H	5	40	42	86.45	**FCP 32**	3.382
33	202	1241	A	9	H	5	50	52	86.55	**FCP 33**	3.3848
34	202	1241	A	9	H	5	60	62	86.65	**FCP 34**	3.3876
35	202	1241	A	9	H	5	70	72	86.75	**FCP 35**	3.3904
36	202	1241	A	9	H	5	80	82	86.85	**FCP 36**	3.3932
37	202	1241	A	9	H	5	90	92	86.95	**FCP 37**	3.3961
38	202	1241	A	9	H	5	100	102	87.05	**FCP 38**	3.3989
39	202	1241	A	9	H	5	110	112	87.15	**FCP 39**	3.4017
40	202	1241	A	9	H	5	120	122	87.25	**FCP 40**	3.4045
41	202	1241	A	9	H	5	130	132	87.35	**FCP 41**	3.4073
42	202	1241	A	9	H	5	140	142	87.45	**FCP 42**	3.4101
43	202	1241	A	9	H	6	0	2	87.56	**FCP 43**	3.4132
44	202	1241	A	9	H	6	10	12	87.66	**FCP 44**	3.416
45	202	1241	A	9	H	6	20	22	87.76	**FCP 45**	3.4188
46	202	1241	A	9	H	6	30	32	87.86	**FCP 46**	3.4216
47	202	1241	A	9	H	6	40	42	87.96	**FCP 47**	3.4244
48	202	1241	A	9	H	6	50	52	88.06	**FCP 48**	3.4272
49	202	1241	A	9	H	6	60	62	88.16	**FCP 49**	3.43

No.	Leg	Site	Hole	Core	T	Sec.	Top	Bot	Depth (mcd)	SEM-tub / sample	age (Ma)
50	202	1241	A	9	H	6	70	72	88.26	**FCP 50**	3.4326
51	202	1241	A	9	H	6	80	82	88.36	**FCP 51**	3.4351
52	202	1241	A	9	H	6	90	92	88.46	**FCP 52**	3.4377
53	202	1241	A	9	H	6	100	102	88.56	**FCP 53**	3.4403
54	202	1241	A	9	H	6	110	112	88.66	**FCP 54**	3.4429
55	202	1241	A	9	H	6	120	122	88.76	**FCP 55**	3.4454
56	202	1241	A	9	H	6	130	132	88.86	**FCP 56**	3.448
57	202	1241	A	9	H	6	140	142	88.96	**FCP 57**	3.4506
58	202	1241	A	9	H	7	0	2	89.07	**FCP 58**	3.4534
59	202	1241	A	9	H	7	10	12	89.17	**FCP 59**	3.456
MISSING SAMPLES DUE TO SAMPLING GAP:											
60	202	1241	C	6	H	3	20	22	89.23	**FCP 60**	3.4576
61	202	1241	C	6	H	3	30	32	89.33	**FCP 61**	3.4601
62	202	1241	C	6	H	3	40	42	89.43	**FCP 62**	3.4627
63	202	1241	C	6	H	3	50	52	89.53	**FCP 63**	3.4653
64	202	1241	C	6	H	3	60	62	89.63	**FCP 64**	3.4679
65	202	1241	C	6	H	3	70	72	89.73	**FCP 65**	3.4704
66	202	1241	C	6	H	3	80	82	89.83	**FCP 66**	3.473
67	202	1241	C	6	H	3	90	92	89.93	**FCP 67**	3.4762
68	202	1241	C	6	H	3	100	102	90.03	**FCP 68**	3.4795
69	202	1241	C	6	H	3	110	112	90.13	**FCP 69**	3.4827
70	202	1241	C	6	H	3	120	122	90.23	**FCP 70**	3.4859
71	202	1241	C	6	H	3	130	132	90.33	**FCP 71**	3.4892
72	202	1241	C	6	H	3	140	142	90.43	**FCP 72**	3.4924
73	202	1241	C	6	H	4	0	2	90.53	**FCP 73**	3.4957
74	202	1241	C	6	H	4	10	12	90.63	**FCP 74**	3.4989
75	202	1241	C	6	H	4	20	22	90.73	**FCP 75**	3.5021
76	202	1241	C	6	H	4	30	32	90.83	**FCP 76**	3.5054
77	202	1241	C	6	H	4	40	42	90.93	**FCP 77**	3.5086
78	202	1241	C	6	H	4	50	52	91.03	**FCP 78**	3.5119
79	202	1241	C	6	H	4	60	62	91.13	**FCP 79**	3.5151
80	202	1241	C	6	H	4	70	72	91.23	**FCP 80**	3.5183
81	202	1241	C	6	H	4	80	82	91.33	**FCP 81**	3.5216
82	202	1241	C	6	H	4	90	92	91.43	**FCP 82**	3.5248
83	202	1241	C	6	H	4	100	102	91.53	**FCP 83**	3.528
84	202	1241	C	6	H	4	110	112	91.63	**FCP 84**	3.5313
85	202	1241	C	6	H	4	120	122	91.73	**FCP 85**	3.5345
86	202	1241	C	6	H	4	130	132	91.83	**FCP 86**	3.5377
87	202	1241	C	6	H	4	140	142	91.93	**FCP 87**	3.541
88	202	1241	C	6	H	5	0	2	92.03	**FCP 88**	3.5442
89	202	1241	C	6	H	5	10	12	92.13	**FCP 89**	3.5475
90	202	1241	A	10	H	2	10	12	92.22	**FCP 90**	3.5504
91	202	1241	A	10	H	2	20	22	92.32	**FCP 91**	3.5535
92	202	1241	A	10	H	2	30	32	92.42	**FCP 92**	3.5564
93	202	1241	A	10	H	2	40	42	92.52	**FCP 93**	3.5594
94	202	1241	A	10	H	2	50	52	92.62	**FCP 94**	3.5623
95	202	1241	A	10	H	2	60	62	92.72	**FCP 95**	3.5653
96	202	1241	A	10	H	2	70	72	92.82	**FCP 96**	3.5682
97	202	1241	A	10	H	2	80	82	92.92	**FCP 97**	3.5712

No.	Leg	Site	Hole	Core	T	Sec.	Top	Bot	Depth (mcd)	SEM-tub / sample	age (Ma)
98	202	1241	A	10	H	2	90	92	93.02	**FCP 98**	3.5742
99	202	1241	A	10	H	2	100	102	93.12	**FCP 99**	3.5771
100	202	1241	A	10	H	2	110	112	93.22	**FCP 100**	3.5801
101	202	1241	A	10	H	2	120	122	93.32	**FCP 101**	3.583
102	202	1241	A	10	H	2	130	132	93.42	**FCP 102**	3.586
103	202	1241	A	10	H	2	140	142	93.52	**FCP 103**	3.5889
104	202	1241	A	10	H	3	0	2	93.62	**FCP 104**	3.5919
105	202	1241	A	10	H	3	10	12	93.72	**FCP 105**	3.5949
106	202	1241	A	10	H	3	20	22	93.82	**FCP 106**	3.5978
107	202	1241	A	10	H	3	30	32	93.92	**FCP 107**	3.6008
108	202	1241	A	10	H	3	40	42	94.02	**FCP 108**	3.6037
109	202	1241	A	10	H	3	50	52	94.12	**FCP 109**	3.6067
110	202	1241	A	10	H	3	60	62	94.22	**FCP 110**	3.6096
111	202	1241	A	10	H	3	70	72	94.32	**FCP 111**	3.6126
112	202	1241	A	10	H	3	80	82	94.42	**FCP 112**	3.6155
113	202	1241	A	10	H	3	90	92	94.52	**FCP 113**	3.6185
114	202	1241	A	10	H	3	100	102	94.62	**FCP 114**	3.6214
115	202	1241	A	10	H	3	110	112	94.72	**FCP 115**	3.6244
116	202	1241	A	10	H	3	120	122	94.82	**FCP 116**	3.6274
117	202	1241	A	10	H	3	130	132	94.92	**FCP 117**	3.6303
118	202	1241	A	10	H	3	140	142	95.02	**FCP 118**	3.6333
119	202	1241	A	10	H	4	0	2	95.12	**FCP 119**	3.6362
120	202	1241	A	10	H	4	10	12	95.22	**FCP 120**	3.6392
121	202	1241	A	10	H	4	20	22	95.32	**FCP 121**	3.6421
122	202	1241	A	10	H	4	30	32	95.42	**FCP 122**	3.6451
123	202	1241	A	10	H	4	40	42	95.52	**FCP 123**	3.648
124	202	1241	A	10	H	4	50	52	95.62	**FCP 124**	3.651
125	202	1241	A	10	H	4	60	62	95.72	**FCP 125**	3.654
126	202	1241	A	10	H	4	70	72	95.82	**FCP 126**	3.657
127	202	1241	A	10	H	4	80	82	95.92	**FCP 127**	3.66
128	202	1241	A	10	H	4	90	92	96.02	**FCP 128**	3.663
129	202	1241	A	10	H	4	100	102	96.12	**FCP 129**	3.666
130	202	1241	A	10	H	4	110	112	96.22	**FCP 130**	3.669
131	202	1241	A	10	H	4	120	122	96.32	**FCP 131**	3.672
132	202	1241	A	10	H	4	130	132	96.42	**FCP 132**	3.675
133	202	1241	A	10	H	4	140	142	96.52	**FCP 133**	3.678
134	202	1241	A	10	H	5	0	2	96.62	**FCP 134**	3.681
135	202	1241	A	10	H	5	10	12	96.72	**FCP 135**	3.684
136	202	1241	A	10	H	5	20	22	96.82	**FCP 136**	3.687
137	202	1241	A	10	H	5	30	32	96.92	**FCP 137**	3.69
138	202	1241	A	10	H	5	40	42	97.02	**FCP 138**	3.693
139	202	1241	A	10	H	5	50	52	97.12	**FCP 139**	3.696
140	202	1241	A	10	H	5	60	62	97.22	**FCP 140**	3.699

Final Closure interval Caribbean

Nr.	Leg	Site	Hole	Core	T	Sec.	Top	Bot	Depth (mbsf)	SEM-Tub / sample	Age tuned (Ma)
1	165	1000	A	12	H	2	45	47	100.25	**FCC 1**	3.3012
2	165	1000	A	12	H	2	54	56	100.35	**FCC 2**	3.3047
3	165	1000	A	12	H	2	65	67	100.45	**FCC 3**	3.3083
4	165	1000	A	12	H	2	75	77	100.55	**FCC 4**	3.3118
5	165	1000	A	12	H	2	85	87	100.65	**FCC 5**	3.3154
6	165	1000	A	12	H	2	95	97	100.75	**FCC 6**	3.3189
7	165	1000	A	12	H	2	105	107	100.85	**FCC 7**	3.3224
8	165	1000	A	12	H	2	115	117	100.95	**FCC 8**	3.326
9	165	1000	A	12	H	2	125	127	101.05	**FCC 9**	3.3286
10	165	1000	A	12	H	2	135	137	101.15	**FCC 10**	3.3312
11	165	1000	A	12	H	2	145	147	101.25	**FCC 11**	3.3337
12	165	1000	A	12	H	3	5	7	101.35	**FCC 12**	3.3363
13	165	1000	A	12	H	3	15	17	101.45	**FCC 13**	3.3389
14	165	1000	A	12	H	3	25	27	101.55	**FCC 14**	3.3415
15	165	1000	A	12	H	3	35	37	101.65	**FCC 15**	3.3441
16	165	1000	A	12	H	3	45	47	101.75	**FCC 16**	3.3466
17	165	1000	A	12	H	3	55	57	101.85	**FCC 17**	3.3492
18	165	1000	A	12	H	3	65	67	101.95	**FCC 18**	3.3518
19	165	1000	A	12	H	3	75	77	102.05	**FCC 19**	3.3544
20	165	1000	A	12	H	3	85	87	102.15	**FCC 20**	3.357
21	165	1000	A	12	H	3	95	97	102.25	**FCC 21**	3.3596
22	165	1000	A	12	H	3	105	107	102.35	**FCC 22**	3.3621
23	165	1000	A	12	H	3	115	117	102.45	**FCC 23**	3.3647
24	165	1000	A	12	H	3	124	126	102.54	**FCC 24**	3.367
25	165	1000	A	12	H	3	135	137	102.65	**FCC 25**	3.3699
26	165	1000	A	12	H	3	142	144	102.72	**FCC 26**	3.3717
27	165	1000	A	12	H	4	5	7	102.85	**FCC 27**	3.375
28	165	1000	A	12	H	4	15	17	102.95	**FCC 28**	3.3776
29	165	1000	A	12	H	4	25	27	103.05	**FCC 29**	3.3802
30	165	1000	A	12	H	4	35	37	103.15	**FCC 30**	3.3828
31	165	1000	A	12	H	4	45	47	103.25	**FCC 31**	3.3854
32	165	1000	A	12	H	4	55	57	103.35	**FCC 32**	3.3879
33	165	1000	A	12	H	4	65	67	103.45	**FCC 33**	3.3905
34	165	1000	A	12	H	4	75	77	103.55	**FCC 34**	3.3931
35	165	1000	A	12	H	4	85	87	103.65	**FCC 35**	3.3957
36	165	1000	A	12	H	4	94	96	103.74	**FCC 36**	3.398
37	165	1000	A	12	H	4	107	109	103.87	**FCC 37**	3.4009
38	165	1000	A	12	H	4	115	117	103.95	**FCC 38**	3.4026
39	165	1000	A	12	H	4	125	127	104.05	**FCC 39**	3.4048
40	165	1000	A	12	H	4	135	137	104.15	**FCC 40**	3.407
41	165	1000	A	12	H	4	145	147	104.25	**FCC 41**	3.4092
42	165	1000	A	12	H	5	5	7	104.35	**FCC 42**	3.4114
43	165	1000	A	12	H	5	15	17	104.45	**FCC 43**	3.4135
44	165	1000	A	12	H	5	25	27	104.55	**FCC 44**	3.4157
45	165	1000	A	12	H	5	35	37	104.65	**FCC 45**	3.4179
46	165	1000	A	12	H	5	45	47	104.75	**FCC 46**	3.4201
47	165	1000	A	12	H	5	55	57	104.85	**FCC 47**	3.4223
48	165	1000	A	12	H	5	65	67	104.95	**FCC 48**	3.4245
49	165	1000	A	12	H	5	75	77	105.05	**FCC 49**	3.4267

Nr.	Leg	Site	Hole	Core	T	Sec.	Top	Bot	Depth (mbsf)	SEM-Tub / sample	Age tuned (Ma)
50	165	1000	A	12	H	5	85	87	105.15	**FCC 50**	3.4289
51	165	1000	A	12	H	5	95	97	105.25	**FCC 51**	3.4311
52	165	1000	A	12	H	5	105	107	105.35	**FCC 52**	3.4332
53	165	1000	A	12	H	5	115	117	105.45	**FCC 53**	3.4354
54	165	1000	A	12	H	5	125	127	105.55	**FCC 54**	3.4376
55	165	1000	A	12	H	5	135	137	105.65	**FCC 55**	3.4398
56	165	1000	A	12	H	5	145	147	105.75	**FCC 56**	3.442
57	165	1000	A	12	H	6	5	7	105.85	**FCC 57**	3.4444
58	165	1000	A	12	H	6	15	17	105.95	**FCC 58**	3.4469
59	165	1000	A	12	H	6	25	27	106.05	**FCC 59**	3.4493
60	165	1000	A	12	H	6	35	37	106.15	**FCC 60**	3.4517
61	165	1000	A	12	H	6	45	47	106.25	**FCC 61**	3.4541
62	165	1000	A	12	H	6	55	57	106.35	**FCC 62**	3.4566
63	165	1000	A	12	H	6	65	67	106.45	**FCC 63**	3.459
64	165	1000	A	12	H	6	75	77	106.55	**FCC 64**	3.4614
65	165	1000	A	12	H	6	85	87	106.65	**FCC 65**	3.4638
66	165	1000	A	12	H	6	95	97	106.75	**FCC 66**	3.4662
67	165	1000	A	12	H	6	105	107	106.85	**FCC 67**	3.4687
68	165	1000	A	12	H	6	115	117	106.95	**FCC 68**	3.4711
69	165	1000	A	12	H	6	125	127	107.05	**FCC 69**	3.4735
70	165	1000	A	12	H	6	135	137	107.15	**FCC 70**	3.4759
71	165	1000	A	12	H	6	145	147	107.25	**FCC 71**	3.4784
72	165	1000	A	12	H	7	5	7	107.35	**FCC 72**	3.4808
73	165	1000	A	12	H	7	15	17	107.45	**FCC 73**	3.4832
74	165	1000	A	12	H	7	23	25	107.53	**FCC 74**	3.4852
75	165	1000	B	2	R	1	5	7	107.85	**FCC 75**	3.4929
76	165	1000	B	2	R	1	15	17	107.95	**FCC 76**	3.4954
77	165	1000	B	2	R	1	25	27	108.05	**FCC 77**	3.4978
78	165	1000	B	2	R	1	35	37	108.15	**FCC 78**	3.5002
79	165	1000	B	2	R	1	45	47	108.25	**FCC 79**	3.5026
80	165	1000	B	2	R	1	55	57	108.35	**FCC 80**	3.5051
81	165	1000	B	2	R	1	65	67	108.45	**FCC 81**	3.5075
82	165	1000	B	2	R	1	75	77	108.55	**FCC 82**	3.5099
83	165	1000	B	2	R	1	85	87	108.65	**FCC 83**	3.5123
84	165	1000	B	2	R	1	95	97	108.75	**FCC 84**	3.5148
85	165	1000	B	2	R	1	105	107	108.85	**FCC 85**	3.5172
86	165	1000	B	2	R	1	115	117	108.95	**FCC 86**	3.5196
87	165	1000	B	2	R	1	125	127	109.05	**FCC 87**	3.522
88	165	1000	B	2	R	1	135	137	109.15	**FCC 88**	3.5244
89	165	1000	B	2	R	1	145	147	109.25	**FCC 89**	3.5269
90	165	1000	B	2	R	2	5	7	109.35	**FCC 90**	3.5293
91	165	1000	B	2	R	2	15	17	109.45	**FCC 91**	3.5317
92	165	1000	B	2	R	2	25	27	109.55	**FCC 92**	3.5341
93	165	1000	B	2	R	2	35	37	109.65	**FCC 93**	3.5366
94	165	1000	B	2	R	2	45	47	109.75	**FCC 94**	3.539
95	165	1000	B	2	R	2	55	57	109.85	**FCC 95**	3.5411
96	165	1000	B	2	R	2	65	67	109.95	**FCC 96**	3.5431
97	165	1000	B	2	R	2	75	77	110.05	**FCC 97**	3.5452
98	165	1000	B	2	R	2	85	87	110.15	**FCC 98**	3.5472
99	165	1000	B	2	R	2	95	97	110.25	**FCC 99**	3.5493

Nr.	Leg	Site	Hole	Core	T	Sec.	Top	Bot	Depth (mbsf)	SEM-Tub / sample	Age tuned (Ma)
100	165	1000	B	2	R	2	105	107	110.35	**FCC 100**	3.5513
101	165	1000	B	2	R	2	115	117	110.45	**FCC 101**	3.5534
102	165	1000	B	2	R	2	125	127	110.55	**FCC 102**	3.5554
103	165	1000	B	2	R	2	135	137	110.65	**FCC 103**	3.5575
104	165	1000	B	2	R	2	145	147	110.75	**FCC 104**	3.5596
105	165	1000	B	2	R	3	5	7	110.85	**FCC 105**	3.5616
106	165	1000	B	2	R	3	15	17	110.95	**FCC 106**	3.5637
107	165	1000	B	2	R	3	25	27	111.05	**FCC 107**	3.5657
108	165	1000	B	2	R	3	35	37	111.15	**FCC 108**	3.5678
109	165	1000	B	2	R	3	45	47	111.25	**FCC 109**	3.5698
110	165	1000	B	2	R	3	55	57	111.35	**FCC 110**	3.5719
111	165	1000	B	2	R	3	65	67	111.45	**FCC 111**	3.5739
112	165	1000	B	2	R	3	75	77	111.55	**FCC 112**	3.576
113	165	1000	B	2	R	3	85	87	111.65	**FCC 113**	3.5781
114	165	1000	B	2	R	3	95	97	111.75	**FCC 114**	3.5801
115	165	1000	B	2	R	3	105	107	111.85	**FCC 115**	3.5822
116	165	1000	B	2	R	3	115	117	111.95	**FCC 116**	3.5842
117	165	1000	B	2	R	3	125	127	112.05	**FCC 117**	3.5863
118	165	1000	B	2	R	3	135	137	112.15	**FCC 118**	3.5883
119	165	1000	B	2	R	3	145	147	112.25	**FCC 119**	3.5904
120	165	1000	B	2	R	4	5	7	112.35	**FCC 120**	3.5924
121	165	1000	B	2	R	4	15	17	112.45	**FCC 121**	3.5945
122	165	1000	B	2	R	4	25	27	112.55	**FCC 122**	3.5966
123	165	1000	B	2	R	4	35	37	112.65	**FCC 123**	3.5986
124	165	1000	B	2	R	4	45	47	112.75	**FCC 124**	3.6007
125	165	1000	B	2	R	4	55	57	112.85	**FCC 125**	3.6027
126	165	1000	B	2	R	4	65	67	112.95	**FCC 126**	3.6048
127	165	1000	B	2	R	4	75	77	113.05	**FCC 127**	3.6068
128	165	1000	B	2	R	4	85	87	113.15	**FCC 128**	3.6089
129	165	1000	B	2	R	4	95	97	113.25	**FCC 129**	3.6109
130	165	1000	B	2	R	4	105	107	113.35	**FCC 130**	3.613
131	165	1000	B	2	R	4	115	117	113.45	**FCC 131**	3.6151
132	165	1000	B	2	R	4	125	127	113.55	**FCC 132**	3.6171
133	165	1000	B	2	R	4	135	137	113.65	**FCC 133**	3.6192
134	165	1000	B	2	R	4	145	147	113.75	**FCC 134**	3.6212
135	165	1000	B	2	R	5	5	7	113.85	**FCC 135**	3.6233
136	165	1000	B	2	R	5	15	17	113.95	**FCC 136**	3.6253
137	165	1000	B	2	R	5	25	27	114.05	**FCC 137**	3.6274
138	165	1000	B	2	R	5	35	37	114.15	**FCC 138**	3.6301
139	165	1000	B	2	R	5	45	47	114.25	**FCC 139**	3.6328
140	165	1000	B	2	R	5	55	57	114.35	**FCC 140**	3.6356
141	165	1000	B	2	R	5	65	67	114.45	**FCC 141**	3.6383
142	165	1000	B	2	R	5	75	77	114.55	**FCC 142**	3.641
143	165	1000	B	2	R	5	85	87	114.65	**FCC 143**	3.6437
144	165	1000	B	2	R	5	95	97	114.75	**FCC 144**	3.6464
145	165	1000	B	2	R	5	105	107	114.85	**FCC 145**	3.6491
146	165	1000	B	2	R	5	115	117	114.95	**FCC 146**	3.6519
147	165	1000	B	2	R	5	125	127	115.05	**FCC 147**	3.6546
148	165	1000	B	2	R	5	135	137	115.15	**FCC 148**	3.6573
149	165	1000	B	2	R	5	145	147	115.25	**FCC 149**	3.66

Sample processing

sample	abundance counts	coccolith size measurements	grain size analysis	stable isotope measurements bulk fine-fraction	stable isotope measurements foraminifers (b+p)
BBP 1	x		x	x	x
BBP 2	x	x	x	x	x
BBP 3	x	x	x	x	x
BBP 4	x	x	x	x	x
BBP 5	x	x	x	x	x
BBP 6	x		x	x	x
BBP 7	x	x	x	x	x
BBP 8	x	x	x	x	x
BBP 9	x		x	x	x
BBP 10	x	x	x	x	x
BBP 11	x		x	x	x
BBP 12	x	x	x	x	x
BBP 13	x		x	x	x
BBP 14	x	x	x	x	x
BBP 15	x		x	x	x
BBP 16	x	x	x	x	x
BBP 17	x		x	x	x
BBP 18	x	x	x	x	x
BBP 19	x		x	x	x
BBP 20	x	x	x	x	x
BBP 21	x	x	x	x	x
BBP 22	x		x	x	x
BBP 23	x	x	x	x	x
BBP 24	x		x	x	x
BBP 25	x	x	x	x	x
BBP 26	x	x	x	x	x
BBP 27	x		x	x	x
BBP 28	x	x	x	x	x
BBP 29	x	x	x	x	x
BBP 30	x		x	x	x
BBP 31	x		x	x	x
BBP 32	x	x	x	x	x
BBP 33	x	x	x	x	x
BBP 34	x	x	x	x	x
BBP 35	x	x	x	x	x
BBP 36	x	x	x	x	x
BBP 37	x	x	x	x	x
BBP 38	x	x	x	x	x
BBP 39	x	x	x	x	x
BBP 40	x	x	x	x	x
BBP 41	x	x	x	x	x
BBP 42	x	x	x	x	x
BBP 43	x	x	x	x	x
BBP 44	x	x	x	x	x
BBP 45	x	x	x	x	x
BBP 46	x		x	x	x
BBP 47	x		x	x	x
BBP 48	x	x	x	x	x

sample	abundance counts	coccolith size measurements	grain size analysis	stable isotope measurements bulk fine-fraction	stable isotope measurements foraminifers (b+p)
BBP 49	x	x	x	x	x
BBP 50	x		x	x	x
BBP 51	x	x	x	x	x
BBP 52	x		x	x	x
BBP 53	x		x	x	x
BBP 54	x	x	x	x	x
BBP 55	x		x	x	x
BBP 56	x	x	x	x	x
BBP 57	x	x	x	x	x
BBP 58	x	x	x	x	x
BBP 59	x	x	x	x	x
BBP 60	x	x	x	x	x
BBP 61	x		x	x	x
BBP 62	x		x	x	x
BBP 63	x	x	x	x	x
BBP 64	x		x	x	x
BBP 65	x		x	x	x
BBP 66	x	x	x	x	x
BBP 67	x	x	x	x	x
BBP 68	x	x	x	x	x
BBP 69	x	x	x	x	x
BBP 70	x		x	x	x
BBP 71	x	x	x	x	x
BBP 72	x	x	x	x	x
BBP 73	x		x	x	x
BBP 74	x		x	x	x
BBP 75	x	x	x	x	x
BBP 76	x		x	x	x
BBP 77	x	x	x	x	x
BBP 78	x		x	x	x
BBP 79	x		x	x	x
BBP 80	x	x	x	x	x
BBP 81	x		x	x	x
BBP 82	x		x	x	x
BBP 83	x		x	x	x
BBP 84	x	x	x	x	x
BBP 85	x	x	x	x	x
BBP 86	x	x	x	x	x
BBP 87	x	x	x	x	x
BBP 88	x	x	x	x	x
BBP 89	x		x	x	x
BBP 90	x		x	x	x
BBP 91	x	x	x	x	x
BBP 92	x		x	x	x
BBP 93	x	x	x	x	x
BBP 94	x	x	x	x	x
BBP 95	x		x	x	x
BBP 96	x	x	x	x	x
BBP 97	x		x	x	x

sample	abundance counts	coccolith size measurements	grain size analysis	stable isotope measurements bulk fine-fraction	stable isotope measurements foraminifers (b+p)
BBP 98	x		x	x	x
BBP 99	x	x	x	x	x
BBP 100	x		x	x	x
BBP 101	x		x	x	x
BBP 102	x	x	x	x	x
BBP 103	x		x	x	x
BBP 104	x	x	x	x	x
BBP 105	x	x	x	x	x
BBP 106	x		x	x	x
BBP 107	x	x	x	x	x
BBP 108	x	x	x	x	x
BBP 109	x	x	x	x	x
BBP 110	x	x	x	x	x
BBP 111	x	x	x	x	x
BBP 112	x	x	x	x	x
BBP 113	x	x	x	x	x
BBP 114	x	x	x	x	x
BBP 115	x	x	x	x	x
BBP 116	x	x	x	x	x
BBP 117	x	x	x	x	x
BBP 118	x	x	x	x	x
BBP 119	x		x	x	x
BBP 120	x		x	x	x
BBP 121	x	x	x	x	x
BBP 122	x		x	x	x
BBP 123	x		x	x	x
BBP 124	x	x	x	x	x
BBP 125	x		x	x	x
BBP 126	x		x	x	x
BBP 127	x	x	x	x	x
BBP 128	x		x	x	x
BBP 129	x		x	x	x
BBP 130	x	x	x	x	x
BBP 131	x		x	x	x
BBP 132	x		x	x	x
BBP 133	x	x	x	x	x
BBP 134	x		x	x	x
BBP 135	x		x	x	x
BBP 136	x	x	x	x	x
BBP 137	x		x	x	x
BBP 138	x		x	x	x
BBP 139	x		x	x	x
BBP 140	x		x	x	x
BBP 141	x		x	x	x
BBP 142	x	x	x	x	x
BBP 143	x	x	x	x	x
BBP 144	x	x	x	x	x
BBP 145	x	x	x	x	x
BBP 146	x	x	x	x	x

sample	abundance counts	coccolith size measurements	grain size analysis	stable isotope measurements bulk fine-fraction	stable isotope measurements foraminifers (b+p)
BBP 147	x		x	x	x
BBP 148	x		x	x	x
BBP 149	x	x	x	x	x
BBC 1	x			x	
BBC 2			x	x	
BBC 3	x	x		x	
BBC 4			x	x	
BBC 5	x	x		x	
BBC 6			x	x	
BBC 7	x	x		x	
BBC 8			x	x	
BBC 9	x	x		x	
BBC 10			x	x	
BBC 11	x	x		x	
BBC 12			x	x	
BBC 13	x	x		x	
BBC 14			x	x	
BBC 15	x	x		x	
BBC 16			x	x	
BBC 17	x	x		x	
BBC 18			x	x	
BBC 19	x	x		x	
BBC 20			x	x	
BBC 21	x	x		x	
BBC 22			x	x	
BBC 23	x	x		x	
BBC 24			x	x	
BBC 25	x	x		x	
BBC 26			x	x	
BBC 27	x			x	
BBC 28			x	x	
BBC 29	x			x	
BBC 30			x	x	
BBC 31	x	x		x	
BBC 32			x	x	
BBC 33	x			x	
BBC 34			x	x	
BBC 35	x	x		x	
BBC 36			x	x	
BBC 37	x			x	
BBC 38			x	x	
BBC 39	x			x	
BBC 40			x	x	
BBC 41	x			x	
BBC 42			x	x	
BBC 43	x			x	
BBC 44			x	x	
BBC 45	x	x		x	
BBC 46			x	x	

sample	abundance counts	coccolith size measurements	grain size analysis	stable isotope measurements bulk fine-fraction	stable isotope measurements foraminifers (b+p)
BBC 47	x			x	
BBC 48			x	x	
BBC 49	x			x	
BBC 50			x	x	
BBC 51	x			x	
BBC 52			x	x	
BBC 53	x			x	
BBC 54			x	x	
BBC 55	x	x		x	
BBC 56			x	x	
BBC 57	x			x	
BBC 58			x	x	
BBC 59	x			x	
BBC 60			x	x	
BBC 61	x			x	
BBC 62			x	x	
BBC 63	x			x	
BBC 64			x	x	
BBC 65	x	x		x	
BBC 66			x	x	
BBC 67	x			x	
BBC 68			x	x	
BBC 69	x			x	
BBC 70			x	x	
BBC 71	x			x	
BBC 72			x	x	
BBC 73	x			x	
BBC 74			x	x	
BBC 75	x	x		x	
BBC 76			x	x	
BBC 77	x	x		x	
BBC 78			x	x	
BBC 79	x	x		x	
BBC 80			x	x	
BBC 81	x	x		x	
BBC 82			x	x	
BBC 83	x	x		x	
BBC 84			x	x	
BBC 85	x			x	
BBC 86			x	x	
BBC 87	x	x		x	
BBC 88			x	x	
BBC 89	x	x		x	
BBC 90			x	x	
BBC 91	x	x		x	
BBC 92			x	x	
BBC 93	x			x	
BBC 94			x	x	
BBC 95	x			x	

sample	abundance counts	coccolith size measurements	grain size analysis	stable isotope measurements bulk fine-fraction	stable isotope measurements foraminifers (b+p)
BBC 96			x	x	
BBC 97	x			x	
BBC 98			x	x	
BBC 99	x			x	
BBC 100			x	x	
BBC 101	x	x		x	
BBC 102			x	x	
BBC 103	x			x	
BBC 104			x	x	
BBC 105	x			x	
BBC 106			x	x	
BBC 107	x			x	
BBC 108			x	x	
BBC 109	x			x	
BBC 110				x	
BBC 111	x	x	x	x	
BBC 112				x	
BBC 113	x			x	
BBC 114			x	x	
BBC 115	x			x	
BBC 116				x	
BBC 117	x	x	x	x	
BBC 118				x	
BBC 119	x	x		x	
BBC 120			x	x	
BBC 121	x	x		x	
BBC 122				x	
BBC 123	x	x	x	x	
BBC 124				x	
BBC 125	x	x		x	
BBC 126			x	x	
BBC 127	x	x		x	
BBC 128				x	
BBC 129	x		x	x	
BBC 130				x	
BBC 131	x			x	
BBC 132			x	x	
BBC 133	x			x	
BBC 134				x	
BBC 135	x	x	x	x	
BBC 136				x	
BBC 137	x			x	
BBC 138			x	x	
BBC 139	x			x	
BBC 140				x	
BBC 141	x		x	x	
BBC 142				x	
BBC 143	x			x	
BBC 144			x	x	

sample	abundance counts	coccolith size measurements	grain size analysis	stable isotope measurements bulk fine-fraction	stable isotope measurements foraminifers (b+p)
BBC 145	x	x		x	
BBC 146				x	
BBC 147	x		x	x	
BBC 148				x	
BBC 149	x			x	
BBC 150			x	x	
BBC 151	x			x	
BBC 152				x	
BBC 153	x			x	
BBC 154				x	
BBC 155	x			x	
BBC 156				x	
BBC 157				x	
BBC 158				x	
BBC 159				x	
BBC 160				x	
BBC 161				x	
BBC 162				x	
BBC 163				x	
BBC 164				x	
BBC 165				x	
BBC 166				x	
BBC 167				x	
BBC 168				x	
BBC 169				x	
BBC 170				x	
BBC 171				x	
BBC 172				x	
BBC 173				x	
BBC 174				x	
BBC 175				x	
BBC 176				x	
BBC 177				x	
BBC 178				x	
BBC 179				x	
BBC 180				x	
BBC 181				x	
BBC 182				x	
BBC 183				x	
BBC 184				x	
BBC 185				x	
BBC 186				x	
BBC 187				x	
BBC 188				x	
BBC 189				x	
BBC 190				x	
BBC 191				x	
BBC 192				x	
BBC 193				x	

sample	abundance counts	coccolith size measurements	grain size analysis	stable isotope measurements bulk fine-fraction	stable isotope measurements foraminifers (b+p)
BBC 194				x	
BBC 195				x	
BBC 196				x	
BBC 197				x	
BBC 198				x	
BBC 199				x	
BBC 200				x	
BBC 201				x	
BBC 202				x	
BBC 203				x	
BBC 204				x	
BBC 205				x	
BBC 206				x	
BBC 207				x	
BBC 208				x	
BBC 209				x	
FCP 1	x	x		x	
FCP 2			x	x	
FCP 3	x			x	
FCP 4			x	x	
FCP 5				x	
FCP 6	x		x	x	
FCP 7				x	
FCP 8			x	x	
FCP 9	x			x	
FCP 10			x	x	
FCP 11				x	
FCP 12	x	x		x	
FCP 13			x	x	
FCP 14				x	
FCP 15	x			x	
FCP 16			x	x	
FCP 17				x	
FCP 18	x			x	
FCP 19			x	x	
FCP 20				x	
FCP 21	x			x	
FCP 22			x	x	
FCP 23				x	
FCP 24	x			x	
FCP 25			x	x	
FCP 26				x	
FCP 27	x			x	
FCP 28			x	x	
FCP 29				x	
FCP 30	x			x	
FCP 31			x	x	
FCP 32				x	
FCP 33	x			x	

sample	abundance counts	coccolith size measurements	grain size analysis	stable isotope measurements bulk fine-fraction	stable isotope measurements foraminifers (b+p)
FCP 34			x	x	
FCP 35				x	
FCP 36	x			x	
FCP 37			x	x	
FCP 38				x	
FCP 39	x			x	
FCP 40			x	x	
FCP 41				x	
FCP 42	x			x	
FCP 43			x	x	
FCP 44				x	
FCP 45	x			x	
FCP 46			x	x	
FCP 47				x	
FCP 48	x			x	
FCP 49			x	x	
FCP 50				x	
FCP 51	x			x	
FCP 52			x	x	
FCP 53				x	
FCP 54	x			x	
FCP 55			x	x	
FCP 56				x	
FCP 57	x			x	
FCP 58			x	x	
FCP 59				x	
FCP 88			x	x	
FCP 89				x	
FCP 90	x			x	
FCP 91			x	x	
FCP 92				x	
FCP 93	x			x	
FCP 94			x	x	
FCP 95				x	
FCP 96	x			x	
FCP 97			x	x	
FCP 98				x	
FCP 99	x			x	
FCP 100			x	x	
FCP 101				x	
FCP 102	x			x	
FCP 103			x	x	
FCP 104				x	
FCP 105	x			x	
FCP 106			x	x	
FCP 107				x	
FCP 108	x			x	
FCP 109			x	x	
FCP 110				x	

sample	abundance counts	coccolith size measurements	grain size analysis	stable isotope measurements bulk fine-fraction	stable isotope measurements foraminifers (b+p)
FCP 111	x			x	
FCP 112			x	x	
FCP 113				x	
FCP 114	x			x	
FCP 115			x	x	
FCP 116				x	
FCP 117	x			x	
FCP 118			x	x	
FCP 119				x	
FCP 120	x			x	
FCP 121			x	x	
FCP 122				x	
FCP 123	x			x	
FCP 124			x	x	
FCP 125				x	
FCP 126	x	x		x	
FCP 127			x	x	
FCP 128				x	
FCP 129	x			x	
FCP 130			x	x	
FCP 131				x	
FCP 132	x			x	
FCP 133			x	x	
FCP 134				x	
FCP 135	x	x		x	
FCP 136			x	x	
FCP 137				x	
FCP 138	x			x	
FCP 139			x	x	
FCP 140				x	
FCC 1	x	x	x	x	
FCC 2	x			x	
FCC 3	x			x	
FCC 4			x	x	
FCC 5				x	
FCC 6	x			x	
FCC 7			x	x	
FCC 8				x	
FCC 9	x			x	
FCC 10			x	x	
FCC 11				x	
FCC 12	x	x		x	
FCC 13			x	x	
FCC 14				x	
FCC 15	x			x	
FCC 16			x	x	
FCC 17				x	
FCC 18	x			x	
FCC 19			x	x	

sample	abundance counts	coccolith size measurements	grain size analysis	stable isotope measurements bulk fine-fraction	stable isotope measurements foraminifers (b+p)
FCC 20				x	
FCC 21	x			x	
FCC 22			x	x	
FCC 23				x	
FCC 24	x			x	
FCC 25			x	x	
FCC 26				x	
FCC 27	x			x	
FCC 28			x	x	
FCC 29				x	
FCC 30	x			x	
FCC 31			x	x	
FCC 32				x	
FCC 33	x			x	
FCC 34			x	x	
FCC 35				x	
FCC 36	x			x	
FCC 37			x	x	
FCC 38				x	
FCC 39	x			x	
FCC 40			x	x	
FCC 41				x	
FCC 42	x			x	
FCC 43			x	x	
FCC 44				x	
FCC 45	x			x	
FCC 46			x	x	
FCC 47				x	
FCC 48	x			x	
FCC 49			x	x	
FCC 50				x	
FCC 51	x			x	
FCC 52			x	x	
FCC 53				x	
FCC 54	x			x	
FCC 55				x	
FCC 56				x	
FCC 57	x			x	
FCC 58				x	
FCC 59				x	
FCC 60	x			x	
FCC 61				x	
FCC 62				x	
FCC 63	x			x	
FCC 64				x	
FCC 65				x	
FCC 66	x			x	
FCC 67				x	
FCC 68				x	

sample	abundance counts	coccolith size measurements	grain size analysis	stable isotope measurements bulk fine-fraction	stable isotope measurements foraminifers (b+p)
FCC 69	x			x	
FCC 70				x	
FCC 71				x	
FCC 72	x			x	
FCC 73				x	
FCC 74				x	
FCC 75	x			x	
FCC 76				x	
FCC 77				x	
FCC 78	x			x	
FCC 79				x	
FCC 80				x	
FCC 81	x			x	
FCC 82				x	
FCC 83				x	
FCC 84	x			x	
FCC 85				x	
FCC 86				x	
FCC 87	x			x	
FCC 88				x	
FCC 89				x	
FCC 90	x			x	
FCC 91				x	
FCC 92				x	
FCC 93	x			x	
FCC 94				x	
FCC 95				x	
FCC 96	x			x	
FCC 97				x	
FCC 98				x	
FCC 99	x			x	
FCC 100				x	
FCC 101				x	
FCC 102	x			x	
FCC 103				x	
FCC 104				x	
FCC 105	x			x	
FCC 106				x	
FCC 107				x	
FCC 108	x			x	
FCC 109				x	
FCC 110				x	
FCC 111	x			x	
FCC 112				x	
FCC 113				x	
FCC 114	x			x	
FCC 115				x	
FCC 116				x	
FCC 117	x			x	

sample	abundance counts	coccolith size measurements	grain size analysis	stable isotope measurements bulk fine-fraction	stable isotope measurements foraminifers (b+p)
FCC 118				x	
FCC 119				x	
FCC 120	x	x		x	
FCC 121				x	
FCC 122				x	
FCC 123	x			x	
FCC 124				x	
FCC 125				x	
FCC 126	x			x	
FCC 127				x	
FCC 128				x	
FCC 129	x			x	
FCC 130				x	
FCC 131				x	
FCC 132	x	x		x	
FCC 133				x	
FCC 134				x	
FCC 135	x			x	
FCC 136				x	
FCC 137				x	
FCC 138	x			x	
FCC 139				x	
FCC 140				x	
FCC 141	x			x	
FCC 142				x	
FCC 143				x	
FCC 144	x			x	
FCC 145				x	
FCC 146				x	
FCC 147	x			x	
FCC 148				x	
FCC 149	x			x	

Table A3-3 Mean carbonate masses and resulting carbonate masses given for minimal and maximal length for selected coccolith species.

SITE	Species	*F. profunda*	*Reticulofenestra* sp.	*R. minuta / D. productus* -group	*R. minutula / R. haquii* -group	*R. pseudoumbilicus* M	*R. pseudoumbilicus*	*Calcidiscus* sp.	*C. leptoporus* S	*C. leptoporus* I	*C. leptoporus* L	*C. leptoporus* XL	*Coccolithus pelagicus*	*Umbilicosphaera* sp.	*U. jafari*	*U. rotula*	*Helicosphaera* sp.	*Pontosphaera* sp.	*Syracosphaera* sp.	*R. clavigera*	*S. apsteinii*	x-fold difference in total coccolith carbonate between min. + max.
BBP	mean length	1.89	3.71	2.43	3.90	5.69	7.82	6.53	3.78	6.67	8.75	11.01	7.54				10.78					**3.4**
	mean mass	0.68	9.80	2.06	8.57	25.58	65.79	77.49	12.77	66.06	144.23	291.09	73.42				183.47					**-**
	mass at min size	0.18	0.11	0.11	3.65	16.88	46.31	3.58	3.58	27.00	110.59	216.00	26.37				73.05					**7.1**
	mass at max size	2.37	115.9	3.65	16.88	46.31	115.9	383.6	27.00	110.59	216.00	383.61	204.73				415.84					
BBC	mean length	2.49	4.07	2.37	3.97	5.78	7.10	6.97	3.96	6.57	8.90	10.00	8.09	3.73	2.94	4.83	9.15	8.55	3.45	6.45	24.00	**0.3**
	mean mass	1.65	11.65	1.94	8.87	26.78	48.35	87.00	14.38	63.19	154.22	216.00	95.78	9.52	4.02	17.18	113.40	100.01	1.96	25.16	7464.96	**-**
	mass at min size	0.22	0.58	0.58	3.65	16.88	46.31	8.49	8.49	27.00	110.59	216.00	23.04		1.19	9.50	30.64	19.20	0.32	3.70		**7.6**
	mass at max size	6.44	50.4	3.65	16.88	46.31	50.39	216	27.00	110.59	216.00	216.00	398.58		9.50	26.08	216.77	347.13	5.37	67.50		
FCP	mean length	2.50	3.21	2.26	3.72			6.21	3.59	6.45	8.73	10.80	6.24	3.60	2.75	4.45	7.88					**2.6**
	mean mass	1.72	5.76	1.75	7.27			78.27	10.79	61.96	145.65	273.26	39.36	8.28	3.24	13.33	69.39					**-**
	mass at min size	0.40	0.46	0.46	3.65			5.27	5.27	27.00	110.59	216.00		2.05	2.05	8.64	24.87					**4.3**
	mass at max size	7.38	16.88	3.65	16.88			311.67	27.00	110.59	216.00	311.67		16.42	8.64	16.42	115.75					
FCC	mean length	3.74	3.80	2.39	3.94	5.39	7.20	6.81	4.31	6.54	8.97	10.66		3.91	3.18	5.03	8.16	8.36	3.74	7.59	16.83	**0.7**
	mean mass	5.61	8.86	1.98	8.66	21.23	50.39	93.50	17.73	64.27	158.42	262.91		10.69	5.02	19.42	79.39	94.04	2.80	53.48	2973.22	**-**
	mass at min size	0.65	0.55	0.55	3.65	16.88	46.31	8.64	8.64	27.00	110.59	216.00		1.38	1.38	9.50	21.73	22.95	0.30	6.57	590.07	**13.5**
	mass at max size	16.64	50.39	3.65	16.88	46.31	50.39	328.51	27.00	110.59	216.00	328.51		30.50	9.50	30.50	170.06	170.06	9.65	523.96	5988.37	